Universidade do Minho
Escola de Engenharia

Sylvie de Oliveira Ribeiro

Tailoring electroactive polymer nanocomposites for novel muscle tissue engineering applications

outubro de 2019

Tailoring electroactive polymer nanocomposites for novel muscle tissue engineering applications
Sylvie de Oliveira Ribeiro
UMinho | 2019

Universidade do Minho
Escola de Engenharia

Sylvie de Oliveira Ribeiro

Tailoring electroactive polymer nanocomposites for novel muscle tissue engineering applications

Tese de Doutoramento
Doutoramento em Engenharia de Materiais

Trabalho efetuado sob a orientação do
Professor Senentxu Lanceros-mendez
da
Professora Andreia Castro Gomes
e do
Professor Carlos Baleizão

outubro de 2019

DIREITOS DE AUTOR E CONDIÇÕES DE UTILIZAÇÃO DO TRABALHO POR TERCEIROS

ACKNOWLEDGEMENTS

And here comes the end of this long and challenging journey. First of all, I would like to thank all people who directly or indirectly contributed to the achievement of this thesis.

I want to thank the financial support of the Foundation for Science and Technology-(FCT), grant SFRH/BD/111478/2015.

To Professor Senentxu Lanceros-Mendez, my supervisor, a very special thank for all the accompaniment, help, continuous support and knowledge given to me over these years. It's an honor to have been your PhD student and I hope that we "jump" more walls together. A huge thanks to my co-supervisors Professora Andreia Gomes and Professor Carlos Baleizão for receiving me so well in your groups, for your ideas and scientific knowledge provided and for your friendship during this step.

I also want to thank the good times spent in the ARC Centre for Electromaterials Science, University of Wollongong and off course, in special, all the support given by Professor Michael Higgings.

To all the members of Electroactive Smart Material group (ESM), I would like to thank all the help along this journey, the companionship and the amazing team spirit given. In a special way I wish to thank my friend Juliana Oliveira, my "Ju", for the friendship. Thanks for all the support, good moments that we shared and good memories that we created.

I would like to thank all my closest friends for the unconditional support, encouragement, laughter and good moments, and also being by my side in the difficult times, not only during the development of this thesis, but in all the journey of the life.

To my parents, the most special thank. Thank you for all the affection, strength, advices, support, friendship and the most important, love. Thank you for being my examples. What I am today, I owe it to you and this thesis would not exist without you.

To Clarisse and Melanie, my big and little sisters, my eternal supports and my unconditional loves. I am so proud to have you as sisters. Thank you for everything you do for me and to see me laugh. I would not be the same without you. To Pedro, my brother from another mother, thank you for all the good moments, support, love and all the sense of humor since you came into my life. To Joel, thank you for all the help, friendship, affection and all the shared laugthers.

At last, and most importantly, I thank my husband Luis that has been always my pillar, to believe in me and for always being by my side. Thank you, my love, for your patience, support, encouragement and for your unconditional love. "The measure of Love is to love without measure". Love you.

STATEMENT OF INTEGRITY

I hereby declare having conducted this academic work with integrity. I confirm that I have not used plagiarism or any form of undue use of information or falsification of results along the process leading to its elaboration.

I further declare that I have fully acknowledged the Code of Ethical Conduct of the University of Minho.

Desenvolvimento de nanocompósitos baseados em polímeros eletroativos para novas aplicações em engenharia de tecido muscular.

Os distúrbios a nível do músculo-esquelético têm vindo a crescer continuamente a nível mundial, exigindo novas estratégias para atingir uma regeneração estrutural e funcional. Os polímeros piezoelétricos tem despertado interesse, oferecendo novas oportunidades para a engenharia de tecido do músculo-esquelético, uma vez que estes são electromecanicamente ativos, permitindo a estimulação mecano-elétrica dos tecidos.

Neste trabalho, poli(fluoreto de vinilideno) (PVDF), o polímero biocompatível com a maior resposta piezoelétrica foi processado na forma de filmes, fibras e membranas porosas. Biomateriais compósitos foram produzidos com a introdução de nanopartículas de sílica com variação de diâmetro, quantidade e funcionalização, assim como com nanopartículas magnetostritivas ($CoFe_2O_4$). Deste modo, foi desenvolvida uma plataforma de polímeros eletroativos com características biomiméticas estruturais e com transdução mecano- e magnetoelétrica até um $d_{33} \approx |24|$ pC.N^{-1} e α_{33}= 16.15 mV.cm^{-1}Oe^{-1}.

O efeito da carga superficial dos filmes de PVDF na adesão e diferenciação celular foi investigado. A organização do citoesqueleto de mioblastos C2C12 aderidas a diferentes amostras de PVDF foi estudada por imunofluorescência e as interações entre uma única célula e o PVDF através de Espectroscopia de Força de uma Única Célula. Os mioblastos C2C12 cultivados nas amostras com carga superficial apresentaram uma morfologia mais alongada, independentemente de a carga ser negativa ou positiva. Foi determinado como as propriedades da superfície do material, tanto em termos de polarização (carga superficial positiva ou negativa) como de morfologia (filmes ou fibras) influenciam a diferenciação dos mioblastos, mostrando que o PVDF promove a diferenciação miogénica conforme evidenciado pela fusão e maturação, comprimento, diâmetro e número dos miotubos. As superfícies carregadas melhoram a fusão das células musculares em miotubos diferenciados e o uso de fibras de PVDF orientadas promovem o alinhamento celular.

A estimulação dinâmica magnetoelétrica permitiu melhorar o índice de maturação do miotubo comparativamente às condições estáticas, sendo ainda melhorado com a combinação de estímulos químicos (meio de diferenciação) chegando até 70%. A estimulação dinâmica mecano-elétrica direta tem o mesmo efeito que a magnetoelétrica.

Assim, este trabalho demonstra que a estimulação mecano-elétrica é uma nova abordagem para aplicações em engenharia de tecido músculo-esquelético.

Palavras chave: Biomateriais, engenharia de tecido, estímulo mecano-elétrico, músculo-esquelético, polímeros piezoelétricos.

Tailoring electroactive polymer nanocomposites for novel muscle tissue engineering applications

The prevalence of skeletal muscle disorders has been steadily increasing worldwide, requiring new strategies for their structural and functional regeneration. Piezoelectric polymers have attracted interest offering new opportunities for skeletal muscle tissue engineering (TE), since they are electromechanically active, allowing tissue mechano-electric and electro-mechanical stimulation.

In this work, piezoelectric poly(vinylidene fluoride) (PVDF), the biocompatible polymer with the highest piezoelectric response, has been processed in the form of films, fibres and porous membranes. Composite biomaterials were also produced with the incorporation of silica nanoparticles with different diameters, functionalization and content, as well as magnetostrictive nanoparticles ($CoFe_2O_4$). This allowed a full set of electroactive polymers with biomimetic structural features and mechano- and magnetoelectric transduction up to $d_{33} \approx |24|$ pC.N^{-1} and α_{33}= 16.15 mV.cm^{-1}Oe^{-1}.

The effect of the surface charge of PVDF films on cell adhesion and differentiation was investigated. The cytoskeletal organization of C2C12 myoblasts adhered to different PVDF samples was studied by immunofluorescence and the interactions between single live cells and PVDF were analyzed by Single Cell Force Spectroscopy. C2C12 myoblasts seeded on samples with surface charge showed a more elongated morphology, independently of the charge being negative or positive. It was further determined how the surface properties of the material, both in terms of the poling state (positive or negative net surface charge) and their morphology (films or fibres) influence myoblast differentiation, showing that PVDF promotes myogenic differentiation as evidenced by myotube fusion and maturation index, length, diameter and number. Charged surfaces improve the fusion of muscle cells into differentiated myotubes and the use of oriented β-PVDF electrospun fibres scaffolds cell alignment.

Magnetoelectric dynamic stimulation allowed to improve myotube maturation index comparatively to the static conditions being further enhanced with the combination of chemical stimuli (differentiation medium) up to ≈ 70%. Further, direct mechanoelectric dynamic stimulation also increases the maturation index of myotubes.

Thus, this work convincingly demonstrates that mechano-electrical stimulation is a novel and suitable approach for skeletal muscle TE applications.

Keywords: Biomaterials, mechano-electrical stimuli, piezoelectric polymer, skeletal muscle, tissue engineering.

Table of contents

List of figures

List of tables

List of symbols

A	Electrode area
A_α	Absorbance – α-PVDF
A_β	Absorbance – β-PVDF
C	Capacity
d	Thickness
d_{33}	Piezoelectric coefficient
E	Young's modulus
ε_0	Vacuum permittivity
ε'	Real part of dielectric constant
ε''	Imaginary part of dielectric constant
ε_{break}	Stain-to-Failure
f	Frequency
F_β	β-phase content
H_{AC}	Amplitude of the AC magnetic field
I	current
K_α	Absorption coefficient of α-PVDF
K_β	Absorption coefficient of β-PVDF
L	Distance between electrodes
R	Electrical resistance
t	Tickness of the piezoelectric layer
$\tan \delta$	Dielectric loss
T_m	Melting temperature
V	Voltage
ω	Angular frequency
wt.%	Weight percentage
X_c	Degree of crystallinity
x	Amount of the α-phase
y	Amount of the β -phase
α_{33}	Transverse Magnetoelectric voltage coefficient
ΔH_α	Enthalpy of pure crystalline α-phase

ΔH_β	Enthalpy of pure crystalline β-phase
ΔHf	Melting enthalpy
ΔV	Output voltage
σ	Direct current electrical conductivity
σ'	Real part of the complex electrical conductivity
σ_{break}	Ultimate tensile strength

List of abbreviations

A

AFM	Atomic Force Microscopy
ATR	Attenuated Total Reflection

B

BM	Basal Medium
BSA	Bovine Serum Albumin

C

CFO	$CoFe_2O_4$

D

DAPI	4',6-diamidino-2-phenylindole
DLS	Dynamic light scattering
DM	Differentiation Medium
DMEM	Dulbecco's Modified Eagle's Medium
DMF	N, N-dimethylformamide
DMSO	Dimethyl sulfoxide
DSC	Differential Scanning Calorimetry
DTG	Differential Thermogravimetric

E

ECM	Extracellular matrix

F

FA	Focal Adhesion
FBS	Fetal Bovine Serum
FITC	Phalloidin Fluorescein Isothiocyanate
FTIR	Fourier Transformed Infrared Spectroscopy

M

ME	Magnetoelectric
MHC	Myosin Heavy Chain
MSNPs	Mesoporous silica nanoparticles
MTS	(3-(4,5-dimethylthiazol-2-yl)-5-(3-carboxymethoxyphenyl)-2-(4-sulfophenyl)-2H-tetrazolium)
MTT	3-(4,5-Dimethylthiazol-2-yl)-2,5-diphenyltetrazolium bromide

N

NMR	Nuclear Magnetic Resonance

P

P/S	Penicillin/Streptomycin
PANI	Poly(aniline)
PBS	Phosphate Buffer Solution
PDI	Perylenediimide derivative
PHB	Poly(hydroxybutyrate)
PLLA	Poly(L-lactic acid)
PVDF	Poly(vinylidene fluoride)
P(VDF-TrFE)	Poly[(vinylidene fluoride-co-trifluoroethylene)

S

SCFS	Single Cell Force Spectroscopy
SD	Standard Deviation
S.E.M.	Standard Error of the Mean
SEM	Scanning Electron Microscope
SiNPs	Silica nanoparticles

T

TCPS	Tissue Culture Polystyrene
TE	Tissue Engineering
TEM	Transmission Electron Microscopy
TEOS	Tetraethyl Orthosilicate
TGA	Thermogravimetric Analysis
TRITC	Tetramethylrhodamine B isothiocyanate

V

VSM	Vibrating Sample Magnetometer

W

WCA	Water Contact Angle

To my parents,

my sisters and my dear Luis

"A dream you dream alone is only a dream. A dream you dream together is reality."

John Lennon

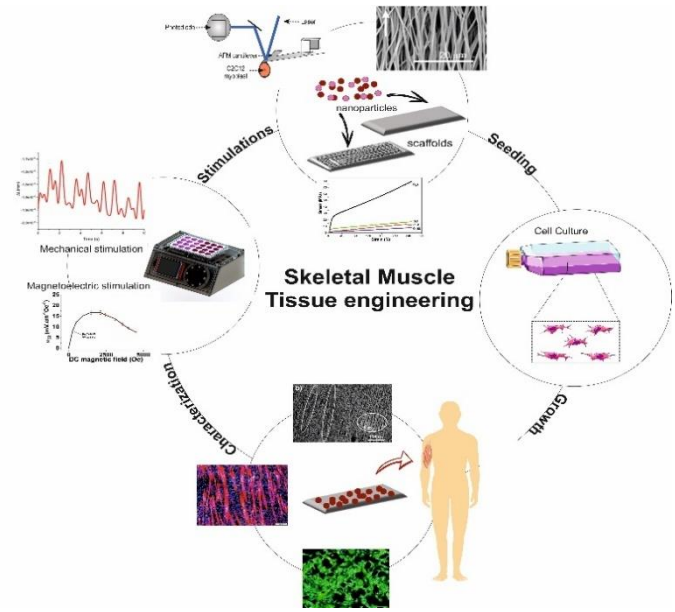

Chapter 1. Introduction

Tissue engineering and regenerative medicine are increasingly taking advantage of active materials, allowing to provide specific cues to the cells. In particular, the use of electroactive polymers that deliver an electrical signal to the cells upon mechanical solicitation, create new scientific and technological opportunities, as they in fact mimic signals and effects that occur in living tissues, allowing the development of suitable microenvironments for tissue regeneration. This chapter is based on a novel overall strategy for skeletal muscle tissue engineering that is based on the notion that muscle cells are subjected to mechano-electrical stimuli in their natural *in vivo* microenvironment and that piezo- and magnetoelectric polymers, used as scaffolds, are suitable for delivering those cues.

This chapter is based on the following publication: **S. Ribeiro**, C. Garcia-Astrain, M.M. Fernandes, S. Lanceros-Méndez and C. Ribeiro, *Chapter 13 - Multidimensional Biomechanics Approaches Though Electrically and Magnetically Active Microenvironments*; in *Advances in Biomechanics and Tissue Regeneration*, 2018, 253-267 and **S. Ribeiro**, D. M. Correia, C. Ribeiro and S. Lanceros-Méndez, *Electrospun Polymeric Smart Materials for Tissue Engineering Applications*; in *Electrospun Biomaterials and Related Technologies*, 2018, 251-282.

1.1 Tissue engineering

Injury, disease and congenital malformation have always been part of the human experience. Tissue and organ failures produced as a result of injury (or other type of damage) are one of the most devastating and costly problems in medicine. Tissue or organs transplantation and reconstruction in these patients is severely limited by readiness of compatible donors, apart from constituting the most expensive therapies available, costing billions of dollars a year [1]. Mechanical devices or artificial prosthetics have also been used but pose important limitations as they do not restore the tissue/organ function, are not intended for integration into the host tissue and may induce inflammatory response in the host [2].

It is within this context that tissue engineering (TE) emerges as a significant alternative or complementary solution. The term *tissue engineering* was initially defined by the attendees of the first National Science Foundation sponsored meeting in 1988 as "application of the principles and methods of engineering and life sciences toward fundamental understanding of structure-function relationship in normal and pathological mammalian tissues and the development of biological substitutes for the repair or regeneration of tissue or organ function" [3]. In 1993, Langer and Vacanti summarized the early developments in this field and defined TE as an interdisciplinary field that applies the principles of engineering and life sciences toward the development of biological substitutes that restore, maintain or improve tissue or organ function [4].

The classical TE approach has been mainly focusing on associating cells with the supporting matrix, also called biomaterials or scaffolds, that essentially act as a template for tissue formation by allowing cells to adhere, migrate, differentiate and produce tissue. The scaffolds are typically seeded with cells and occasionally have added growth factors, or subjected to biophysical stimuli in the form of a bioreactor [5, 6]. Typically, the combination of cells, signals and scaffold is often referred to as TE triad [1, 3].

The field relies extensively on the use of scaffolds to provide the appropriate environment for regeneration of tissues and organs. A number of key considerations are important when designing or determining the suitability of a scaffold for use in TE, such as biocompatibility, biodegradability, mechanical properties, scaffold architecture, manufacturing technology and finally the selection of biomaterial [7].

Over the years, TE embraced that biomimetic microenvironments are key components to successful cell culture and TE *in vitro.*

TE approaches usually involve a biocompatible material in combination with cells and different stimuli to repair tissues or organs (figure 1.1).

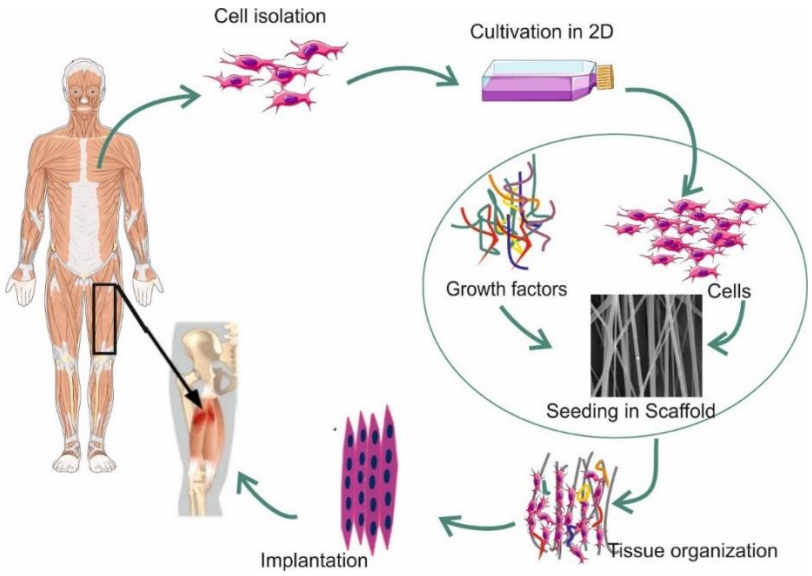

Figure 1.1. Tissue engineering strategies for muscle regeneration.

Cell adhesion is influenced by several parameters such as scaffold surface chemistry and surface charge or topography, among others. For example, to induce stem cell differentiation to the desired lineage, stems cells require extracellular stimuli, such as chemical (growth factors) and physical cues (i.e. mechanical stimulation). Physical signals are particularly relevant, as cell development is influenced by these stimuli and cell activity can be potentiated in *in vitro* models that mimic the body's microenvironment. Moreover, cell adhesion, proliferation and differentiation can also be regulated by using active scaffolds which provide the appropriate environment for specific cell responses. The effect of external stimuli over cell attachment is also a key point, since focal adhesions (FAs) are the predominant mechanism by which cells mechanically connect to and apply traction forces on the extracellular matrix (ECM) [8]. Although the cellular response to electrical stimuli remains largely unknown, some regulatory membrane proteins and enzymes are sensitive to electric fields. When a cell attaches to a surface, it receives information from the environment by means of these ion channels and receptors present in its membrane and starts developing FAs [9].

The relevance of electrical phenomena in the human body was realized in the 18th century by von Haller and later by Galvani and Volta who demonstrated the dependence of muscles and nervous cells from electricity [10]. Major functions of cells, such as metabolism and growth, are influenced by electrical processes at different stages. Cells maintain a difference in potential across membranes and reduce it when necessary, can switch current on and off as well as vary current flow or store charge [11]. Among the different cues determining tissue functionality, electrical and electromechanical ones are crucial for tissues such as bone or muscle [12]. The movement and migration can be guided by electric fields in a

variety of different cell types such as corneal, epidermal and epithelial cells [13-16]. Moreover, these electric fields can also modulate the phenotypes of vascular endothelial cells, regenerate nerve fibres and influence ligament healing [17-19].

1.1.1 Principles for electric and mechanical cues

Tissue development, repair and/or regeneration of cells and organs, as well as cell behaviour and function, require multiple physiological cues, not only the (bio)chemical ones, but also physical signals, namely electrical and mechanical [20, 21].

Relatively to the mechanical forces, it is known that the cells are constantly exposed to them (depending on the tissue, they can be shear, compressive or tensile forces) [22], which in turn exert forces on their environment, modulating their behaviour (cell migration, proliferation and differentiation) [20, 23]. Also, they play a key role in diverse cellular processes, ranging from proliferation to transcription to organogenesis [24] due to, for example, the FAs complexes and the internal remodeling of the cytoskeletal architecture, the signalization of the second messenger (such as the intracellular Ca^{2+}) or gene expression changes. So, cells are constantly monitoring the extracellular parameters of the surrounding microenvironment in order to respond to these changes appropriately and modify their behaviour accordingly, through a process termed mechanotransduction [25]. Essentially, each cellular process must begin with mechanotransduction, which is the conversion of the mechanical forces into biochemical or electrical signals that will remodel the cells and tissues at the structural and functional level [26].

The microenvironment found is dependent on the tissue and can be highly unique. For example, skeletal muscle cells are found embedded in a 3D tissue undergoing mechanical stretch and compression and endothelial cells are found in a 2D interface in contact with fluid, exposed to stretch and compression during pulsatile blood flow but also to fluid shear stress [24, 27]. In this way, for the design of the mechanical platforms, the mechanobiological niche of each tissue must be taken into consideration.

The bioelectrical fields are generated by specific ion channels and pumps within cell membranes and guide the development and regeneration of many tissues, such as cartilage, nervous system and vascular endothelial cells [28, 29].

The knowledge that cells and tissues are able to sense physical stimuli and translate them into biochemical and biological responses, has been paving the way for the development of novel smart materials to be applied in regenerative medicine [30, 31].

One such example is the development of electrically and magnetically active materials/scaffolds for TE purposes. These materials are able to efficiently promote cell seeding, growth and differentiation, taking advantage of the mechanotransduction properties of the cells [11]. Living cells show many properties that are typical from electrical systems. They generate electromotive force, use varying resistances in series or in parallel, regulate the potentials difference whenever needed, switch on and off, control and rectify current flow store charge. Across the plasma membrane, an electrical voltage is present and inside the cell the environment remains more negative than the outside [11]. Due to all these properties, the application of small electric fields on different cells such as corneal [13, 14] and epithelial [16], has been described to guide them to in culture. Electric fields have also been reported to modulate phenotypes of vascular endothelial cells [17], to enhance nerve fibre outgrowth *in vitro* [18] and have been widely used in bone and cartilage regeneration [19, 29, 32].

Therefore, materials capable of inducing a surface electrical charge able to stimulate the growth of cells and tissues in culture constitute a suitable approach for TE applications.

In this context, smart materials show strong advantages with respect to conventional scaffolds providing additional cues to the cell and supporting the development of suitable microenvironments and can be used as innovative active biomimetic template for the regeneration of damaged tissue [33].

1.2 Smart materials

Smart materials constitute a key technology supporting novel products with unique capabilities [34]. The adjective “smart” implies that these materials are able to react to changes in their environment in a predetermined way [34, 35].

Thus, smart materials are able to respond to specific single or multiple external stimuli in a controllable, predictable and reproducible way [35]. Only some materials show certain intrinsic characteristics which can be exploited in products, systems or structures that in turn exhibit “smart” behaviour [36].

In particular, the available literature describes a variety of smart materials playing an increasing role in a wide range of TE strategies. This strong increase of smart materials development for TE applications is due to improvement of the limitations of conventional scaffolds, which are simply used in a passive way, i.e. as support for cells and tissues. It is observed that for specific cells and tissues, the active behaviour of the material used for the scaffold can be used as an advantage, providing the necessary stimuli for proper tissue regeneration [33].

Many stimuli can play an important role in the development and function of the human body. Some of these stimuli can be artificially controlled, such as light, magnetic or electric field, or naturally promoted by a physiological environment, such as electrical, temperature or pH changes, within the body. Thus, variations of pH can be found in muscle cells after muscle activity or in the brain, and pH variations also promote many cellular processes [37]. Mechanical stimuli are also constantly occurring in throughout the lifespan of human body cells, playing a particularly relevant role in bone formation and ECM production [12].

Some studies exploit the application of electrical or mechanical stimuli without the use of active polymers (such as conductive or piezoelectric). However, in recent years, active polymers have been used for different TE areas (such as regeneration of bone, muscle, nerve, among others) in order to induce these stimuli more naturally, taking advantage of the existence of electrical or mechanical signals of the body.

Piezoelectric polymers are among the smart materials most commonly used for TE. Many tissues of human body such as bone [38], nervous tissue [39] and muscle [40] are controlled by electrical signals, and piezoelectric materials allow the application of electrical signals to the cells through mechano-electrical transduction. They have shown suitability for TE due to their capacity of varying surface charge when a mechanical load is applied, without need of direct connection to an external voltage source (figure 1.2).

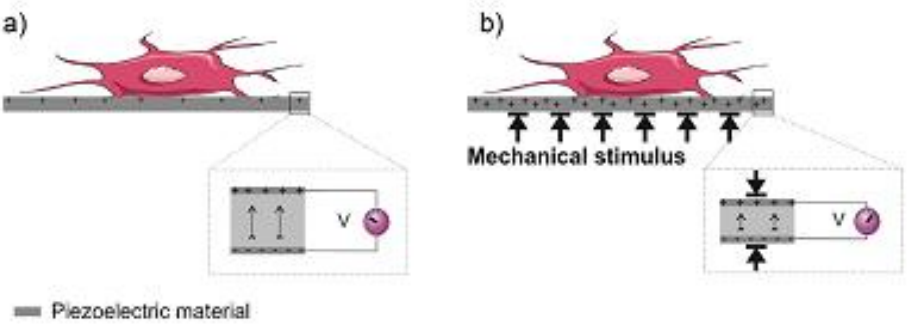

Figure 1.2. Schematic representation of the piezoelectric effect (piezoelectric material representation at the bottom of the image) and corresponding cell culture on piezoelectric supports (a) without and (b) with mechanical stimulus, the later leading to an electrical potential variation of the materials which is, in turn, influences cell response [12].

In some cases, the scaffolds structures should be accomplished with the few natural and synthetic materials available for a specific smart response, reinforced by other (nano)materials in order to achieve

multifunctional smart materials. Some of these materials are, for example, the inclusion of magnetic sensitivity by using magnetic fillers, and electrical sensitivity/conductivity by using electrically conducting fillers such as carbon or silver nanotubes or nanowires, among others [36]. The inability of engineered materials to mimic the natural properties of tissue is a major roadblock that can be solved by resourcing to nanotechnology.

1.2.1 Polymer-based multifunctional nanocomposites

Strong efforts have been put into research to reach the actual needs in term of materials characteristics. Nanotechnology has demonstrated a strong impact in the area of materials science by providing, among others, a new generation of nanocomposites with enhanced functionalities to overcome the limitations of traditional materials [41]. Due to their improved mechanical, thermal, physical, biological and chemical properties than bulk materials, nanoparticles are an interesting solution as functional agents to include into polymers films. Among the different nanocomposites, polymer-based nanocomposites have become a prominent area of current research [41, 42], allowing the development of advanced multifunctional materials with tailorable properties for a broad range of applications in areas such as food packaging [43], sensors and actuators [44, 45], biomedical field [46, 47], among others.

Generally, these nanocomposites are designed specifically to take advantage of the properties of the fillers together with the ductility, flexibility and processability of the organic polymers [47, 48].

Different kind of nanoparticles have been used on and added to polymeric matrices, such as magnetic nanoparticles in order to obtain magnetoelectric (ME) and multiferroic composites for sensors and cell stimulation [49]; Ag particles for larger dielectric response and antimicrobial properties [50]; zeolites to increase the dielectric and functional properties, and controlled drug release [51]; ceramic fillers to improve electroactivity [52] and carbon nanotubes to enhance dielectric and mechanical properties [53]. On the other hand, once fillers have been introduced into the polymer matrix, biomaterial–cell interaction is modified and novel bioactivity or even suppression of biocompatibility can occur [54, 55].

Additionally, among the wide range of fillers that can be added, the magnetic/magnetostrictive nanoparticles have attracted increasing attention as they generate ME composite materials that allow the use of an external magnetic field to remotely trigger mechanical and electrical stimuli onto growing tissues [56]. Silica nanoparticles (SiNPs) also have huge potential for TE applications due to their properties and the possibility to incorporate drug or growth/differentiation factors that can improve/complete the

multifunctional systems for tissue regeneration. In this sense, the focus has been mainly on these two types of fillers described above that have been extensively used in TE.

1.2.1.1 Silica nanoparticles

Silica is the most common oxide on earth with a mean abundance of about 37 wt.% [57]. SiNPs, which belong to the Organization of Economic Cooperation and Development (OECD) list of interest and are among the most utilized nanomaterials in industrial nanotechnologies, can present a variety of forms: crystalline, simple amorphous and mesoporous [58].

Among inorganic materials, silica is especially adequate for biomedical applications as it is biocompatible, endogenous (present in bones), and generally recognized as safe by the U.S. Food and drug Administration (US-FDA) [59]. SiNPs are not only easy to synthesize with controlled diameter and low size dispersion but also amiable to rich conjugation chemistry, which allows the incorporation of different groups into the silica network, such as drugs, inorganic complexes, fluorescent dyes (to improve the photophysical and photochemical performance of the dyes) [60-64]. Owing to these characteristics, SiNPs have been used as supports or carriers for drug delivery [65] and imaging [66, 67]. Some studies have also investigated the use of SiNPs in combination with polymers for biomedical applications. The use of SiNPs to produce hybrid hydrogels with poly(hydroxyethylmethacrylate) showed an improvement on cell adhesion and proliferation of 3T3-fibroblast cells when 10 and 30% of SiNPs concentrations were used [68]. The same happen for PEG hydrogels that enhance initial cell adhesion, promote cell spreading and increase the metabolic activity when SiNPs are added to the hydrogel [69]. *Chrissafis* et al. found that incorporating silica nanoparticles substantially increased tensile strength and Young's modulus of poly(vinyl pyrrolidone), chitosan or poly(vinyl alcohol) based hydrogels [70] and more recently a simple and effective method for the production of mechanically-responsive scaffolds using SiNPs into a biocompatible polymer has been presented, in order to evaluate the effect of the change mechanical properties on cellular functions [71]. SiNPs embedded electrospun fiber mats have been also used for drug delivery in bone TE with PLGA and PLLA as well as for nerve and wound healing tissue regeneration [72, 73]. To date, research on SiNPs in TE has dominantly focused on bone regeneration given that the diversified functions of SiNPs are qualified with various demands in bone TE [74]. The application of SiNPs in other TE areas, namely skeletal muscle TE, has scarcely been addressed, so more effort should be devoted to conduct an in-depth study on the suitability of SiNPs in these fields.

1.2.1.2 Magnetic, magnetomechanic and magnetoelectric materials

Another strategy able to induce mechanotransduction on cells is the application of magnetic stimuli on magnetic responsive materials. The use of such materials in biomedicine has been widely explored, mainly if we consider the possibility of preparing nanoscaled magnets. They possess important properties that have allowed applications in different medical areas including neurology [75], ophthalmology [76], dentistry [77] and cardiology [78], among others. In fact, the size of these magnetic nanomaterials plays a key role as it imparts unique properties to the material. Specific interactions with cells, viruses and proteins, which ultimately induce cellular growth or death, and the possibility of entering the organism and reach locations inaccessible to other materials [79, 80], are just a few examples of the important properties these materials hold. Moreover, these nanoparticles are easily functionalized with other materials, permitting enhanced interactions and specific binding to the targeted biological entities, which ultimately results in colloidal stability and biocompatibility [81]. Also, one of the advantages of using magnetic nanomaterials in biomedicine is the fact that they are easily traceable and localized inside the body through the action of a magnetic field, thus using minimally invasive methods [82].

Magnetic nanomaterials can be obtained in different morphologies, such as magnetic micro/nanoparticles, which may be categorized into different structures: pure metals (Co, Fe, Ni, Ti) and metal oxides (iron oxides Fe_2O_3 or Fe_3O_4 and ferrites such as $BaFe_{12}O_{19}$ and $CoFe_2O_4$ (CFO)) in order to obtain magnetic nanocomposites [83, 84]. Magnetic nanoparticles have been commonly used with a variety of cells and tissues for TE applications [85]. Also, they have been playing an important role in cell separation and immunoassays, drug targeting and delivery, gene delivery and transfection [86], as well as magnetic resonance imaging (MRI) contrast agents [87, 88]. These particles vary in size, surface chemistry, magnetic properties and bulk chemistry and often consist of a magnetic iron oxide core coated with a biocompatible polymer. This allows their functionalization enabling them to attach binding molecules such as antibodies, peptides and other functional groups [89]. Magnetic nanoparticles may be linked to functional sites, such as the cell membrane and/or on internal cellular components, thus acting as transducers of magnetic fields and enabling the non-invasive control of various cellular functions [30]. Early findings have shown that by functionalizing magnetic microparticles with ligands able to interact with different receptors on the cells surface, it was possible to study the mechanical linkage between the cell membrane receptor and the cytoskeletal network [90]. Since then, basic scientific research has been conducted on a variety of cell types to evaluate the mechanotransduction phenomenon assisted by these particles and respective coatings [91-97].

These types of magnetic nanoparticles may be incorporated as a filler to obtain composites with ME properties. The obtained nanocomposites are very interesting materials since it becomes possible to remotely mechanical and/electrically stimulate tissues from outside of the human body [98, 99] and for specific cell cultures in bioreactors [100]. Therefore, in cases when the patient is immobilized due to serious health issues, or when the natural mechanical stimulus does not occur, decreasing the effectiveness of piezoelectric materials, this type of smart materials may hold an interesting advantage.

In this sense, examples of such materials are those possessing mechano-electric, magnetic and ME properties. Mechano-electric materials are mainly constituted by piezoelectric polymers that respond to mechanical stimuli, inducing an electrical charge in the material (Figure 1.3A). Magnetic and ME materials are composites comprising magnetic or magnetostrictive particles and a piezoelectric polymer. Because of their magnetic component, they sense a magnetic field that induces a mechanical stimulation on the scaffold due to the incorporated magnetic or magnetostrictive properties, which further induce an electrical polarization variation due to the piezoelectric phase present in the same scaffold (Figure 1.3B and C).

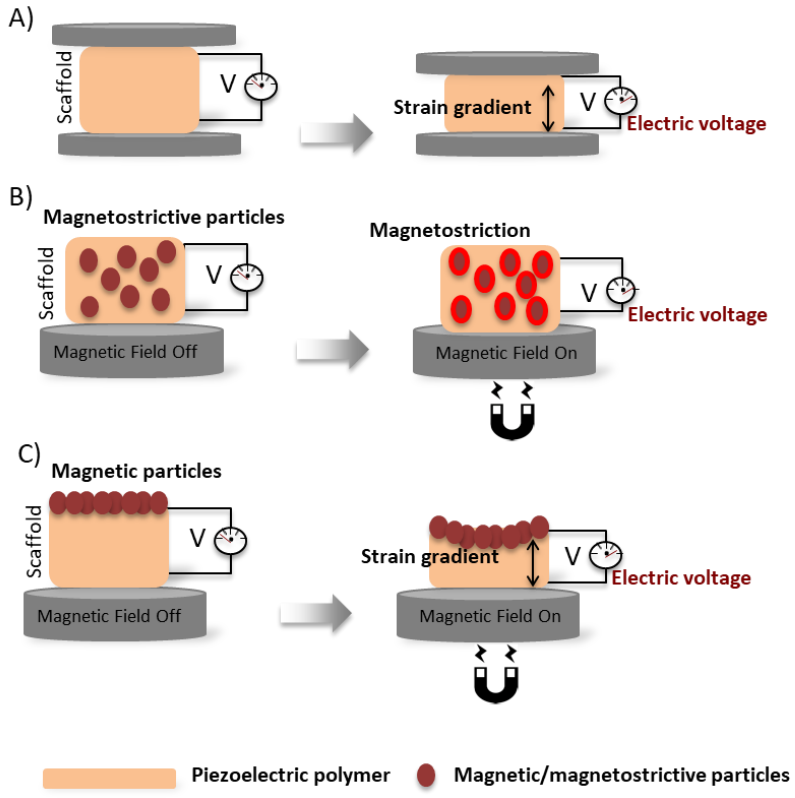

Figure 1.3. Schematic representation of the (A) mechano-electric properties of a scaffold upon the application of mechanical stimuli and (B) and (C) magnetoelectric properties of scaffolds upon the application of magnetic stimuli.

1.2.2 Scaffold design

Nevertheless, not only the mechanical and electrical stimuli are important to obtain promising results in regenerating, maintaining, or improving tissue functions in the human body. The architecture of the scaffolds used for TE is also of critical importance. Intuitively, the best scaffold for an engineered tissue should be the extracellular matrix of the target tissue in its native state [101]. The fabrication technique for TE scaffolds depends almost entirely on the bulk and surface properties of the material and the proposed function of the scaffold. Each method presents distinct advantages and disadvantages, and the appropriate technique is selected to meet the requirements for the specific tissue type [102]. In the last years, significant advances have been achieved in the development of definite scaffolds geometries including hydrogels, three-dimensional polymeric scaffold, microspheres, acellular scaffolds and fibres scaffolds, among others [102]. Furthermore, it is important refer that scaffolds should have an interconnected pore structure and high porosity to ensure cellular penetration and adequate diffusion of nutrients to cells within the construct and to the extracellular matrix formed by these cells [103].

Various engineering materials, including ceramics, metals (alloys), polymers and composites, have been developed to replace/support the function of biological materials. Metal, alloys and ceramics materials are being replaced by polymers because the developing scaffolds with the optimal characteristics, such as the strength, rate of degradation, porosity, and microstructure, as well as their shapes and sizes, are more readily and reproducibly controlled in polymeric scaffolds. Polymers are light weight, inexpensive, mechanically and electrically tough and show excellent compatibility with other organic and inorganic materials for the development of multifunctional hybrid systems [101].

As mechanical stimuli found throughout many human body activities, piezoelectric materials and mechano-electrical transduction demonstrate large potential for TE. Table 1.1 summarizes the main studies on scaffold morphologies that can be used to produce piezoelectric materials in the form of films, fibres, porous membranes and 3D scaffolds [12] for TE applications.

Table 1.1. Scaffold designs from piezoelectric materials for different tissue engineering applications. Adapted from [12].

Applications	Scaffold design	Piezoelectric materials	References
Bone regeneration or bone TE	Films	Poly(vinylidene fluoride)(PVDF)/copolymers Poly(L-lactic acid)(PLLA) Poly(hydroxybutyrate)(PHB)/copolymers	[38, 104-108] [109] [110]
	Fibres	PVDF/copolymers PLLA PHB/copolymer Composite poly(lactic acid) /demineralized bone powders	[111] [112] [110, 113] [114]
	3D blends / blends membranes (porous)	PVDF/copolymers PHB/copolymers Composite PVDF/starch/natural rubber (NR) Composite Poly(vinylidene fluoride-co-trifluoroethylene) (P(VDF-TrFe))/strarch/NR	[115] [116] [115] [115]
	Membranes	P(VDF-TrFe)/Barium titanate	[117]
	3D porous scaffold	PLLA covered with bonelike apatite Apatite/collagen	[118] [118]
Muscle regeneration	Films	PVDF	[40]
	Fibres	PVDF Composite Au-PLLA	[40, 119] [120]
	Meshes	PVDF	[121]
Nerve regeneration	Films	PVDF P(VDF-TrFE)	[18, 122, 123] [18, 124]
	Fibres	P(VDF-TrFE) Collagen	[124, 125] [126]
	Blends membranes (porous)	PVDF	[127]
	Channels/tubes	PVDF P(VDF-TrFe)	[128, 129] [130]
	3D porous scaffold	PLLA	[131]
	3D gel matrices	Collagen	[132]

1.2.2.1 Electrospinning

The development of nanofibres has widened the scope for fabricating scaffolds that can potentially mimic the architecture of natural human tissue at the nanometer scale. There are three main techniques

available for the synthesis of nanofibres: electrospinning, self-assembly and phase separation [102]. Electrospinning (ES) has attracted much attention not only because of its versatility in spinning a wide variety of polymeric fibres but also because of its consistency in producing fibres with submicron thickness [133]. The technique can be easily employed in the laboratory and can be scaled up to an industrial process [134]. The setup essentially consists on a capillary tube, a needle, attached to a syringe filled with the polymer solution, a grounded collector and a high voltage power supply connected to the capillary and the collector (figure 1.4) [134].

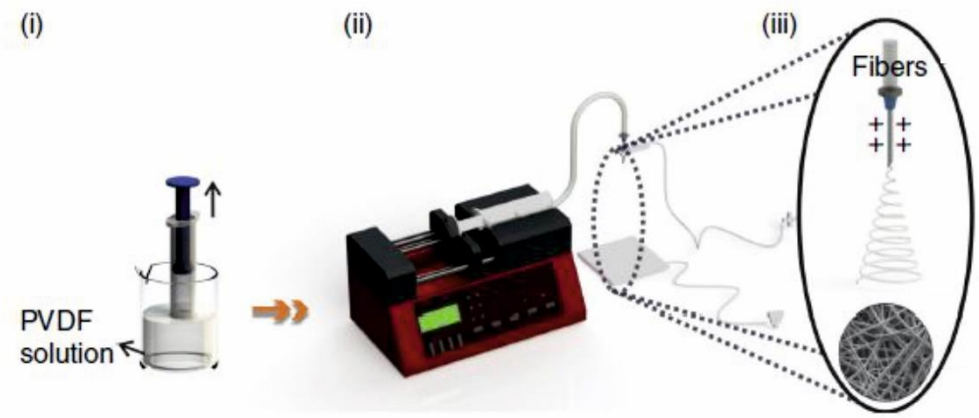

Figure 1.4. Schematic representation of the preparation of β-PVDF fibres by electrospinning. (i) The PVDF solution is poured into a syringe; (ii) the syringe pump is turned on to apply a positive voltage to the needle and (iii) fibres will be formed according to the solution concentration [135].

During the electrospinning process, a polymer solution is held at the needle tip through surface tension. The application of an electric field using the high-voltage source causes a charge to be induced within the polymer, resulting in charge repulsion within the solution. This electrostatic force opposes the surface tension; eventually, the charge repulsion overcomes the surface tension, causing the initiation of a jet. As this jet travels, the solvent evaporates, and an appropriate collector can be used to capture the polymer fibre [136].

Electrospun fibre scaffolds have a high surface to volume ratio and, together with their microporous structure, can enhance cell adhesion, migration, proliferation and differentiated function, all of which are highly desired properties for TE applications [137]. Polymers can be easily processed by electrospinning and consequently, this potential makes smart electrospun polymers materials viable candidate for bone, neuronal, cardiac, and muscle, among others, TE applications. Table 1.2 summarizes some electrospun polymers with specific smart functions, together with the respectively application.

Table 1.2. Some relevant electrospun smart materials for different tissue engineering.

Effect of smart material	Tissue engineering applications	Polymers	References
Piezoelectric	Bone	Collagen	[138]
		Cellulose	[139]
		Chitin	[140]
		Keratin	[141]
		PVDF	[111]
		PHB	[142]
		PLLA	[143]
	Muscle	Collagen	[144]
		PVDF	[40]
	Nerve	PHB	[145]
		PLLA	[146]
	Others Applications (skin substitutes or wound healing, cartilage)	PHB	[147]
		PLLA	[148]
		Collagen	[149, 150]
Conductive Scaffolds	Cardiac	Poly(aniline) (PANI)	[151, 152]

1.3 Smart materials for tissue engineering

Many tissues in the human body undergo physical stimulation, namely through electrical and mechanical stimuli (figure 1.5a). Figure 1.5b shows the tissues that can be stimulated with the designed platform to improve tissue regeneration. In addition, there are also tissues in the human body which are piezoelectric. In this sense, it is important to use active materials, notably piezoelectric polymers for TE which in recent years has been validated as a promising approach because they can give the electrical and mechanical stimuli that tissues require.

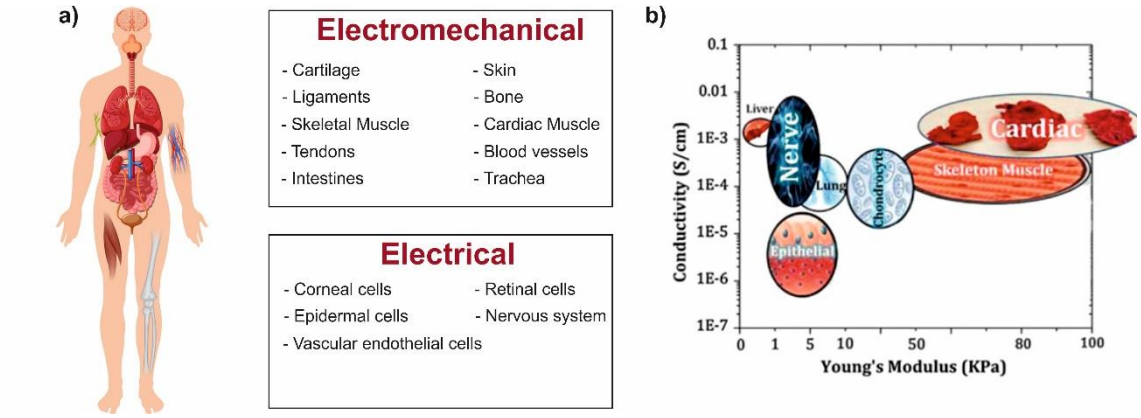

Figure 1.5. (a) Representative human body tissues and cells in which electrical and electromechanical signals are relevant; (b) conductivity and mechanical properties of different tissue. Adapted from [153].

In particular, piezoelectric and ME polymers with different morphologies have been used with different cell type. However, most of these studies were performed in static conditions. The piezoelectric and ME effect is only proven when dynamic conditions (either mechanical or electrical) are applied (Table 1.3), otherwise, only the suitability of the materials and the significance of the surface charge, when the material is poled, are demonstrated [12].

Table 1.3. Biomaterial, cell culture condition and cells used for different applications.

Biomaterial	Conditions	Cells	Application	Ref.
PVDF positively poled	-Mechanical stimulation	Goat marrow	Bone	[106]
	-Mechanical stimulation in vertical vibration -Frequency = 1Hz -Amplitude ≈1mm	MC3T3-E1 pre-osteoblast		[38]
PVDF negatively poled	-Mechanical stimulation in vertical vibration -Frequency = 1 Hz -Maximum amplitude ≈1mm	Human adipose stem		[108]
Terfenol-D/P(VDF-TrFE)	-Magnetic stimulation; -Active time = 16 h (10 min of active time and 20 min of repose time); -Non-active time = 8 h; -Frequency = 0.3 Hz; -Displacement of permanent magnets ≈ 20 mm; -Maximum value = 230 Oe; -ME voltages = 0.115 mV.	MC3T3-E1 pre-osteoblast		[154]
Colagen type I	-Stretched cyclically along the long axis -Frequency = 1 Hz -Magnitude = 10 000 μstrain (1%) -Number of cycles = 1800 -Time = every day for 30 min over a period of 3 weeks.	Human osteoblastic precursor		[155]
PVDF and P(VDF-TrFe)	-Sinusoidal output (vibrational forces); -Peak voltage ≈ 2.5mV; -Frequency = 1200Hz -Standard incubator shelves	Mouse neuroblastoma	Nerve	[156]
PLLA/PANI	-A silver electrode and a platinum electrode were inserted to opposite ends of the nanofibrous scaffold; -Constant voltage = 1.5 V; -Time = 60 min; -Electric field = 100 mV/mm.	Nerve stem cells		[157]
Polyurethane/PVDF	-Intermittent deformation of 8% -Frequency = 0.5 Hz	NIH3T3	Wound healing	[158]

PVDF and its copolymers constitute the most used piezoelectric polymer for TE due to their stronger piezoelectric response [67]. In particular, most of the studies describing cell response under dynamic stimulation use PVDF as a support for cell proliferation and differentiation. Rodrigues *et al.* showed that

β-PVDF positively charged films provide an adequate environment for enhancing the growth and differentiation of goat marrow cells into osteoblast in dynamic conditions, being an ideal support for the seeding and the development of undifferentiated cells towards a desired phenotype [106]. The combination of biochemical and physical stimuli can successful mimic a biomimetic microenvironment present in the human body. Ribeiro *et al.* showed that PVDF negatively charged films [107] under dynamic conditions, more specifically mechanical stimulation, lead to enhanced osteogenic differentiation of human adipose stem cells, which was confirmed by detection of higher alkaline phosphatase activity [108]. In the presence of PVDF films, MC3T3-E1 pre-osteoblast cells showed different responses. In the presence of positively charged β-PVDF films and with mechanical stimuli, higher osteoblast adhesion and proliferation was observed [38]. These results were confirmed in *in vivo* studies where β-PVDF films were implanted into a bone defect, significantly demonstrating more defect closure and bone remodeling. In this case, the mechanical solicitations are obtained by the rat movements [159]. Other piezoelectric polymers such as collagen type I have also been used, where 3D samples mechanically stretched to promote proliferation and differentiation of human osteoblastic precursor cells through gene expression regulation related to the early and late stages of osteoblastic differentiation [155].

A novel approach for TE applications has been achieved with biomaterials with ME response. Magnetoelectric Terfenol-D/P(VDF-TrFe) composites promote ≈25% of MC3T3-E1 pre-osteoblast cell proliferation when the cells are cultured under mechanical and electrical stimulation remotely triggered by varying magnetic field [56]. ME electrospun fibres based on CFO/PVDF [160] have also been reported, with suitable ME response for TE applications.

For muscle regeneration, although this tissue type is not piezoelectric, it was already proven that a charged surface enhances cell proliferation [40]. However, until now, the studies under dynamic conditions with piezoelectric biomaterials are yet to be performed contrarily to bone tissue. Previous studies reported that skeletal muscle cells exhibited viscoelastic behaviour that changed during differentiation: the apparent elastic modulus increased from 11.5 ± 1.3 kPa for undifferentiated myoblasts to 45.3 ± 4.0 kPa after eight days of differentiation [161]. The electrical conductivity of the native skeletal muscle tissue is approximately 0.04-0.5 S/m [162].

1.4 Skeletal Muscle tissue engineering

Although many cell types constitute the human body, they are organized into four broad categories of tissues: epithelial, connective, muscle and nervous. Each of these categories is characterized by

specific functions that contribute to the overall health and maintenance of the human body [163]. Muscle tissue is characterized by properties that allow movement. Muscle cells are excitable since they respond to a stimulus. They are contractile, meaning they can shorten and generate a pulling force. When attached between two movable objects, in other words, between bones, contractions of the muscles cause the bones to move. Some muscle movement is voluntary, which means it is under conscious control. For example, a person decides to open a book and read a chapter on anatomy. Other movements are involuntary, meaning they are not under conscious control, such as the contraction of your pupil in bright light [164, 165]. Muscle tissue is classified into three types according to structure and function: skeletal [166] , cardiac [167] and smooth[168].

With more than 600 individual muscles, skeletal muscle represents the largest tissue mass of the body and is essential for motion and support. Skeletal muscles are distinct from both cardiac and smooth muscles in that they can be voluntary controlled by the organism [169]. Furthermore, the creation of skeletal muscle tissue using TE methods holds promise for the treatment of a variety of muscle diseases, including skeletal myopathies such as muscular dystrophy or spinal muscular atrophy [170]; in addition, traumatic injury, aggressive tumor ablation, and prolonged denervation are common clinical situations that often result in significant loss of muscle tissue and require subsequent surgical reconstruction [171].

Skeletal muscle exhibits a high degree of structural organization (figure 1.6). Each muscle is composed of thousands of multinucleate muscle fibres (differentiated (fused) muscle cells), which run in parallel to each other and have relatively consistent diameter [172].

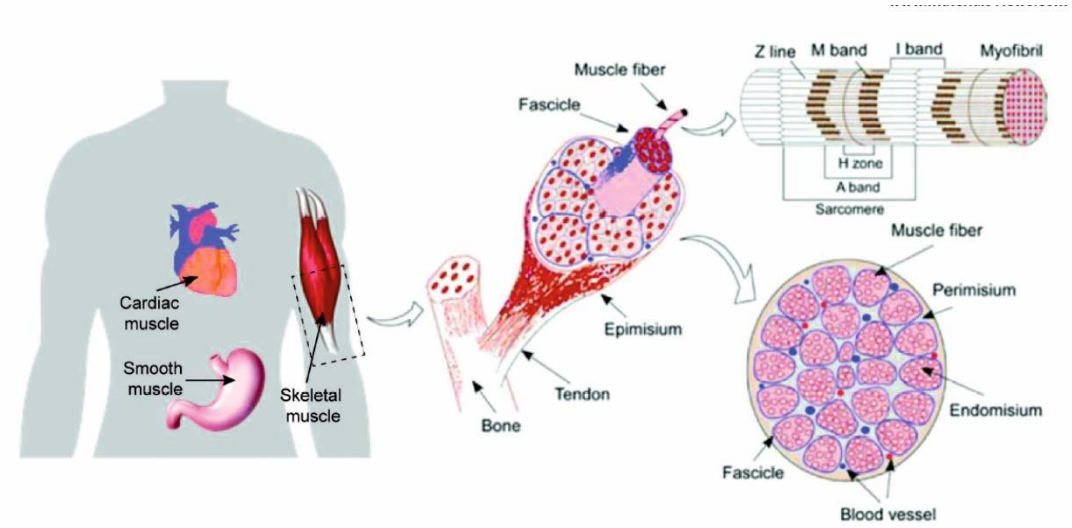

Figure 1.6. Schematic illustration of anatomic structures and organization of skeletal muscle tissue [173].

Each muscle fibre is densely packed with myofibrils throughout their core, and as such organelles such as nuclei and mitochondria are located peripherally in the mature muscle fibre [174]. The myofibrils contain repeating contractile units termed sarcomeres (approximately 2.3 μm long), which form the basis for muscular contraction and thus force its production, as well as endowing skeletal muscle with its striated appearance [172].

The structure of the sarcomere was first published in 1953, revealing that each repeating sarcomere principally contained two fibrous proteins, thin actin filaments and thick myosin ones, organized in a precise manner [175, 176]. Actin and myosin proteins represent approximately 70% of the total protein content of a single fibre and are the main component of sarcomeres [177]. According to the structure and function of skeletal muscle, the requirements of engineered muscle are as follows: reconstructed muscle is a parallel alignment of myofibrils with myosin/actin filaments, intracellular calcium storage, and acetylcholine receptors, which are needed for creating direct forces and functional use [171].

Myofibrils are bundled within the massive cytoplasm of a multinucleated syncytium, the muscle cell or myofibre; motoneuron connections in the cell membrane (the sarcolemma) regulate the flow of calcium ions through the sarcoplasmic reticulum, necessary for the contraction of the myofibrils [178].

It should be noted that skeletal muscle fibres differ in their phenotypes depending on their myosin heavy chain isoform, which results in differences in twitch speed. Type I fibres express slow-twitch myosin heavy chain (MHC) isoforms and are suited for endurance while type II fibres express fast-twitch MHCs that are suited for short and high intensity work [179].

Differentiation of mononucleated myoblasts into differentiated multinucleated myotubes can be analysed by investigating the expression of marker genes that play distinct roles during myogenesis. Among these genes, myogenic regulator factors (MRF) play essential roles [180]. These transcription factors contain a basic helix loop helix DNA-binding domain and function as promoters for several muscle specific genes. Two important transcription factors of myogenesis are Myo and myogenin, both members of the MRF family. MyoD, acting as a myogenic differentiation factor, is upregulated in the early stages of myogenesis and induces fusion of myoblasts and reduction of proliferation. It accomplishes this by up regulating cell cycle inhibitors (p21) and downregulating cell-cycle activators, such as cyclins and cyclin-dependent kinases [181]. Myogenin arises in later stages of differentiation and acts more specifically in the formation of multinucleated muscle tissue, as seen in myogenin-deficient knock-out mice which terminate muscle formation due to insufficient myoblast fusion [182]. Both transcription factors are upregulated during the process of skeletal muscle formation and can function as markers of

differentiation. Mature myotubes can be identified by CD 56, alpha-sarcomeric actin, myogenin, MRF 4, MyoD or Myf 5 stainings (Table 1.4) [183].

Table 1.4. Markers of skeletal muscle differentiation. Adapted of [184].

	Expression Markers
Muscle derived cell	CD 34
Satellite cell	CD34, CD 56, Myf 5, desmin
Myotube	CD 56, alpha-sarcomeric actin, myosin heavy chains, Myogenin, MRF 4, desmin

Several intracellular pathways are responsible for enhancing proliferation and differentiation expression of cell genes during muscle development.

1.4.1 Mechanical and electrical signals for engineered skeletal muscle

Skeletal muscles are continuously under mechanical tension *in vivo*, either as an antagonist or an agonist during eccentric contractions as well as the nerve-induced electrical activation of skeletal muscle that is indispensable for normal tissue development and contractile function [185, 186]. These microenvironments present in the human body demonstrate that this tissue reacts to electro-mechanical stimuli. So, it is important to study the effects in cell cultures combining chemical and physical stimulations [187].

Electrical stimulation is of particular interest because of the indisputable role of the electrical cues issued by the central nervous system during the development of skeletal muscles *in vivo* [188]. The parameters of the applied electric field can be modulated, according to the desired type of response. It has been shown that depending on whether the regimen applied is direct or alternative, and depending on the voltage/intensity range, it accelerates sarcomere assembly, promoting cell proliferation, differentiation, and/or muscle cell alignment [186, 189-196]. Some studies pointed out that electrical stimulation makes intracellular calcium release possible [197]. Others showed that it acts via the activation of PI3K, p38 signaling pathways [198].

In parallel, mechanical stresses also play a role in muscle cell growth, differentiation, and function because of the contractile and elastic nature of skeletal muscle [199]. When cells grow on a scaffold, a variety of stretch regimes can be applied. Thus, by modulating the cycle, stretching elongation and duration, muscle cell changes and functionality can be modulated [200-207]. It seems that cell stretching

induces the activation of FAK via integrin, leading to an increase in gene expression [208]. Other studies suggest that stretching may also influence the passage of calcium via the ion channels [209, 210] and activate PI3K and p38 signaling pathways [211, 212].

More importantly, there is growing evidence that a combination of chemical and physical stimulations in addition to surface topography and scaffold composition may be a solution for generating safe and functional muscle constructs *in* vitro [177, 178].

Biomaterials based on conducting polymers are especially useful for engineering electrical-sensitive tissues such as skeletal muscles, cardiac muscles, nerves, skin and bones [213]. Relatively to the skeletal muscle, the literature demonstrates more studies with the aligned conductive nanofibres since the aligned structure of the scaffolds can mimic the anisotropic structure of elongated myofibres in skeletal muscle [213-218].

However, although conducting polymers were shown to be biocompatible *in vitro*, systematic and long-term studies of their *in vivo* biocompatibility and biodegradability are still needed. In this sense, the piezoelectric polymers can introduce the biocompatibility as well the mechanical and electric stimulus that skeletal muscle tissue need. These polymers already demonstrated huge potential for bone tissue on static and dynamic conditions, and previous studies already demonstrated that these polymers have influence on C2C12 myoblast proliferation in static conditions using PVDF polymer through the surface charge. Previous studies have demonstrated that negatively charged surface of PVDF improve cell adhesion and proliferation and that the directional growth of the myoblast cells can be achieved through the use of aligned fibres. It was observed that fibre orientation influences cell behaviour in the scaffold, C2C12 myoblast cells alignment along the direction of the fibres within the matrix [40].

1.5 Objectives

The main objective of this work was the development of multifunctional piezoelectric nanocomposite scaffolds with selected architectures and fillers for biomedical applications, in particular for skeletal muscle TE applications, being those cells subjected to electromechanical stimuli during their normal functioning in order to evaluate their biological response.

In summary, the main specific objectives of this work were:

- The production and characterization of silica nanoparticles with tailor made characteristics (fluorescent, charged groups and different diameters).
- The production of scaffolds, films and other microstructures such as electrospinning, with controlled morphology and surface properties of different electroactive polymer composites.

- Evaluation of the influence of the scaffold parameters (morphology, surface wettability, roughness, electroactivity) on growth, proliferation and differentiation of muscle cells.
- The study the selected scaffolds for myoblast culture under static and dynamical conditions by electrical and mechanical stimulation.

1.6 Structure of the work and methodology

The present thesis is divided in seven chapters, six of them based on published or submitted scientific manuscripts. The sequence of these chapters intended to provide a comprehensive and logical account of the progress achieved during the present research as well as the research methodology used. The work was based preferentially on piezoelectric polymer PVDF, due to its biocompatibility, highest piezoelectric constant and the different morphologies that can be easily obtained. A summary of the work covered in each chapter is briefly described below.

Chapter 1 presents the motivation of the thesis giving a general introduction to the work. The main objectives and the structure of the thesis are also presented. It is of notice that the specific state of the art on the different issues related to the present work is provided in each of different chapters.

After, to better understand the importance of physical stimuli for the cells and the potential of piezoelectric polymers to give these stimuli, **Chapter 2** is based on the two published works where SiNPs were incorporated in PVDF matrix in order to improve the piezoelectric phase by nucleation of the β-phase of PVDF. Additionally, these nanoparticles may be used for drug delivery of proliferation/differentiation factors. So, this chapter is dedicated to the production of PVDF nanocomposites with different morphologies, such as porous and non-porous films, and fibres with SiNPs with different content, diameter and functionalization. Structural, morphological, optical, thermal and mechanical properties of the nanocomposites were evaluated. The wettability of the samples was also reported. Cytotoxicity and cell proliferation studies were also performed.

Therefore, the functionalization of SiNPs can nucleate the electroactive phase of PVDF, however it is also important to study the introduction of other active nanoparticles that can give stimulation to the cells. Another important parameter is the morphology of the biomaterial and since the microenvironment of muscle in the human body is fibrillar, piezoelectric fibres were produced in order to mimic this morphology. For this, **Chapter 3** reports on the production of PVDF aligned and randomly oriented fibres by electrospinning with and without magnetic nanoparticles and the influence of fibre orientation on their

mechanical properties by strain-stress assays. The angle between the stretch direction and the fibre direction was varied as well as the stretching level up to 100%. The influence of these parameters on the morphology, fibre average diameter and orientation, wettability, electroactive phase content and degree of crystallinity was studied. The young modulus and respective yield point were also evaluated and related with the others. The potential application of the CFO/PVDF fibres was also evaluated through cytotoxicity studies.

Before studying the effect of physical stimuli on muscle differentiation with the different nanocomposites and bioreactors (dynamic conditions), it is important understand the influence of PVDF surface properties, in terms of the poling state, positive or negative net surface charge. In this way, **Chapter 4** evaluates the influence of this parameter and also of the morphology, films and fibres, on myoblast differentiation under static conditions by immunofluorescence staining. The quantitative analysis by myotube fusion, maturation index, length, diameter and number of myotubes was presented and discussed.

The cell material interactions also play a key role in the development of scaffold-based TE. As it was verified that the surface charge of biomaterial improves the cell differentiation, and knowing that cell adhesion will influence cell behaviour, namely cell proliferation and differentiation, **Chapter 5** focuses on the influence of the PVDF surface charge on cell adhesion. The cytoskeletal organization of C2C12 myoblast cells on PVDF with and without proteins was studied by immunofluorescence staining characterizing cell length and diameter. The interactions between single live cells and PVDF were analyzed using an Atomic Force Microscopy (AFM) technique termed Single Cell Force Spectroscopy (SCFS) and related with cytoskeletal variations.

After verification that the surface charge of piezoelectric polymer can enhance myoblast differentiation, it is important to study the effect of mechanic-electrical stimuli the cell differentiation. For that, CFO/P(VDF-TrFE) films were produced. Therefore, **Chapter 6** is dedicated to study the influence of the polarization of electroactive CFO/P(VDF-TrFE) films on the biological response of myoblast cells cultivated under static and dynamic conditions. Myoblast differentiation was analyzed by immunofluorescence staining and creatine kinase functional assay. The quantitative analysis of myotube fusion, maturation index, length, diameter and number of myotubes was presented and discussed. The mechano-electrical stimuli given to the cells through the use of these films was also quantified.

Finally, **Chapter 7** compiles the main conclusions of the work presented in this thesis and proposes some suggestions for future work research directions.

1.7 References

1. Lanza, R., Langer, R. and Vacanti, J.P., *Principles of Tissue Engineering: Fourth Edition*. Principles of Tissue Engineering: Fourth Edition. 2013. p. 1-1887.
2. Shafiee, A. and Atala, A., *Tissue Engineering: Toward a New Era of Medicine*. Annual Review of Medicine, 2017. **68**: p. 29-40.
3. Chapekar, M.S., *Tissue engineering: Challenges and opportunities.* Journal of Biomedical Materials Research, 2000. **53**(6): p. 617-620.
4. Langer, R. and Vacanti, J.P., *Tissue engineering.* Science, 1993. **260**(5110): p. 920-926.
5. Meyer, U., et al., *Fundamentals of tissue engineering and regenerative medicine*. Springer, 2009. p. 1-1049.
6. Griffith, L.G. and Naughton, G., *Tissue engineering - Current challenges and expanding opportunities.* Science, 2002. **295**(5557): p. 1009-1014.
7. O'Brien, F.J., *Biomaterials & scaffolds for tissue engineering.* Materials Today, 2011. **14**(3): p. 88-95.
8. Burridge, K. and Guilluy, C., *Focal adhesions, stress fibers and mechanical tension.* Experimental Cell Research, 2016. **343**(1): p. 14-20.
9. Ning, C.Y., et al., *Electroactive polymers for tissue regeneration: Developments and perspectives.* Progress in Polymer Science, 2018. **81**: p. 144-162.
10. Telega, J.J. and Wojnar, R., *Piezoelectric effects in biological tissues.* Journal of Theoretical and Applied Mechanics, 2002. **3**(40): p. 723-759.
11. Ghasemi-Mobarakeh, L., et al., *Application of conductive polymers, scaffolds and electrical stimulation for nerve tissue engineering.* Journal of Tissue Engineering and Regenerative Medicine, 2011. **5**(4): p. e17-e35.
12. Ribeiro, C., et al., *Piezoelectric polymers as biomaterials for tissue engineering applications.* Colloids and Surfaces B: Biointerfaces, 2015. **136**: p. 46-55.
13. Sulik, G.L., et al., *Effects of steady electric fields on human retinal pigment epithelial cell orientation and migration in culture.* Acta Ophthalmologica, 1992. **70**(1): p. 115-122.
14. Zhao, M., et al., *Orientation and directed migration of cultured corneal epithelial cells in small electric fields are serum dependent.* Journal of Cell Science, 1996. **109**(6): p. 1405-1414.
15. Pu, J., et al., *EGF receptor signalling is essential for electric-field-directed migration of breast cancer cells.* Journal of Cell Science, 2007. **120**(19): p. 3395-3403.
16. Wang, E., et al., *Bi-directional migration of lens epithelial cells in a physiological electrical field.* Experimental Eye Research, 2003. **76**(1): p. 29-37.
17. Bouaziz, A., Richert, A., and Caprani, A., *Vascular endothelial cell responses to different electrically charged poly(vinylidene fluoride) supports under static and oscillating flow conditions.* Biomaterials, 1997. **18**(2): p. 107-112.

18. Valentini, R.F., et al., *Electrically charged polymeric substrates enhance nerve fibre outgrowth In vitro.* Biomaterials, 1992. **13**(3): p. 183-190.
19. Chao, P.-H.G., et al., *Effects of Applied DC Electric Field on Ligament Fibroblast Migration and Wound Healing.* Connective Tissue Research, 2007. **48**(4): p. 188-197.
20. Hoon, J.L., Tan, M.H., and Koh, C.G., *The regulation of cellular responses to mechanical cues by rho gtpases.* Cells, 2016. **5**(2): p. 17.
21. Brás-Pereira, C. and Moreno, E., *Mechanical cell competition.* Current Opinion in Cell Biology, 2018. **51**: p. 15-21.
22. Kirby, T.J. and Lammerding, J., *Emerging views of the nucleus as a cellular mechanosensor.* Nature Cell Biology, 2018. **20**(4): p. 373-381.
23. Weaver, V.M., *Cell and tissue mechanics: The new cell biology frontier.* Molecular Biology of the Cell, 2017. **28**(14): p. 1815-1818.
24. Bukoreshtliev, N.V., Haase, K., and Pelling, A.E., *Mechanical cues in cellular signalling and communication.* Cell and Tissue Research, 2013. **352**(1): p. 77-94.
25. Barnes, J.M., Przybyla, L., and Weaver, V.M., *Tissue mechanics regulate brain development, homeostasis and disease.* Journal of Cell Science, 2017. **130**(1): p. 71-82.
26. McCain, M.L. and Parker, K.K., *Mechanotransduction: The role of mechanical stress, myocyte shape, and cytoskeletal architecture on cardiac function.* Pflugers Archiv European Journal of Physiology, 2011. **462**(1): p. 89-104.
27. Trumbull, A., Subramanian, G., and Yildirim-Ayan, E., *Mechanoresponsive musculoskeletal tissue differentiation of adipose-derived stem cells.* BioMedical Engineering Online, 2016. **15**(1): p. 43.
28. Levin, M., *Bioelectric mechanisms in regeneration: Unique aspects and future perspectives.* Seminars in Cell and Developmental Biology, 2009. **20**(5): p. 543-556.
29. Yuan, X., et al., *Electrical stimulation enhances cell migration and integrative repair in the meniscus.* Scientific Reports, 2015. **4**: p. 3674.
30. H. Cartmell, S. and Dobson, J., *The Use of Magnetic Particles in Tissue Engineering*, in *Nanotechnologies for the Life Sciences*. Challa, S. et al., Editors, Wiley-VCH, 2011. p. 293-308.
31. Bidan, C.M., et al., *Magneto-active substrates for local mechanical stimulation of living cells.* Scientific Reports, 2018. **8**(1): p. 1464.
32. Baker, B., Becker, R.O., and Spadaro, J., *A Study of Electrochemical Enhancement of Articular Cartilage Repair.* Clinical Orthopaedics and Related Research, 1974. **102**: p. 251-267.
33. Ravichandran, R., et al., *Advances in Polymeric Systems for Tissue Engineering and Biomedical Applications.* Macromolecular Bioscience, 2012. **12**(3): p. 286-311.
34. Bogue, R., *Smart materials: a review of capabilities and applications.* Assembly Automation, 2014. **34**(1): p. 16-22.
35. Xia, F. and Jiang, L., *Bio-inspired, smart, multiscale interfacial materials.* Advanced Materials, 2008. **20**(15): p. 2842-2858.
36. Ferreira, A.D.B.L., Nóvoa, P.R.O. and Marques, A.T., *Multifunctional Material Systems: A state-of-the-art review.* Composite Structures, 2016. **151**: p. 3-35.
37. Cardoso, V.F., Ribeiro, C. and Lanceros-Mendez, S., *Metamorphic biomaterials*, in *Bioinspired Materials for Medical Applications*, Rodrigues, L. and Mota, M., Editor, Elsevier-Woodhead Publishing, 2016. p. 69-99.

38. Ribeiro, C., et al., *Enhanced proliferation of pre-osteoblastic cells by dynamic piezoelectric stimulation.* Rsc Advances, 2012. **2**(30): p. 11504-11509.
39. Seil, J.T. and Webster, T.J., *Electrically active nanomaterials as improved neural tissue regeneration scaffolds.* Wiley Interdisciplinary Reviews-Nanomedicine and Nanobiotechnology, 2010. **2**(6): p. 635-647.
40. Martins, P.M., et al., *Effect of poling state and morphology of piezoelectric poly(vinylidene fluoride) membranes for skeletal muscle tissue engineering.* RSC Advances, 2013. **3**(39): p. 17938-17944.
41. Paul, D.R. and Robeson, L.M., *Polymer nanotechnology: Nanocomposites.* Polymer, 2008. **49**(15): p. 3187-3204.
42. Pandey, N., Shukla, S.K. and Singh, N.B., *Water purification by polymer nanocomposites: an overview.* Nanocomposites, 2017. **3**(2): p. 47-66.
43. Narayanan, K.B. and Han, S.S., *Dual-crosslinked poly(vinyl alcohol)/sodium alginate/silver nanocomposite beads – A promising antimicrobial material.* Food Chemistry, 2017. **234**: p. 103-110.
44. Muller, K., et al., *Review on the Processing and Properties of Polymer Nanocomposites and Nanocoatings and Their Applications in the Packaging, Automotive and Solar Energy Fields.* Nanomaterials, 2017. **7**(4): p. 74.
45. Raji, M., et al., *Effect of silane functionalization on properties of polypropylene/clay nanocomposites.* Composites Part B: Engineering, 2018. **146**: p. 106-115.
46. Ribeiro, C., et al., *Piezoelectric polymers as biomaterials for tissue engineering applications*, Colloids and Surfaces B: Biointerfaces, 2015. **136**: p. 46-55.
47. Cardoso, V., et al., *Fluorinated Polymers as Smart Materials for Advanced Biomedical Applications.* Polymers, 2018. **10**(2): p. 161.
48. Nunes-Pereira, J., et al., *Nanodiamonds/poly(vinylidene fluoride) composites for tissue engineering applications.* Composites Part B: Engineering, 2017. **111**: p. 37-44.
49. Martins, P., et al., *Optimizing piezoelectric and magnetoelectric responses on $CoFe_2O_4$ /P(VDF-TrFE) nanocomposites.* Journal of Physics D: Applied Physics, 2011. **44**(49): p. 495303.
50. Sharma, V.K., R.A. Yngard, and Y. Lin, *Silver nanoparticles: Green synthesis and their antimicrobial activities.* Advances in Colloid and Interface Science, 2009. **145**(1-2): p. 83-96.
51. Lopes, A.C., et al., *Enhancement of the dielectric constant and thermal properties of α-Poly(vinylidene fluoride)/zeolite nanocomposites.* Journal of Physical Chemistry C, 2010. **114**(34): p. 14446-14452.
52. Mendes, S.F., et al., *Effect of filler size and concentration on the structure and properties of poly(vinylidene fluoride)/$BaTiO_3$ nanocomposites.* Journal of Materials Science, 2012. **47**(3): p. 1378-1388.
53. Simoes, R., et al., *Low percolation transitions in carbon nanotube networks dispersed in a polymer matrix: Dielectric properties, simulations and experiments.* Nanotechnology, 2009. **20**(3): p. 035703.
54. Tripathi, G., Choudhury, P. and Basu, B., *Development of polymer based biocomposites: A review.* Materials Technology, 2010. **25**(3-4): p. 158-176.

55. Ramakrishna, S., et al., *Biomedical applications of polymer-composite materials: A review.* Composites Science and Technology, 2001. **61**(9): p. 1189-1224.
56. Ribeiro, C., et al., *Proving the suitability of magnetoelectric stimuli for tissue engineering applications.* Colloids and Surfaces B-Biointerfaces, 2016. **140**: p. 430-436.
57. Allègre, C.J., et al., *The chemical composition of the Earth.* Earth and Planetary Science Letters, 1995. **134**(3-4): p. 515-526.
58. Uboldi, C., et al., *Amorphous silica nanoparticles do not induce cytotoxicity, cell transformation or genotoxicity in Balb/3T3 mouse fibroblasts.* Mutation Research - Genetic Toxicology and Environmental Mutagenesis, 2012. **745**(1-2): p. 11-20.
59. Chen, Y., Chen, H. and Shi, J., *In vivo bio-safety evaluations and diagnostic/therapeutic applications of chemically designed mesoporous silica nanoparticles.* Advanced Materials, 2013. **25**(23): p. 3144-3176.
60. Bao, G., Mitragotri, S. and Tong, S., *Multifunctional nanoparticles for drug delivery and molecular imaging*. Annual Review of Biomedical Engineering, 2013. **15**: p. 253-282.
61. Ribeiro, T., Baleizão, C. and Farinha, J.P.S., *Synthesis and characterization of perylenediimide labeled core-shell hybrid silica-polymer nanoparticles.* Journal of Physical Chemistry C, 2009. **113**(42): p. 18082-18090.
62. Ribeiro, T., et al., *NIR and visible perylenediimide-silica nanoparticles for laser scanning bioimaging.* Dyes and Pigments, 2014. **110**: p. 227-234.
63. Ribeiro, T., et al., *Formation of hybrid films from perylenediimide-labeled core-shell silica-polymer nanoparticles.* Journal of Colloid and Interface Science, 2013. **401**: p. 14-22.
64. Ribeiro, T., et al., *High performance NIR fluorescent silica nanoparticles for bioimaging.* RSC Advances, 2013. **3**(24): p. 9171-9174.
65. Argyo, C., et al., *Multifunctional mesoporous silica nanoparticles as a universal platform for drug delivery.* Chemistry of Materials, 2014. **26**(1): p. 435-451.
66. Kim, J., Piao, Y. and Hyeon, T., *Multifunctional nanostructured materials for multimodal imaging, and simultaneous imaging and therapy.* Chemical Society Reviews, 2009. **38**(2): p. 372-390.
67. Santiago, A.M., et al., *Multifunctional Hybrid Silica Nanoparticles with a Fluorescent Core and Active Targeting Shell for Fluorescence Imaging Biodiagnostic Applications.* European Journal of Inorganic Chemistry, 2015. **2015**(27): p. 4579-4587.
68. Schiraldi, C., et al., *Development of hybrid materials based on hydroxyethylmethacrylate as supports for improving cell adhesion and proliferation.* Biomaterials, 2004. **25**(17): p. 3645-3653.
69. Gaharwar, A.K., et al., *Photocrosslinked nanocomposite hydrogels from PEG and silica nanospheres: Structural, mechanical and cell adhesion characteristics.* Materials Science and Engineering C, 2013. **33**(3): p. 1800-1807.
70. Chrissafis, K., et al., *Thermal and dynamic mechanical behavior of bionanocomposites: Fumed silica nanoparticles dispersed in poly(vinyl pyrrolidone), chitosan, and poly(vinyl alcohol).* Journal of Applied Polymer Science, 2008. **110**(3): p. 1739-1749.
71. Griffin, M., et al., *Development of mechano-responsive polymeric scaffolds using functionalized silica nano-fillers for the control of cellular functions.* Nanomedicine: Nanotechnology, Biology, and Medicine, 2016. **12**(6): p. 1725-1733.

72. Song, B., Wu, C. and Chang, J., *Dual drug release from electrospun poly(lactic-co-glycolic acid)/mesoporous silica nanoparticles composite mats with distinct release profiles.* Acta Biomaterialia, 2012. **8**(5): p. 1901-1907.
73. Qiu, K., et al., *Doxorubicin-loaded electrospun poly(l-lactic acid)/mesoporous silica nanoparticles composite nanofibers for potential postsurgical cancer treatment.* Journal of Materials Chemistry B, 2013. **1**(36): p. 4601-4611.
74. Chen, L., Zhou, X. and He, C., *Mesoporous silica nanoparticles for tissue-engineering applications.* Wiley Interdisciplinary Reviews: Nanomedicine and Nanobiotechnology, 2019. **11**(6): p. e1573.
75. Howard, M.A., et al., *Magnetic neurosurgery.* Stereotact Funct Neurosurg, 1996. **66**(1-3): p. 102-107.
76. Ergeneman, O., et al., *Wireless Intraocular Microrobots: Opportunities and Challenges*, in *Surgical Robotics: Systems Applications and Visions*, Rosen, J., Hannaford, B. and Satava, R.M., Editors. Springer US: Boston, 2011. p. 271-311.
77. Qu, X.Z., et al., *Post-operative hemimaxillectomy rehabilitation using prostheses supported by zygoma implants and remaining natural teeth.* Clinics, 2016. **71**: p. 575-579.
78. Da Costa, A., et al., *Robotic magnetic navigation for ablation of human arrhythmias.* Medical Devices, 2016. **9**: p. 331-339.
79. Faraji, M., Yamini, Y. and Rezaee, M., *Magnetic nanoparticles: Synthesis, stabilization, functionalization, characterization, and applications.* Journal of the Iranian Chemical Society, 2010. **7**(1): p. 1-37.
80. Medeiros, S.F., et al., *Stimuli-responsive magnetic particles for biomedical applications.* International Journal of Pharmaceutics, 2011. **403**(1): p. 139-161.
81. Gil, S. and Mano, J.F., *Magnetic composite biomaterials for tissue engineering.* Biomaterials Science, 2014. **2**(6): p. 812-818.
82. Teresa, J.M.D., et al., *From magnetoelectronic to biomedical applications based on the nanoscale properties of advanced magnetic materials.* International Journal of Nanotechnology, 2005. **2**(1-2): p. 3-22.
83. Kudr, J., et al., *Magnetic Nanoparticles: From Design and Synthesis to Real World Applications.* Nanomaterials, 2017. **7**(9): p. 243.
84. Cardoso, V.F., et al., *Advances in Magnetic Nanoparticles for Biomedical Applications.* Advanced Healthcare Materials, 2018. **7**(5): p. 1700845.
85. Ito, A. and Honda, H., *Magnetic Nanoparticles for Tissue Engineering*, in *Nanotechnologies for the Life Sciences*. 2007.
86. McBain, S.C., Yiu, H.H.P. and Dobson, J., *Magnetic nanoparticles for gene and drug delivery.* International Journal of Nanomedicine, 2008. **3**(2): p. 169-180.
87. Dobson, J., *Gene therapy progress and prospects: magnetic nanoparticle-based gene delivery.* Gene Therapy, 2006. **13**(4): p. 283-287.
88. Weissleder, R., et al., *Ultrasmall superparamagnetic iron oxide: characterization of a new class of contrast agents for MR imaging.* Radiology, 1990. **175**(2): p. 489-493.

89. Neuberger, T., et al., *Superparamagnetic nanoparticles for biomedical applications: Possibilities and limitations of a new drug delivery system.* Journal of Magnetism and Magnetic Materials, 2005. **293**(1): p. 483-496.
90. Wang, N., Butler, J.P. and Ingber, D.E., *Mechanotransduction across the cell surface and through the cytoskeleton.* Science, 1993. **260**(5111): p. 1124-1127.
91. Bausch, A.R., et al., *Local measurements of viscoelastic parameters of adherent cell surfaces by magnetic bead microrheometry.* Biophysical Journal, 1998. **75**(4): p. 2038-2049.
92. Bausch, A.R., Möller, W. and Sackmann, E., *Measurement of Local Viscoelasticity and Forces in Living Cells by Magnetic Tweezers.* Biophysical Journal, 1999. **76**(1): p. 573-579.
93. D'Addario, M., et al., *Regulation of Tension-induced Mechanotranscriptional Signals by the Microtubule Network in Fibroblasts.* Journal of Biological Chemistry, 2003. **278**(52): p. 53090-53097.
94. Glogauer, M., Ferrier, J. and McCulloch, C.A., *Magnetic fields applied to collagen-coated ferric oxide beads induce stretch-activated Ca^{2+} flux in fibroblasts.* American Journal of Physiology-Cell Physiology, 1995. **269**(5): p. C1093-C1104.
95. Glogauer, M., et al., *Calcium ions and tyrosine phosphorylation interact coordinately with actin to regulate cytoprotective responses to stretching.* Journal of Cell Science, 1997. **110**(1): p. 11-21.
96. Glogauer, M. and Ferrier, J., *A new method for application of force to cells via ferric oxide beads.* Pflügers Archiv European Journal of Physiology, 1998. **435**(2): p. 320-327.
97. Pommerenke, H., et al., *The Mode of Mechanical Integrin Stressing Controls Intracellular Signaling in Osteoblasts.* Journal of Bone and Mineral Research, 2002. **17**(4): p. 603-611.
98. Dobson, J., *Remote control of cellular behaviour with magnetic nanoparticles.* Nature Nanotechnology, 2008. **3**(3): p. 139-143.
99. Guduru, R. and Khizroev, S., *Magnetic Field-Controlled Release of Paclitaxel Drug from Functionalized Magnetoelectric Nanoparticles.* Particle & Particle Systems Characterization, 2014. **31**(5): p. 605-611.
100. Ribeiro, C., et al., *Proving the suitability of magnetoelectric stimuli for tissue engineering applications.* Colloids and Surfaces B: Biointerfaces, 2016. **140**: p. 430-436.
101. Chan, B.P. and Leong, K.W., *Scaffolding in tissue engineering: General approaches and tissue-specific considerations.* European Spine Journal, 2008. **17**(SUPPL. 4): p. S467-S479.
102. Dhandayuthapani, B., et al., *Polymeric Scaffolds in Tissue Engineering Application: A Review.* International Journal of Polymer Science, 2011. **2011**: p. 290602.
103. O'Brien, F.J., *Biomaterials & scaffolds for tissue engineering.* Materials Today, 2011. **14**(3): p. 88-95.
104. Frias, C., et al., *Polymeric piezoelectric actuator substrate for osteoblast mechanical stimulation.* Journal of Biomechanics, 2010. **43**(6): p. 1061-1066.
105. Reis, J., et al., *A New Piezoelectric Actuator Induces Bone Formation In Vivo: A Preliminary Study.* Journal of Biomedicine and Biotechnology, 2012. **2012:** p. 613403.
106. Rodrigues, M.T., et al., *beta-PVDF Membranes Induce Cellular Proliferation and Differentiation in Static and Dynamic Conditions*. Materials Science Forum, 2008. **587-588**: p. 72-76.

107. Parssinen, J., et al., *Enhancement of adhesion and promotion of osteogenic differentiation of human adipose stem cells by poled electroactive poly(vinylidene fluoride).* Journal of Biomedical Materials Research Part A, 2015. **103**(3): p. 919-928.
108. Ribeiro, C., et al., *Dynamic piezoelectric stimulation enhances osteogenic differentiation of human adipose stem cells.* Journal of Biomedical Materials Research Part A, 2015. **103**(6): p. 2172-2175.
109. Ikada, Y., et al., *Enhancement of bone formation by drawn poly(L-lactide).* Journal of Biomedical Materials Research, 1996. **30**(4): p. 553-558.
110. Wang, Y.-W., et al., *Evaluation of three-dimensional scaffolds made of blends of hydroxyapatite and poly(3-hydroxybutyrate-co-3-hydroxyhexanoate) for bone reconstruction.* Biomaterials, 2005. **26**(8): p. 899-904.
111. Damaraju, S.M., et al., *Structural changes in PVDF fibers due to electrospinning and its effect on biological function.* Biomedical Materials, 2013. **8**(4): p. 045007.
112. Prabhakaran, M.P., Venugopal, J. and Ramakrishna, S., *Electrospun nanostructured scaffolds for bone tissue engineering.* Acta Biomaterialia, 2009. **5**(8): p. 2884-2893.
113. Paşcu, E.I., Stokes, J. and McGuinness, G.B., *Electrospun composites of PHBV, silk fibroin and nano-hydroxyapatite for bone tissue engineering.* Materials Science and Engineering: C, 2013. **33**(8): p. 4905-4916.
114. Ko, E.K., et al., *In Vitro Osteogenic Differentiation of Human Mesenchymal Stem Cells and In Vivo Bone Formation in Composite Nanofiber Meshes.* Tissue Engineering Part A, 2008. **14**(12): p. 2105-2119.
115. Marques, L., et al., *Subcutaneous tissue reaction and cytotoxicity of polyvinylidene fluoride and polyvinylidene fluoride-trifluoroethylene blends associated with natural polymers.* Journal of Biomedical Materials Research Part B-Applied Biomaterials, 2013. **101**(7): p. 1284-1293.
116. Mota, C., et al., *Additive manufacturing of poly[(R)-3-hydroxybutyrate-co-(R)-3-hydroxyhexanoate] scaffolds for engineered bone development.* Journal of Tissue Engineering and Regenerative Medicine, 2014. **11**(1): p. 175-186.
117. Gimenes, R., et al., *Composites PVDF-TrFE/BT used as bioactive membranes for enhancing bone regeneration*, in *Smart Structures and Materials 2004: Electroactive Polymer Actuators and Devices*, BarCohen, Y., Editor. 2004. p. 539-547.
118. Chen, Y., et al., *PLLA scaffolds with biomimetic apatite coating and biomimetic apatite/collagen composite coating to enhance osteoblast-like cells attachment and activity.* Surface & Coatings Technology, 2006. **201**(3-4): p. 575-580.
119. Inui, A., et al., *Potency of double-layered Poly L-lactic Acid scaffold in tissue engineering of tendon tissue.* International Orthopaedics, 2010. **34**(8): p. 1327-1332.
120. McKeon-Fischer, K.D. and Freeman, J.W., *Characterization of electrospun poly(L-lactide) and gold nanoparticle composite scaffolds for skeletal muscle tissue engineering.* Journal of Tissue Engineering and Regenerative Medicine, 2011. **5**(7): p. 560-568.
121. Jansen, P.L., et al., *Surgical mesh as a scaffold for tissue regeneration in the esophagus.* European Surgical Research, 2004. **36**(2): p. 104-111.

122. Valentini, R.F., et al., *Patterned neuronal attachment and outgrowth on surface modified, electrically charged fluoropolymer substrates.* Journal of Biomaterials Science, Polymer Edition, 1994. **5**(1-2): p. 13-36.
123. Royo-Gascon, N., et al., *Piezoelectric substrates promote neurite growth in rat spinal cord neurons.* Annals of Biomedical Engineering, 2013. **41**(1): p. 112-122.
124. Lee, Y.S. and Arinzeh, T.L., *The influence of piezoelectric scaffolds on neural differentiation of human neural stem/progenitor cells.* Tissue Engineering - Part A, 2012. **18**(19-20): p. 2063-2072.
125. Lee, Y.-S., Collins, G. and Arinzeh, T.L., *Neurite extension of primary neurons on electrospun piezoelectric scaffolds.* Acta Biomaterialia, 2011. **7**(11): p. 3877-3886.
126. De Guzman, R.C., Loeb, J.A. and VandeVord, P.J., *Electrospinning of Matrigel to Deposit a Basal Lamina-Like Nanofiber Surface.* Journal of Biomaterials Science, Polymer Edition, 2010. **21**(8-9): p. 1081-1101.
127. Young, T.H., et al., *Surface modification of microporous PVDF membranes for neuron culture.* Journal of Membrane Science, 2010. **350**(1-2): p. 32-41.
128. Aebischer, P., et al., *Piezoelectric guidance channels enhance regeneration in the mouse sciatic nerve after axotomy.* Brain Research, 1987. **436**(1): p. 165-168.
129. Delaviz, H., et al., *Repair of peripheral nerve defects using a polyvinylidene fluoride channel containing nerve growth factor and collagen gel in adult rats.* Cell Journal, 2011. **13**(3): p. 137-142.
130. Fine, E.G., et al., *Improved nerve regeneration through piezoelectric vinylidenefluoride-trifluoroethylene copolymer guidance channels.* Biomaterials, 1991. **12**(8): p. 775-780.
131. Evans, G.R.D., et al., *Clinical long-term in vivo evaluation of poly(L-lactic acid) porous conduits for peripheral nerve regeneration.* Journal of Biomaterials Science, Polymer Edition, 2000. **11**(8): p. 869-878.
132. O'Shaughnessy, T.J., Lin, H.J. and Ma, W., *Functional synapse formation among rat cortical neurons grown on three-dimensional collagen gels.* Neuroscience Letters, 2003. **340**(3): p. 169-172.
133. Bhardwaj, N. and Kundu, S.C., *Electrospinning: A fascinating fiber fabrication technique.* Biotechnology Advances, 2010. **28**(3): p. 325-347.
134. Ramakrishna, S., et al., *An introduction to electrospinning and nanofibers*. Lim, T.C. et al., Editors. World Scientific, 2005. p. 1-382.
135. Ribeiro, C., et al., *Electroactive poly(vinylidene fluoride)-based structures for advanced applications.* Nature Protocols, 2018. **13**(4): p. 681-704.
136. Pham, Q.P., Sharma, U. and Mikos, A.G., *Electrospinning of polymeric nanofibers for tissue engineering applications: A review.* Tissue Engineering, 2006. **12**(5): p. 1197-1211.
137. Cui, W.G., Zhou, Y. and Chang, J., *Electrospun nanofibrous materials for tissue engineering and drug delivery.* Science and Technology of Advanced Materials, 2010. **11**(1): p. 014108.
138. Venugopal, J., et al., *Mineralization of osteoblasts with electrospun collagen/hydroxyapatite nanofibers.* Journal of Materials Science: Materials in Medicine, 2008. **19**(5): p. 2039-2046.

139. Singh, B.N., et al., *Carboxymethyl cellulose enables silk fibroin nanofibrous scaffold with enhanced biomimetic potential for bone tissue engineering application.* Carbohydrate Polymers, 2016. **151**: p. 335-347.
140. Pangon, A., et al., *Hydroxyapatite-hybridized chitosan/chitin whisker bionanocomposite fibers for bone tissue engineering applications.* Carbohydrate Polymers, 2016. **144**: p. 419-427.
141. Zhao, X., et al., *Calcium phosphate coated Keratin–PCL scaffolds for potential bone tissue regeneration.* Materials Science and Engineering: C, 2015. **49**: p. 746-753.
142. Sadat-Shojai, M., *Electrospun Polyhydroxybutyrate/Hydroxyapatite Nanohybrids: Microstructure and Bone Cell Response.* Journal of Materials Science & Technology, 2016. **32**(10): p. 1013-1020.
143. Fernandes, J.S., et al., *Reinforcement of poly-l-lactic acid electrospun membranes with strontium borosilicate bioactive glasses for bone tissue engineering.* Acta Biomaterialia, 2016. **44**: p. 168-177.
144. Venugopal, J., et al., *In vitro study of smooth muscle cells on polycaprolactone and collagen nanofibrous matrices.* Cell Biology International, 2005. **29**(10): p. 861-867.
145. Kose, S., et al., *Evaluation of biocompatibility of random or aligned electrospun polyhydroxybutyrate scaffolds combined with human mesenchymal stem cells.* Turkish Journal of Biology, 2016. **40**(2): p. 410-419.
146. Yu, Y., et al., *The Interactions Between Aligned Poly(L-Lactic Acid) Nanofibers and SH-SY5Y Cells In Vitro.* Journal of Nanoscience and Nanotechnology, 2016. **16**(6): p. 6407-6413.
147. Sadeghi, D., et al., *Electrospun poly(hydroxybutyrate)/chitosan blend fibrous scaffolds for cartilage tissue engineering.* Journal of Applied Polymer Science, 2016. **133**(47): p. 44171.
148. Mohiti-Asli, M., et al., *Ibuprofen loaded PLA nanofibrous scaffolds increase proliferation of human skin cells in vitro and promote healing of full thickness incision wounds in vivo.* Journal of Biomedical Materials Research Part B: Applied Biomaterials, 2015. **105**(2): p. 327-339.
149. Jha, B.S., et al., *Electrospun Collagen: A Tissue Engineering Scaffold with Unique Functional Properties in a Wide Variety of Applications.* Journal of Nanomaterials, 2011. **2011**: p. 348268.
150. Wang, J., et al., *Evaluation of the potential of rhTGF- β3 encapsulated P(LLA-CL)/collagen nanofibers for tracheal cartilage regeneration using mesenchymal stems cells derived from Wharton's jelly of human umbilical cord.* Materials Science and Engineering: C, 2017. **70**: p. 637-645.
151. Borriello, A., et al., *Optimizing PANI doped electroactive substrates as patches for the regeneration of cardiac muscle.* Journal of Materials Science: Materials in Medicine, 2011. **22**(4): p. 1053-1062.
152. Li, M., et al., *Electrospinning polyaniline-contained gelatin nanofibers for tissue engineering applications.* Biomaterials, 2006. **27**(13): p. 2705-2715.
153. Saberi, A., et al., *Electrically Conductive Materials: Opportunities and Challenges in Tissue Engineering.* Biomolecules, 2019. **9**(9): p. 448.
154. Correia, D.M., et al., *Processing and size range separation of pristine and magnetic poly(l-lactic acid) based microspheres for biomedical applications.* Journal of Colloid and Interface Science, 2016. **476**: p. 79-86.

155. Ignatius, A., et al., *Tissue engineering of bone: effects of mechanical strain on osteoblastic cells in type I collagen matrices.* Biomaterials, 2005. **26**(3): p. 311-318.
156. Valentini, R.F., et al., *Electrically charged polymeric substrates enhance nerve-fiber outgrowth invitro.* Biomaterials, 1992. **13**(3): p. 183-190.
157. Prabhakaran, M.P., et al., *Electrospun conducting polymer nanofibers and electrical stimulation of nerve stem cells.* Journal of Bioscience and Bioengineering, 2011. **112**(5): p. 501-507.
158. Guo, H.F., et al., *Piezoelectric PU/PVDF electrospun scaffolds for wound healing applications.* Colloids and Surfaces B-Biointerfaces, 2012. **96**: p. 29-36.
159. Ribeiro, C., et al., *In vivo demonstration of the suitability of piezoelectric stimuli for bone reparation.* Materials Letters, 2017. **209**: p. 118-121.
160. Gonçalves, R., et al., *Magnetoelectric $CoFe_2O_4$/polyvinylidene fluoride electrospun nanofibres.* Nanoscale, 2015. **7**(17): p. 8058-8061.
161. Collinsworth, A.M., et al., *Apparent elastic modulus and hysteresis of skeletal muscle cells throughout differentiation.* American Journal of Physiology - Cell Physiology, 2002. **283**(4 52-4): p. C1219-C1227.
162. Zarrintaj, P., et al., *Agarose-based biomaterials for tissue engineering.* Carbohydrate Polymers, 2018. **187**: p. 66-84.
163. Jarmey, C., *The Concise Book of Muscles*. North Atlantic Books, 2008. p. 1-192.
164. Kendall, F.P., McCreary, E.K. and Provance, P.G., *Muscles: Testing and Function with Posture and Pain*. Lippincott Williams & Wilkins, 2005. p. 1-560.
165. Vogel, S. and A. DeFerrari, *Prime Mover: A Natural History of Muscle*. W. W. Norton & Company, 2003. p. 1-383.
166. Brack, A.S. and Rando, T.A., *Tissue-specific stem cells: Lessons from the skeletal muscle satellite cell.* Cell Stem Cell, 2012. **10**(5): p. 504-514.
167. Haraguchi, Y., et al., *Concise review: Cell therapy and tissue engineering for cardiovascular disease.* Stem Cells Translational Medicine, 2012. **1**(2): p. 136-141.
168. Zhang, L., et al., *Musculature Tissue Engineering to Repair Abdominal Wall Hernia.* Artificial Organs, 2012. **36**(4): p. 348-352.
169. Chal, J. and Pourquié, O., *Making muscle: Skeletal myogenesis in vivo and in vitro.* Development, 2017. **144**(12): p. 2104-2122.
170. Longo, U.G., et al., *Tissue engineered strategies for skeletal muscle injury.* Stem Cells International, 2012. **2012**: p. 175038.
171. Liao, H. and Zhou, G.Q., *Development and progress of engineering of skeletal muscle tissue.* Tissue Engineering - Part B: Reviews, 2009. **15**(3): p. 319-331.
172. Lieber, R.L., *Skeletal muscle structure, function, and plasticity*. Lippincott Williams & Wilkins, 2011. p. 1-304.
173. Jana, S., Levengood, S.K.L. and Zhang, M., *Anisotropic Materials for Skeletal-Muscle-Tissue Engineering.* Advanced Materials, 2016. **28**(48): p. 10588-10612.
174. Sciote, J.J. and Morris, T.J., *Skeletal muscle function and fibre types: The relationship between occlusal function and the phenotype of jaw-closing muscles in human.* Journal of Orthodontics, 2000. **27**(1): p. 15-30.

175. Hanson, J. and Huxley, H.E., *Structural basis of the cross-striations in muscle.* Nature, 1953. **172**(4377): p. 530-532.
176. Huxley, H.E., *Electron microscope studies of the organisation of the filaments in striated muscle.* BBA - Biochimica et Biophysica Acta, 1953. **12**(1-2): p. 387-394.
177. Beldjilali-Labro, M., et al., *Biomaterials in tendon and skeletal muscle tissue engineering: Current trends and challenges.* Materials, 2018. **11**(7): p. 1116.
178. Vigodarzere, G.C. and Mantero, S., *Skeletal muscle tissue engineering: Strategies for volume tric constructs.* Frontiers in Physiology, 2014. **5**: p. 362.
179. Bottinelli, R. and Reggiani, C., *Human skeletal muscle fibres: Molecular and functional diversity.* Progress in Biophysics and Molecular Biology, 2000. **73**(2-4): p. 195-262.
180. Brand-Saberi, B., *Genetic and epigenetic control of skeletal muscle development.* Annals of Anatomy, 2005. **187**(3): p. 199-207.
181. Kitzmann, M. and Fernandez, A., *Crosstalk between cell cycle regulators and the myogenic factor MyoD in skeletal myoblasts.* Cellular and Molecular Life Sciences, 2001. **58**(4): p. 571-579.
182. Hasty, P., et al., *Muscle deficiency and neonatal death in mice with a targeted mutation in the myogenin gene.* Nature, 1993. **364**(6437): p. 501-506.
183. Sinanan, A.C.M., Buxton, P.G. and Lewis, M.P., *Muscling in on stem cells.* Biology of the Cell, 2006. **98**(4): p. 203-214.
184. Stern-Straeter, J., et al., *Advances in skeletal muscle tissue engineering.* In Vivo, 2007. **21**(3): p. 435-444.
185. Atherton, P.J., et al., *Cyclic stretch reduces myofibrillar protein synthesis despite increases in FAK and anabolic signalling in L6 cells.* Journal of Physiology, 2009. **587**(14): p. 3719-3727.
186. Khodabukus, A. and Baar, K., *Defined electrical stimulation emphasizing excitability for the development and testing of engineered skeletal muscle.* Tissue Engineering - Part C: Methods, 2012. **18**(5): p. 349-357.
187. Christ, G.J., et al., *Skeletal Muscle Tissue Engineering*, in *Stem Cell Biology and Tissue Engineering in Dental Sciences*. VishWaKarma, A., et al., Editors. Elsevier, 2014. p. 567-592.
188. Campion, D.R., et al., *Regulation of skeletal muscle development by the central nervous system in the fetal pig.* Growth, 1978. **42**(2): p. 189-204.
189. Nakajima, A., et al. *Effect of pulsatile electric field on cultured muscle cells in vitro*. Journal of systemics, 2012. **10**(1): p. 1-6.
190. Hosseini, V., et al., *Engineered contractile skeletal muscle tissue on a microgrooved methacrylated gelatin substrate.* Tissue Engineering - Part A, 2012. **18**(23-24): p. 2453-2465.
191. Sirivisoot, S. and Harrison, B.S., *Skeletal myotube formation enhanced by electrospun polyurethane carbon nanotube scaffolds.* International journal of nanomedicine, 2011. **6**: p. 2483-2497.
192. Ostrovidov, S., et al., *Myotube formation on gelatin nanofibers - Multi-walled carbon nanotubes hybrid scaffolds.* Biomaterials, 2014. **35**(24): p. 6268-6277.
193. Serena, E., et al., *Electrophysiologic stimulation improves myogenic potential of muscle precursor cells grown in a 3D collagen scaffold.* Neurological Research, 2008. **30**(2): p. 207-214.

194. Langelaan, M.L.P., et al., *Advanced maturation by electrical stimulation: Differences in response between C2C12 and primary muscle progenitor cells.* Journal of Tissue Engineering and Regenerative Medicine, 2011. **5**(7): p. 529-539.
195. Stern-Straeter, J., et al., *Impact of electrical stimulation on three-dimensional myoblast cultures - A real-time RT-PCR study.* Journal of Cellular and Molecular Medicine, 2005. **9**(4): p. 883-892.
196. Bajaj, P., et al., *Patterning the differentiation of C2C12 skeletal myoblasts.* Integrative Biology, 2011. **3**(9): p. 897-909.
197. Buvinic, S., et al., *ATP released by electrical stimuli elicits calcium transients and gene expression in skeletal muscle.* Journal of Biological Chemistry, 2009. **284**(50): p. 34490-34505.
198. Eltit, J.M., et al., *Membrane electrical activity elicits inositol 1,4,5-trisphosphate-dependent slow Ca^{2+} signals through a Gβγ/phosphatidylinositol 3-kinase γ pathway in skeletal myotubes.* Journal of Biological Chemistry, 2006. **281**(17): p. 12143-12154.
199. Zöllner, A.M., et al., *Stretching Skeletal Muscle: Chronic Muscle Lengthening through Sarcomerogenesis.* PLoS ONE, 2012. **7**(10): p. e45661.
200. Valentin, J.E., et al., *Functional skeletal muscle formation with a biologic scaffold.* Biomaterials, 2010. **31**(29): p. 7475-7484.
201. Pennisi, C.P., et al., *Uniaxial cyclic strain drives assembly and differentiation of skeletal myocytes.* Tissue Engineering - Part A, 2011. **17**(19-20): p. 2543-2550.
202. Boonen, K.J.M., et al., *Effects of a combined mechanical stimulation protocol: Value for skeletal muscle tissue engineering.* Journal of Biomechanics, 2010. **43**(8): p. 1514-1521.
203. Okano, T., et al., *Tissue engineering of skeletal muscle: Highly dense, highly oriented hybrid muscular tissues biomimicking native tissues.* ASAIO Journal, 1997. **43**(5): p. M749-M753.
204. Candiani, G., et al., *Cyclic mechanical stimulation favors myosin heavy chain accumulation in engineered skeletal muscle constructs.* Journal of Applied Biomaterials and Biomechanics, 2010. **8**(2): p. 68-75.
205. Powell, C.A., et al., *Mechanical stimulation improves tissue-engineered human skeletal muscle.* American Journal of Physiology - Cell Physiology, 2002. **283**(5 52-5): p. C1557-C1565.
206. Ahmed, W.W., et al., *Myoblast morphology and organization on biochemically micro-patterned hydrogel coatings under cyclic mechanical strain.* Biomaterials, 2010. **31**(2): p. 250-258.
207. Moon, D.G., et al., *Cyclic mechanical preconditioning improves engineered muscle contraction.* Tissue Engineering - Part A., 2008. **14**(4): p. 473-482.
208. Zhang, S.J., Truskey, G.A. and Kraus, W.E., *Effect of cyclic stretch on β1D-integrin expression and activation of FAK and RhoA.* American Journal of Physiology - Cell Physiology, 2007. **292**(6): p. C2057-C2069.
209. Hara, M., et al., *Calcium influx through a possible coupling of cation channels impacts skeletal muscle satellite cell activation in response to mechanical stretch.* American Journal of Physiology - Cell Physiology, 2012. **302**(12): p. C1741-C1750.
210. Tatsumi, R., et al., *Release of hepatocyte growth factor from mechanically stretched skeletal muscle satellite cells and role of pH and nitric oxide.* Molecular Biology of the Cell, 2002. **13**(8): p. 2909-2918.

211. Hanke, N., et al., *Passive mechanical forces upregulate the fast myosin heavy chain IId/x via integrin and p38 MAP kinase activation in a primary muscle cell culture.* American Journal of Physiology - Cell Physiology, 2010. **298**(4): p. C910-C920.
212. Adam, R.M., et al., *Signaling through P13K/AKT mediates stretch and PDGF-BBdependent DNA synthesis in bladder smooth muscle cells.* Journal of Urology, 2003. **169**(6): p. 2388-2393.
213. Guo, B. and Ma, P.X., *Conducting Polymers for Tissue Engineering.* Biomacromolecules, 2018. **19**(6): p. 1764-1782.
214. Gilmore, K.J., et al., *Skeletal muscle cell proliferation and differentiation on polypyrrole substrates doped with extracellular matrix components.* Biomaterials, 2009. **30**(29): p. 5292-5304.
215. Gelmi, A., Higgins, M.J. and Wallace, G.G., *Physical surface and electromechanical properties of doped polypyrrole biomaterials.* Biomaterials, 2010. **31**(8): p. 1974-1983.
216. Broda, C.R., et al., *A chemically polymerized electrically conducting composite of polypyrrole nanoparticles and polyurethane for tissue engineering.* Journal of Biomedical Materials Research - Part A, 2011. **98 A**(4): p. 509-516.
217. Ostrovidov, S., et al., *Gelatin-Polyaniline Composite Nanofibers Enhanced Excitation-Contraction Coupling System Maturation in Myotubes.* ACS Applied Materials and Interfaces, 2017. **9**(49): p. 42444-42458.
218. Chen, M.C., Sun, Y.C. and Chen, Y.H., *Electrically conductive nanofibers with highly oriented structures and their potential application in skeletal muscle tissue engineering.* Acta Biomaterialia, 2013. **9**(3): p. 5562-5572.

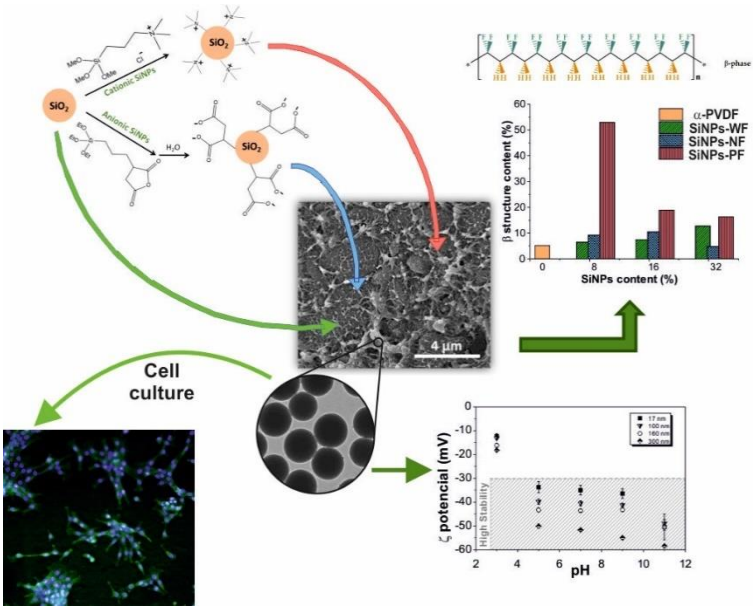

Chapter 2. Multifunctional platform based on electroactive polymers and silica nanoparticles for tissue engineering applications

Poly(vinylidene fluoride) can be processed with various morphologies and dimensionalities by different methods. The introduction of nanoparticles into a matrix can improve the piezoelectric phase of the material and offer new functions important for regulating cell response, such drug delivery (proliferation/differentiation factors). This chapter builds on how different SiNPs diameter and functionalizations influence the features of the produced nanocomposites, such as physico-chemical properties and electroactive β-phase content. Cell viability was also characterized using myoblasts seeded on nanocomposites with all the different morphologies and containing SiNPs of varying diameters in order to evaluate the potential of these materials for muscle tissue engineering.

This chapter is based on the following publications: **S. Ribeiro**, T. Ribeiro, C. Ribeiro, D.M. Correia, J.P.S. Farinha, A.C. Gomes, C. Baleizão and S. Lanceros-Méndez, *Multifunctional Platform Based on Electroactive Polymers and Silica Nanoparticles for Tissue Engineering Applications*; Nanomaterials, 8(11), 933, 2018 and **S. Ribeiro**, R. Meira, D.M. Correia, C. R. Tubio, C. Ribeiro, C. Baleizão and S. Lanceros-Méndez, *Silica nanoparticles surface charge modulation of the electroactive phase content and physical-chemical properties of poly(vinylidene fluoride) nanocomposites*; Submitted 2019.

2.1 Introduction

The development of advanced multifunctional materials is essential for the development of society [1]. Nanocomposites are among the most important materials for an increasing number of applications due to the possibility of tailoring materials properties to meet specific application demands in areas ranging from sensors and actuators [2, 3] to food packaging [4, 5] and TE [6, 7], among others. The introduction of inorganic nanomaterials into polymers allows the combination of the rigidity and high thermal stability of the inorganic material with the ductility, flexibility and processability of the organic polymers [8], as well as the introduction/tuning of further functionalities such as magnetic [9], mechanical[10] or electrical properties [11, 12]. Typical nanomaterials include nanoparticles, nanotubes, nanofibres, fullerenes and nanowires [13]. Among nanomaterials, silica is widely present in the environment and has several key features [14].

Properties of silica nanoparticles (SiNPs), such as high mechanical strength, permeability, thermal and chemical stability, relatively low refractive index, high surface area and the fact of being used for coatings of other particles, such as magnetic and quantum dots [15-17], make these nanoparticles highly applicable [18]. Furthermore, their biocompatibility and the different possibilities to functionalize them are the basis of their large potential for biomedicine and TE applications [19]. Silica nanostructures have been extensively used as supports or carriers in drug delivery [20, 21], nanomedicine [22, 23] and bioanalysis [24]. Their characteristics can be tuned during synthesis to obtain a wide range of particle diameters ranging from 20 to 500 nm, different pore sizes and the incorporation of molecules such as drugs or fluorophores [24], as well as magnetic nanostructures [25]. Mesoporous silica nanoparticles (MSNPs) [20, 26] have attracted particular attention for their functionalization versatility. Silica-based mesoporous nanoparticles, due to the strong Si-O bond compared to liposomes and dendrimers, are more resistant to degradation and mechanical stress, inhibiting the need of any external stabilization of the MSNPs [27, 28].

With respect to TE, different tissues require different microenvironments for suitable regeneration [29]. Thus, muscle tissue displays electromechanical response and needs electrical stimulation to support ionic exchange, mainly sodium by calcium ion [30]. In this context, electroactive polymers such as magnetoelectric [31, 32], piezoelectric and conductive polymers [33], among others [34], show strong potential for TE applications. Among the different electroactive polymers, piezoelectric polymers have already shown their suitability for TE [6, 29] due to their capacity to vary surface charge when a mechanical load is applied or vice versa. These materials can play a significant role because the electric stimulation can be found in many living tissues of human body, namely neural tissue [35] and bone [36,

37], and it can provide electromechanical solicitations for muscle [38]. PVDF is the biocompatible piezoelectric polymer with the highest piezoelectric response. It can crystallize in five differentiated crystalline phases α, β, γ, δ, $\mathcal{E}$, being the β-phase the one with the highest piezoelectric response and consequently the most desirable for applications in areas such as sensors and actuators, biomedicine or energy harvesting, where an active electrical response is needed [39, 40]. It can also be processed in different morphologies, including films, fibres, spheres, membranes, and 3D scaffolds [29, 41] providing a suitable platform for TE.

In order to further exploit the applicability of PVDF in regenerative medicine, polymer nanocomposites based on PVDF using silica nanoparticles with different diameters and different functionalizations were prepared, improving the electroactive characteristics of PVDF with the aforementioned characteristics of MSNPs for biomedical applications. Together with the physico-chemical characteristics of the developed composites, their biocompatibility was evaluated in murine myoblast cells.

2.2 Experimental Section

2.2.1 Materials

PVDF (Solef 1010) was purchased from Solvay and N,N-dimethylformamide (DMF) from Merck. Absolute ethanol (EtOH, 99.5%), ammonium hydroxide solution (NH_4OH, 28% in water), tetraethyl orthosilicate (TEOS, 99%), N-trimethoxysilylpropyl-N,N,N-trimethylammonium chloride (50% in methanol), and 3-triethoxysilylpropylsuccinic anhydride (95%) were purchased from Sigma-Aldrich and used as received. Toluene was distilled over calcium hydride prior to use. Deionized water from a Millipore (Oeiras, Portugal) system Milli-Q ≥ 18 MΩ cm was used in the synthesis of the silica nanoparticles. Perylenediimide derivative (PDI) was synthesized according to the literature [42].

2.2.2 Silica Nanoparticles

2.2.2.1 Preparation of silica nanoparticles

The fluorescent silica nanoparticles, doped with fluorescent dye (PDI) were prepared by a modified Stöber method [6, 18]. Water, absolute ethanol, and PDI (previously dispersed in ethanol, 1×10^{-6} M) were mixed and after 30 min, the ammonia solution was added to the mixture, followed by TEOS. The reaction was kept under stirring at constant temperature for 24 h. After that time, the nanoparticles were recovered and washed with ethanol (3 cycles of centrifugation). Nanoparticle centrifugation was performed on a centrifuge Sigma 2K15, with a 12 141 rotor. The nanoparticles were redispersed in ethanol and dried

at 50 °C in a ventilated oven. The experimental details for the different diameters are provided in Table 2.1.

Table 2.1. Experimental details used for the preparation of the SiNPs.

Particle diameter (nm)	EtOH (g)	H_2O (g)	PDI solution (mL)	NH_3 (mL)	TEOS (mL)	Reaction temperature (°C)
17	84.13	7.99	3	1.51	4.46	50
100	105.73	4.65	4	6.68	9.00	30
160	53.18	11.03	4	2.67	4.46	50
300	53.18	11.03	4	2.67	4.46	30

The Silica nanoparticles-PDI without any functionalization (SiNPs-WF) with the lower diameter, were used to perform two different types of functionalization, anionic and cationic groups in the surface of nanoparticles. Their chemical structure was presented in figure 2.1 and the properties of these nanoparticles are shown in table 2.2.

2.2.2.1.1 Cationic Silica Nanoparticles

The modification of the SiNP surface with cationic groups was performed by dispersing 1.1 g of SiNP in a solution of N-trimethoxysilylpropyl-N,N,N-trimethylammonium chloride (0.6 mL) in dry toluene (55 mL). The reaction mixture was left under reflux and argon atmosphere for 24 h. The nanoparticles were recovered and washed with ethanol (three cycles of centrifugation) and then redispersed in ethanol and dried at 50 °C in a ventilated oven. The surface modification was confirmed and quantified by Nuclear Magnetic Resonance (NMR), following a method described in the literature [43]. These nanoparticles are denominated SiNPs-PF due to the presence of a positive group (NMe_3^+) in the SiNPs surface (table 2.2).

2.2.2.1.2 Anionic Silica Nanoparticles

The procedure to modify the SiNP surface with anionic groups was similar to the one used for cationic functionalization but using 3-triethoxysilylpropylsuccinic anhydride (0.3 mL) as modifying agent. To hydrolyze the anhydride and obtain the anionic carboxylate groups, the nanoparticles were suspended in 50 mL of water and left under stirring at 70 °C for 6 h. The nanoparticles were recovered and washed with ethanol and dried at 50 °C in a ventilated oven. The surface modification was confirmed and

quantified by NMR, following a method described in the literature [43]. These nanoparticles are denominated SiNPs-NF due to the presence of a negative group (COO^-) in the SiNPs surface (table 2.2).

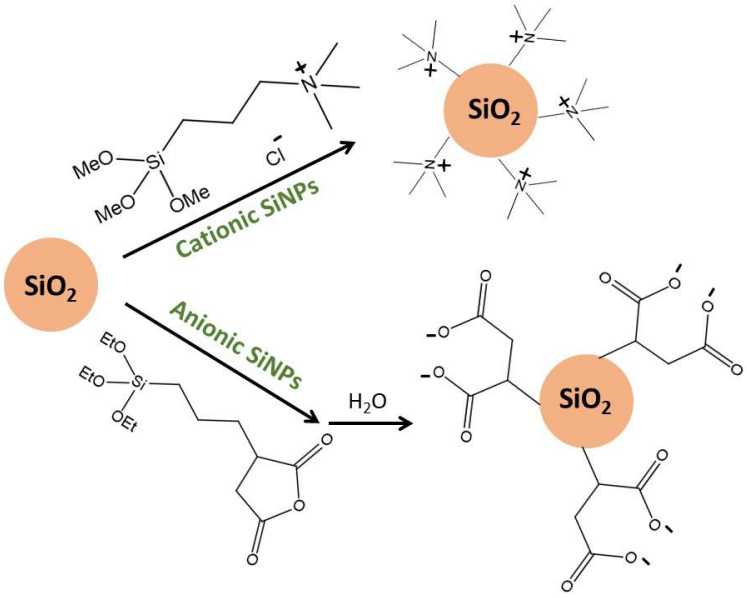

Figure 2.1. Schematic representation of the chemical structure of the SiNPs without and with positive and negative functionalization.

2.2.2.2 Characterization of the SiNPs

Transmission electron microscopy: Transmission electron microscopy (TEM) images were obtained on a Hitachi transmission electron microscope (model H-8100 with a LaB6 filament) with an acceleration voltage of 200 kV. One drop of the dispersion of particles in ethanol was placed on a carbon grid and dried in air before observation. The images were processed with the Fiji software.

Zeta potential: The surface charge of the nanoparticles was estimated with the use of zeta potential instrument (Zetasizer NANO ZS-ZEN3600, Malvern). The zeta potential of the fluorescent SiNPs with different diameters and functionalizations were evaluated at different pH (3, 5, 6, 7, 11, 13). To adjust the pH, it was used a solution of HCl (1M) and NaOH (1M). The average value and standard deviation for each sample were obtained from 6 measurements.

Hydrodynamic diameters and zeta potential values of the nanoparticles were obtained using a Zetasizer Nano ZS equipped with a 4 mW He–Ne solid-state laser operating at 633 nm and backscattered light detected at 173°. To determine the hydrodynamic diameter of the nanoparticles, the autocorrelated function was analyzed by the CONTIN method. Zeta potentials were calculated from electrophoretic

mobility using the Smoluchowski relationship. Disposable folded capillary cells (DTS1070) were used for the measurement of zeta potentials. All measurements were performed in triplicate.

Table 2.2. Characterization of Silica Nanoparticles without and with functionalization (negative and positive).

	Diameter (DLS)	Functionalization (NMR)		Zeta-potencial (mV) at pH=6	Denomination
		$mmol.g^{-1}$	$Molecules.nm^{-2}$		
SiNP		——	——	-25.8 ± 1.54	WF
Ani-SiNP	16 ± 1 nm	0.76	1.9	-34.3 ± 1.08	NF
Cat-SiNP		1.0	2.5	8.64 ± 0.58	PF

2.2.3 Nanocomposite samples

2.2.3.1 Preparation of the SiNPs/PVDF nanocomposites

To evaluate the different diameters, SiNPs/PVDF nanocomposites were prepared with 16 wt.% of SiNPs by dispersing the respective mass of SiNPs in the DMF solvent within an ultrasound bath for 4 h at room temperature, to ensure good dispersion of the nanoparticles and avoid nanoparticles agglomeration. The filler concentration was selected based in [44], as it shows a suitable filler content without compromising the mechanical characteristics of the polymer matrix and allowing a suitable dispersion of the filler. After obtain a good dispersion of the nanoparticles, PVDF was added with a concentration of 20 wt.% and the solution was magnetically stirred at room temperature until the complete dissolution of the polymer. The materials were then prepared by different production methods [41].

First, SiNPs/PVDF samples (porous and non-porous films) were prepared by solution casting on a clean glass substrate and, in some cases, melted at different temperatures for different times (table 2.3). The different preparation conditions allow to tailor both porosity and to study the possibility of the nucleation of the electroactive β-phase of the polymer by the fillers [45]. The thickness of the films ranges from 30 to 50 μm.

Table 2.3. Denomination, relevant preparation conditions and morphology of the PVDF and nanocomposite samples prepared in this work.

Morphology	Temperature (°C)	Time to melt/dry (min)	Diameter of the nanoparticles (nm)	Samples morphology (P: porous; NP: non-porous)	Denomination
Films (F)	90	30	—	NP	F90-NP
			17	NP	F90-17NP
			100	NP	F90-100NP
			160	NP	F90-160NP
			300	NP	F90-300NP
	210	10		NP	F210-17NP
	Room temperature (Tamb)	—		P	FTamb-17P
Oriented fibres (O)	—	—	17	P	O-17P
Random fibres (R)	—	—		P	R-17P

For SiNPs/PVDF electrospun fiber mats, the solution was placed in a plastic syringe (10 mL) fitted with a steel needle with inner diameter of 0.5 mm. After an optimization procedure, electrospinning was conducted with a high voltage power supply from Glasman (model PS/FC30P04) at 14 kV with a feed rate of 0.5 $mL.h^{-1}$ (with a syringe pump from Syringepump). The electrospun fibres were collected in an aluminum plate (placed at 20 cm from the needle) and in a rotating drum (1500 rpm) to obtain random and oriented nanofibres, respectively.

Table 2.3 summarizes the main characteristics of the samples and the corresponding denomination that refers the type of sample and processing temperature, the nanoparticle diameter and the composite morphology. For example, F90-17NP is a film (F) obtained at 90 °C (90) with nanoparticles with a diameter of 17 nm (17), which is non-porous (NP).

To study the different functionalizations into PVDF matrix, the preparation of the pristine PVDF films, PVDF was first dissolved in DMF, under magnetic stirring, in a polymer concentration of 15 wt.%, following the guidelines presented in [41]. The SiNPs/PVDF nanocomposites were prepared by the same method as mentioned above, but with 8, 16 and 32 wt.% of each three different SiNPs nanoparticles (SiNPs-WF, -NF and -PF). The pH of the prepared SiNPs/PVDF mixture was approximately 6 [46]. The PVDF and

SiNPs/PVDF nanocomposites films were obtained then by the solvent casting method. The samples were produced by spreading the solution on a clean glass substrate followed by polymer melting and solvent evaporation at 210 °C for 10 min. Films with a typical thickness of 30 to 50 µm were then obtained after cooling down the samples to room temperature. It is to notice that this procedure is the typically one used to obtain PVDF in the α-phase [41, 45].

2.2.3.2 Characterization of the SiNPs/PVDF nanocomposites samples

Scanning electron microscopy: A desktop scanning electron microscope (SEM) (Phenom ProX, Netherlands) was used to observe the morphology and microstructure of the PVDF and SiNPs/PVDF nanocomposites. This technique was also used to observe the cell morphology seeded on the different fibrous samples. All the samples were added to the aluminium pin stubs with electrically conductive carbon adhesive tape (PELCO TabsTM). The aluminium pin stub was then placed on a phenom Charge Reduction sample Holder. All results were acquired using the ProSuite Software. The images were obtained with an acceleration voltage of 10 kV. All results were acquired using the ProSuite software.

Laser scanning confocal fluorescence microscopy: Laser scanning confocal fluorescence microscopy images were obtained with a Leica TCS SP5 laser scanning microscope (Leica Mycrosystems CMS GmbH, Mannheim, Germany) using an inverted microscope (DMI6000), a HCX PL APO CS 10x dry immersion objective (10x magnification and 0.4 numerical aperture) and a HC PL FLUOTAR 50x dry immersion objective (50x magnification and 0.8 numerical aperture). Imaging used the 488 nm line of an argon ion laser.

Water contact angle measurements: Water contact angle (WCA) measurements (sessile drop in dynamic mode) were performed at room temperature in a Data Physics OCA20 set up using ultrapure water as the test liquid. The samples wettability was determined by using water drops (3 µL) placed onto the surface of the samples. Each sample was measured at six different locations and the mean WCA and standard deviation were calculated.

Fourier transform infrared spectroscopy: Fourier transformed infrared spectroscopy (FTIR) measurements in attenuated total reflectance (ATR) mode were performed at room temperature, using a Nicolet Nexus 670 FTIR-spectrophotometer with Smart Orbit Accessory equipment. The analysis was performed from 4000 to 600 cm^{-1}, after 64 scans with a resolution of 4 cm^{-1}.

The spectrum of each sample was used to determine the relative content of the electroactive β-phase in the composite samples, by using the method presented in [45]. In short, the β-phase content (F_β) was calculated by equation 2.1.

$$F_\beta = \frac{A_\beta}{\left(\frac{K_\beta}{K_\alpha}\right) \times A_\alpha + A_\beta} \qquad (2.1)$$

where A_β are the absorbance at $840\ cm^{-1}$, and $K_\beta = 7.7 \times 10^4\ cm^2 mol^{-1}$ is the absorption coefficient corresponding to the β-phase, A_α is the absorbance at $760\ cm^{-1}$ and $K_\alpha = 6.1 \times 10^4\ cm^2 mol^{-1}$ is the absorption coefficient corresponding to the α-phase.

Thermal properties: Differential scanning calorimetry (DSC) was carried out with a DSC 6000 Perkin Elmer instrument. Samples were cut from the middle region of the films and placed in aluminum pans. Then, the samples were heated from 30 to 200 °C at a rate of 10 °C.min^{-1} under a flowing nitrogen atmosphere.

From the melting in the DSC thermograms, the degree crystallinity (X_c) of the samples was calculated by the following equation 2.2 [45].

$$X_c = \frac{\Delta H_f}{x\Delta H_\alpha + y\Delta H_\beta} \qquad (2.2)$$

where ΔH_f is the melting enthalpy of the sample, x and y represent the α- and β-phase content present in the sample, respectively, and ΔH_α and ΔH_β are the melting enthalpies for a 100% α-PVDF (93.04 J.g^{-1}) and β-PVDF (104.4 J.g^{-1}) crystalline sample respectively. The crystallinity values were adjusted by the effective fraction of PVDF in the nanocomposite.

Thermogravimetry analyses were performed with a thermal analyzer 6000 Perkin Elmer instrument. For the measurements, approximately 10 mg of samples were transferred to open ceramic crucibles and measurements were performed between 25 and 900 °C at a heating rate of 10 °C.min^{-1} under a flowing nitrogen atmosphere.

Mechanical characterization: Mechanical measurements were carried out with a universal testing machine (Shimadzu model AG-IS) at room temperature, in the tensile mode and at a test velocity of 1 mm.min^{-1}, with a load cell of 50 N. The tests were performed on rectangular samples (30 x 10 mm) with a thickness between 30 and 50 μm (Fischer Dualscope 603-478, digital micrometer).

The mechanical parameters were calculated from the average of triplicate measurements. The Hook's law was used to obtain the effective Young's modulus (E) of PVDF and SiNPs/PVDF nanocomposite samples in the linear elastic zone between 0 and 1% strain.

Electrical and Dielectric measurements

The electrical conductivity of the samples was evaluated from the current (I) - voltage (V) characteristic curves using an automated Keithley 487 picoammeter/voltage source. Before analysis, gold electrodes with 5 mm diameter were deposited on both sides of the samples by magnetron sputtering (Scancoat Six SEM Sputter Coater). The current intensity was measured while applying voltages between -0.1 V and +0.1 V (step of 0.01 V). The electrical resistance (R) was determined from the slope of the *I-V* curves and the d.c. (direct current) electrical conductivity (σ) was obtained from equation 2.3.

$$\sigma = \frac{1}{(\frac{RA}{L})} \qquad (2.3)$$

where R is the resistance in Ohm, A is the electrode area in square meters and L is the distance between electrodes in meters.

Dielectric measurements were carried out in the parallel plate capacitor configuration using a Quadtech 1920 LCR precision meter. The real (ε') and imaginary (ε'') part of the dielectric function were obtained from the measurement of the capacity (C) and the dielectric losses (tan δ) at room temperature in the frequency range of 100 Hz to 1 MHz with an applied voltage of 0.5 V. ε' and ε'' were calculated with the equation 2.4 and 2.5.

$$\varepsilon' = \frac{C.d}{\varepsilon_0.A} \qquad (2.4)$$

and

$$\varepsilon'' = tan\,\delta.\varepsilon' \qquad (2.5)$$

where C is the capacitance, ε_0 is the permittivity of vacuum (8.85×10^{-12} F m^{-1}), A is the electrode area and d is the thickness of samples.

For these measurements, circular gold electrodes of 5 mm diameter were deposited by a magnetron sputtering with a Polaron Coater SC502 onto both sides of each sample.

The a.c. (alternate current) electrical conductivity (σ') of PVDF and SiNPs/PVDF composites was obtained from the dielectric measurements by the equation 2.6.

$$\sigma' = \omega \cdot \varepsilon_0 \cdot \varepsilon'' = \omega \cdot \varepsilon_0 \cdot \varepsilon' \cdot tan\ \delta \qquad (2.6)$$

where ε_0 (8.85 × 10^{-12} F.m^{-1}) is the permittivity of the free space, $\omega = 2\,\pi f$ is the angular frequency, ε' and ε'' are the real and imaginary part of the dielectric constant (equations 4 and 5), respectively, and $tan\ \delta = \varepsilon''/\ \varepsilon'$.

2.2.3.3 Cell culture experiments

2.2.3.3.1 Sample sterilization

The samples were sterilized by multiple immersions into 70% ethanol for 30 min each and to remove any residual solvent, they were washed 5 times in a phosphate buffered saline (PBS) 1x solution for 5 min each. Each side of the samples was then exposed to ultraviolet light for 1 h.

2.2.3.3.2 Cell culture

Murine myoblasts (C2C12 cell line) were cultivated in Dulbecco's Modified Eagle's Medium (DMEM, Gibco) with 4.5 g.L^{-1} containing 10% of Fetal Bovine Serum (FBS, Biochrom) and 1% of Penicillin/Streptomycin (P/S, Biochrom). The cells were grown in 75 cm^2 cell-culture flask at 37 °C in a humidified air containing 5% CO_2 atmosphere. Every two days, the culture medium was changed. The cells were trypsinized with 0.05% trypsin-EDTA when reached 60-70% confluence. For the cytotoxicity assays, SiNPs/PVDF nanocomposites with different morphologies were cut according the ISO_10993-12. The extraction ratio (surface area or mass/volume) was 6 cm^2.mL^{-1}. To analyze cell morphology and viability, the materials were cut into 6 mm of diameter. PVDF films without nanoparticles were used as control.

2.2.3.3.3 Cytotoxicity assay by the indirect contact

C2C12 cells were seeded at the density of 2×10^4 cells.mL^{-1} in 96-well tissue culture polystyrene plates. Cells were allowed to attach for 24 h, after which the culture medium was removed and the conditioned medium (the medium that was in contact with the samples) was added to the wells (100 µL). Afterwards, the cells were incubated for 24 or 72 h, and the number of viable cells was quantified by (3 (4,5 Dimethylthiazol 2 yl) 2,5 diphenyltetrazolium bromide) (MTT) assay. The cells received MTT solution (5 mg.mL^{-1} in PBS dissolved in DMEM in proportion of 10%) and were incubated in the dark at 37 °C for 2 h. The medium was then removed and 100 µL of DMSO/well was added to dissolve the precipitated

formazan. The quantification was determined by measuring the absorbance at 570 nm using a microplate reader. All quantitative results were obtained from four replicate samples and controls and were analyzed as the average of viability ± standard deviation (SD).

2.2.3.3.4 Direct contact and Proliferation

Since MTT interferes with the materials, it had chosen the MTS that having the same theoretical base but with soluble reaction product. C2C12 cells (4 000) were seeded on each sample. After 24 h and 72 h, the viable cell number was determined using the (3-(4,5-dimethylthiazol-2-yl)-5-(3-carboxymethoxyphenyl)-2-(4-sulfophenyl)-2H-tetrazolium) (MTS) assay. At the desired time points, the MTS reagent was added into each well in proportion of 1 part to 5 of DMEM medium and, incubated at 37 °C for 2 h. The absorbance was detected at 490 nm with a microplate reader. Experimental data were obtained from four replicates.

2.2.3.3.5 Immunofluorescence staining

Using the same time-points as in the proliferation assays, the nanocomposite samples were subjected to immunofluorescence staining to analyze the cytoskeleton morphology of the cells, verifying also the cell viability and adhesion. At each time point, the medium of each well was removed, the samples were washed with PBS and the cells fixed with 4% formaldehyde for 10 min at 37 °C in a 5% CO_2 incubator. After fixation, the samples were washed with PBS 1x (three times) and incubated for 45 min at room temperature in 0.1 μg mL^{-1} of phalloidin-fluorescein isothiocyanate (FITC, Sigma). Then, the samples were incubated for 5 min with 1 μg mL^{-1} of 4,6-diamidino-2-phenylindole (DAPI, Sigma). Afterwards, the samples were washed again with PBS 1x (three times) and one time with distillate water. Finally, the samples were visualized in a fluorescence microscopy (Olympus BX51 Microscope).

2.3 Results and discussion

2.3.1 Influence of different SiNPs diameters

2.3.1.1 Morphology and size of the silica nanoparticles

The morphology and the size of the SiNPs were analyzed from TEM images (figure 2.2). The spherical nanoparticles prepared by the Stober method [47] were prepared in four different diameters: 17 ± 2, 100 ± 18, 160 ± 17 and 300 ± 37 nm. The corresponding histograms are presented as insets in figure 2.2.

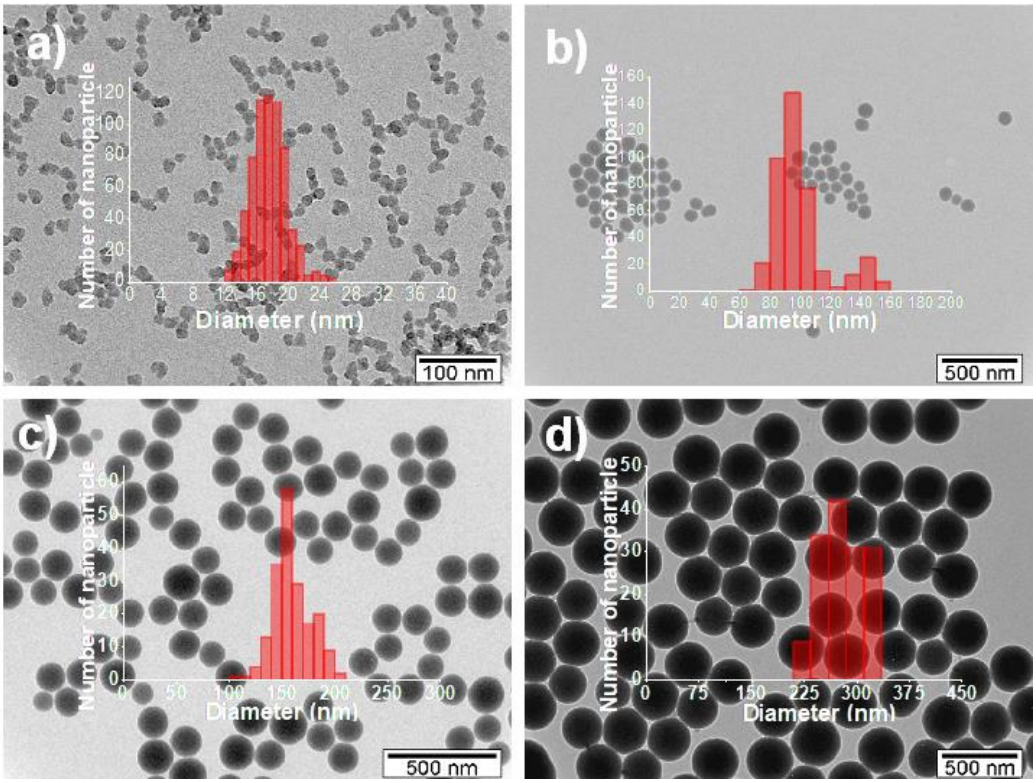

Figure 2.2. TEM images of SiNPs-PDI with different particle size: (a) 17 ± 2 nm, (b) 100 ± 18nm, (c) 160 ± 17nm and (d) 300 ± 37nm.

2.3.1.2 Surface charge of the nanoparticles

Figure 2.3 shows the zeta potential of aqueous dispersions of the different SiNPs at different pH to analyse the periphery charge of the particles.

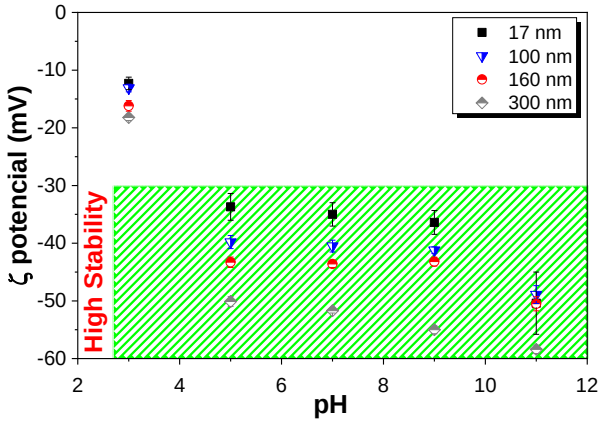

Figure 2.3. Zeta potential of the different SiNPs nanoparticles at different pH.

The particles are considered more stable with a zeta potential above +30 mV or below -30 mV. This fact is due to the electrostatic repulsions between the nanoparticles that prevent their aggregation. Figure 2.3 shows that all nanoparticles are more stable at pH ≥ 5, independently of their average diameter. On

the other hand, nanoparticles with higher average diameters are more stable. The isoelectric point of SiNPs is close to pH 2 so, from this pH upwards, the silica nanoparticles are negatively charged in acidic, neutral and basic environments, which can be taken to advantage, as it has been demonstrated that the interactions between negatively charged nanoparticle surfaces and the positive charge density of the CH_2 groups of the PVDF polymer, can promote the nucleation of the electroactive β-phase of the polymer [46].

2.3.1.3 Morphology of the nanocomposites

The morphology of the nanocomposites was assessed by SEM. Figure 2.4 shows the different morphologies obtained after the different processing methods as well as the variations due to the introduction of fillers with different diameters. Figure 2.4 shows the cross section (figure 2.4a-2.4c) of the nanocomposites and electrospun fibres samples (figure 2.4d) with 16 wt.% of SiNPs.

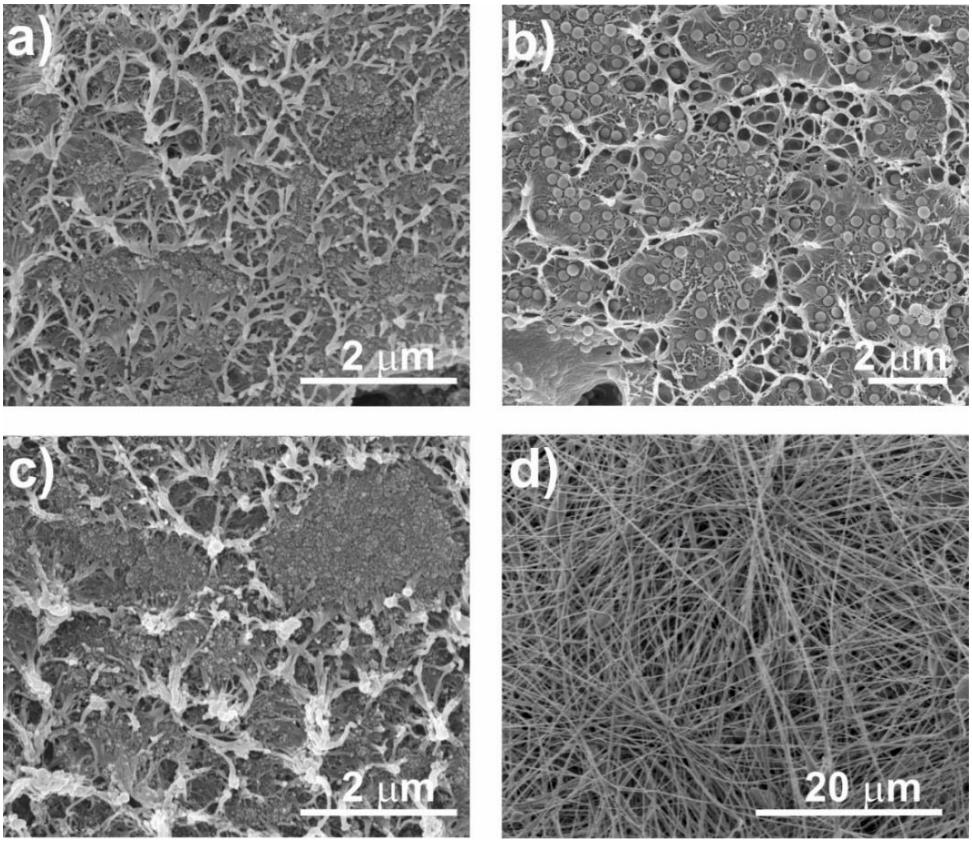

Figure 2.4. Cross section SEM micrographs of SiNPs/PVDF nanocomposite samples with nanoparticles of different diameters and different processing conditions: (a) F90-17NP, (b) F90-300NP, (c) F210-17NP, (d) R-17P.

Figures 2.4a and 2.4b present the differences between the samples obtained at 90 °C with SiNPs of different diameters, showing that the higher diameter particles are well-dispersed in the PVDF polymer

matrix, contrary to the SiNPs with lower diameter that present particles agglomerates. Furthermore, a small porosity is observed (figure 2.4a), which is in agreement with the literature [48].

It is to notice that the nanoparticles act as nucleation agents for crystallization in PVDF composites [49], which can be verified with the results obtained, indicating a good interfacial interaction between the PVDF chains and silica nanoparticles.

Figure 2.4a and 2.4c show the differences in composite morphology due to the crystallization process. The samples obtained at 90 °C (figure 2.4a and 2.4b) present a slightly more porous morphology than the ones obtained at 210 °C (figure 2.4c).

Once the SiNPs with 17 nm do not show a suitable dispersion in the films, electrospinning has been used in order to produce fibres with well dispersed particles. Relatively to the fibres (figure 2.4d), smooth randomly oriented fibres with encapsulated particles are observed, with no particles at the surface.

This result is confirmed by the confocal images represented in figure 2.5. It was observed that the introduction of the particles increases the fibre diameter (243 ± 89 to 339 ± 92 nm). Oriented fibres with SiNPs were also produced (data not shown), verifying also the particles encapsulation within the fibres and fibre diameter of 683 ± 140 nm. The increase of fibre diameter with the incorporation of the SiNPs is attributed to the higher viscosity of the solution, with also hinders fibre stretching by the applied field. The higher diameter of the oriented fibres comparatively to the randomly oriented fibres is attributed to the merging of aligned fibrils that crystallize simultaneously [50].

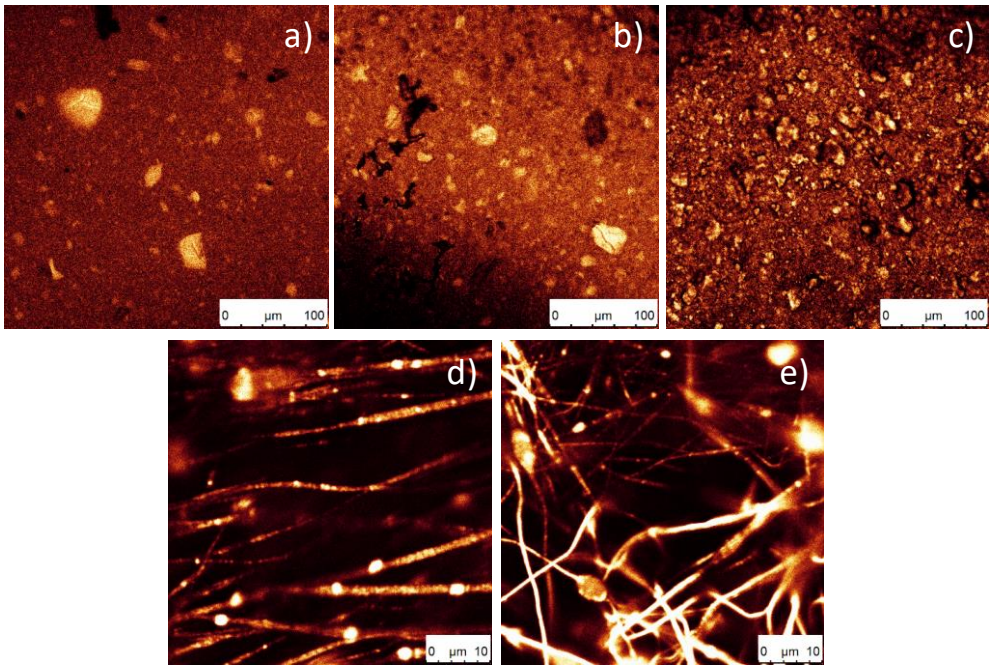

Figure 2.5. Representative confocal images of SiNPs/PVDF nanocomposites with different morphologies: (a) F210-17NP, (b) F90-17NP, (c) Ftamb-17P, (d) O-17P and (e) R-17P.

2.3.1.4 Confocal fluorescence microscopy of the nanocomposites

The incorporation of PDI in the silica nanoparticles can increase their application range, in particular, for biomedical applications, as it allows their tracking and localization [18, 51]. In figure 2.5, the orange colour identifies the fluorescence of the nanoparticles, higher colour intensity indicates a higher number of nanoparticles present. Figures 2.5a, 2.5b and 2.5c show that as the processing temperature decreases, a larger aggregation of nanoparticles is observed. In figure 2.5a, where the temperature is higher, more homogeneous samples were obtained.

Relatively to the oriented and random fibres, figure 2.5d and 2.5e, respectively, it is observed that the nanoparticles are present and included within the fibres.

2.3.1.5 Wettability of the nanocomposites

Material surface characteristics are essential in demining cell response in TE applications. In this sense, the static WCA was measured on the different SiNPs/PVDF nanocomposites and the values are presented in figure 2.6.

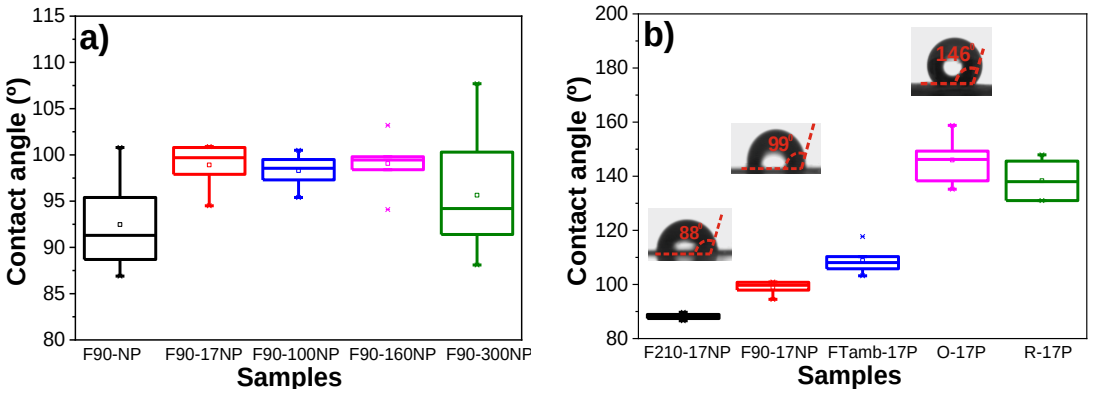

Figure 2.6. Water contact angle of the SiNPs/PVDF nanocomposites: (a) PVDF with the SiNPs with different diameters processed at 90 °C and (b) SiNPs/PVDF samples with silica nanoparticles (17 nm) with different morphologies.

The introduction of the Si nanoparticles increases the WCA values, independently of the diameter of the silica nanoparticles [52], to around 100° excepting for the samples with silica nanoparticles with the highest diameter (F90-300NP). This increase is attributed to the hydrophobic properties of the silica nanoparticles [52]. The WCA of the samples with the nanoparticles with the highest diameter show a higher range of WCA values, which is explained by the variation in the diameter of the nanoparticles, as observed in figure 2.2. Regarding figure 2.6b, the WCA for the composite samples with the smallest silica

nanoparticles show that the WCA of PVDF fibres increases significantly when compared to the one of PVDF films, and the WCA of the oriented PVDF fibres is slightly higher than the one for randomly oriented PVDF fibres, showing a WCA of 146.0 ± 7.2°. These results support the idea that the increase of the hydrophobicity of electrospun samples is mainly related to the membrane morphology [8], the fibres being significantly more hydrophobic than films. In the case of PVDF films, the WCA is also higher for the films with higher porosity as already reported for pristine films [44].

2.3.1.6 Structural properties and electroactive phase content of the nanocomposites

FTIR-ATR spectra allow to identify and quantify (equation 2.1) the polymer phase present in the samples and, therefore, to evaluate possible modifications induced by the introduction of silica nanoparticles (Figure 2.7).

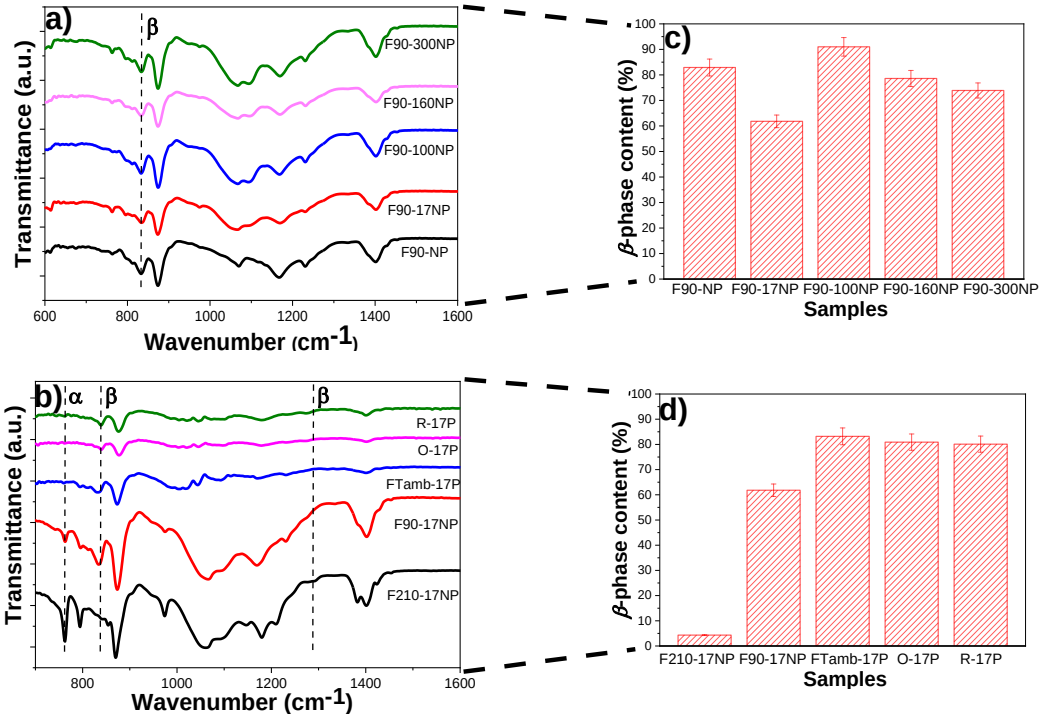

Figure 2.7. FTIR spectra of (a) neat PVDF and SiNPs/PVDF nanocomposites with silica nanoparticles of different diameters processed at 90 °C and (b) different morphologies of SiNPs nanocomposites prepared with the smallest nanoparticles. The β-phase content for the different sample is represented in c) and d).

Figure 2.7a shows the FTIR spectra of the different samples prepared at 90 °C as well as the corresponding quantification of the β-phase content (figure 2.7c, calculated after equation 2.1). The

characteristic bands of β-PVDF (840 cm^{-1}) is present in all samples, with low traces of α-PVDF (bands at 766, 855 cm^{-1}), with the exception of F210-17NP. This is mainly attributed to the processing temperature [48], which mainly governs the solvent evaporation kinetics and the polymer crystallization in the β-phase for processing at temperatures below 90 °C [45]. The introduction of SiNPs in PVDF does not significantly change the β-phase content, independently of the SiNPs content and average diameter. The β-phase value of pristine PVDF is 83 ± 3.3% and for the nanocomposites F90-17NP, F90-100NP, F90-160NP and F90-300NP, is 62 ± 2.5, 91 ± 3.6, 79 ± 3.1 and 74 ± 3%, respectively (figure 2.7c). On the other hand, figure 2.7d shows that depending on the nanocomposite morphology, the polymer crystallizes in different phase, mainly due to the different processing conditions. Thus, electrospinning involves room temperature solvent evaporation and polymer stretching during jet formation, both favorable conditions for the crystallization of the polymer fibres in the β-phase [50]. With respect to the films, the F210-17NP nanocomposite, which is processed by a melting and recrystallization process, crystallizes in the α-phase and shows that the addition of SiNPs does not induce the nucleation of the electroactive β-phase of the polymer, as observed in previous study with Fe_3O_4 spherical nanoparticles [53]. On the other hand, the porous samples, as well as the fibres, are prepared after solvent evaporation at room temperature, conditions leading to the crystallization in the β-phase. This fact is not affected by the introduction of the nanoparticles. Thus, it is concluded that the presence of the nanoparticles does not induce strong interactions with the polymer chain, leading to the nucleation of a specific phase, as observed with other fillers such as CFO [54] and NaY zeolite [44]. Thus, processing temperature and solvent/polymer ratio remains the main factor determining polymer phase content in those composites [41, 45].

2.3.1.7 Thermal behaviour of the nanocomposites

The DSC scans allow to determine the melting temperature and the degree of polymer crystallinity (figure 2.8).

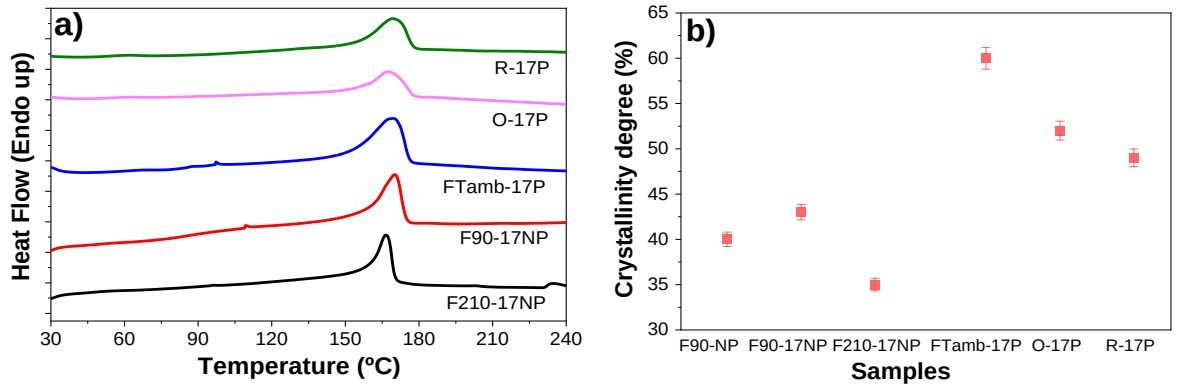

Figure 2.8. (a) DSC thermographs and (b) degree of crystallinity of the SiNPs/PVDF nanocomposites with different morphologies and with the fillers of lowest average diameter.

All the samples show an endothermic peak around 168 °C corresponding to the polymer melting of the crystalline phase [45], thus, both processing conditions and incorporation of the filler does not affect the melting temperature. The degree of crystallinity was calculated (equation 2.2) from the enthalpy of the melting peak of the DSC thermograms. It is not notice that the samples prepared by solvent evaporation at 90 °C and after melting and recrystallization show a lower degree of crystallinity than the samples prepared by solvent evaporation at room temperature, which also includes the electrospun samples (figure 2.8b). The pristine PVDF film processed at 90 °C shows a degree of crystallinity of ≈ 40%, which slightly increases with the introduction of the SiNPs and with the size of the SiNPs, being 43% for F90-17NP and 55% for F90-160NP (data not shown). Relatively to the different morphologies (figure 2.8a), the endothermic peak value is lower for the sample processed at 210 °C, indicating a lower degree of crystallinity if the sample, attributed to the fillers acting as defects during the crystallization from the melt [55]. Inclusion of the nanoparticles in the fibres does not significantly alters the crystallinity degree of the O-17P (52%) and R 17P (49%) with respect to the pristine polymer oriented fibres (50% [8]).

The latter is ascribed to the combined effect of solvent evaporation at room temperature and stretching during the crystallization process that overcome the effect of the presence of NP.

2.3.1.8 Mechanical properties of the nanocomposites

The mechanical properties of the materials are essential parameters to design a scaffold suitable for tissues with different mechanical characteristics. The characteristic mechanical strain-stress curves of samples with different morphology, filler type and content are presented in figure 2.9.

Figure 2.9a shows the stress-strain curves for the nanocomposites prepared with fillers with different average diameter after a melting process and figure 2.9b refers to the nanocomposites with the same

SiNPs (17 nm) after different processing conditions. Independently of the filler average diameter or processing conditions all samples show the typical mechanical behaviour of PVDF [56] characterized by the elastic region, yielding and plastic region, i.e. the typical behaviour of a thermoplastic elastomer.

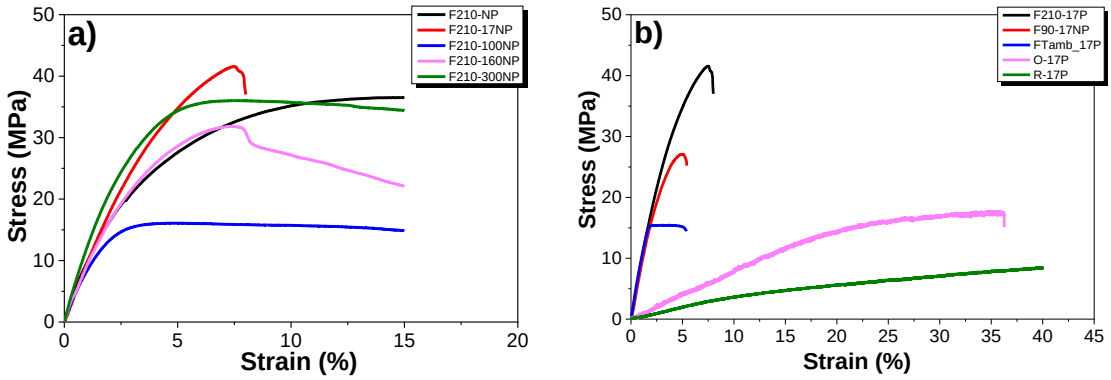

Figure 2.9. Stress-Strain curves for (a) SiNPs/PVDF nanocomposites with different SiNPs average diameters within the PVDF matrix and (b) for nanocomposites obtained after different processing conditions.

The Young modulus of the samples was calculated from the linear zone of elasticity between 0 and 1% strain, as presented in figure 2.10.

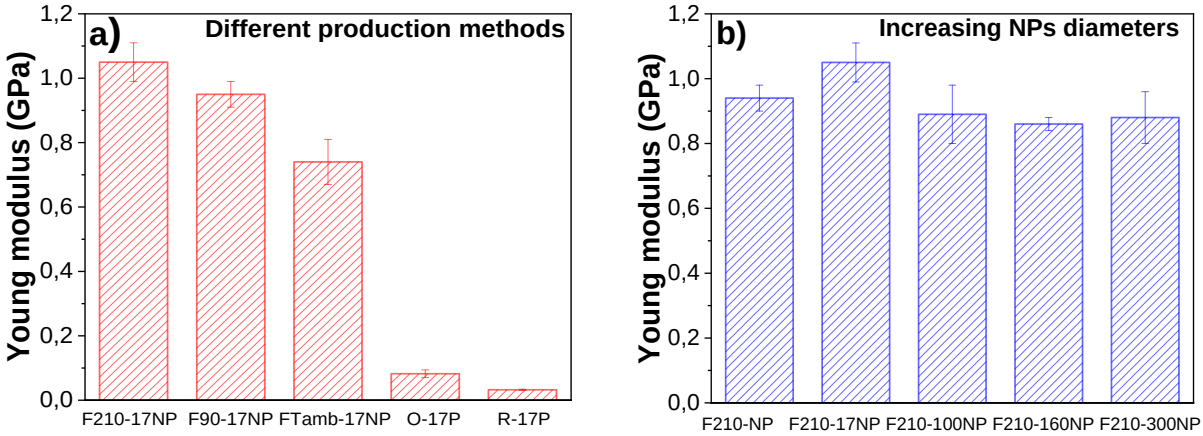

Figure 2.10. Young modulus of the SiNPs/PVDF nanocomposites varying (a) the processing method and (b) the average diameters of the SiNPs. The values shown as mean ± SD.

The characteristic features of the strain-stress curves are similar for all the materials, demonstrating that the mechanical characteristics are not strongly dependent on nanoparticle diameter. Further, the introduction of particles with different diameters does not significantly affect the Young modulus of the pristine PVDF (F210-NP) - 0.94 ± 0.04 GPa. However, a slight improvement of the Young modulus is

observed for the samples prepared with smaller silica nanoparticles (F210-17NP): 1.05 ± 0.06 GPa, this is in line with reports showing that the modulus increases as the particle size decreases [57]. Relatively to the different production methods for the polymer films, F210-NP, F90-17NP and Ftamb-17P, it is observed that the more porous is the structure, the lower is the Young modulus, 0.83 ± 0.16 GPa for FTamb-17P. On the other hand, oriented fibres (O-17P) show higher Young modulus (0.082 ± 0.012 GPa) than the random fiber samples (R-17P) (0.032 ± 0.002 GPa) due to the larger number of fibres along the stretch direction [8].

Relatively to the other samples, the production method has a relevant influence on their mechanical response, as the samples prepared at room temperature by solvent evaporation showing lower Young modulus than those obtained at 210 °C, due to the porous nature of the former and the compact structure of the later, as was also visible in the SEM images (figure 2.4).

2.3.1.9 Cell culture studies

In order to explore the potential use of the developed materials in TE applications, it is necessary to evaluate the putative cytotoxicity of the samples. The study of metabolic activity of C2C12 myoblasts, evaluated with the MTS assay, was applied to all samples and the results for 24 and 72 h are presented in figure 2.11. Thus, the effects associated with introducing fluorescent SiNPs with different sizes is analyzed as well as the effect of the different microstructures/morphologies.

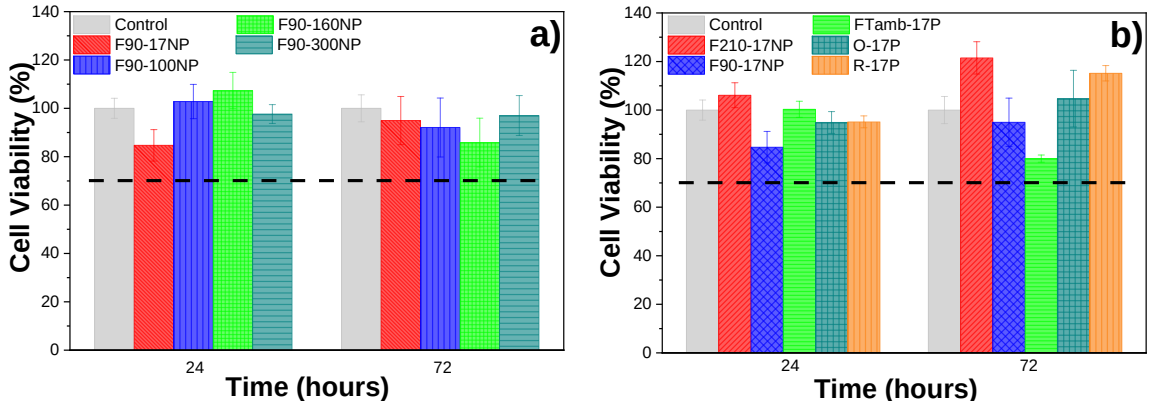

Figure 2.11. Cytotoxicity indirect test of (a) samples prepared with nanoparticles of different diameters and prepared by solvent evaporation at 90 °C and (b) samples prepared with SiNPs of 17 nm diameter after different processing methods and therefore with different morphologies.

It has been already reported that PVDF is biocompatible and shows no cytotoxicity to C2C12 cells for 24 or 72 h [29, 38]. The SiNPs are also biocompatible for many cells including C2C12 myoblasts [58-60].

Thus, figure 2.11 shows that none of the samples are cytotoxic, independently of the nanoparticle diameter and of the material morphology. It is to notice that despite both materials being biocompatible, the result is not evident, as polymer-filler interface effects or solvent retained in the nanoparticles or in the interface areas, can lead to cytotoxic effects. According to the ISO standard 10993-5, samples are considered cytotoxic when cells suffer a viability reduction larger than 30%. The measured cell viability values are all higher than 70%, confirming the cytocompatibility of the SiNPs/PVDF nanocomposites.

C2C12 myoblasts were used in previous studies to analyze cell proliferation of cultures grown on porous [61] and non-porous [38] PVDF films as well as fibres [38], with the verification that C2C12 cells proliferate better on piezoelectric β-PVDF "poled" samples. The samples obtained in this work were studied to determine the suitability for TE applications, namely muscle tissue.

The MTS (figure 2.12), immunofluorescence (figure 2.13) and SEM (figure 2.14) assays were used to assess cell viability and morphology in the different samples. Relatively to the proliferation results (Figure 2.12), the cell viability has been obtained in relation to the sample of F90-NP at 24 h (equation 2.7).

$$Cell\ Viability\ (\%) = \left(\frac{Absorbance\ of\ samples\ at\ 72h}{Absorbance\ of\ F90\text{-}NP\ at\ 24h} \times 100\right) - cell\ viability\ of\ F90\text{-}NP\ at\ 24h \quad (2.7)$$

Figure 2.12 shows that cell viability of the samples increases after 72 h of cell culture, independently of the SiNPs diameters (figure 2.12a) and the morphology of the materials (figure 2.12b), when compared with the sample without particles (F90-NP). No significant differences are observed between the samples and the negative control (F90-NP), revealing that C2C12 myoblast proliferation is not affected by the presence of SiNPs in the PVDF matrix. In fact, it has been reported that SiNPs included in different polymers improves cell attachment and proliferation, and enhances cellular processes [62-63], which is in agreement with the obtained results.

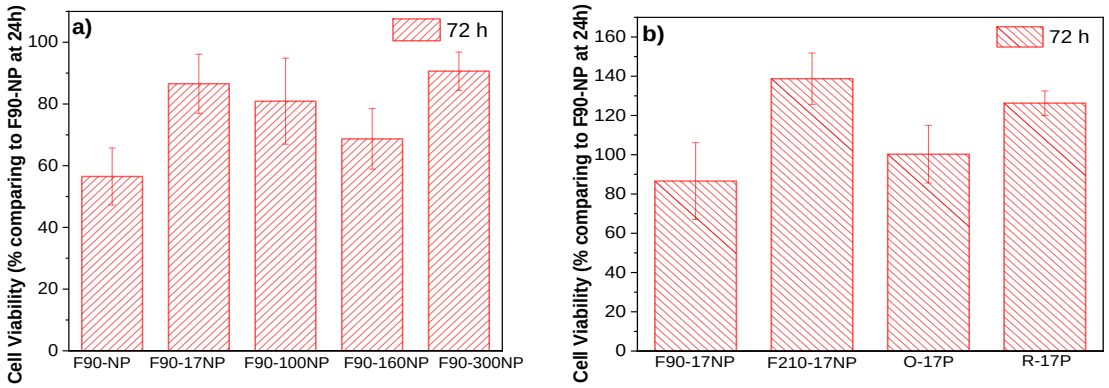

Figure 2.12. Cell proliferation of C2C12 cells seeded on (a) SiNPs/PVDF samples prepared at 90 °C with different sized nanoparticles and (b) SiNPs/PVDF samples with different morphologies.

Cell cytoskeleton morphology, viability and adhesion were analyzed by fluorescence microscopy for porous and non porous films and SEM for fibre samples.

Independently of the nanoparticles diameters and the sample morphology, it is observed that the cell behaviour is similar. Bigger cell agglomerates are observed with increasing nanoparticles diameter (which also show larger nanoparticle agglomerates) on the samples (figure 2.13 a-d). This fact is associated with the interaction between serum proteins and nanoparticles present on the PVDF matrix, as it has been reported that negative surface charge enhance the adsorption of proteins with isoelectric point more than 5.5 such as immunoglobulin G that can be important for C2C12 myoblasts [64-65]. Cell cultures on PVDF fibres prepared with the smaller silica nanoparticles were analyzed by SEM and figure 2.14 shows the cell morphology of C2C12 cells after 72 h of cell culture on oriented and random PVDF fiber nanocomposites.

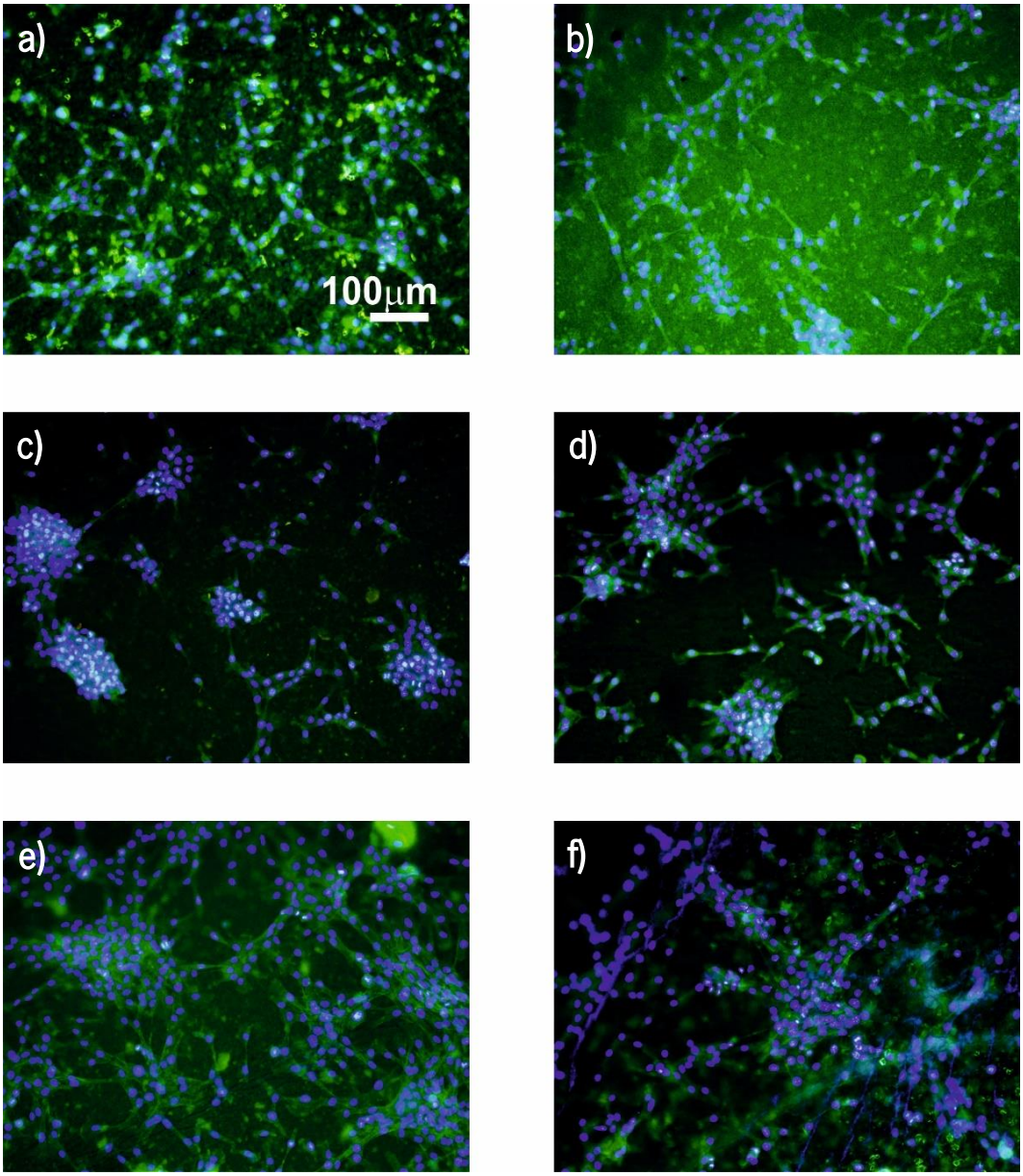

Figure 2.13. Representative images of C2C12 myoblast culture after 72 h on (a) F90-17NP, (b) F90-100NP, (c) F90-160NP, (d) F90-300NP, (e) F210-17NP and (f) FTamb-17P samples (nucleus stained with DAPI-blue and cytoskeleton stained with FITC-green). Scale bar = 100 μm for all the samples.

These representative images demonstrate that in the presence of fibrillar microstructure the muscle cells orientate their cytoskeleton along the fibres, which is in agreement with the literature [38]. In this way, in the presence of oriented fibres, the cells share a similar architecture to the natural muscle cells in living systems.

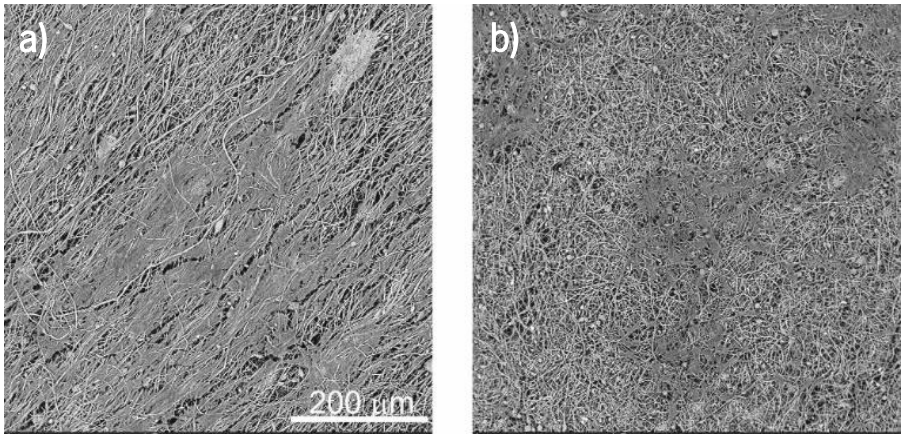

Figure 2.14. Cell morphology obtained by SEM of C2C12 myoblasts seeded on PVDF fibres: (a) O-17P and (b) R-17P, after 3 days of culture. The scale bar is 200 µm for all samples.

Thus, the overall results prove the potential of the use of SiNPs/PVDF piezoelectric nanocomposites for muscle TE. Physical and chemical stimuli are important factors to obtain tissues with characteristics similar to those of natural living tissues in the human body, developing therefore specific biomimetic microenvironments for different tissues, attending their specific biophysico-chemical needs. The developed platform presents nanocomposites with different morphologies (membranes and fibres), piezoelectric β-phase and SiNPs diameter (from 17 to 300 nm), which makes it an interesting and complete platform for TE.

Furthermore, this platform will allow further studies applying mechanical stimuli on the nanocomposites obtained in this work with specific bioreactors [36] applying mechanical and/or mechanoelectrical stimuli. It may also take advantage of the SiNPs capacity to include specific biomolecules or to develop drug delivery systems, or more specifically, differentiation factors to promote directed myogenic differentiation. This will allow not only a deeper knowledge of the necessary stimuli for muscle tissue regeneration, but also more effective therapies.

After the study with different diameter of SiNPs, the functionalization of these nanoparticles was performed in order to verify if this parameter can nucleate the β-phase of PVDF.

2.3.2 Influence of different SiNPs functionalizations

2.3.2.1 Characterization of the silica nanoparticles

The SiNPs morphology was analyzed by TEM and the corresponding hydrodynamic size was obtained by DLS (figure 2.15a). The zeta potential in aqueous dispersions at different pH for the three different SiNPs was also evaluated (figure 2.15b).

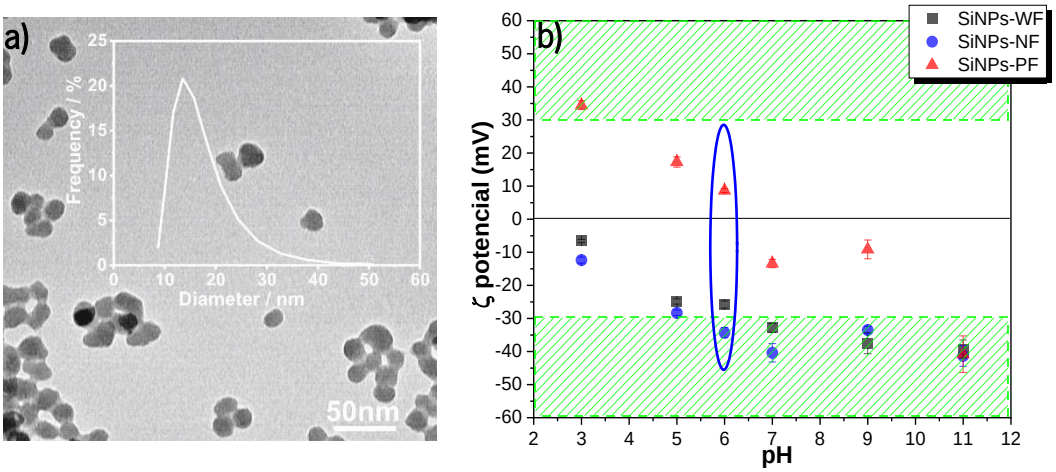

Figure 2.15. (a) Representative TEM images of SiNPs doped with PDI and the respective size by DLS and (b) zeta potential values at different pH for the three different nanoparticle types.

The TEM image of figure 2.15a show that the SiNPs present a spherical shape. From the dynamic light scattering measurements presented as inset in figure 2.15a, the diameter of the SiNPs is ≈ 16 ± 1 nm.

The surface charge and the stability of the three different types of SiNPs (WF, NF and PF) against aggregation was evaluated by the zeta potential measurements of the NPs in aqueous dispersions at different pH between 3 and 11 (figure 2.15b).

Figure 2.15b shows that SiNPs-WF and NF are negatively charged, independently of the pH, increasing the surface charge with increasing pH. On the other hand, for the SiNPs-PF the positive charge (pH ≤ 6) decreases and turns to negative values with increasing pH for pH > 6. Further, SiNPs-WF and SiNPs-NF are more stable than SiNPs-PF for pH higher than 5, the stabilty of SiNPs-PF (pH higher than |-30| mV) being observed pH above 10 and below 4. In these pH ranges, the -potential values indicate higher peripheral charge values, contributing for the nanoparticle repulsion and stability, preventing aggregation and precipitation [66].

2.3.2.2 Morphological evaluation of the nanocomposites

The morphology of the SiNPs/PVDF nanocomposite samples with different SiNPs contents and types was analyzed by SEM. Figure 2.16 shows the cross-section SEM images of pristine PVDF and SiNPs-PF/PVDF nanocomposites with 8 and 32 wt.% SiNPs-PF. Similar results are observed for the other nanocomposites with different contents and SiNPs types.

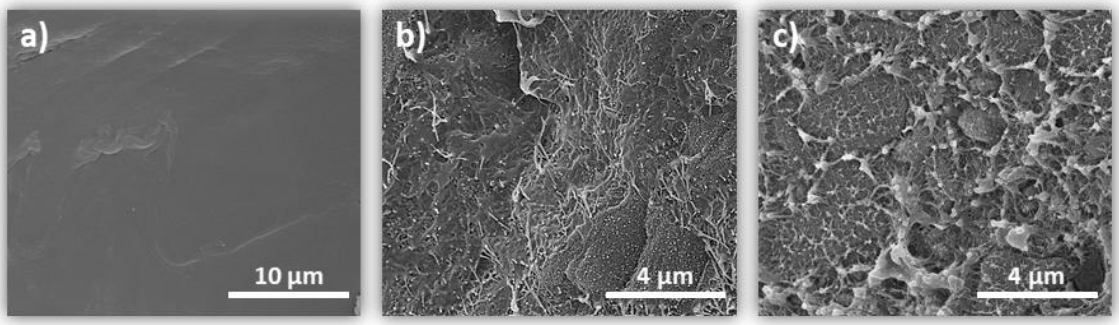

Figure 2.16. Cross section SEM images of (a) pristine α-PVDF, (b) 8 wt.% SiNPs-PF/PVDF and (c) 32 wt.% SiNPs-PF/PVDF.

Figure 2.16a shows that the PVDF film presents a homogeneous and flat surface morphology without the absence of pores. Figure 2.16b shows that the SiNPs-PF are well dispersed within the polymer for the lower filler contents but that, for the largest filler concentrations (figure 2.16c), some agglomeration occurs although without the presence of large silica clusters. As the same morphological features are observed for SiNPs-WF and SiNPs-NF nanocomposites, it is demonstrated that the surface charge of the SiNPs does not have a relevant effect on the morphology of composites.

2.3.2.3 Samples Wettability

Surface wettability was assessed for the different nanocomposites through the sessile drop technique and the results are presented in figure 2.17.

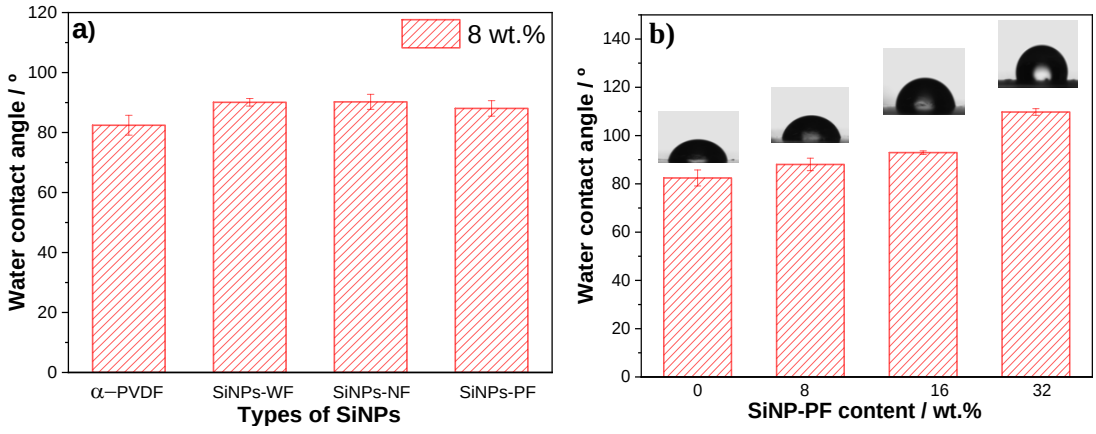

Figure 2.17. Water contact angle measurement for pure PVDF and the different nanocomposite films (mean ± SD). (a) nanocomposites with different SiNPs surface functionalization and (b) SiNPs-PF/PVDF nanocomposites with different filler content.

Figure 2.17a shows that there are no significant differences in the surface wettability of the PVDF composites containing different SiNPs. All the samples show WCA values around 90°, which are slightly higher than pristine α-PVDF, which shows a WCA of 82°. Figure 2.17b also shows that higher content of silica nanoparticles leads to a higher increase in the WCA values of all the samples, up to ≈ 110° for the samples with 32 wt.% filler content. This increase of the hydrophobicity is associated to the increase of the surface roughness, related to the inclusion of the fillers [67]. In fact, it is to notice that the surface chemistry is the same for pristine polymer and nanocomposites, as the fillers are within the polymer matrix and not at the surface. This correlation between morphology and hydrophobicity in PVDF microporous membranes with increasing has been reported for SiNPs fillers [68] as well as for NaY incorporation into PVDF [44].

2.3.2.4 Structural Characterization

In order to evaluate the variation in the crystalline phase content of PVDF due to the inclusion of SiNPs with different surface charges and content, FTIR-ATR measurements were performed (figure 2.18).

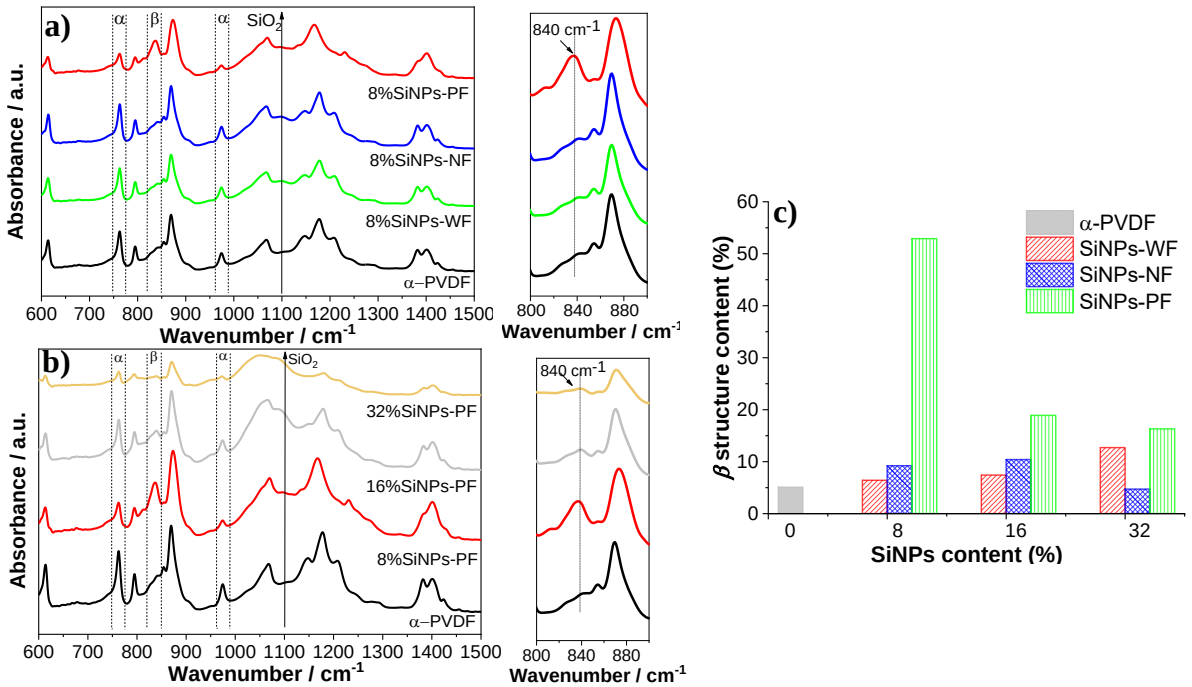

Figure 2.18. ATR-FTIR spectra of (a) nanocomposites with 8 wt.% filler content of the SiNPs with different surface functionalization (without, negative and positive functionalization, WF, NF and PF, respectively) and (b) three different SiNP contents (8, 16 and 32 wt.%) for the SiNPs-PF/PVDF nanocomposites. (c) β-PVDF phase content for the different composites.

Figures 2.18a and 2.18b show the FTIR spectra of α-PVDF and the different nanocomposites prepared after polymer melting and solvent evaporation at 210 °C as well as the corresponding quantification of the β-phase content present in the nanocomposites, calculated after equation 2.1 (figure 2.18c).

The chemical structure of PVDF is composed by the repetition unit -CH_2-CH_2- along the polymer chain and characteristic vibrational modes can be used for the identification and quantification of the α- and β-phases [45]. In particular, the absorption band at 766 cm^{-1} corresponds to the α-phase and is related to stretching of the CF_2, whereas the band at 840 cm^{-1} corresponds to the β-phase and is related to the CH_2 stretching In Figures 2.18a and 2.18b the absorption band characteristic of the SiNPs is identified at 1100 cm^{-1}, and is related to the anti-symmetric stretching mode of the Si-O-Si group [69]. Thus, it confirmed the successful inclusion of SiNPs in the PVDF nanocomposites. Further, the intensity of this absorption band increases with increasing SiNPs content from 8 to 32 wt.%.

Figure 2.18a and 2.18b show that no chemical modifications occur in the PVDF polymer chain upon the incorporation of the fillers, however, it is observed that the intensity of the absorption band at 840 cm^{-1}, related to the β-phase of the polymer, increases for the sample containing silica nanoparticles with positive functionalization.

In fact, as figure 2.18c shows, the type and content of SiNPs influence significantly the content of β-phase. Comparatively to the pristine PVDF film, which shows a β-phase content of ≈ 5%, the nanocomposites with 8 wt.% SiNPs content with fillers without and with negative and positive functionalization, show β-phase contents of 6, 9 and 53%, respectively. In this sense, the inclusion of positive SiNPs induce a significant increase of the electroactive phase, contrarily to the other nanoparticles, being an indicative that the SiNPs-PF acts as nucleating agents of this phase during the PVDF crystallization [45], mainly due to the interaction between the CF_2 groups of PVDF with the positive charge of the SiNPs. Further, these results are also an indicative that this positive particle functionalization leads to a more effective particle-polymer chain interaction than the negative functionalization of the fillers.

It has been reported that nanoparticles with negative surface charge are more efficient in promoting the nucleation of the β-phase of PVDF [45, 70, 71]. Nevertheless, it has been also proven that not just the surface charge, but also the size and shape of the nanoparticles influences this process [53, 70]. Thus, in the present case the interplay of SiNPs filler size (table 2.2) and positive functionalization improve the nucleation of the electroactive phase more efficiently due to improved local particle-chain interactions. In fact, it has been shown that the addition of small organic positively charged molecules in the molten

state results in polar phases dominated by β-phase PVDF once these molecules excluded the possibility of lattice matching or epitaxial crystallization [72].

Further, the relative β-phase content in the samples also depends on the content of filler within the polymer matrix. For SiNPs-WF/PVDF nanocomposites, the β-phase slightly increases with increasing SiNPs-WF content from 6 to 12.7%. However, a decrease in the electroactive phase is observed with increasing filler content of charged SiNPs into the polymer matrix from 8 to 32 wt.%. Relatively to the SiNPs with negative functionalization, these nanocomposites present a slightly higher value of β-phase than pristine α-PVDF, 10.4% (with 16 wt.% filler content) that decreases with the introduction of 32 wt.% of nanoparticles (5%). A similar behaviour is observed for the SiNPs-PF/PVDF samples, decreasing the content of β-phase with increasing SiNPs content. This behaviour has been already reported in the literature for related nanoparticles [69] and other types of nanoparticles [73] and in attributed to the loss of efficient particle-polymer interactions once nanofiller agglomerations occur for larger filler contents.

The piezoelectricity of the β-phase nucleated nanocomposite samples was evaluated by measuring d_{33} coefficient of corona poled samples, leading to a d_{33} around 5 pC.N^{-1} for the 8 wt.% SiNPs-PF/PVDF sample. This d_{33} value is lower than for pristine β-PVDF [41, 45] without fillers, mostly due to increased mechanical stiffness and interfacial effects, however being among the highest values among polymer materials and suitable for applications.

2.3.2.5 Thermal characterization

To investigate the influence of SiNPs type and content in the thermal properties of PVDF, DSC and TGA analysis was performed. Figures 2.19a and 2.19b show the DSC thermograms of neat PVDF and the different SiNPs/PVDF nanocomposites.

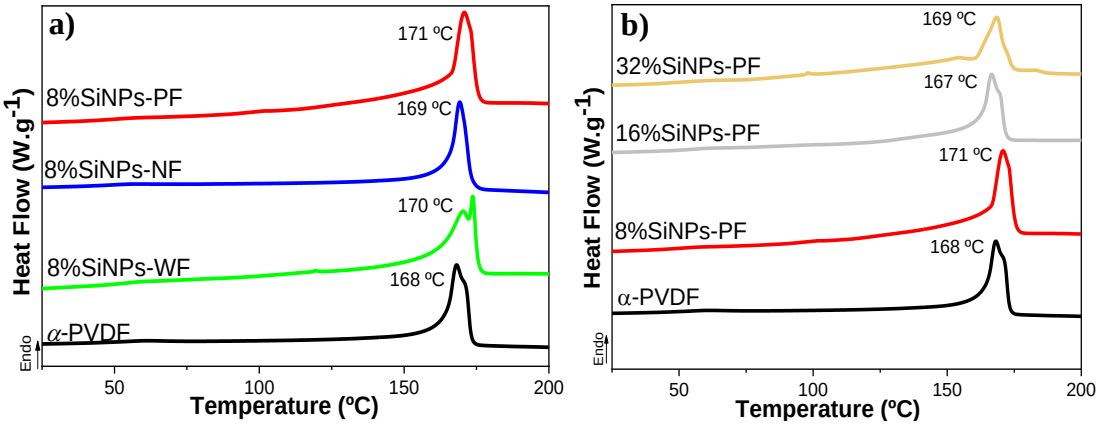

Figure 2.19. DSC thermograms for SiNPs nanocomposites with different (a) types of SiNPs for a filler content of 8 wt.% and (b) different SiNPs-PF contents.

Neat α-PVDF exhibits an intense endothermic peak at 168 °C corresponding to the melting peak of PVDF [45]. The inclusion of different types and contents of SiNPs does not lead to any relevant modification in the melting behaviour (figure 2.19a and 2.19b) of the samples, the nanocomposite films being also characterized by a single peak corresponding to the melting temperature between 167-171 °C. The melting temperature, the enthalpy associated to each endothermic peak and the degree of crystallinity of the samples, as obtained after equation 2.2, are presented in table 2.4.

Table 2.4. T_m and degree of crystallinity of PVDF and SiNPs/PVDF nanocomposites samples.

SAMPLE	wt.% SINPS	TYPE OF SINPS	T_m (°C)	X_c (%)
α-PVDF	—	—	168	57.2 ± 1.14
SINPS/PVDF	8	WF	170	50.5 ± 1.01
		NF	169	49.1 ± 0.98
		PF	171	51.1 ± 1.02
	16	PF	167	47.5 ± 0.95
	32	PF	169	30.3 ± 0.61

Table 2.4 shows the melting temperature, T_m, and degree of crystallinity, X_c, of PVDF and SiNPs/PVDF nanocomposite samples. It is verified that the crystallinity of PVDF (≈ 57%) suffers a similar decrease by the inclusion of the fillers (8 wt.% of SiNPs-WF ≈ 51%, SiNPs-NF ≈ 49% and SiNPs-PF ≈ 51%), independently of the SiNPs surface charge. Further, the decrease of the degree of crystallinity is more pronounced for larger filler contents (32 wt.%, the SiNPs ≈ 30%) showing that the fillers act as defects during the crystallization of the polymer. No significant differences are observed in the melting temperature, being the variations within experimental error (2%).

The thermal degradation of PVDF and the different SiNPs/PVDF nanocomposites is presented in figure 2.20.

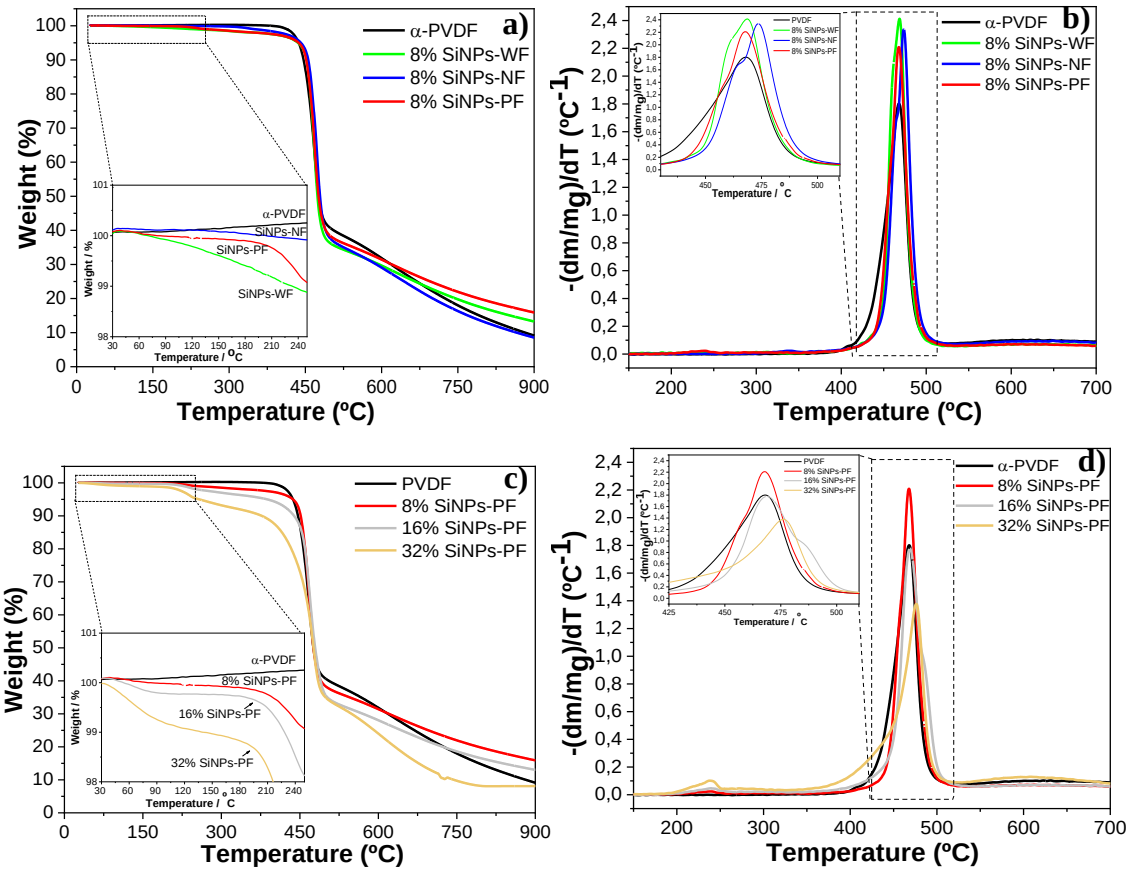

Figure 2.20. TGA thermograms (a, c) and corresponding first derivatives (b, d) for (a, b) nanocomposites with 8 wt.% SiNPs with different functionalizations and (c, d) SiNPs-PF nanocomposites with different SiNPs contents.

Figure 2.20a and 2.20c shows that all samples are characterized by a similar thermal degradation profile, independently to the filler type and concentration. The thermal degradation of the different PVDF samples occurs in one main weight loss step, corresponding to the scission of the carbon-hydrogen (C-H) bonds, followed by the carbon-fluorine bonds (C-F) due to the strength of the C-F bonds when compared with the C-H bonds [74]. Figures 2.20c also allow to identify a weight loss starting at temperature below 60 °C, which is proportional to the filler content and therefore related to degradation at the filler-polymer interface, in particular due to the nanofiller functionalization. The Differential Thermogravimetric, DTG, analysis (Fig. 2.20b and 2.20d) allows to identify the temperature of maximum rate of weight loss, which is approximately 467 °C for PVDF, with no significative differences for the different SiNPs/PVDF film composites.

2.3.2.6 Mechanical characterization

The mechanical stress-strain response of the samples is presented in figure 2.21. The corresponding Young's modulus, tensile strength and strain-to-failure are presented in table 2.5.

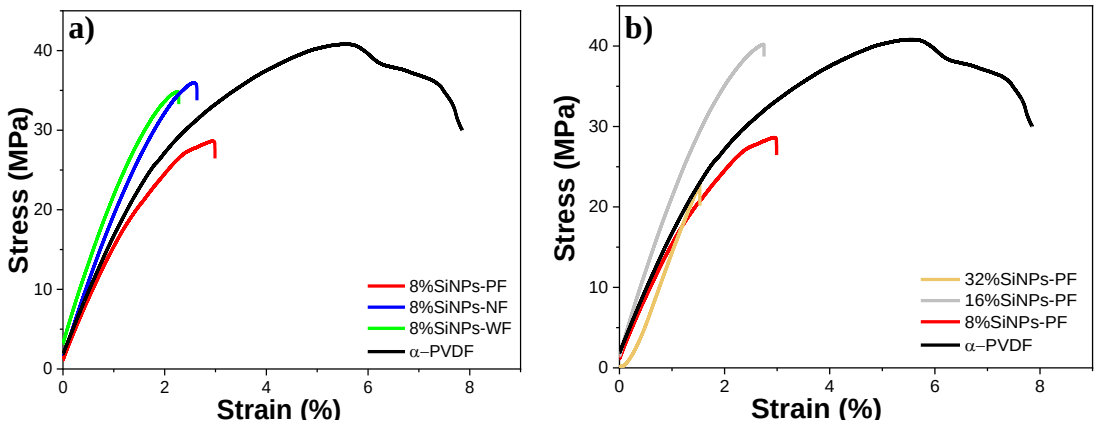

Figure 2.21. Representative stress-strain curves of the PVDF samples with (a) 0, 8, 16 and 32 wt.% SiNPs-PF nanoparticles and (b) SiNPs/PVDF nanocomposites with 8 wt.% of SiNPs with different surface characteristics.

Figure 2.21 shows that all samples show the typical behaviour of PVDF, characteristic of thermoplastic materials, showing a nearly linear region for strains below 1%, followed by a plastic deformation stage before the sample undergoes fracture. The main different of pristine PVDF with the nanocomposites is that, for the later, the elongation at break is significantly lower. Pristine PVDF shows an average Young's modulus of 1.23 ± 0.68 GPa, an average ultimate tensile strength of 37.42 ± 2.21 MPa and an average strain-to-failure of 7.30 ± 1.13% (Table 2.5), within the typical value range of PVDF films [8, 75].

Table 2.5. Mechanical properties of α-PVDF and SiNPs/PVDF nanocomposites incorporating 8, 16 and 32 wt.% of SiNPs with different surface functionalizations. E – Young's modulus; σ_{break} – ultimate tensile strength; ε_{break} – strain-to-failure.

Sample	E ± StdDev (MPa)	σ_{break} ± StdDev (MPa)	ε_{break} ± StdDev (%)
α-PVDF	1231 ± 48	37.42 ±2.21	7.30 ± 1.13
8 wt.% - WF	1463 ± 131	40.39 ± 8.49	4.69 ± 2.27
8 wt.% - NF	1500 ± 141	35.49 ± 2.09	3.21 ± 0.57
8 wt.% - PF	1492 ± 131	30.94 ± 4.11	2.85 ± 0.48
16 wt.% - PF	1916 ± 154	39.39 ± 3.70	2.59 ± 0.17
32 wt.% - PF	1925 ± 146	22.96 ± 0.92	1.34 ± 0.18

Table 2.5 shows that, independently of the SiNPs type, the Young's modulus increases with the incorporation of the SiNPs fillers as well as with increasing filler content. Thus, the Young's modulus is 1916 and 1925 MPa, respectively for 16 and 32 wt.%, which is a ≈ 56% increase with respect to pure PVDF. Thus, the inclusion of the filler acts as reinforcement of the material as demonstrated for others nanofillers [8]. Relatively to the ultimate tensile strength and strain, SiNPs/PVDF nanocomposites films shows a lower elongation at fracture than the pristine polymer, which decreases with increasing SiNPs content, with no significant differences between the different types of silica nanoparticles. This decrease on tensile strength is related to the defective interfaces between polymer and nanofillers, leading to act as defects, leading to early fracture [76].

2.3.2.7 Electrical response

The effect of the SiNPs inclusion in the dielectric response of PVDF was evaluated as a function of frequency (Figure 2.22).

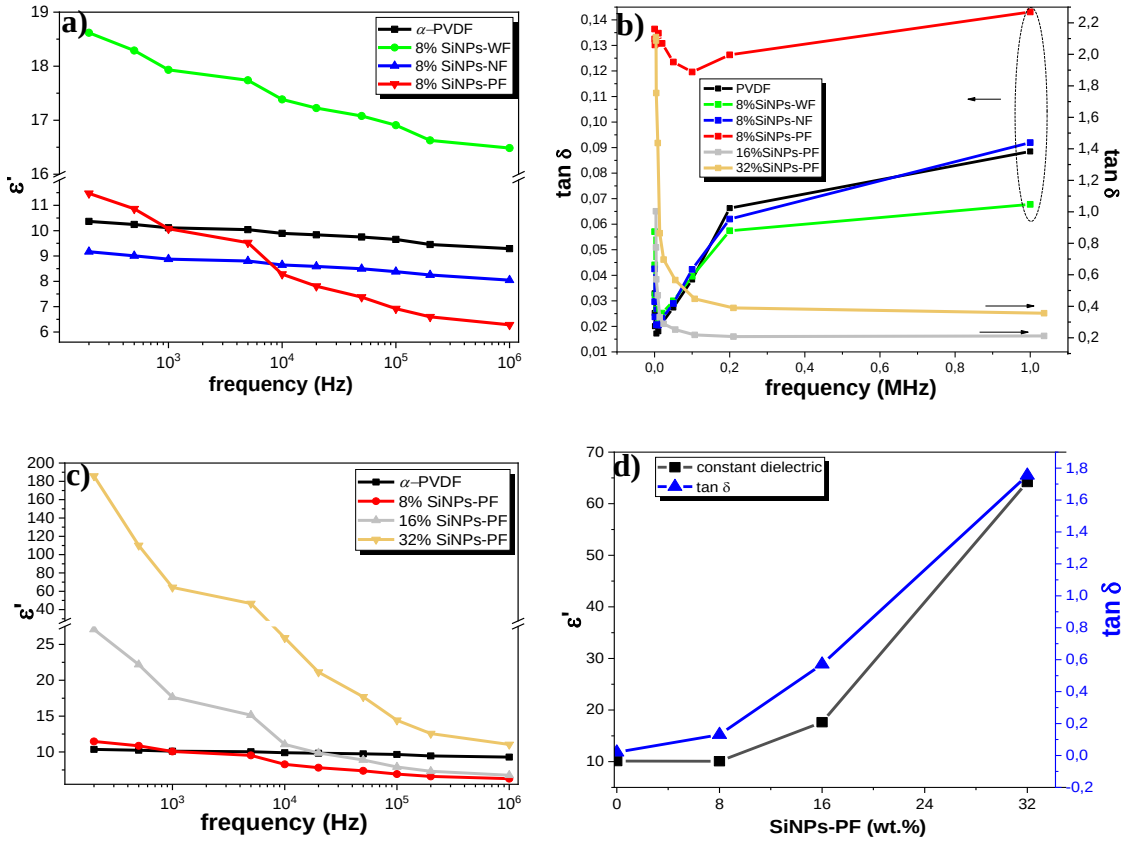

Figure 2.22. Frequency dependence of the real part of the dielectric permittivity (a) for the pristine polymer and nanocomposites with 8 wt.% filler content with fillers with different functionalization and (c) SiNPs/PVDF nanocomposites with positive functionalized nanoparticles at different filler contents. Frequency dependence of the (b) loss tangent for all nanocomposites and (d) dielectric constant and loss tangent for a frequency of 1 kHz as a function of filler content.

Independently of the filler type and content, the dielectric constant decreases with increasing the frequency, showing the relaxation behaviour of dipolar dynamics [77]. It is also worth noticing that the dielectric constant of the composites depends on the nature of SiNPs and content (figure 2.22a and 2.22c). Thus, the highest dielectric constant values are observed for 8% SiNPs-WF (Figure 2.22a), whereas the lowest values are observed for the SiNPs-NF and SiNPs-PF, indicative of the interaction between the SiNPs with the PVDF polymer chain, that reduces the segmental motion of PVDF chain, as well as Maxwell-Wagner-Sillars interfacial contributions [78] induced by the introduction of the non-treated nanofillers, promoting a reduction in the electrical polarization variations under applied field. In fact, this is also verified by the lower frequency dependence of the dielectric constant with frequency for the composites with charged nanofillers. On the other hand, the dielectrically response strongly increases

with increasing filler content, due both to the dielectric contribution to the filler and to the increase number of polymer-filler interfaces (figure 2.22c).

The frequency dependence of the dielectric loss tangent (tan δ) for PVDF and SiNPs/PVDF composites is shown in figure 2.22b for various frequencies and figure 2.22d for 1 kHz as a function of filler content. The tan δ of a material denotes quantitatively dissipation of the electrical energy. The tan δ is higher than PVDF for all the composites except for the 8 wt.% SiNPs-WF/PVDF and SiNPs-NF/PVDF composites which no significative differences (figure 2.22b) were observed, demonstrating the interfacial contributions and increased electrical conductivity. Thus, the tan δ also increases with increasing filler content in the polymer matrix (figure 2.22d).

The a.c. and d.c. conductivity of pristine PVDF and SiNPs/PVDF composites were evaluated, and the results are shown in figure 2.23.

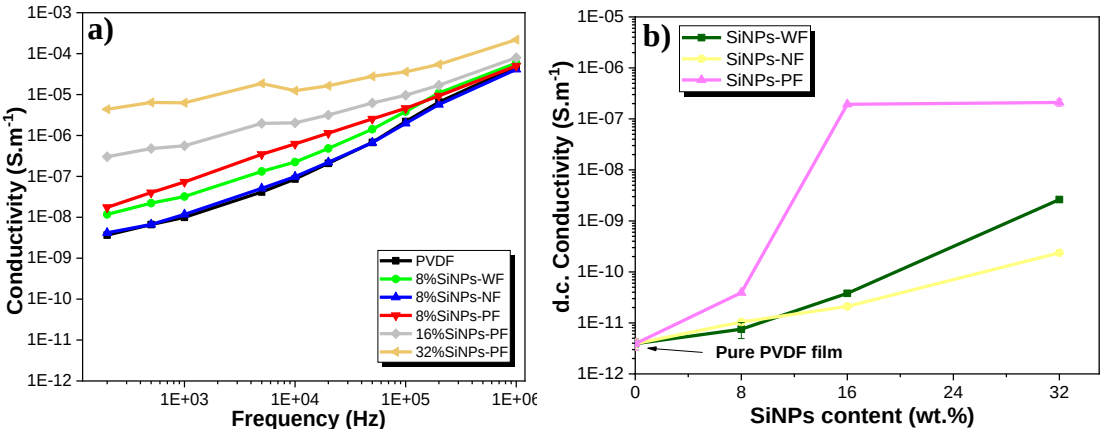

Figure 2.23. Electrical a.c. e d.c. conductivity of pristine PVDF pure and the different nanocomposites as a function of (a) frequency and (b) SiNPs type and content.

Independently of the SiNPs functionalization and functionalization type, the introduction of SiNPs within the polymer matrix substantially improves the electrical a.c. (figure 2.23a) and d.c. (figure 2.23b) conductivity of the films, which further increases with increasing frequency and SiNPs content, respectively. This increase is more noticeable for the PVDF films containing positive functionalized SiNPs (up to 2.1×10^{-7} S.m^{-1}) being an indicative of higher mobility of charges species at the particle-polymer interfaces. From figure 2.23, it is also noticed that the electrical conductivity values of the negative functionalized SiNPs are lower than those of non-functionalized SiNPs, reaching a maximum of 2.4×10^{-9} S.m^{-1} and 2.6×10^{-9} S.m^{-1}, respectively. The obtained results can be related with the content of the electroactive phase: the incorporation of positive functionalized SiNPs leads to the highest β-phase

content, when compared with the negative and non-functionalized SiNPs, resulting from the higher interactions between the positive charge of the particles and the PVDF. These interactions enhance the polar phase content, which improves charges mobility and, therefore, electrical conductivity [79].

2.4 Conclusions

Different parameters important for TE, such as materials morphology, porosity and the PVDF electroactive phase, were modified in the obtained membranes.

Different diameters of silica nanoparticles have been introduced within PVDF polymer matrix to obtain multifunctional samples for TE applications.

It is observed that the introduction of the SiNPs fillers in the PVDF matrix decreases its wettability. Further, it is shown that the filler diameter does not significantly affects the properties of the polymer matrix, such as physico-chemical, thermal and mechanical properties.

SiNPs with specific surface functionalization allows to tailor the electroactive β-phase content of PVDF. Positive SiNPs functionalization allows to obtain ≈ 53% β-phase content with 8 wt.% filler content. These results lead to the conclusion that the formation of the polar phase is due to interactions between the positively charged SiNPs surface and the CF_2 dipoles. The mechanical properties depend on the content of SiNPs but is independent of the functionalization type as well as the degree of crystallinity of the samples, which depends on filler content rather than on filler type. Finally, the electrical response of the composites, increase of the dielectric constant and electrical conductivity, is mainly determined by interfacial effects which depend on particle surface charge and content.

Cytotoxicity assays with C2C12 cells show no cytotoxic associated with neat PVDF and composites with different SiNPs diameters and sample morphologies.

Thus, it is demonstrated that the developed platform of PVDF materials with silica nanoparticles demonstrates a large potential for TE applications allowing to develop electromechanically active microenvironments with different morphologies with SiNPs allowing protein functionalization and/or controlled release of specific drugs and/or growth or differentiation factors according the targeted application. In this way, the present work opens new perspectives for advanced composites comprising electroactive PVDF and SiNPs, with tailorable electro-mechanical properties for specific applications.

2.5 References

1. Camargo, P.H.C., Satyanarayana, K.G. and Wypych, F., *Nanocomposites: Synthesis, Structure, Properties and New Application Opportunities.* Materials Research-Ibero-American Journal of Materials, 2009. **12**(1): p. 1-39.

2. Muller, K., et al., *Review on the Processing and Properties of Polymer Nanocomposites and Nanocoatings and Their Applications in the Packaging, Automotive and Solar Energy Fields.* Nanomaterials, 2017. **7**(4): p. 74.
3. Raji, M., et al., *Effect of silane functionalization on properties of polypropylene/clay nanocomposites.* Composites Part B: Engineering, 2018. **146**: p. 106-115.
4. Ribeiro, S., et al., *Electrospun styrene-butadiene-styrene elastomer copolymers for tissue engineering applications: Effect of butadiene/styrene ratio, block structure, hydrogenation and carbon nanotube loading on physical properties and cytotoxicity.* Composites Part B: Engineering, 2014. **67**: p. 30-38.
5. Narayanan, K.B. and Han, S.S., *Dual-crosslinked poly(vinyl alcohol)/sodium alginate/silver nanocomposite beads - A promising antimicrobial material.* Food Chemistry, 2017. **234**: p. 103-110.
6. Santiago, A.M., et al., *Multifunctional Hybrid Silica Nanoparticles with a Fluorescent Core and Active Targeting Shell for Fluorescence Imaging Biodiagnostic Applications.* European Journal of Inorganic Chemistry, 2015. **2015**(27): p. 4579-4587.
7. Cardoso, V.F., et al., *Fluorinated polymers as smart materials for advanced biomedical applications.* Polymers, 2018. **10**(2): p. 161.
8. Maciel, M.M., et al., *Relation between fiber orientation and mechanical properties of nano-engineered poly(vinylidene fluoride) electrospun composite fiber mats.* Composites Part B: Engineering, 2018. **139**: p. 146-154.
9. Cardoso, V.F., et al., *Advances in Magnetic Nanoparticles for Biomedical Applications.* Advanced Healthcare Materials, 2017. **7**(5): p. 1700845.
10. Liu, D., et al., *Cavitation in strained polyethylene/aluminium oxide nanocomposites.* European Polymer Journal, 2017. **87**: p. 255-265.
11. Xu, D., et al., *Dielectric and electromechanical properties of modified cement/polymer based 1-3 connectivity piezoelectric composites containing inorganic fillers.* Composites Science and Technology, 2015. **114**: p. 72-78.
12. Liu, D., et al., *Influence of nanoparticle surface coating on electrical conductivity of LDPE/Al_2O_3 nanocomposites for HVDC cable insulations.* IEEE Transactions on Dielectrics and Electrical Insulation, 2017. **24**(3): p. 1396-1404.
13. Li, Y., et al., *One-dimensional metal oxide nanotubes, nanowires, nanoribbons, and nanorods: Synthesis, characterizations, properties and applications.* Critical Reviews in Solid State and Materials Sciences, 2012. **37**(1): p. 1-74.
14. Chen, L., et al., *Novel functional silica nanoparticles for rubber vulcanization and reinforcement.* Composites Science and Technology, 2017. **144**: p. 11-17.
15. Bergren, M.R., et al., *High-Performance $CuInS_2$ Quantum Dot Laminated Glass Luminescent Solar Concentrators for Windows.* ACS Energy Letters, 2018. **3**(3): p. 520-525.
16. Marinins, A., et al., *Light-Converting Polymer/Si Nanocrystal Composites with Stable 60-70% Quantum Efficiency and Their Glass Laminates.* ACS Applied Materials and Interfaces, 2017. **9**(36): p. 30267-30272.
17. Meinardi, F., et al., *Highly efficient luminescent solar concentrators based on earth-Abundant indirect-bandgap silicon quantum dots.* Nature Photonics, 2017. **11**(3): p. 177-185.

18. Ribeiro, T., et al., *NIR and visible perylenediimide-silica nanoparticles for laser scanning bioimaging.* Dyes and Pigments, 2014. **110**: p. 227-234.
19. Asefa, T. and Tao, Z.M., *Biocompatibility of Mesoporous Silica Nanoparticles.* Chemical Research in Toxicology, 2012. **25**(11): p. 2265-2284.
20. Rodrigues, A.S., et al., *Intrinsically Fluorescent Silica Nanocontainers: A Promising Theranostic Platform.* Microscopy and Microanalysis, 2013. **19**(5): p. 1216-1221.
21. Jiao, J., et al., *Fluorescent carbon dot modified mesoporous silica nanocarriers for redox-responsive controlled drug delivery and bioimaging.* Journal of Colloid and Interface Science, 2016. **483**: p. 343-352.
22. Burns, A., Ow, H. and Wiesner, U., *Fluorescent core-shell silica nanoparticles: towards "Lab on a Particle" architectures for nanobiotechnology.* Chemical Society Reviews, 2006. **35**(11): p. 1028-1042.
23. Chen, F., et al., *Multifunctional nanomedicine with silica: Role of silica in nanoparticles for theranostic, imaging, and drug monitoring.* Journal of Colloid and Interface Science, 2018. **521**: p. 261-279.
24. Yan, J., et al., *Dye-doped nanoparticles for bioanalysis.* Nano Today, 2007. **2**(3): p. 44-50.
25. Cardoso, V.F., et al., *Comparative study of sol-gel methods for the facile synthesis of tailored magnetic silica spheres.* Materials Research Express, 2016. **3**(7): p. 075402.
26. Slowing, I.I., et al., *Mesoporous silica nanoparticles: structural design and applications.* Journal of Materials Chemistry, 2010. **20**(37): p. 7924-7937.
27. Liong, M., et al., *Multifunctional inorganic nanoparticles for imaging, targeting, and drug delivery.* Acs Nano, 2008. **2**(5): p. 889-896.
28. Bharti, C., et al., *Mesoporous silica nanoparticles in target drug delivery system: A review.* International Journal of Pharmaceutical Investigation, 2015. **5**(3): p. 124-133.
29. Parssinen, J., et al., *Enhancement of adhesion and promotion of osteogenic differentiation of human adipose stem cells by poled electroactive poly(vinylidene fluoride).* Journal of Biomedical Materials Research Part A, 2015. **103**(3): p. 919-928.
30. Gilbert, J.R. and Meissner, G., *Sodium-Calcium ion-exchange in skeletal-muscle sarcolemmal vesicles.* Journal of Membrane Biology, 1982. **69**(1): p. 77-84.
31. Brito-Pereira, R., et al., *Magnetoelectric response on Terfenol-D/ P(VDF-TrFE) two-phase composites.* Composites Part B: Engineering, 2017. **120**: p. 97-102.
32. Ribeiro, C., et al., *Proving the suitability of magnetoelectric stimuli for tissue engineering applications.* Colloids and Surfaces B-Biointerfaces, 2016. **140**: p. 430-436.
33. Ribeiro, S., et al., *Electrospun Polymeric Smart Materials for Tissue Engineering Applications*, in: *Electrospun Biomaterials and Related Technologies,* Almodovar, J., Editor, Springer International Publishing, 2017. p. 251-282.
34. Cardoso, V.F., Ribeiro, C. and Lanceros-Mendez, S., *Metamorphic biomaterials*, in *Bioinspired Materials for Medical Applications*, Rodrigues, L. and Mota, M., Editor, Elsevier-Woodhead Publishing, 2016. p. 69-99.
35. Lee, Y.S., Collins, G. and Arinzeh, T.L., *Neurite extension of primary neurons on electrospun piezoelectric scaffolds.* Acta Biomaterialia, 2011. **7**(11): p. 3877-3886.

36. Ribeiro, C., et al., *Enhanced proliferation of pre-osteoblastic cells by dynamic piezoelectric stimulation.* Rsc Advances, 2012. **2**(30): p. 11504-11509.
37. Ribeiro, C., et al., *Dynamic piezoelectric stimulation enhances osteogenic differentiation of human adipose stem cells.* Journal of Biomedical Materials Research Part A, 2015. **103**(6): p. 2172-2175.
38. Martins, P.M., et al., *Effect of poling state and morphology of piezoelectric poly(vinylidene fluoride) membranes for skeletal muscle tissue engineering.* RSC Advances, 2013. **3**(39): p. 17938-17944.
39. Gomes, J., et al., *Influence of the β-phase content and degree of crystallinity on the piezo-and ferroelectric properties of poly(vinylidene fluoride).* Smart Materials and Structures, 2010. **19**(6): p. 065010.
40. Ruan, L., et al., *Properties and Applications of the β Phase Poly(vinylidene fluoride).*Polymers, 2018. **10**(3): p. 228.
41. Ribeiro, C., et al., *Electroactive poly(vinylidene fluoride)-based structures for advanced applications.* Nature Protocols, 2018. **13**(4): p. 681-704.
42. Ribeiro, T., Baleizão, C. and Farinha, J.P.S., *Synthesis and characterization of perylenediimide labeled core-shell hybrid silica-polymer nanoparticles.* Journal of Physical Chemistry C, 2009. **113**(42): p. 18082-18090.
43. Crucho, C.I.C., Baleizão, C. and Farinha, J.P.S., *Functional Group Coverage and Conversion Quantification in Nanostructured Silica by 1H NMR.* Analytical Chemistry, 2017. **89**(1): p. 681-687.
44. Lopes, A.C., et al., *Effect of filler content on morphology and physical-chemical characteristics of poly(vinylidene fluoride)/NaY zeolite-filled membranes.* Journal of Materials Science, 2014. **49**(9): p. 3361-3370.
45. Martins, P., Lopes, A.C. and Lanceros-Mendez, S., *Electroactive phases of poly(vinylidene fluoride): Determination, processing and applications.* Progress in Polymer Science, 2014. **39**(4): p. 683-706.
46. Martins, P., et al., *Role of nanoparticle surface charge on the nucleation of the electroactive β-poly(vinylidene fluoride) nanocomposites for sensor and actuator applications.* Journal of Physical Chemistry C, 2012. **116**(29): p. 15790-15794.
47. Stober, W., Fink, A. and Bohn, E., *Controlled growth of monodisperse silica spheres in micron size range*. Journal of Colloid and Interface Science,1968. **26**(1): p. 62-69.
48. Ferreira, J.C.C., et al., *Variation of the physicochemical and morphological characteristics of solvent casted poly(vinylidene fluoride) along its binary phase diagram with dimethylformamide.* Journal of Non-Crystalline Solids, 2015. **412**: p. 16-23.
49. Sencadas, V., et al., *Influence of ferrite nanoparticle type and content on the crystallization kinetics and electroactive phase nucleation of poly(vinylidene fluoride).* Langmuir, 2011. **27**(11): p. 7241-7249.
50. Ribeiro, C., et al., *Influence of processing conditions on polymorphism and nanofiber morphology of electroactive poly(vinylidene fluoride) electrospun membranes.* Soft Materials, 2010. **8**(3): p. 274-287.

51. Ribeiro, T., et al., *High performance nir fluorescent silica nanoparticles for bioimaging*. RSC Advances, 2013. **3**(24): p. 9171-9174.
52. Ribeiro, T., Baleizao, C. and Farinha, J.P.S., *Functional Films from Silica/Polymer Nanoparticles.* Materials, 2014. **7**(5): p. 3881-3900.
53. Sebastian, M.S., et al., *Understanding nucleation of the electroactive β-phase of poly(vinylidene fluoride) by nanostructures.* RSC Advances, 2016. **6**(114): p. 113007-113015.
54. Martins, P., Costa, C.M. and Lanceros-Mendez, S., *Nucleation of electroactive β-phase poly(vinilidene fluoride) with $CoFe_2O_4$ and $NiFe_2O_4$ nanofillers: A new method for the preparation of multiferroic nanocomposites*. Applied Physics A : Materials Science and Processing, 2011. **103**(1): p. 233-237.
55. Costa, C.M., et al., *Effect of the microsctructure and lithium-ion content in poly[(vinylidene fluoride)-co-trifluoroethylene]/lithium perchlorate trihydrate composite membranes for battery applications*. Solid State Ionics, 2012. **217**: p. 19-26.
56. Zeng, F., Liu, Y. and Sun, Y., *Mechanical properties and fracture behavior of poly(vinylidene fluoride)-polyhedral oligomeric silsesquioxane nanocomposites by nanotensile testing*, 13th International Conference on Fracture, 2013. **6**: p. 4862-4869.
57. Xu, Y.L., Yu, L.Y. and Han, L.F., *Polymer-nanoinorganic particles composite membranes: A brief overview*. Frontiers of Chemical Engineering in China, 2009. **3**(3): p. 318-329.
58. Beck, G.R., et al., *Bioactive silica-based nanoparticles stimulate bone-forming osteoblasts, suppress bone-resorbing osteoclasts, and enhance bone mineral density in vivo*. Nanomedicine, 2012. **8**(6): p. 793-803.
59. Liu, D., et al., *Biocompatible silica nanoparticles-insulin conjugates for mesenchymal stem cell adipogenic differentiation*. Bioconjugate Chemistry, 2010. **21**(9): p. 1673-1684.
60. Poussard, S., et al., *Internalization and fate of silica nanoparticles in c2c12 skeletal muscle cells: Evidence of a beneficial effect on myoblast fusion*. International Journal of Nanomedicine, 2015. **10**: p. 1479-1492.
61. Nunes-Pereira, J., et al., *Poly(vinylidene fluoride) and copolymers as porous membranes for tissue engineering applications*. Polymer Testing, 2015. **44**: p. 234-241.
62. Mehrasa, M., et al., *Incorporation of mesoporous silica nanoparticles into random electrospun plga and plga/gelatin nanofibrous scaffolds enhances mechanical and cell proliferation properties*. Materials Science and Engineering C, 2016. **66**: p. 25-32.
63. Mehrasa, M., et al., *Incorporation of zeolite and silica nanoparticles into electrospun pva/collagen nanofibrous scaffolds: The influence on the physical, chemical properties and cell behavior*. International Journal of Polymeric Materials and Polymeric Biomaterials, 2016. **65**(9): p. 457-465.
64. Gessner, A., et al., *Influence of surface charge density on protein adsorption on polymeric nanoparticles: Analysis by two-dimensional electrophoresis*. European Journal of Pharmaceutics and Biopharmaceutics, 2002. **54**(2): p. 165-170.
65. Aggarwal, P., et al., *Nanoparticle interaction with plasma proteins as it relates to particle biodistribution, biocompatibility and therapeutic efficacy.* Advanced Drug Delivery Reviews, 2009. **61**(6): p. 428-437.

66. Teixeira, S., et al., *Photocatalytic degradation of recalcitrant micropollutants by reusable $Fe_3O_4/SiO_2/TiO_2$ particles.* Journal of Photochemistry and Photobiology A: Chemistry, 2017. **345**: p. 27-35.
67. Sun, H., et al., *Preparation of superhydrophobic nanocomposite fiber membranes by electrospinning poly(vinylidene fluoride)/silane coupling agent modified SiO_2 nanoparticles.* Journal of Applied Polymer Science, 2017. **134**(13): p. 44501.
68. Zaherzadeh, A., Karimi-Sabet, J. and Mousavian, A., *Study the Effects of SiO_2 Nanoparticle on the Hydrophobic Properties of PVDF Composite Membrane*. 2014.
69. Kar, E., et al., *Enhancement of electroactive β phase crystallization and dielectric constant of PVDF by incorporating GeO_2 and SiO_2 nanoparticles.* Physical Chemistry Chemical Physics, 2015. **17**(35): p. 22784-22798.
70. Lopes, A.C., et al., *Nanoparticle size and concentration dependence of the electroactive phase content and electrical and optical properties of Ag/poly(vinylidene fluoride) composites.* ChemPhysChem, 2013. **14**(9): p. 1926-1933.
71. Wu, Y., et al., *The role of surface charge of nucleation agents on the crystallization behavior of poly(vinylidene fluoride).* Journal of Physical Chemistry B, 2012. **116**(24): p. 7379-7388.
72. Liang, C.L., et al., *Induced formation of dominating polar phases of poly(vinylidene fluoride): Positive ion-CF_2 Dipole or Negative Ion-CH_2 dipole interaction.* Journal of Physical Chemistry B, 2014. **118**(30): p. 9104-9111.
73. Thakur, P., et al., *Effect of in situ synthesized Fe_2O_3 and Co_3O_4 nanoparticles on electroactive β phase crystallization and dielectric properties of poly(vinylidene fluoride) thin films.* Physical Chemistry Chemical Physics, 2015. **17**(2): p. 1368-1378.
74. Correia, D.M., et al., *Physicochemical properties of poly(vinylidene fluoride-trifluoroethylene)/poly(ethylene oxide) blend membranes for lithium ion battery applications: Influence of poly(ethylene oxide) molecular weight.* Solid State Ionics, 2014. **268**(Part A): p. 54-67.
75. Mejri, R., et al., *Effect of ionic liquid anion and cation on the physico-chemical properties of poly(vinylidene fluoride)/ionic liquid blends.* European Polymer Journal, 2015. **71**: p. 304-313.
76. Kim, J.W., Cho, W.J. and Ha, C.S., *Morphology, crystalline structure, and properties of poly(vinylidene fluoride)/silica hybrid composites.* Journal of Polymer Science, Part B: Polymer Physics, 2002. **40**(1): p. 19-30.
77. Mendes, S.F., et al., *Influence of filler size and concentration on the low and high temperature dielectric response of poly(Vinylidene fluoride)/$Pb(Zr_{0.53}\ Ti_{0.47})O_3$ composites.* Journal of Polymer Research, 2012. **19**(9): p. 9967.
78. Lopes, A.C., et al., *Dielectric relaxation, ac conductivity and electric modulus in poly(vinylidene fluoride)/NaY zeolite composites.* Solid State Ionics, 2013. **235**: p. 42-50.
79. Kundu, M., et al., *On the Relevance of the Polar β-Phase of Poly(vinylidene fluoride) for High Performance Lithium-Ion Battery Separators.* Journal of Physical Chemistry C, 2017. **121**(47): p. 26216-26225.

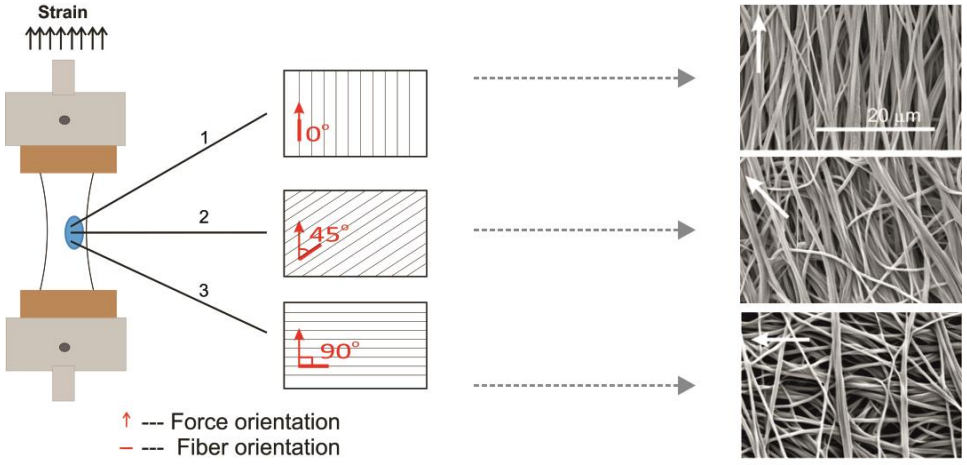

Chapter 3. Relation between fibre orientation and mechanical properties of nano engineered poly(vinylidene fluoride) electrospun composite fibre mats

This chapter reports the development of nano-engineered PVDF aligned and randomly oriented fibres by electrospinning with and without $CoFe_2O_4$ magnetostrictive nanoparticles as a suitable material for tissue engineering applications. The addition of active nanoparticles allow the magnetoelectric response on the composite fibre mats and opens large application potential for non-contact tissue engineering strategies. The influence of fibre orientation and addition of magnetostrictive nanoparticles on their mechanical properties through young modulus and yield point has been studied. The physico-chemical properties and the electroactive β-phase were also evaluated. C2C12 and 3T3 cell cytotoxicity on these fibres was assessed, to study their potential use for tissue engineering applications.

This chapter is based on the following publication: **S. Ribeiro**, M.M. Maciel, C. Ribeiro, A. Francesko, A. Maceiras, J.L. Vilas, S. Lanceros-Méndez, *Relation between fibre orientation and mechanical properties of nano engineered poly(vinylidene fluoride) electrospun composite fibre mats*; Composites Part B: Engineering, 139, 146-154, 2018.

3.1 Introduction

The origin of electrospinning can be traced back to 1902 [1]. Several other methods exist for fabricating fibres, but electrospinning has proven to be one the most promising and versatile emerging technique for manufacturing fibres [2, 3]. This technique is suitable for processing both synthetic and natural polymers into nano-/micro-scale fibrous materials [4]. The most attractive features of this process are simplicity, versatility and low cost manufacturing. In particular, electrospinning gained a large popularity for TE applications as a potential mean for the production of scaffolds [5]. This technique allows the fabrication of scaffolds with suitable topology, microstructure and mechanical properties that altogether mimic the native physiological environment [6].

All cells in the ECM receive mechanical, chemical and external stimuli, which influence how cells will behave, grow and function [7]. In a similar way, electrospun nanofibres can mimic the different types of ECM to give the necessary stimuli to the cells in order to produce a viable and functional tissue [8, 9]. For example, the mechanical and structural properties of a scaffold play an important role in determining the morphology of attached cells and their cellular functions. Therefore, the mechanical properties are useful for modulating cell behaviour, as well as to provide adequate tension and strength to resist to the forces from the cell cytoskeleton [10]. The cells perceive the fibres characteristics, the fibre diameter, and display different behaviour accordingly. Indeed, it has been reported that osteoblast cells grow faster and migrate well into the materials with large fibre diameter, however, differentiate faster on fibres with smaller diameters [11]. The orientation of the fibres is another key factor that can influence how cell migration, proliferation, differentiation and maturation occur. It has been verified that aligned fibres, contrary to randomly oriented ones, can successfully promote the regeneration of axons, reinnervation of muscles and reforming new neuromuscular junctions [12].

Currently, different types of electrospun fibres are being tested for engineering different types of tissues, including skin [13], cardiac [14, 15], ligaments [16], neural [17, 18] and bone [19, 20]. The discovery of smart materials capable of providing a specific response when they are stimulated opens new opportunities especially in the production of scaffolds able to mimic the biophysical cues necessary for tissues to become functional. A good example is in bone regeneration where the shear strain is important to initiate the process, being a balance between biochemical and biophysical stimulus [21].

Further, the use of electrospun fibre mats goes beyond TE and extends to other applications, such as drug and gene delivery [22], water treatment [23], filtration membranes [23, 24], food packaging [25, 26], textile manufacturing [27], antibacterial agent [28, 29] and energy [30], where the proper evaluation of the mechanical response is essential. However, till now the mechanical properties of fibre mats have

not been properly evaluated, probably due to the difficulty to assess the contribution of fibre orientation, entanglement and material properties themselves. In the specific context of TE and due to many tissues reaction to electrical and/or mechanical stimulation [31], the mechanical properties of scaffolds should be better understood in the context of the dynamic and multi-directional loading environments that scaffolds will be subjected to when placed *in vivo*.

PVDF is a piezoelectric polymer with the highest piezoelectric, pyroelectric and ferroelectric responses, among polymers. PVDF is a biocompatible and non-biodegradable polymer [32], showing also excellent mechanical strength and processability in a variety of forms and shapes [33]. This polymer and its co-polymers have been also largely used in TE applications [34]. For example, in skeletal muscle TE it has been reported that the morphology of electroactive PVDF improve the directional growth of myoblast cells [35], which enhances the importance of the study of macroscopic deformation of fibres.

The incorporation of nanoparticles can further allow to tune the properties of polymers [36-39]. Ferrites are an important class of magnetic materials that have gained increasing attention of the scientific community due to their wide range of application in sensors, electronics, magnetic recording, electrical and automobile industries as well as their increasing use in biotechnology and biomedical applications [40-42]. In particular, CFO nanoparticles show high permeability and good saturation magnetization. They are magnetically "soft", being easily magnetized and demagnetized, and electrically insulating, being also stable physically and chemically [43, 44].

As previously indicated, different cell functions can be regulated by mechanical signals [45], and in particular, the microstructure of a biomaterial affects the mechanotransduction of cells. Accordingly, the study on the influence of scaffolds topography on cell behaviour can provide a basis for the study of the mechanobiology in the context of topographical cues received from the nearest microenvironment. The PVDF films with and without magnetostrictive nanoparticles have already been investigated relatively to their morphological, physico-chemical properties, magnetic and dielectric response [36, 46, 47]. In line with the above, this study investigates the macroscopic deformations in materials comprising oriented fibres, in particular, how their microstructure modulates the effect of the applied tensions and consequent deformations. In such way, this work aims to assess the influence of PVDF and PVDF magnetic composite fibres orientation (aligned and randomly oriented) on the strain and Young modulus when a mechanical force is applied.

3.2 Experimental Section

3.2.1 Materials

PVDF (Solef 5130, M_W 1,000-1,200 kg.mol^{-1}) was purchased from Solvay, DMF from Merck and CFO nanoparticles (35–55 nm) were purchased from Nanoamor.

3.2.2 Electrospinning

PVDF was dissolved with a concentration of 20 wt.% in DMF at room temperature under constant magnetic stirring. For the preparation of composite fibres, 5, 10 and 20 wt.% of CFO nanoparticles were added to the polymer solution, using the procedure described in [48]. In order to obtain the PVDF fibres, the same procedure as described on Chapter 2 (section 2.2.3.1) was performed (with a steel needle with inner diameter of 0.5 mm at 14 kV with a feed rate of 0.5 mL.h^{-1}). Oriented and random oriented fibres were prepared.

3.2.3 Sample Characterization

Mechanical characterization

Mechanical measurements were performed on rectangular samples (25 x 10 mm) with thickness between 10-50 μm (Fischer Dualscope 603-478, digital micrometer). All samples were mechanically tested at room temperature on a universal testing machine, Linkam TST350 tensile stress testing system (Linkam Scientific Instruments, Surrey, UK) in the tensile mode at a test velocity of 1 mm.min^{-1} with a loading cell of 20 N, excepting for the oriented fibres evaluated along the fibre direction, where a 200 N load cell was used. The mechanical parameters were calculated from the average of triplicate measurements. The Young's modulus was determined as presented on chapter 2 (section 2.2.3.2).

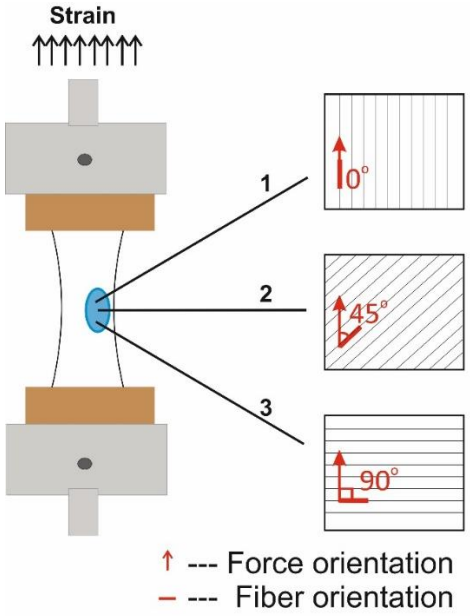

Figure 3.1. Schematic representation of the different mechanical experiments, where stretching was applied along different angles with respect to the orientation of the fibres.

The stretching of the samples (3, 16 and 100%) was performed in three different directions (0, 45 and 90°) relative to the fibre orientation (Figure 3.1). To maintain the performed stretching, a fixing sprayed paint was used. The denomination of the different samples is presented in Table 3.1.

Table 3.1. Denomination of the different fibre mat samples of PVDF stressed with different stretching angle with respect to the aligned fibres.

PVDF Fibres	Angle of stretching	Significance	Sample denomination	Load cell (N)
Oriented fibres	0°	Stretching along the same direction of the fibres orientation	O_0	200
	45°	Stretching at 45° with respect to the fibres orientation	O_45	20
	90°	Stretching at 90° with respect to the fibres direction.	O_90	20
Random fibres	No orientation	—	NO	20

Morphological analysis

Oriented and randomly oriented fibrous mats, with and without cobalt ferrite nanoparticles, and sputter-coated with gold (Polaron sputter coating) were imaged in a Quanta 650 (FEI) field-emission SEM. Images were obtained prior to stretching and at different deformations along the stretching process with magnifications of ×1K, ×5K and ×20K. The ImageJ software was used for determination of diameter of the individual fibres.

Fourier transform infrared spectroscopy

Structural analysis of the samples was evaluated by FTIR measurements were carried out in ATR described on Chapter 2 (section 2.2.3.2). Volume fraction of the electroactive β-phase in the all produced nanofibre was also determined by the equation 2.1 showed on Chapter 2 (section 2.2.3.2).

Thermal properties

The thermal properties of the samples were determined by DSC described on Chapter 2 (section 2.2.3.2). The degree crystallinity of the samples was calculated from the DSC thermograms according the equation 2.2 on Chapter 2 (section 2.2.3.2).

Water contact angle measurements

Wettability of the samples was determined by measuring the WCA at room temperature as described on Chapter 2 (section 2.2.3.2).

3.2.4 Cytotoxicity evaluation of samples

Sample sterilization

For the in vitro assays, samples without and with different concentrations of CFO nanoparticles were cut according the ISO_10993-12. The extraction ratio (surface area or mass/volume) was 6 $cm^2.mL^{-1}$. These samples were sterilized as presented on Chapter 2 (section 2.2.3.3.1).

Cell culture and cytotoxicity assay

C2C12 mouse myoblast and 3T3 fibroblast cells were grown separately in 75 cm^2 cell culture flask using the same medium. The composition of the medium and the conditions of cell culture are the same as described on Chapter 2 (section 2.2.3.3.2). C2C12 and 3T3 cells were seeded in the 96-well tissue culture polystyrene plate at the density of 2×10^4 $cells.mL^{-1}$ for both and incubated for 24 h to allow the cell attachment on the plate. The cytotoxicity assay by the indirect contact were performed as described on chapter 2 (section 2.2.3.3.3).

All quantitative results were obtained from four replicates samples and controls and were analyzed as the average of viability ± SD.

3.3 Results and Discussion

3.3.1 Morphological and mechanical response of PVDF fibre mats

The influence of the fibre orientation on the mechanical response when the samples are stretched along different angles with respect to the orientation of the fibre was evaluated using the stress-strain measurements (Figure 3.2) and their respective young modulus and yield point are present in Table 3.2.

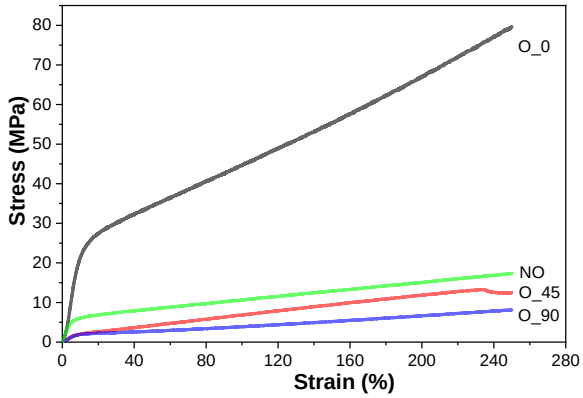

Figure 3.2. Mechanical response of the PVDF fibres: stress-strain characteristic behaviour for stretching along 0, 45 and 90 ° with respect to the orientation of the fibres.

Table 3.2. Young modulus and yield point of PVDF fibres for stretching at 0, 45 and 90° with respect to fibre orientation. Values shown as mean ± SD.

	E (MPa)	Yield Strain (%)	Yield Stress (MPa)
O_0	225.27 ± 16.51	11.83 ± 1.24	25.37 ± 1.30
O_45	26.91 ± 1.60	7.51 ± 1.02	1.98 ± 0.54
O_90	23.21 ± 1.48	7.58 ± 0.78	1.75 ± 0.22
NO	129.17 ± 25.15	5.37 ± 0.24	6.96 ± 1.43

In comparison to β-PVDF films that exhibit an effective Young's modulus around 2 GPa [49], the β-PVDF electrospun mats present lower values. The characteristic features of the stress-strain curves are similar for the PVDF samples O_45, O_90 and NO, in contrast to the curve of the sample O_0. It is observed that the random electrospun and oriented mats stretched at 45 and 90° showed lower

mechanical properties than the experiments along the oriented fibre mats at 0 ° due to the lower number of fibres along the stretch direction. All samples of PVDF pure (O_0; O_45; O_90 and NO) break above 200% of strain, independently of angle between orientation fibre and the direction of applied strain. The elastic modulus for the oriented fibres depends significantly on the relative angle between the fibres and the stretch direction (Table 3.2). The sample O_0 showed a higher value of the effective Young modulus, approximately 225 ± 16 MPa, in agreement with previous studies [50], decreasing to 27 ± 2 MPa for O_45 and 23 ± 2 MPa for O_90 (Table 3.2). These results are consistent with previous investigations in related scaffolds where the effective Young's modulus also decreases with increasing angle between fibre orientation and strain direction [51, 52]. This result is explained by the fibre reorientation and collapsing of the porous microstructure once the fibres tend to align towards the direction of applied strain [51]. Thus, depending on the desired applications, it is possible to modulate the applied deformation on the polymer fibres.

The yield point determines the region when the material begins to deform plastically. As expected, yield strain and stress for the O_0 samples are larger than for the other samples: random (NO) and oriented electrospun mats stretched at 45 and 90° (O_45 and O_90). This fact is explained once for the O_0 samples the stress is mostly used for the deformation of the fibres whereas for the other conditions the stress is applied for the reorientation of the fibres along the stretching direction.

After submitting the PVDF fibres to stretching along different relative angles, their morphology was further observed by SEM. Figure 3.3 shows the differences observed in the morphology of the fibre mats when stretching has been applied at different angles and after the application of different strains. The stretching values of 3 and 16% were selected to analyze the morphological variations in the elastic and plastic regions of the mechanical response of the PVDF fibre mats, respectively, while the stretching value of 100% is selected to observe the morphology of the fibre mats at high levels of deformation. The SEM images (Figure 3.3) demonstrate a reorientation of the fibres along the stretching direction, where the reorientation in the O_0 samples is far less pronounced, as the stretching is already performed along the fibre orientation. It is to notice that the alignment of fibres along the stretching direction is a relevant issue for the mechanical response, as it has been verified that an increasing number of aligned fibres in the polymeric electrospun mats can change the mechanical properties significantly, increasing the elastic modulus by 125% and stress yield by 150% [16]. This fact is in agreement with the difference of Young's modulus among the different experimental conditions and samples, as represented in Figure 2.2. Beyond the fibre reorientation, it is also possible to observe that some fibres are grouped in boundless, mainly formed in the samples stretched along different directions than the orientation of the fibres.

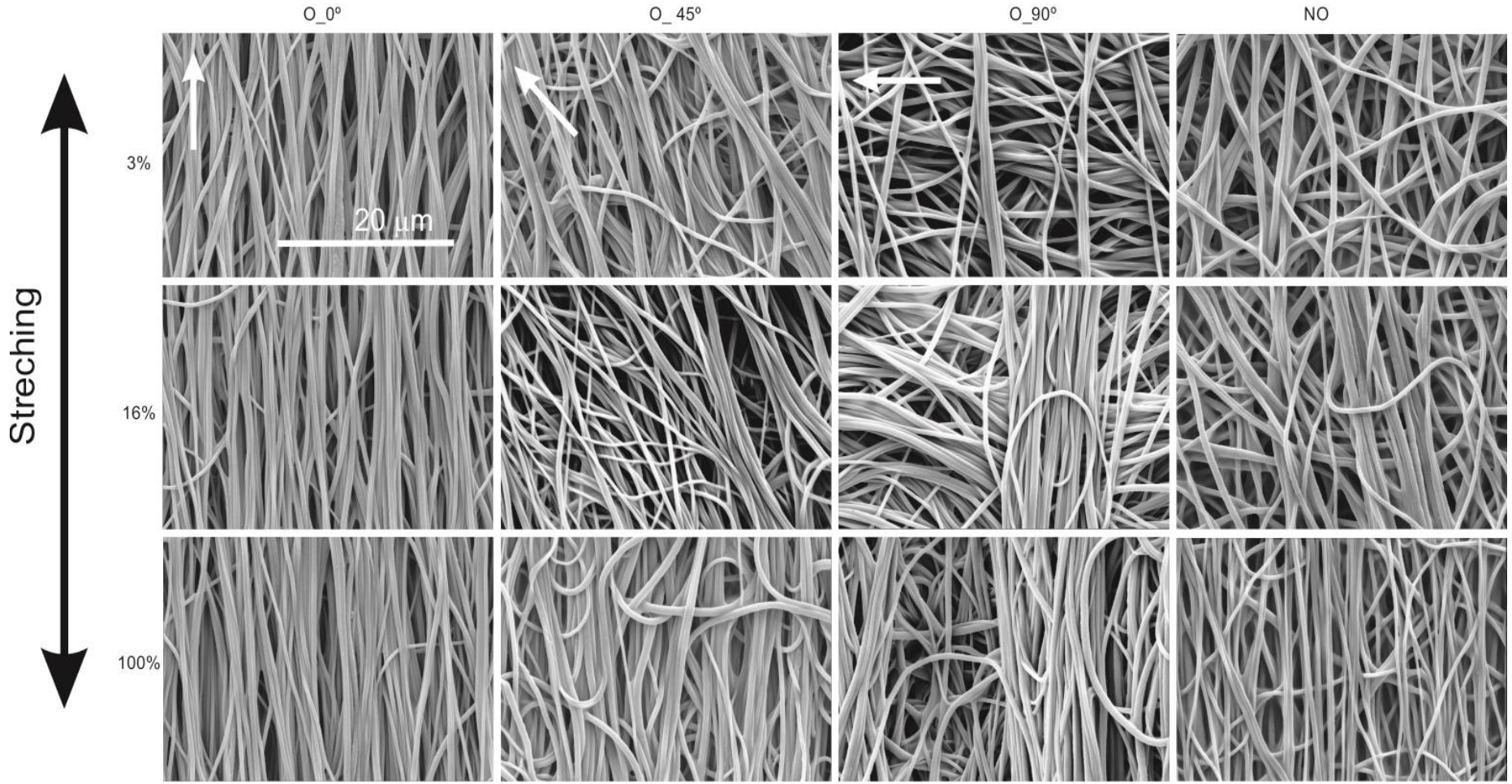

Figure 3.3. Electrospun fibre mat morphology after different angle of stretching relatively to the fibre orientation (indicated by the arrow in the first images).

Electrospun PVDF fibre morphology and properties are affected by processing parameters including initial polymer solution, solvent evaporation and collection procedure, allowing the collection of random or oriented fibres [53]. In the present processing conditions, PVDF random and oriented fibres show a fibre average diameter of 954 ± 90 and 794 ± 198 nm, respectively. The oriented fibres show typically a lower diameter due to the additions stretching of the fibre during the collection process in a rotating drum, in which solvent is still not completely evaporated [53]. Under mechanical stretching, all samples demonstrate a decrease in diameter with the increasing of the applied strain (Figure 3.4). After 100% deformation, the decrease in diameter is more pronounced for the O_0 samples, reaching a diameter of 425 ± 108 nm. This can be explained once the force is applied along the same direction of the fibres, leading mainly to an actual stretching of the fibres, contrary to what happens in O_45 and O_90, where the force has more influence on the fibres reorientation to the stretching direction. Thus, with stretching along O_45 and O_90, the diameters of the fibres decrease just to 589 ± 148 and 751 ± 153 nm, respectively. Further, NO samples after 100% deformation presented a mean diameter of 496 ± 113 nm, being even lower than those for O_45 and O_90. This result is expected, since in the samples with a random fibre orientation, there exist a higher number of fibres along the stretching direction, independently of the direction of stretching, excepting for the stretching of the fibres along O_0.

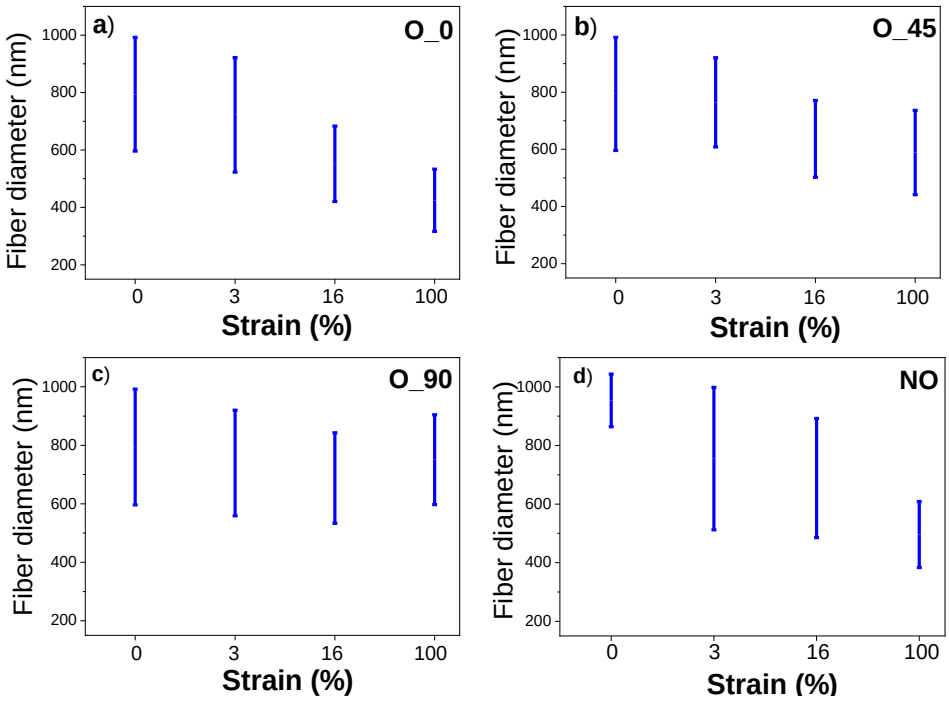

Figure 3.4. Influence of stretching of PVDF electrospun mats in the average fibre diameter as a function of strain: (a) O_0, (b) O_45, (c) O_90 and (d) NO.

Figure 3.5 shows the orientation of PVDF fibres in the O_90 condition as a function of stretching in order to properly quantify the reorientation of the fibres. It is to notice that for a deformation of 16% there is already a clear reorientation of the fibres along the stretching directions and for 100% this reorientation is almost complete. The same behaviour was observed for the other samples.

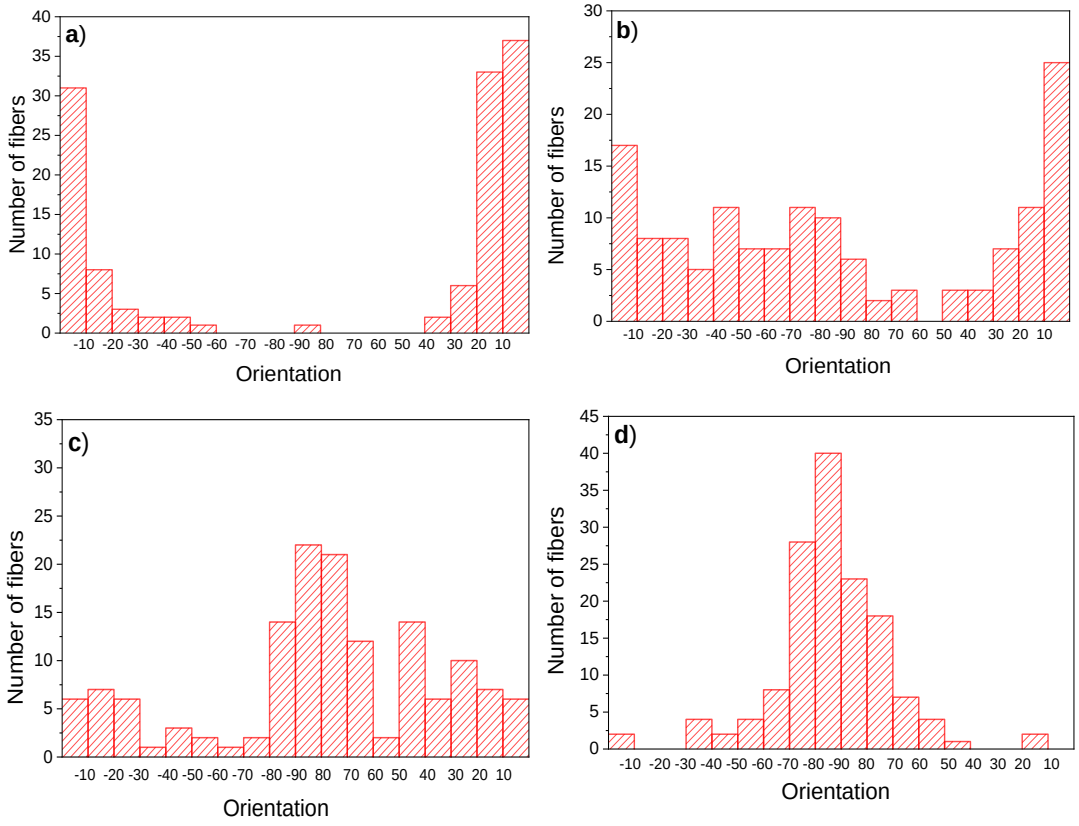

Figure 3.5. Orientation of the fibres in the fibre mat for the O_90 sample (a) without and with (b) 3%, (c) 16% and (d) 100% of stretching.

It is important to notice that the stretching on the PVDF fibres leads to a relevant reorientation and modification of the fibres diameter in the fibre mat, but that others relevant surface properties of the PVDF mats, such as wettability are not significantly affected by the stretching once the samples with or without stretching present values around ≈ 145° and ≈ 133° for oriented and randomly oriented PVDF fibres, respectively [35].

Contrarily to the wettability, others relevant properties of the PVDF mats, such as polymer electroactive phase and degree of crystallinity are affected by the stretching (Figure 3.6 and 3.7). The FTIR-ATR spectra and DSC curves are presented in Figure 3.6 for oriented PVDF electrospun mats, 100% stretched along two different angles between stretching/fibre orientation (0 and 90°). The characteristic bands of the β-phase are present on FTIR-ATR spectra for all the samples analyzed (Figure 3.6a). DSC

scans were performed to investigate possible changes in the degree of crystallinity and melting behaviour, and are characterized by similar endothermic peaks, characteristic of the melting of the polymer (Figure 3.6b).

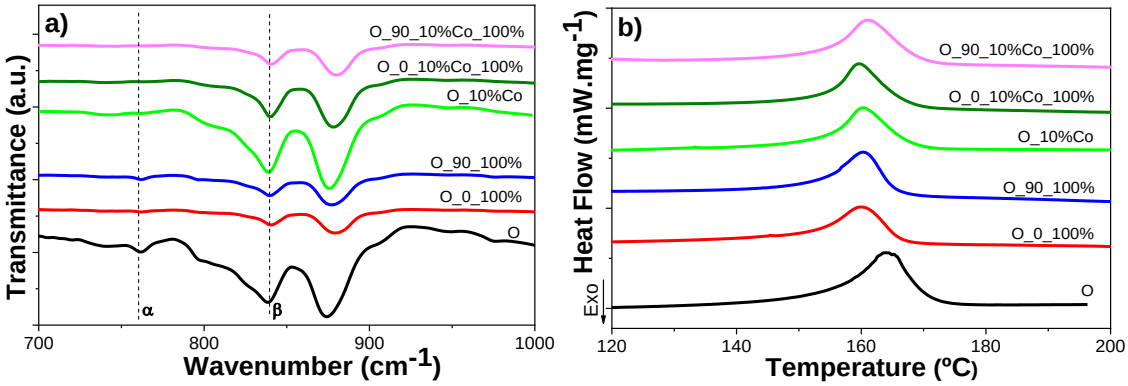

Figure 3.6. (a) FTIR-ATR spectra and (b) DSC curves of oriented PVDF electrospun mats with and without 10 wt.% CFO, 100% stretched along two different angles between stretching/fibre orientation (0 and 90°).

Comparing the PVDF with and without stretching, it is observed a higher decrease of the degree of crystallinity when the angle between the stretching and the fibre orientation is 0°. The values decrease from ≈ 48% for pure PVDF fibres to 30 and 41%, for O_0_100% and O_90_100%, respectively. The electroactive β-phase of the pure PVDF fibres (≈ 83%) shows a small increase for the samples O_0 with 100% of stretching (≈ 92%), however is observed a decrease on β electroactive phase for the sample O_90_100% (≈ 79%). So, the stretching on the same direction of fibre orientation improves the β-phase formation. Thus, whereas stretching decrease the degree of crystallinity mainly by breaking up ill-crystallized crystals in the amorphous-crystalline interface regions, it improves the relative β-phase content of the crystalline phase as the α to β–phase transformation of the polymer chains is improved by stretching both in the crystalline and interfacial amorphous regions of the polymer [33].

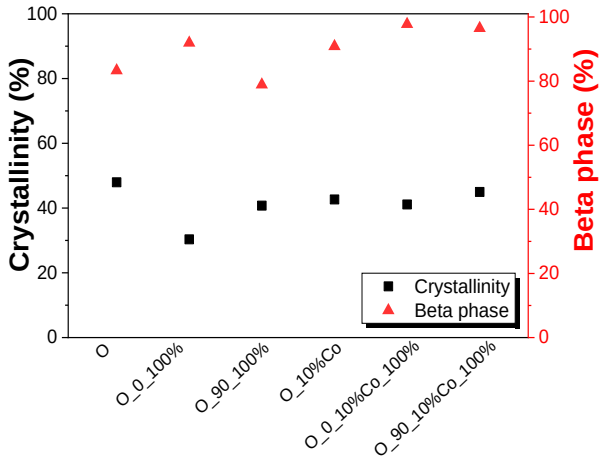

Figure 3.7. Crystallinity degree and beta phase of the different fibres samples with and without stretching. The associated error is 2% for crystallinity degree and 3% for beta phase.

3.3.2 CFO/PVDF fibre mats

The introduction of CFO nanoparticles in PVDF fibres allows to introduce magnetic [54], magnetostrictive and ME properties to the fibre mats [48], with large application potential for TE strategies. In fact, it has been reported that the ME cell stimulation is a suitable approach for novel TE strategies, once ME composites enhanced up to 25% the cell proliferation under the mechanical and electrical stimulation [41].

The FTIR-ATR spectra and DSC curves of PVDF electrospun mats with 10 wt.% CFO with 100% stretched along two different angles between stretching/fibre orientation (0 and 90°) are also presented in Figure 3.6. The introduction of CFO on PVDF samples show a slight decrease of the degree of crystallinity but these values are similar when the stretching is applied (Figure 3.6b and 3.7).

The introduction of CFO nanoparticles on the oriented PVDF fibres results in an increase on the β-phase (≈ 91%) when compared to the PVDF fibres without nanoparticles. This can be explained by the interactions between the negatively charged surface of the CFO nanoparticles and the positively charged polymer CH_2 group that promotes the nucleation of the polar β-phase [47, 48]. The stretching on these samples, CFO/PVDF fibres, also improve the β-phase formation as it happened in the PVDF fibres without nanoparticles (previously mentioned) ≈ 98% for O_0°_10%Co_100% and ≈ 96% for O_90°_10%Co_100%. It is also observed that, contrarily to PVDF fibres, for CFO/PVDF fibres, the β-phase does not decrease significantly when the angle between the stretching and fibre orientation is 90°, attributed to the reinforcement effect of the nanoparticles.

Fibre mats were prepared with filler contents of 5, 10 and 20 wt.% The composite fibre mats (data not shown) are similar to the ones presented in Figure 3.3 and show an average diameter of 417 ± 98 and 442 ± 90 nm, respectively. Therefore, the CFO nanoparticle content has no significant impact on the nanofibres average diameter [48]. The diameters of oriented electrospun PVDF fibres range from around 794 ± 198 nm, so the introduction of CFO nanoparticles makes the nanofibres thinner due to the increase of the electrical conductivity of the solutions and strong electrostatic interactions of the nanoparticles with the polymer chains [36]. CFO nanoparticles make also the diameter of the nanofibre more uniform, due to the increase of the solution conductivity with the addition of CFO. Further, as previously demonstrated, the CFO nanoparticles are well encapsulated in the PVDF fibres without agglomerates [48].

With respect to the mechanical measurements of CFO/PVDF oriented fibres, these samples present similar mechanical properties (Figure 3.8) and stress-strain behaviour than the pure PVDF fibres (Figure 3.2). However, it is possible verified a decrease on (%) strain of break and also a slight increase on the tensile strength for all the PVDF fibres samples with 10 wt.% CFO. The same behaviour is observed for the samples with a concentration of 20 wt.% CFO. Independently of the samples, the strain break of all PVDF fibres with wt.% CFO break above 125% of strain.

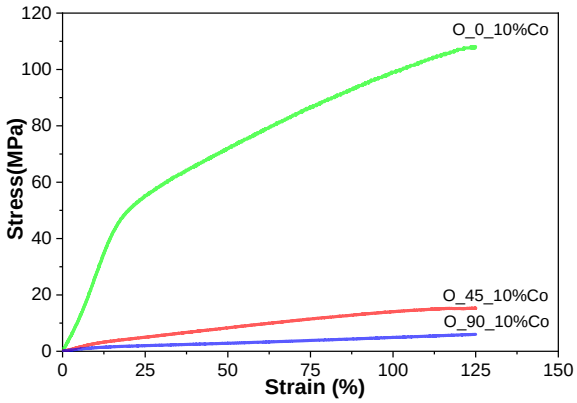

Figure 3.8. Mechanical response of the CFO/PVDF electrospun fibres: stress-strain characteristic behaviour for stretching along 0, 45 and 90° with respect to the orientation of the oriented fibres with 10 wt.% CFO.

Table 3.3 shows the variation of Young's modulus with increasing cobalt ferrite concentration in the PVDF oriented fibres as well as the corresponding yield point for each sample. The introduction of the CFO nanoparticles changes the mechanical properties of the pure fibres. Further, for the O_0 experimental condition, the Young modulus increases with increasing filler concentrations, in particular for filler concentrations up to 10%, stabilizing for higher concentrations. In contrast, when the angle between the stretching and fibre orientation is 90°, the value of the Young modulus shows a slight

decrease with increasing filler content. Relatively to the yield point, the values increase relatively to the pure PVDF fibres independently of the angle between the stretching and fibre orientation (0 or 90°). No significant changes are observed with the increase of CFO nanoparticles concentration. Thus, the inclusion of the filler acts as reinforcement of the material itself, but not of the fibre mat.

Table 3.3. Young modulus and yield point of CFO/PVDF fibres for stretching at 0 and 90° with respect to fibre orientation. Values shown as mean ± SD.

	E (MPa)	Yield point (Strain %)	Yield point (Stress MPa)
0-5% Co_0	250.57 ± 23.80	19.98 ± 2.20	51.87 ± 8.32
0-5% Co_90	23.94 ± 3.51	9.27 ± 1.27	2.32 ± 0.12
0-10% Co_0	308.71 ± 30.62	19.80 ± 2.84	56.40 ± 3.11
0-10% Co_45	25.55 ± 2.66	11.16 ± 0.48	3.16 ± 0.43
0-10% Co_90	14.01 ± 2.47	8.91 ± 1.21	1.44 ± 0.02
0-20% Co_0	287.69 ± 11.85	18.70 ± 0.80	53.91 ± 1.70
0-20% Co_90	10.45 ± 0.27	9.42 ± 0.65	0.98 ± 0.04

3.3.3 Implications in tissue engineering applications

The effect of fibre reorientation under mechanical stretching is particularly relevant for TE applications once it has implications for mechanically guided maturation of specific tissues [55-57]. Thus, it has been demonstrated that the orientation of mesenchymal stem cells and changes in nuclear morphology were strongly dependent on the fibres direction. This was further translated to changes in gene expression depending on fibre alignment [51]. Furthermore, the fibre diameter is a parameter that influence the cell behaviour [58], so it is an important parameter to relate to the applied mechanical solicitation, once different biomedical applications require different diameter values [59].

The relationship between CFO and cells has been studied from the point of view of safety. Several studies have reported the occurrence of some adverse effects, such as changes in cell morphology, mitochondrial function, plasma membrane permeability and apoptosis [60]. It is essential to understand the interactions between biological systems and nanomaterials, so *in vitro* experiments with different cell lines represent a very useful tool [61]. It is to notice that, in particular, the presence of magnetic and

magnetostrictive nanoparticles will allow cell culture under induced magnetomechanical [62] and magnetoelectrical stimuli [41] that can be of relevance for specific cells.

The potential application in TE of these samples leads to study the cytotoxicity of these composite samples, once it is already demonstrated the biocompatibility of the PVDF electrospun mats [35]. Figure 3.9 shows the effects of polymer extract medium on metabolic activity of two cell types, namely C2C12 and 3T3, to analyze the CFO effect before and after 100% stretching of CFO/PVDF fibres. The pure PVDF fibres already demonstrated biocompatibility and potential application in TE [35].

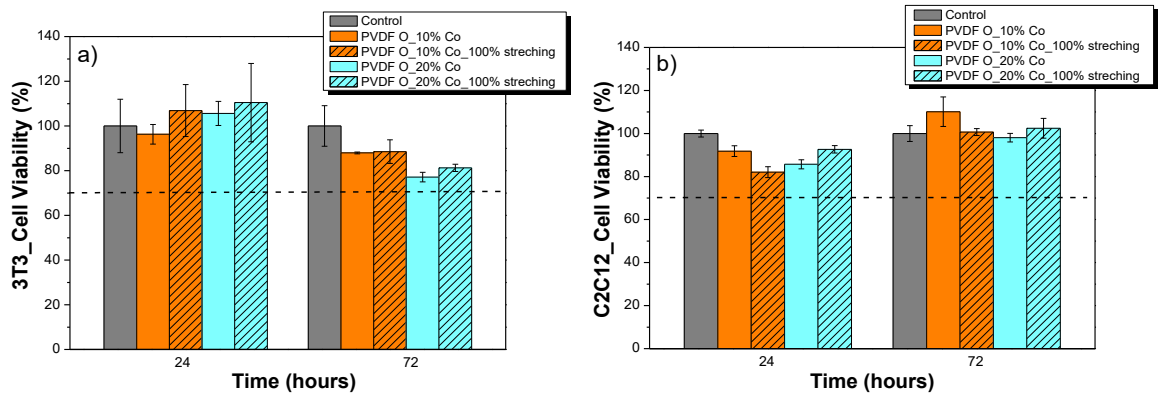

Figure 3.9. Cytotoxicity assay of (a) 3T3 and (b) C2C12 cells in contact with the conditioned media exposed with the different CFO/PVDF samples for 24 and 72 h (relative cell viability was presented as the percentage of control (n = 4) ± SD).

According to the ISO standard 10993-5, it is verified that all the samples are not cytotoxic, once the samples are considered cytotoxic when the cell viability reduction is larger than 30% and after 72 h the cell viability values are higher than 70%. Independently of the CFO concentration (10 and 20%) and with or without stretching. So, these CFO/PVDF fibres are not cytotoxic for the two type of cells used in this work. These results also demonstrate that CFO nanoparticles are well encapsulated on PVDF fibres.

Thus, a novel approach for TE applications can be achieved by materials with a ME response, the ME materials [48, 63]. These materials allow the use of an external magnetic field to remotely control tissue stimulation without the need of patient movement once there combining magnetostrictive and piezoelectric materials. Previous study reported that Terfenol-D/P(VDF-TrFe) composites films being observed that they are able to provide mechanical and electrical stimuli to MC3T3-E1 pre-osteoblast cells being the stimuli remotely triggered by an applied magnetic field films [41]. Electrospun fibres and ME response show thus a large potential for TE, so it will be interesting study the influence and suitability of these CFO/PVDF fibres on cell behaviour.

3.4 Conclusions

PVDF electrospun fibre mats with aligned and randomly oriented fibres were produced and subjected to mechanical stretching along three different directions, 0, 45 and 90°, relative to the fibre orientation within the fibre mats in order to study the variation in fibre mats morphology and mechanical response. The effective Young's modulus for the oriented fibre mats depends significantly on the stretching direction. Being 225, 27 and 23 MPa for the 0, 45 and 90° angles, respectively. All samples demonstrated a reorientation of the fibres along the stretching direction, where the reorientation is less pronounced in the O_0 samples, since the direction of the fibres corresponds to the stretching direction. A decrease in the average diameter of the fibres is also verified with increasing applied strain. The introduction of cobalt ferrite nanoparticles in PVDF fibre mats further slightly changed their mechanical properties, increasing the Young´s Modulus to 308.71 MPa with 10 wt.% of CFO nanoparticles. Additionally, there is an increase of the strain value at break when subjected to stretching at the same direction of the fibres orientation, but a decrease when the angle between the stretching direction and fibre orientation is 90°. These variations must be quantitatively taken into account when the fibre composite mats are used as scaffolds for TE applications.

3.5 References

1. Mirjalili, M. and Zohoori, S., *Review for application of electrospinning and electrospun nanofibres technology in textile industry.* Journal of Nanostructure in Chemistry, 2016. **6**(3): p. 207-213.
2. Jin, L., et al., *Electrospun fibres and tissue engineering.* Journal of Biomedical Nanotechnology, 2012. **8**(1): p. 1-9.
3. Pham, Q.P., Sharma, U. and Mikos, A.G., *Electrospinning of polymeric nanofibres for tissue engineering applications: A review.* Tissue Engineering, 2006. **12**(5): p. 1197-1211.
4. Kai, D., et al., *Electrospun synthetic and natural nanofibres for regenerative medicine and stem cells.* Biotechnology Journal, 2013. **8**(1): p. 59-72.
5. Li, M., et al., *Electrospun protein fibres as matrices for tissue engineering.* Biomaterials, 2005. **26**(30): p. 5999-6008.
6. Chen, H., et al., *Fabrication of nanofibrous scaffolds for tissue engineering applications*, in *Nanomaterials in Tissue Engineering: Fabrication and Application,* Gaharwar, A. K. et al., Editor, Elsevier-Woodhead Publishing, 2013. p. 158-183.
7. Rosso, F., et al., *From Cell-ECM Interactions to Tissue Engineering.* Journal of Cellular Physiology, 2004. **199**(2): p. 174-180.
8. Rozario, T. and DeSimone, D.W., *The extracellular matrix in development and morphogenesis: a dynamic view.* Dev Biol, 2010. **341**(1): p. 126-40.

9. Dike, L.E., et al., *Geometric control of switching between growth, apoptosis, and differentiation during angiogenesis using micropatterned substrates.* In Vitro Cellular and Developmental Biology - Animal, 1999. **35**(8): p. 441-448.
10. Horner, C.B., et al., *Microstructure-dependent mechanical properties of electrospun core–shell scaffolds at multi-scale levels.* Journal of the Mechanical Behavior of Biomedical Materials, 2016. **59**: p. 207-219.
11. Sisson, K., et al., *Fibre diameters control osteoblastic cell migration and differentiation in electrospun gelatin.* J Biomed Mater Res A, 2010. **94**(4): p. 1312-20.
12. Kim, Y.T., et al., *The role of aligned polymer fibre-based constructs in the bridging of long peripheral nerve gaps.* Biomaterials, 2008. **29**(21): p. 3117-27.
13. Liu, N.H., et al., *Electrospinning of poly (ε-caprolactone-co-lactide)/Pluronic blended scaffolds for skin tissue engineering.* Journal of Materials Science, 2014. **49**(20): p. 7253-7262.
14. Kai, D., et al., *Guided orientation of cardiomyocytes on electrospun aligned nanofibres for cardiac tissue engineering.* J Biomed Mater Res B Appl Biomater, 2011. **98**(2): p. 379-86.
15. Albanna, M.Z., et al., *Improving the mechanical properties of chitosan-based heart valve scaffolds using chitosan fibres.* Journal of the Mechanical Behavior of Biomedical Materials, 2012. **5**(1): p. 171-180.
16. Pauly, H.M., et al., *Mechanical properties and cellular response of novel electrospun nanofibres for ligament tissue engineering: Effects of orientation and geometry.* J Mech Behav Biomed Mater, 2016. **61**: p. 258-70.
17. Pires, F., et al., *Neural stem cell differentiation by electrical stimulation using a cross-linked PEDOT substrate: Expanding the use of biocompatible conjugated conductive polymers for neural tissue engineering.* Biochim Biophys Acta, 2015. **1850**(6): p. 1158-68.
18. Gerardo-Nava, J., et al., *Human neural cell interactions with orientated electrospun nanofibres in vitro.* Nanomedicine (Lond), 2009. **4**(1): p. 11-30.
19. Tuzlakoglu, K., et al., *Nano- and micro-fibre combined scaffolds: a new architecture for bone tissue engineering.* J Mater Sci Mater Med, 2005. **16**(12): p. 1099-104.
20. Jing, X., et al., *Hierarchically decorated electrospun poly(ε-caprolactone)/nanohydroxyapatite composite nanofibres for bone tissue engineering.* Journal of Materials Science, 2015. **50**(12): p. 4174-4186.
21. Prendergast, P.J., Huiskes, R. and Søballe, K., *Biophysical stimuli on cells during tissue differentiation at implant interfaces.* Journal of Biomechanics, 1997. **30**(6): p. 539-548.
22. Pillay, V., et al., *A review of the effect of processing variables on the fabrication of electrospun nanofibres for drug delivery applications.* Journal of Nanomaterials, 2013. **2013:** p. 789289.
23. Feng, C., et al., *Preparation and characterization of electro-spun nanofibre membranes and their possible applications in water treatment.* Separation and Purification Technology, 2013. **102**: p. 118-135.
24. Barhate, R.S. and Ramakrishna, S., *Nanofibrous filtering media: Filtration problems and solutions from tiny materials.* Journal of Membrane Science, 2007. **296**(1–2): p. 1-8.
25. Anu Bhushani, J. and Anandharamakrishnan, C., *Electrospinning and electrospraying techniques: Potential food based applications.* Trends in Food Science & Technology, 2014. **38**(1): p. 21-33.

26. Pereira da Silva, J.S., et al., *Fully biodegradable composites based on poly(butylene adipate-co-terephthalate)/peach palm trees fibre.* Composites Part B: Engineering, 2017. **129**: p. 117-123.
27. Lee, S. and Obendorf, S.K., *Developing protective textile materials as barriers to liquid penetration using melt-electrospinning.* Journal of Applied Polymer Science, 2006. **102**(4): p. 3430-3437.
28. Da Silva, F.A.G., et al., *Synthesis and characterization of highly conductive polypyrrole-coated electrospun fibres as antibacterial agents.* Composites Part B: Engineering, 2017. **129**: p. 143-151.
29. Grkovic, M., et al., *Improvement of mechanical properties and antibacterial activity of crosslinked electrospun chitosan/poly (ethylene oxide) nanofibres.* Composites Part B: Engineering, 2017. **121**: p. 58-67.
30. Thavasi, V., Singh, G. and Ramakrishna, S., *Electrospun nanofibres in energy and environmental applications.* Energy and Environmental Science, 2008. **1**(2): p. 205-221.
31. Correia, V., et al., *Design and validation of a biomechanical bioreactor for cartilage tissue culture.* Biomechanics and Modeling in Mechanobiology, 2016. **15**(2): p. 471-478.
32. Nunes-Pereira, J., et al., *Poly(vinylidene fluoride) and copolymers as porous membranes for tissue engineering applications.* Polymer Testing, 2015. **44**: p. 234-241.
33. Ribeiro, C., et al., *Piezoelectric poly(vinylidene fluoride) microstructure and poling state in active tissue engineering.* Engineering in Life Sciences, 2015. **15**(4): p. 351-356.
34. Ribeiro, C., et al., *Piezoelectric polymers as biomaterials for tissue engineering applications.* Colloids and Surfaces B: Biointerfaces, 2015. **136**: p. 46-55.
35. Martins, P.M., et al., *Effect of poling state and morphology of piezoelectric poly(vinylidene fluoride) membranes for skeletal muscle tissue engineering.* RSC Advances, 2013. **3**(39): p. 17938-17944.
36. Martins, P., Lopes, A.C. and Lanceros-Mendez, S., *Electroactive phases of poly(vinylidene fluoride): Determination, processing and applications.* Progress in Polymer Science, 2014. **39**(4): p. 683-706.
37. Ribeiro, S., et al., *Electrospun styrene-butadiene-styrene elastomer copolymers for tissue engineering applications: Effect of butadiene/styrene ratio, block structure, hydrogenation and carbon nanotube loading on physical properties and cytotoxicity.* Composites Part B: Engineering, 2014. **67**: p. 30-38.
38. Wu, Q., et al., *Absorption and mechanical properties of SiCp/PVDF composites.* Composites Part B: Engineering, 2017. **131**: p. 1-7.
39. Nunes-Pereira, J., et al., *Nanodiamonds/poly(vinylidene fluoride) composites for tissue engineering applications.* Composites Part B: Engineering, 2017. **111**: p. 37-44.
40. Rana, S., et al., *On the suitability of nanocrystalline ferrites as a magnetic carrier for drug delivery: Functionalization, conjugation and drug release kinetics.* Acta Biomaterialia, 2007. **3**(2): p. 233-242.
41. Ribeiro, C., et al., *Proving the suitability of magnetoelectric stimuli for tissue engineering applications.* Colloids and Surfaces B-Biointerfaces, 2016. **140**: p. 430-436.
42. Hazra, S. and Ghosh, N.N., *Preparation of Nanoferrites and Their Applications.* Journal of Nanoscience and Nanotechnology, 2014. **14**(2): p. 1983-2000.

43. Ajroudi, L., et al., *Magnetic, electric and thermal properties of cobalt ferrite nanoparticles.* Materials Research Bulletin, 2014. **59**: p. 49-58.
44. Bhowmik, R.N., *Ferromagnetism in lead graphite-pencils and magnetic composite with $CoFe_2O_4$ particles.* Composites Part B: Engineering, 2012. **43**(2): p. 503-509.
45. Han, W.M., et al., *Impact of cellular microenvironment and mechanical perturbation on calcium signalling in meniscus fibrochondrocytes.* European Cells and Materials, 2014. **27**: p. 321-331.
46. Martins, P., et al., *Dielectric and magnetic properties of ferrite/poly(vinylidene fluoride) nanocomposites.* Materials Chemistry and Physics, 2012. **131**(3): p. 698-705.
47. Martins, P., Costa, C.M. and Lanceros-Mendez, S., *Nucleation of electroactive β-phase poly(vinilidene fluoride) with $CoFe_2O_4$ and $NiFe_2O_4$ nanofillers: A new method for the preparation of multiferroic nanocomposites.* Applied Physics A: Materials Science and Processing, 2011. **103**(1): p. 233-237.
48. Gonçalves, R., et al., *Magnetoelectric $CoFe_2O_4$/polyvinylidene fluoride electrospun nanofibres.* Nanoscale, 2015. **7**(17): p. 8058-8061.
49. Fraden, J., *Physical Principles of Sensing*, in *Handbook of Modern Sensors: Physics, Designs, and Applications*, Fraden, J., Editor. Springer-Verlag New York, 2010. p. 53-145.
50. Hadimani, R.L., et al., *Continuous production of piezoelectric PVDF fibre for e-textile applications.* Smart Materials and Structures, 2013. **22**(7): p. 075017.
51. Heo, S.J., et al., *Fiber Stretch and Reorientation Modulates Mesenchymal Stem Cell Morphology and Fibrous Gene Expression on Oriented Nanofibrous Microenvironments.* Annals of Biomedical Engineering, 2011. **39**(11): p. 2780-2790.
52. Wang, H.W., et al., *Analysis of effect of fiber orientation on Young's modulus for unidirectional fiber reinforced composites.* Composites Part B: Engineering, 2014. **56**: p. 733-739.
53. Ribeiro, C., et al., *Influence of Processing Conditions on Polymorphism and Nanofiber Morphology of Electroactive Poly(vinylidene fluoride) Electrospun Membranes.* Soft Materials, 2010. **8**(3): p. 274-287.
54. Martins, P., et al., *Tailored Magnetic and Magnetoelectric Responses of Polymer-Based Composites.* ACS Applied Materials and Interfaces, 2015. **7**(27): p. 15017-15022.
55. Nerurkar, N.L., Elliott, D.M. and Mauck, R.L., *Mechanics of oriented electrospun nanofibrous scaffolds for annulus fibrosus tissue engineering.* Journal of Orthopaedic Research, 2007. **25**(8): p. 1018-1028.
56. Lake, S.P., et al., *Effect of Fiber Distribution and Realignment on the Nonlinear and Inhomogeneous Mechanical Properties of Human Supraspinatus Tendon under Longitudinal Tensile Loading.* Journal of Orthopaedic Research, 2009. **27**(12): p. 1596-1602.
57. Li, W.J., et al., *Engineering controllable anisotropy in electrospun biodegradable nanofibrous scaffolds for musculoskeletal tissue engineering.* Journal of Biomechanics, 2007. **40**(8): p. 1686-1693.
58. Ruder, C., et al., *Influence of fibre diameter and orientation of electrospun copolyetheresterurethanes on smooth muscle and endothelial cell behaviour.* Clinical Hemorheology and Microcirculation, 2013. **55**(4): p. 513-522.

59. Nguyen, A.T., Sathe, S.R. and Yim, E.K.F., *From nano to micro: topographical scale and its impact on cell adhesion, morphology and contact guidance.* Journal of Physics-Condensed Matter, 2016. **28**(18): p. 183001.
60. Jeng, H.A. and Swanson, J., *Toxicity of metal oxide nanoparticles in mammalian cells.* Journal of Environmental Journal of Environmental Science and Health - Part A Toxic/Hazardous Substances & Environmental Engineering, 2006. **41**(12): p. 2699-2711.
61. Bachand, G.D., et al., *Cytotoxicity and inflammation in human alveolar epithelial cells following exposure to occupational levels of gold and silver nanoparticles.* Journal of Nanoparticle Research, 2012. **14**(10): p. 1212.
62. Hu, B., El Haj, A.J. and Dobson, J., *Receptor-Targeted, Magneto-Mechanical Stimulation of Osteogenic Differentiation of Human Bone Marrow-Derived Mesenchymal Stem Cells.* International Journal of Molecular Sciences, 2013. **14**(9): p. 19276-19293.
63. Brito-Pereira, R., et al., *Magnetoelectric response on Terfenol-D/ P(VDF-TrFE) two-phase composites.* Composites - Part B: Engineering, 2017. **120**: p. 97-102.

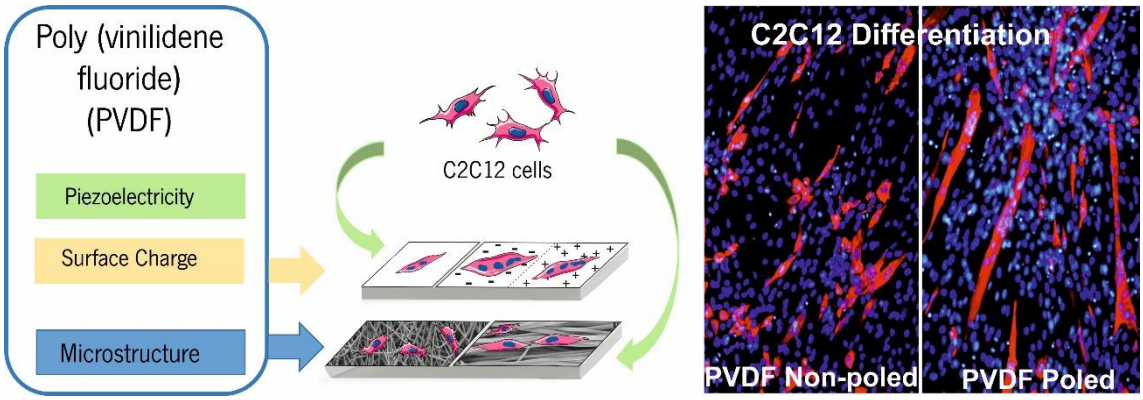

Chapter 4. Electroactive biomaterial surface engineering effects on muscle cells differentiation

PVDF has been proven to be a suitable as a substrate for skeletal muscle tissue engineering in the form of film and fibres in the myoblast proliferation. This chapter describes how the surface properties of the material, both in terms of the poling state (positive or negative net surface charge) and of the morphology (films or fibres) influence myoblast differentiation before dynamic tests. Quantitative analysis of myotube fusion, maturation index, length, diameter and number were evaluated as well as immunofluorescence staining of the myosin heavy chain present in the myotubes.

This chapter is based on the following publication: **S. Ribeiro**, A.C. Gomes, I. Etxebarria, S. Lanceros-Méndez, C. Ribeiro, *Electroactive biomaterial surface engineering effects on muscle cells differentiation*; Materials Science and Engineering C, 92, 868-874, 2018.

4.1 Introduction

The loss or failure of an organ or tissue is one of the most frequent, devastating and costly problems in health care. Musculoskeletal conditions are the most common cause of severe long-term pain and physical disability [1], and they affect hundreds of millions of people around the world [2]. The musculoskeletal system, which includes bone [3], cartilage [4], tendon/ligament [5] and skeletal muscle [6], is becoming the main target for TE because of the high need for regeneration and/or repair.

Skeletal muscles, comprising between 40 to 45% of an adult human body mass, are mainly responsible for generating forces which facilitate voluntary movement, postural support, breathing and locomotion [7]. Skeletal muscle injuries can stem from a variety of events, including direct trauma such as muscle lacerations, contusions or strains, and indirect causes, such as ischemia, infection or neurological dysfunction [8]. In response to minor injuries, skeletal muscle possesses a remarkable robust innate capacity for regeneration [9]. However, severe injuries that result in muscle mass loss of more than 20% can lead to extensive and irreversible fibrosis, scaring and loss of muscle function [10]. In such cases, reparative fibrosis overpowers formation of new muscle, leaving an excess of scar tissue that eventually yields a sub-innervated, malfunctioning muscle. Furthermore, with aging and severe congenital disorders, the loss of muscle mass and function is additionally exacerbated by the reduced self-renewing capacity of satellite cells [9].

In this sense, TE and regenerative medicine are growing fields of interest in human life sciences due to promising results in regenerating, maintaining or improving almost every tissue function of the human body by combining optimized biomaterial scaffolds, cells and growth factors [11]. The biomaterial scaffold acts as a tool to locally control and guide tissue regeneration, more specifically, its architecture and physical properties play an important role from the cell seeding procedure to the processes of cell proliferation and differentiation [12]. In the human body, various biophysical and biochemical stimuli govern the development and maintenance of tissue structure and functionality. Chemical, mechanical, topography/microstructure, electric and magnetic stimuli are critical cues in the formation, function and regeneration of tissues and organs [13-15]. In this sense, *in vivo* electric signals directly influence the development, function and repair of many tissues and organs. Skeletal muscle cells develop endogenous electrical fields in the form of membrane potentials, which demonstrate the importance of the application and modulation of electrical stimuli [16]. Muscle tissue consists of aligned bundles of multinucleated, striated and contractile muscle cells, the myofibres [17]. It has been demonstrated that electrical stimulation not only influences muscle cell phenotype, myosin expression and contractile sarcomere assembly, but can also modulate fiber type switch, and induce contractility in differentiated myotubes

[18]. C2C12 myoblasts, a murine myoblast cell line, is routinely used as an experimental model of skeletal muscle [6]. Myotubes differentiated from C2C12 myoblasts can be used to monitor skeletal muscle cell contraction and activity [19-20]. It has been demonstrated that Ca^{2+} transient fluxes in C2C12 myotubes induced by electrical pulse stimulation can accelerate the combination of functional sarcomeres and stimulate contractile activity of cells [21]. Furthermore, C2C12 skeletal muscle cells cultured on positively and negatively charged polyelectrolyte layer-by-layer polymeric nanofilms demonstrate that negative charge and the increase of the molecular weight promote myotube formation with high fusion index [22].

As electrical signals, in particular electromechanical signals, constitute one of the main physical stimuli present in the human body, electroactive scaffolds based on piezoelectric polymers have shown strong potential for TE [3, 23] with different cellular models, such as C2C12 myoblast [6], MC3T3-E1 pre-osteoblast [24-25], human adipose stem cells [3] and also in *in vivo* study [26]. Piezoelectric polymers are able to induce transient surface charge boosting cell growth and differentiation compared with non-piezoelectric controls. In this way, such electromechanical stimulation can be conducted effectively by piezoelectric polymers, such as PVDF that is a biocompatible polymer with the largest piezoelectric response. PVDF is a semi-crystalline polymer with five known crystalline forms: β, α, γ, δ and ε, the β-phase showing the strongest piezoelectric response [27-28]. Further, materials with a ME response based on the combination of magnetostrictive and piezoelectric materials have been proposed as a new approach for TE [29-30], allowing magnetically induced piezoelectric stimulation of cells.

In this context, the main objective of the present study is to elucidate the influence of the poling state in the behaviour of C2C12 myoblast cell line cultured on β-PVDF films, quantifying the differentiation capabilities of myoblasts, such as the fusion and maturation index. Three kinds of β-PVDF films were used: non-poled - no charged surface, “poled +” - positively charged side of the sample and “poled –” - negatively charged side of the sample. Oriented and random electrospun fibres were used to evaluate the effect of piezoelectric support morphology on cell response. C2C12 differentiation into myotubes was analyzed in order to provide quantitative information on the regeneration potential of skeletal muscle through piezoelectric polymers.

4.2 Experimental Section

4.2.1 Materials

PVDF (Solef 5130, M_w 1,000-1,200 kg/mol) and DMF were purchased from Solvay and Merck, respectively.

4.2.2 Preparation of the samples

A 20 wt.% solution of PVDF in DMF was prepared under magnetic stirring at room temperature until complete dissolution of the polymer. For PVDF films, the solution was spread on a clean glass substrate and heated (J.P. Selecta) to 220 °C for 10 min for solvent evaporation and polymer melting. Then the samples were cooled at room temperature. After that, the polymer is predominantly in the α-PVDF, so to obtain β-PVDF, the conventional stretching is carried out and films with a thickness around 110 µm were obtained [31]. Sample poling (orientation of the dipolar moments along the thickness direction of the samples) was achieved by Corona discharge inside a home-made chamber (10 kV and 10 µA during 120 min at 120 °C) and cooling down to room temperature under applied electric field, after an optimization procedure [31]. The piezoelectric response (d_{33}) of the poled films was obtained with range d_{33}-meter (model 8000, APC Int Ltd). The d_{33} coefficient of the poled samples is ≈ |24| pC.N^{-1} [27].

The PVDF electrospun fibres were processed after the experimental procedure presented in [31-32]. In order to obtain these PVDF electrospun fibres, the same procedure as described on Chapter 2 (section 2.2.3.1) was performed (with a steel needle with inner diameter of 0.5 mm at 14 kV with a feed rate of 0.5 mL.h^{-1}). Oriented and random oriented fibres were prepared.

The surface charge and morphological features of the films and fibres has been previously reported in [33] and [32], respectively. WCA, essential for properly understanding cell materials interaction, is 83.1 ± 2.2°; 51.3 ± 3.1° and 45.0 ± 1.6° for the non-poled, positive poled and negative poled PVDF films, respectively [6]. Further, the WCA is 135.1 ± 3.0° and 115.6 ± 3.3° for oriented and random fibres, respectively [6].

4.2.3 Membrane sterilization

Circular PVDF samples for *in-vitro* assays: non-poled, "poled +", "poled –" β-PVDF films, random and oriented β-PVDF nanofibres, were cut with 13 mm of diameter. The samples sterilization was done as showed on chapter 2 (section 2.2.3.3.1). Then, the samples were placed in a 24-well cell culture plates.

4.2.4 Cell culture

C2C12 cells were grown in 75 cm^2 cell-culture flask. The composition of the medium, i.e. basal medium (BM) and the conditions of cell culture are the same as described on Chapter 2 (section 2.2.3.3.2). C2C12 cells were seeded on the different PVDF films and fibres at a density of 4x10^4 cells.mL^{-1}

and $1x10^5$ cells.mL^{-1}, respectively. The samples were placed in 24-well plates and incubated in BM, as previously described, until becoming confluent. For proliferation assessment, the cells were maintained in BM for 8 days at 37 °C in a saturated humidity atmosphere containing 95% air and 5% CO_2. For the differentiation experiments, in order to induce myotube formation, the BM of the C2C12 cells was changed to differentiation medium (DM) and the culture was also maintained for 8 days, as in the proliferation studies. The DM was composed of DMEM supplemented with 2% FBS and 1% P/S. The decrease of the serum percentage in the medium (DM) leads the cells to be exposed to less factors. Under these conditions, cells stop proliferation and start a differentiation process [34]. In all cultures the medium was renovated daily.

4.2.5 Immunofluorescence staining

After 3, 5 and 8 days of culture in BM or DM, cells seeded on different samples were subjected to immunofluorescence staining to analyse the presence of MHC. MHC are contractile proteins that are part of the thick filaments of the functional unit of the skeletal muscle. In this way, only the functional myotube exhibits MHC, although it appears in the formation of more myotubes. At each timepoint, the medium of each well was removed and the cells were washed with PBS and fixed in 70% ethanol-37% formaldehyde-glacial acetic acid (20:2:1) solution for 10 min at 4 °C and then blocked with a blocking solution (5% goat serum and 0.3% triton X-100 in PBS) for 1 h at room temperature. After this, the samples were incubated with monoclonal mouse IgG_{2B} Clone MF20 antibody (R&D Systems, Catalog number: MAB4470) at 1:50 in 5% goat serum in PBS at room temperature for 1 h, washed in 0.5% PBS-Tween 20 and then labelled with anti-mouse IgG-NL557 secondary antibody (R&D Systems) diluted 1:200, also in 5% donkey serum in PBS at room temperature and in the dark for 1 h. The cells were subsequently counterstained with 1 μg.mL^{-1} of DAPI for 5 min at room temperature in the dark, rinsed in 0.5% PBS-Tween 20 and then with distilled water. The samples were carefully removed from the wells, mounted on slides with the cells facing towards the microscope slide and visualized using a fluorescence microscope (Olympus BX51) with the appropriate filter sets for the used label.

4.2.6 Calculation of fusion and maturation index per area

The fusion index was calculated as the ratio of the nuclei number in myotube with two or more nuclei versus the total number of nuclei. The maturation index was defined as myotubes having five or more nuclei. Myotube number per area was calculated by dividing the number of myotubes in each pattern by the respective area of the pattern and after converted to an area of 1 mm^2. Length, width and the ratio

between them was also calculated. All the tests were calculated using the ImageJ software. Experiments were performed on three samples for each condition, and by analyzing ten images for each sample. The graphs were designed in OriginPro 8.5, and Photoshop CS5 was used to assembly the figures for publication. Data are presented as mean ± standard error of mean (s.e.m.) from triplicates samples of two independent experiments.

4.3 Results

4.3.1 Influence of polymer film polarization on myoblast differentiation

Individual myoblasts fuse to form multinucleated myotubes during myogenic cell differentiation, which can be induced by applying well established protocols. In this study, cells were grown on the materials in the presence of two different culture media: 1) with DM for 8 days to induce cell differentiation and 2) with BM to assess the influence of the poled surface in the expression of the myogenic differentiation marker MHC.

MHC, which is the motor protein of muscle thick filaments that regulates muscle function, was expressed only on the differentiated myotubes. Figure 4.1 shows the fluorescence images of C2C12 myoblasts cultured on different β-PVDF film surfaces (non-poled, “poled +” and “poled –”) and on polystyrene plate with the two different media, BM and DM.

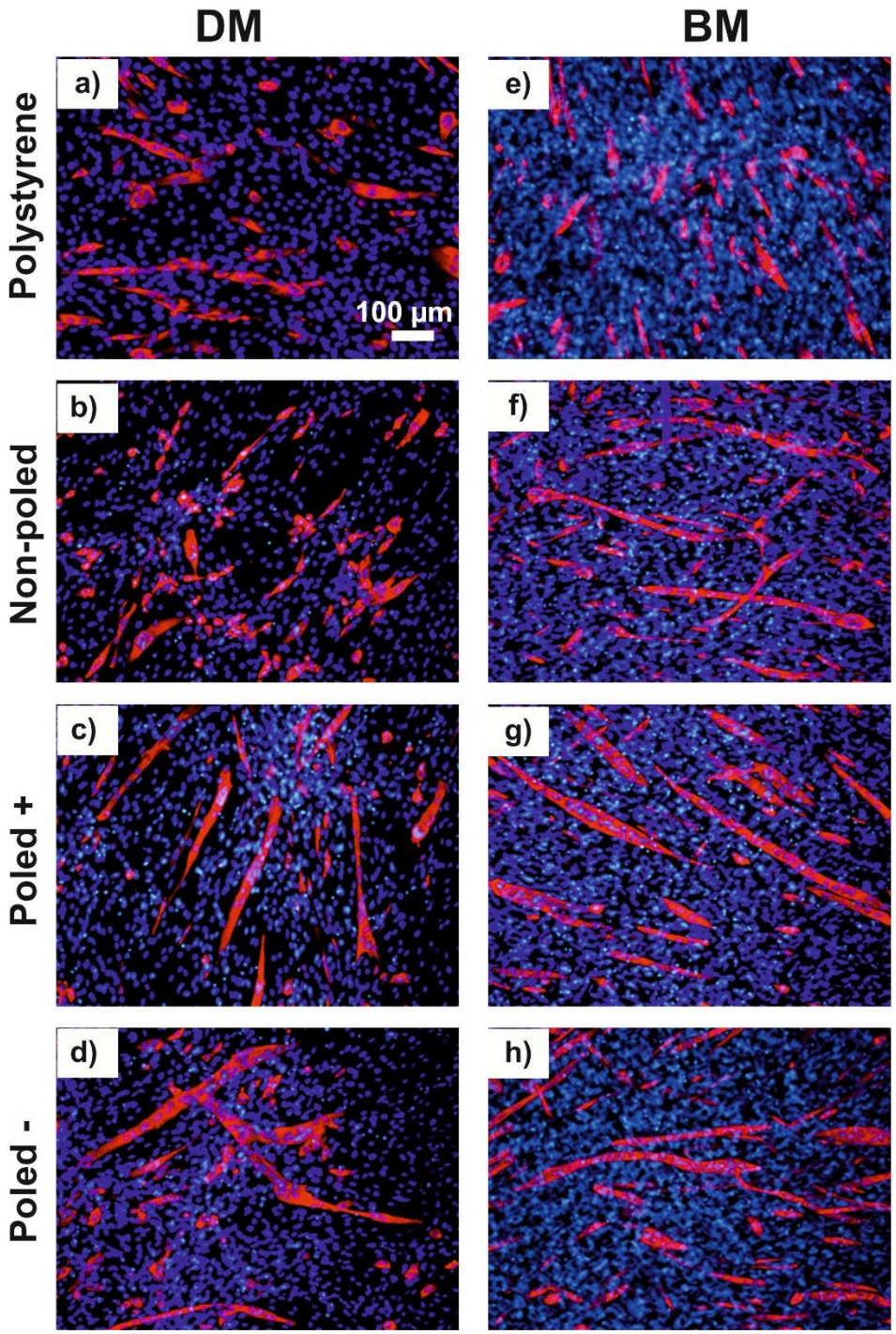

Figure 4.1. Fluorescence microscopy images of myoblasts differentiated on polystyrene and on the different PVDF films for 8 days with different media, containing (a-d) 2% FBS and (e-h)10% FBS. Myofibres were fixed and stained with a MHC-specific antibody (red) and the nuclei counterstained with DAPI (blue). Scale bars represent 100 µm for all images.

As shown in figure 4.1, all the materials with and without surface charge support C2C12 myoblasts differentiation as evidenced by the presence of MHC in all the samples after 8 days of cell culture. Thus, β-PVDF films effectively promote myogenic differentiation of C2C12 myoblast even without DM.

Figure 4.2 shows the fusion and maturation index, which is calculated as the number of fibres in the MHC stained region with more than two nuclei (figure 4.2a) and with five or more nuclei (figure 4.2b), respectively, divided by the total number of myotubes in the vision field.

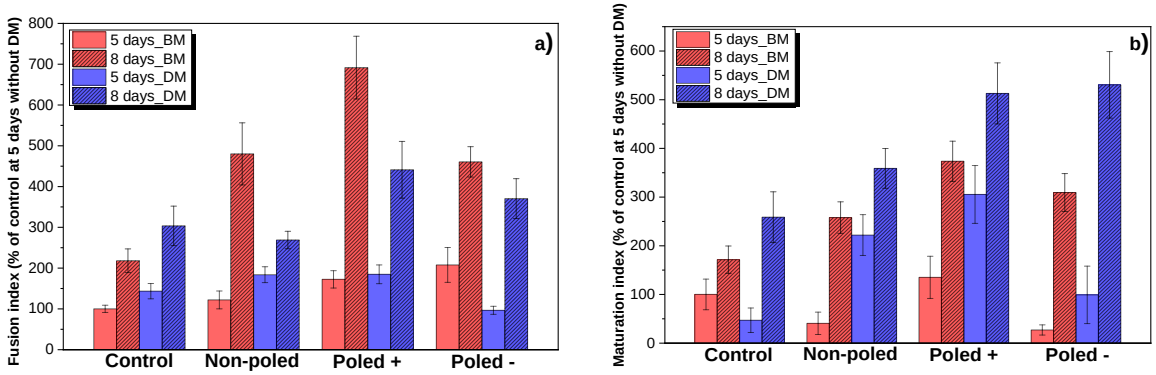

Figure 4.2. Quantification of the (a) fusion and (b) maturation index for the C2C12 cells seeded on control and different β-PVDF films (non-poled, "poled –" and "poled +") with BM and DM for 5 and 8 days of cell culture. The fusion index was calculated as the ratio of the nuclei number in myotubes with two or more nuclei versus the total number of nuclei and the maturation index was calculated as the ratio of the myotube with 5 or more nuclei versus the total number of myotubes. The represented percentage is with respect to the fusion and maturation index of control at 5 days of differentiation without DM.

The results show a progressive increase in differentiation parameters between 5 and 8 days of differentiation for all the samples with either cell culture medium tested. Comparatively to the fusion index in the control at 5 days without DM, the samples β-PVDF "poled –" show higher fusion index relatively to all others. This fact indicates that negatively charged PVDF samples improve C2C12 myoblast cell adhesion and proliferation, which is in agreement with a previous study [6]. β-PVDF "poled –" showed 2.1 fold higher differentiation compared to non-poled β-PVDF (1.2 fold) and "poled +" β-PVDF (1.7 fold). After 8 days of differentiation with the same medium, the fusion index increased in all samples, particularly with "poled +" β-PVDF, which led to 6.92 fold higher fusion index when compared to the others.

Figure 4.2a also shows the fusion index of all samples grown with DM comparatively to the control at 5 days, cultured without DM. Similar values are observed after 5 days of differentiation without DM, however the value is slightly lower for "poled –" β-PVDF. After 8 days, the fusion index values also increase but comparatively lower with regard to the values obtained after 8 days of differentiation with BM. The

materials with surface charge led to higher values than non-poled β-PVDF, while there was no significant differences in differentiation of cells grown on "poled +" or "poled –" β-PVDF.

The maturation index (percentage of myotubes with five or more nuclei) was also used as a parameter to evaluate the differentiation of C2C12 myotubes. These parameter's values were compared with that of cells cultured on control sample for 5 days without DM (figure 4.2b). The cells grown with DM showed for the same sample, highest maturation index than the fusion index. The maturation and fusion indexes at 8 days of differentiation obtained with positive and negatively charged samples, "poled +" β-PVDF and "poled –" β-PVDF, showed no significant differences compared with the control (5 days of differentiation with BM). It is also evident, in figure 4.2b, that cell culture with BM for 5 and 8 days on "poled +" β-PVDF yields the highest fusion index and myotubes with higher maturation when compared with the other samples cultured with the same medium. Thus, on β-PVDF films, the DM can promote myotubes with higher maturation.

The size of myotubes, more specifically their length and diameter, after cell culture with the two media previously described was investigated and the results are shown in figure 4.3.

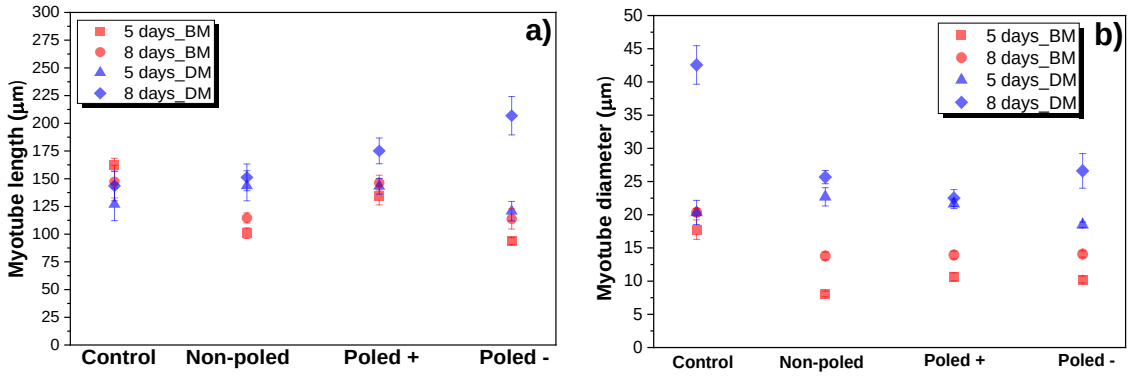

Figure 4.3. Mean of (a) length and (b) diameter of myotubes obtained by fusion of C2C12 cells grown on control and different β-PVDF films (non-poled, "poled –" and "poled +") with either BM or DM for 5 and 8 days of cell culture.

Figure 4.3a shows that higher values of maturation index are also associated with longer myotubes. The myotubes obtained by fusion of C2C12 myoblast cells cultured on samples with DM present the highest values. After 8 days of cell culture with DM, all β-PVDF samples lead to a higher mean length compared to that of the control. Myotubes grow significantly longer between 5 and 8 days with"poled –" β-PVDF with DM, 120.7 ± 8.8 and 206.8 ± 17.3 µm, respectively. "Poled +" β-PVDF and non-poled β-PVDF support myotubes with 175.1 ± 11.6 and 151.2 ± 12.1 µm, respectively, after 8 days with the

same culture medium. Myotubes grown on all PVDF samples with BM are smaller compared to those incubated with DM. The "poled +" β-PVDF samples support the biggest myotubes, with 146.4 ± 6.7 µm, in association with the highest maturation index value. Interestingly, no significant differences exist compared to the size of myotubes at 5 days of differentiation, 134.7 ± 8.4 µm.

The average diameter of the myotubes obtained with the different PVDF samples are presented in figure 4.3b and shows that the diameter means of myotubes cultured on the PVDF samples with DM ranged between 22.5 and 26.6 µm after 8 days of differentiation. "poled –" β-PVDF led to a higher difference in diameter between 5 and 8 days of cell culture. The diameter of myotubes obtained with BM was smaller when compared to the others, as depicted in figure 4.3b (13.8 to 14.1 µm after 8 days of cell proliferation with all PVDF samples).

The myotube number was also quantified and the results are represented in figure 4.4.

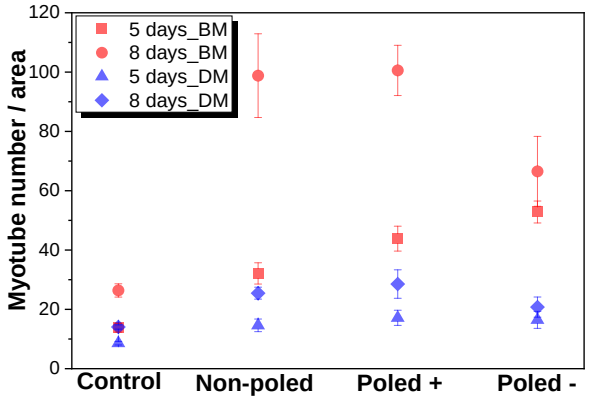

Figure 4.4. Number of myotubes present in 1 mm^2 of the different samples, such as control and β-PVDF films (non-poled, "poled –" and "poled +"), cultured with BM and DM for 5 and 8 days of cell culture.

Figure 4.4 shows that there is a higher number of myotubes per area on the samples cultured with BM, which is in agreement with the previous results once myotubes with higher maturation are obtained with DM, which leads also to larger myotubes and, therefore, to lower number of myotubes per area.

4.3.2 Influence of polymer fiber orientation on myoblast differentiation

The obtained PVDF fibres present a diameter of approximately 500 nm and a WCA of 135.1 ± 3.0° for oriented fibres and slightly lower (115.6 ± 3.3°) for randomly oriented fibres. Relatively to the electroactive beta phase and crystallinity, both PVDF fiber mats show values around 48 and 83%, respectively. It is to notice that after the electrospinning process the fibres are piezoelectric and self-poled

with a positive surface charge [35]. Thus, electrospun fibres essentially represent just a morphological modification with respect to PVDF films.

The different PVDF morphologies were used as supports for cell viability studies in order to improve specific TE approaches [36], in particular for muscle cells, due to their fibrillar microstructure. Electrospun fibres seem to be a promising approach for skeletal muscle TE as they share a similar architecture to the natural living systems of the muscle cells [37]. Figure 4.5 shows the SEM images of C2C12 myoblasts cultured on different PVDF electrospun fibres, oriented and random, after eight days of cell culture with DM.

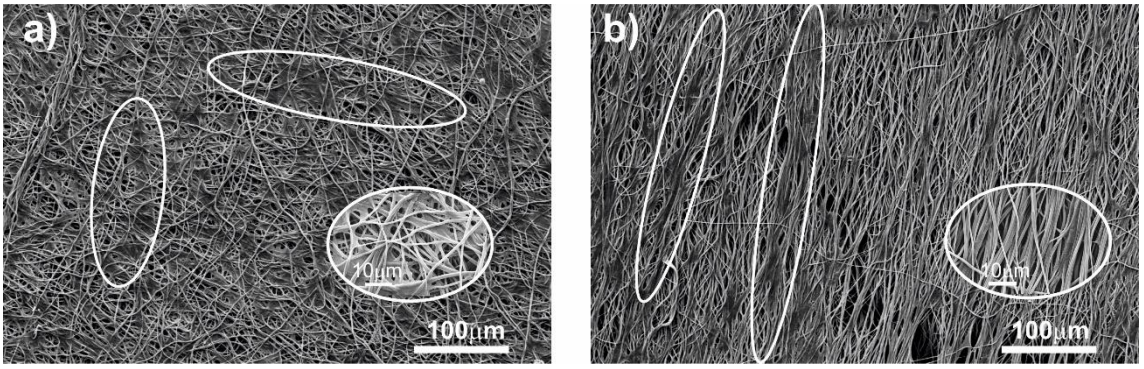

Figure 4.5. SEM micrographs of PVDF (a) random and (b) oriented electrospun fibres with C2C12 myoblast cells after eight days of culture.

4.4 Discussion

PVDF is an electroactive polymer with excellent biocompatibility [6] and a high Young's modulus of 2 GPa [38], the fibres showing a lower effective Young´s modulus around 220 MPa [39], mainly due to fiber reorientation during mechanical stretching. The mechanical characteristics of PVDF influence cellular activities, as PVDF scaffolds can support adhesion, proliferation and differentiation of cells [23, 40]. It has been reported that PVDF directly influences cell adhesion, proliferation and differentiation depending on cell type [3, 41], morphology [42] and poling state [6, 43].

Previous studies reported that after just one day of cell culture, the morphology of C2C12 cells revealed some differences depending on the support given by different PVDF films [6]. It is also demonstrated that the films with surface charge improve myoblast proliferation, wherein β-PVDF "poled –" show the best results. The surface charge is a relevant parameter for cell morphology and proliferation [6], so it is a relevant parameter to take into account for myoblast differentiation.

DM, applied to promote myogenic differentiation of C2C12, includes a lower percentage of serum compared to the BM, used for regular maintenance of this cell line. It is known that upon reduction of

serum present in the medium, the myoblast cell cycle arrests and these cells start to differentiate, align and fuse, forming multinucleated myotubes [44], which are the building blocks for skeletal muscle. Therefore, understanding the differentiation process of C2C12 skeletal myoblasts *in vitro* will allow to get insights on the mechanisms of myogenic differentiation *in vivo*. In this study, after 8 days of cell culture, it was demonstrated that the β-PVDF also influences myoblast differentiation although without significant differences between the two poling states tested, positive and negative.

The samples cultured with DM that show the lowest fusion index, lead to the highest myotube maturation index which can be related with the fact that the DM better supports myotube maturation.

Skeletal muscle generally consists on bundles of multinucleated myofibres and can be distinguished by morphological properties such as shape, orientation innervation, attachment sites and size. These unique properties allow for considerable muscle diversity generating muscles to produce a variety of movements and functions [45]. These properties can be influenced by the surface charge of the material they grow on. The maturation index can also be associated with the size of myotubes [46]. The diameter of the myotube is another relevant parameter as it is an important indicator of the contractile force generation ability of the muscle [47].

The fact that the number of myotubes per area is higher on samples cultured with BM can be inversely correlated with the higher length and maturation index of myotubes obtained with PVDF samples and cultured with DM. In this way, PVDF promoted myogenic differentiation of C2C12 cells as evidenced by this quantitative analysis and also others already discussed here.

It has been demonstrated that the PVDF fibres influence cell morphology [6] and consequently the fiber topography directs cytoskeletal reorganization to orient cells longitudinally along the axis of the fiber [48]. It has been reported that myoblasts likely fuse in an end-to-end configuration, and therefore the linear morphology of the support favors the linear form, rather than irregular myotubes and consequently to reproduce the muscle force [49]. Similarly, the inherent electrical excitability of muscle cells inspired the use of electroactive scaffolds for skeletal muscle TE [50]. Silk fibroin/melanin composite electrospun fibres maintained the proliferation of C2C12 cells and improve the differentiation of the myoblast cells into multinucleate myotube on the aligned fibres compared to the corresponding films, demonstrating the importance of the topography and conductivity of the scaffolds for muscle TE [50].

The surface characteristics of biomaterials, including their topography, plays an essential role in cell behaviour and cellular processes [51-52]. In order to enter into myogenesis (the differentiation process), myoblasts need to exit the cell cycle [53]. During this process, successive events occur and are regulated by several factors, such as transcription factors and regulatory mechanism of several proteins (such as

transforming growth factor β and protein kinase C). So, varying charged surfaces and topographies (figure 4.6), allows to influence those processes at the molecular level through electrostatic interactions, modifying muscle fiber formation and enhancing differentiation of myoblast cells.

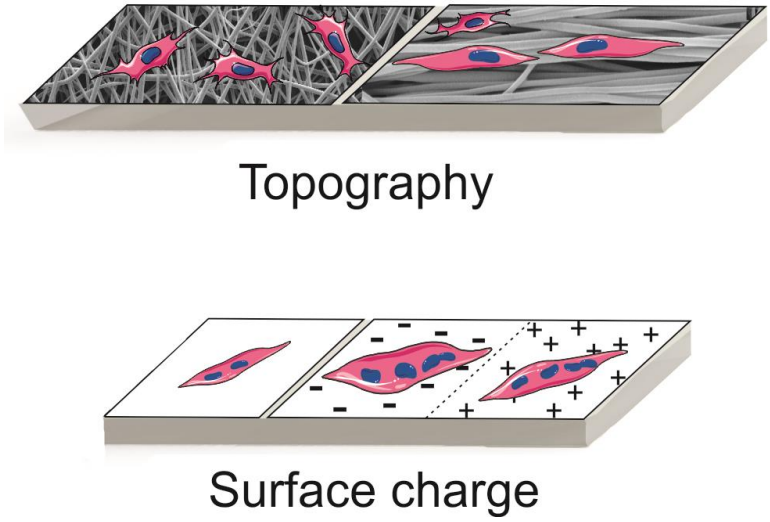

Figure 4.6. Schematic representation of cell behaviour depending on the topography and surface charge.

So, the results prove the potential of the use of piezoelectric biomaterials for muscle TE, allowing the combination of charged and aligned materials to tailor cell response. So, these physical stimuli (electrical signals and scaffolds topography) are important factors to consider to obtain biomimetic tissues. Further, specific bioreactors can apply mechanical stimuli to the piezoelectric scaffolds in order to produce voltage variation that have shown to be suitable for other cell types, such as bone cells [3]. So, under dynamic conditions, the developed samples can further improve myoblast proliferation and differentiation.

4.5 Conclusions

This work demonstrates that charged surfaces of piezoelectric polymers promote myogenic cell differentiation. It is shown that positively charged surfaces of β-PVDF samples with the BM show a higher fusion index comparatively to negatively charged surfaces and non-poled samples. Further, the maturation index is higher for cells grown on surface charged samples in the presence of DM, with no significant differences in positive and negatively charged surfaces. With respect to the effect of the scaffold morphology, oriented electrospun PVDF fibres promote the alignment of the cells that is important for the differentiation and morphology of skeletal muscle tissue in the human body. Therefore, it is demonstrated that electroactive biomaterials are a valuable approach in muscle regeneration therapies.

4.6 References

1. Nijhawan, R., *Visual prediction: Psychophysics and neurophysiology of compensation for time delays.* Behavioral and Brain Sciences, 2008. **31**(2): p. 179-198.
2. Woolf, A.D. and Pfleger, B., *Burden of major musculoskeletal conditions.* Bulletin of the World Health Organization, 2003. **81**(9): p. 646-656.
3. Ribeiro, C., et al., *Piezoelectric poly(vinylidene fluoride) microstructure and poling state in active tissue engineering.* Engineering in Life Sciences, 2015. **15**(4): p. 351-356.
4. Zhu, W.M., et al., *Research Progress of Scaffold Materials in Cartilage Tissue Engineering.* Journal of Biomaterials and Tissue Engineering, 2015. **5**(9): p. 673-679.
5. Tellado, S.F., Balmayor, E.R. and Griensven, M.V., *Strategies to engineer tendon/ligament-to-bone interface: Biomaterials, cells and growth factors.* Advanced Drug Delivery Reviews, 2015. **94**: p. 126-140.
6. Martins, P.M., et al., *Effect of poling state and morphology of piezoelectric poly(vinylidene fluoride) membranes for skeletal muscle tissue engineering.* Rsc Advances, 2013. **3**(39): p. 17938-17944.
7. Järvinen, M.J. and Lehto, M.U.K., *The Effects of Early Mobilisation and Immobilisation on the Healing Process Following Muscle Injuries.* Sports Medicine, 1993. **15**(2): p. 78-89.
8. Huard, J., et al., *Muscle Injuries and Repair: What's New on the Horizon!* Cells Tissues Organs, 2015. **202**(3-4): p. 227-236.
9. Juhas, M. and Bursac, N., *Engineering skeletal muscle repair.* Current Opinion in Biotechnology, 2013. **24**(5): p. 880-886.
10. Turner, N.J. and Badylak, S.F., *Regeneration of skeletal muscle.* Cell and Tissue Research, 2012. **347**(3): p. 759-774.
11. Chaudhuri, R., et al., *Biomaterials and cells for cardiac tissue engineering: Current choices.* Materials Science and Engineering: C, 2017. **79**: p. 950-957.
12. Melchels, F.P.W., et al., *Effects of the architecture of tissue engineering scaffolds on cell seeding and culturing.* Acta Biomaterialia, 2010. **6**(11): p. 4208-4217.
13. Balint, R., Cassidy, N.J. and Cartmell, S.H., *Electrical Stimulation: A Novel Tool for Tissue Engineering.* Tissue Engineering Part B-Reviews, 2013. **19**(1): p. 48-57.
14. Liao, S., Chan, C.K. and Ramakrishna, S., *Stem cells and biomimetic materials strategies for tissue engineering.* Materials Science and Engineering: C, 2008. **28**(8): p. 1189-1202.
15. Mansouri, N. and Bagheri, S., *The influence of topography on tissue engineering perspective.* Materials Science and Engineering: C, 2016. **61**: p. 906-921.
16. Handschin, C., et al., *External physical and biochemical stimulation to enhance skeletal muscle bioengineering.* Advanced Drug Delivery Reviews, 2015. **82**: p. 168-175.
17. Bach, A.D., et al., *Skeletal muscle tissue engineering.* Journal of Cellular and Molecular Medicine, 2004. **8**(4): p. 413-422.
18. Qazi, T.H., et al., *Biomaterials based strategies for skeletal muscle tissue engineering: Existing technologies and future trends.* Biomaterials, 2015. **53**: p. 502-521.
19. Kaji, H., et al., *Electrically induced contraction of C2C12 myotubes cultured on a porous membrane-based substrate with muscle tissue-like stiffness.* Biomaterials, 2010. **31**(27): p.6981

20. Akimoto, T., et al., *Mechanical stretch is a down-regulatory signal for differentiation of C2C12 myogenic cells.* Materials Science and Engineering: C, 2001. **17**(1): p. 75-78.
21. Fujita, H., Nedachi, T. and Kanzaki, M., *Accelerated de novo sarcomere assembly by electric pulse stimulation in C2C12 myotubes.* Experimental Cell Research, 2007. **313**(9): p. 1853-1865.
22. Ricotti, L., et al., *Quantification of growth and differentiation of C2C12 skeletal muscle cells on PSS-PAH-based polyelectrolyte layer-by-layer nanofilms.* Biomedical Materials, 2011. **6**(3): p. 031001.
23. Ribeiro, C., et al., *Piezoelectric polymers as biomaterials for tissue engineering applications.* Colloids and Surfaces B-Biointerfaces, 2015. **136**: p. 46-55.
24. Ribeiro, C., et al., *Enhanced proliferation of pre-osteoblastic cells by dynamic piezoelectric stimulation.* Rsc Advances, 2012. **2**(30): p. 11504-11509.
25. Ribeiro, C., et al., *Fibronectin adsorption and cell response on electroactive poly(vinylidene fluoride) films.* Biomedical Materials, 2012. **7**(3): p. 035004.
26. Ribeiro, C., et al., *In vivo demonstration of the suitability of piezoelectric stimuli for bone reparation.* Materials Letters, 2017. **209**: p. 118-121.
27. Gomes, J., et al., *Influence of the beta-phase content and degree of crystallinity on the piezo- and ferroelectric properties of poly(vinylidene fluoride).* Smart Materials & Structures, 2010. **19**(6): p. 065010.
28. Low, Y.K.A., et al., *β-Phase poly(vinylidene fluoride) films encouraged more homogeneous cell distribution and more significant deposition of fibronectin towards the cell–material interface compared to α-phase poly(vinylidene fluoride) films.* Materials Science and Engineering: C, 2014. **34**(1): p. 345-353.
29. Goncalves, R., et al., *Magnetoelectric $CoFe_2O_4$/polyvinylidene fluoride electrospun nanofibres.* Nanoscale, 2015. **7**(17): p. 8058-8061.
30. Ribeiro, C., et al., *Proving the suitability of magnetoelectric stimuli for tissue engineering applications.* Colloids and Surfaces B-Biointerfaces, 2016. **140**: p. 430-436.
31. Ribeiro, C., et al., *Electroactive poly(vinylidene fluoride)-based structures for advanced applications.* Nature Protocols, 2018. **13**(4): p. 681-704.
32. Ribeiro, C., et al., *Influence of processing conditions on polymorphism and nanofiber morphology of electroactive poly(vinylidene fluoride) electrospun membranes.* Soft Materials, 2010. **8**(3): p. 274-287.
33. Nunes, J.S., et al., *Relationship between the microstructure and the microscopic piezoelectric response of the alpha- and beta-phases of poly(vinylidene fluoride).* Applied Physics a-Materials Science & Processing, 2009. **95**(3): p. 875-880.
34. Rodgers, B.D., et al., *Myostatin stimulates, not inihibits, C2C12 myoblast proliferation.* Endocrinology, 2014. **155**(3): p. 670-675.
35. Sencadas, V., et al., *Local piezoelectric response of single poly(vinylidene fluoride) electrospun fibers.* Physica Status Solidi (A) Applications and Materials Science, 2012. **209**(12): p. 2605-2609.
36. Correia, D.M., et al., *Strategies for the development of three dimensional scaffolds from piezoelectric poly(vinylidene fluoride).* Materials & Design, 2016. **92**: p. 674-681.

37. Sun, B., et al., *Electrospun anisotropic architectures and porous structures for tissue engineering.* Journal of Materials Chemistry B, 2015. **3**(27): p. 5389-5410.
38. Fraden, J., *Physical Principles of Sensing*, in *Handbook of Modern Sensors: Physics, Designs, and Applications*, Fraden, J., Editor. Springer-Verlag New York, 2010. p. 53-145.
39. Maciel, M.M., et al., *Relation between fiber orientation and mechanical properties of nano-engineered poly(vinylidene fluoride) electrospun composite fiber mats.* Composites Part B: Engineering, 2018. **139**: p. 146-154.
40. Augustine, R., et al., *Electrospun poly(vinylidene fluoride-trifluoroethylene)/zinc oxide nanocomposite tissue engineering scaffolds with enhanced cell adhesion and blood vessel formation.* Nano Research, 2017. **10**(10): p. 3358-3376.
41. Ribeiro, C., et al., *Surface roughness dependent osteoblast and fibroblast response on poly(l-lactide) films and electrospun membranes.* Journal of Biomedical Materials Research Part A, 2015. **103**(7): p. 2260-2268.
42. Nunes-Pereira, J., et al., *Poly(vinylidene fluoride) and copolymers as porous membranes for tissue engineering applications.* Polymer Testing, 2015. **44**: p. 234-241.
43. Parssinen, J., et al., *Enhancement of adhesion and promotion of osteogenic differentiation of human adipose stem cells by poled electroactive poly(vinylidene fluoride).* Journal of Biomedical Materials Research Part A, 2015. **103**(3): p. 919-928.
44. Andres, V. and Walsh, K., *Myogenin expression, cell cycle withdrawal, and phenotypic differentiation are temporally separable events that precede cell fusion upon myogenesis.* Journal of Cell Biology, 1996. **132**(4): p. 657-666.
45. Rochlin, K., et al., *Myoblast fusion: When it takes more to make one.* Developmental Biology, 2010. **341**(1): p. 66-83.
46. Bajaj, P., et al., *Patterning the differentiation of C2C12 skeletal myoblasts.* Integrative Biology, 2011. **3**(9): p. 897-909.
47. Ikeda, K., et al., *Improved contractile force generation of tissue-engineered skeletal muscle constructs by IGF-I and Bcl-2 gene transfer with electrical pulse stimulation.* Regenerative Therapy, 2016. **3**: p. 38-44.
48. Jana, S., Levengood, S.K.L. and Zhang, M.Q., *Anisotropic Materials for Skeletal-Muscle-Tissue Engineering.* Advanced Materials, 2016. **28**(48): p. 10588-10612.
49. Clark, P., et al., *Alignment of myoblasts on ultrafine gratings inhibits fusion in vitro.* International Journal of Biochemistry & Cell Biology, 2002. **34**(7): p. 816-825.
50. Manchineella, S., et al., *Pigmented Silk Nanofibrous Composite for Skeletal Muscle Tissue Engineering.* Advanced Healthcare Materials, 2016. **5**(10): p. 1222-1232.
51. Sanz-Herrera, J.A. and Reina-Romo, E., *Cell-Biomaterial Mechanical Interaction in the Framework of Tissue Engineering: Insights, Computational Modeling and Perspectives.* International Journal of Molecular Sciences, 2011. **12**(11): p. 8217-8244.
52. Kasemo, B. and Lausmaa, J., *Surface properties and processes of the biomaterial-tissue interface.* Materials Science and Engineering: C, 1994. **1**(3): p. 115-119.
53. Ostrovidov, S., et al., *Skeletal Muscle Tissue Engineering: Methods to Form Skeletal Myotubes and Their Applications.* Tissue Engineering Part B-Reviews, 2014. **20**(5): p. 403-436.

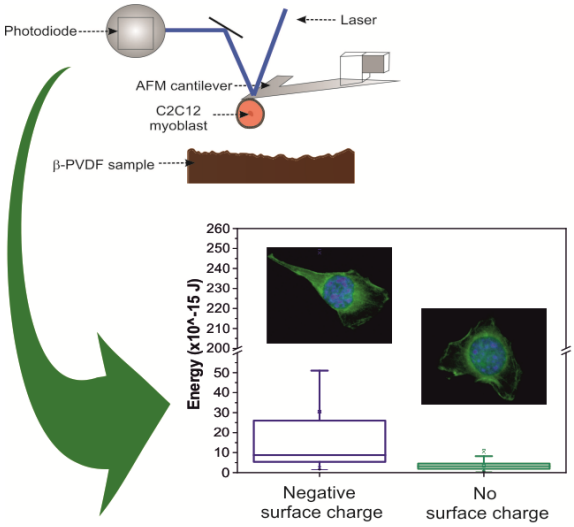

Chapter 5. Surface charge mediated cell-surface interaction on piezoelectric materials

PVDF are the polymers with the largest piezoelectric response. Cell-material interactions play an essential role in the development of scaffold-based tissue engineering strategies. Being Surface characteristics are very important properties of materials for tissue engineering. This chapter describes the influence of the surface charge of piezoelectric PVDF on cell adhesion. The cytoskeletal organization and focal adhesions of C2C12 myoblast cells on different PVDF samples was studied by immunofluorescence staining with and without FBS. The study of the interactions between single live cells and PVDF were analyzed using an AFM technique termed SCFS was evaluated obtaining the quantification of adhesion force, adhesion energy and detachment length.

This chapter is based on the following publication: **S. Ribeiro**, C. Puckert, C. Ribeiro, A.C. Gomes, M.J. Higgins, S. Lanceros-Méndez, *Surface charge mediated cell-surface interaction on piezoelectric materials*; Submitted 2019.

5.1 Introduction

Piezoelectric materials undergoing mechanical deformation generate an overall surface charge variation (direct piezoelectric effect) or expand/contract in the presence of an applied voltage [1]. Piezoelectricity was first reported in 1880 by Jacques and Pierre Curie [2] and since then piezoelectric materials have been used in different areas such as energy harvesting, sensors and actuators, electronics, biotechnology and, more recently, TE [3-5]. In particular, piezoelectric polymers are attractive for these applications due to them being easily tailored at the nano-, micro- and macroscale, produced at low-temperatures and at relatively low cost, and characterized by their flexibility and light weight [6]. A variety of natural and synthetic piezoelectric polymers with different surface properties, such as surface charge or roughness, have recently emerged as biomaterials for TE applications [7]. The use of natural polymers is still inferior to their synthetic counterparts due to their poor mechanical and electrical properties, as well as their often-difficult processing (i.e. isolation/extraction and the possibility to produce larger quantities) and their fabrication, which is less straightforward at this stage. As such, the synthetic piezoelectric polymers have been the largest group of biocompatible polymers used for TE [8], mainly acting as a passive support for cell proliferation and differentiation.

Many of the major functions in cells and organs of the human body are controlled by ionic currents, electric fields, ion flow and voltage gradients produced by ion channels and pumps, which are key regulators of cell proliferation, migration and differentiation [9]. Herein, it has been shown that piezoelectric materials can be relevant for TE strategies by enabling electrical stimulation via a mechanical stimulus, which is important for a range of tissues like bone, tendons, ligaments, cartilage and muscle [10, 11]. It is important to emphasize that skeletal muscle is not a piezoelectric tissue, such as bone, but critically requires electro-mechanical stimulus to promote tissue growth and development and, for this reason, piezoelectric polymers represent a promising new approach for skeletal muscle TE [12]. Piezoelectric polymeric biomaterials such as poly(vinylidene fluoride), PVDF, have been shown to have the necessary biocompatibility and deliver electro-mechanical stimulus to specific cell types [13-15]. More specifically, the effect of PVDF surface charge on the proliferation [14] and differentiation [15] of C2C12 myoblast cells has previously been demonstrated (Figure 5.1). Analysis of the cell differentiation showed that the maturation index of the formed myotubes was higher on electrically poled samples consisting of surface charges in the presence of differentiation medium, with no significant differences between the positively ("poled +") and negatively ("poled –") charged surfaces. C2C12 proliferation on β-PVDF showed that surface charge (of the poled samples) promoted the elongation of the cells after 1 day. In contrast to the morphology, where both polarizations ("poled +" and "poled –") promoted the elongation, it was

found that C2C12 proliferation was higher on the "poled –" β-PVDF. To rationalize effects from the physical surface properties, earlier studies have shown that β-PVDF films have a surface roughness of ≈ 42 nm from peak-to-peak, with no differences between the non-poled and poled β-PVDF samples [16]. However, the polarization of the PVDF electroactive crystalline phase was shown to affect the wettability of the films. The non-poled β-PVDF films were more hydrophobic, with a WCA of 76.8°, whereas the poled β-PVDF films with surface charge had lower WCA of 31.8° and 51° for "poled +" and "poled –", respectively [17], suggesting that surface charge and energy play a role in determining the C2C12 proliferation and differentiation.

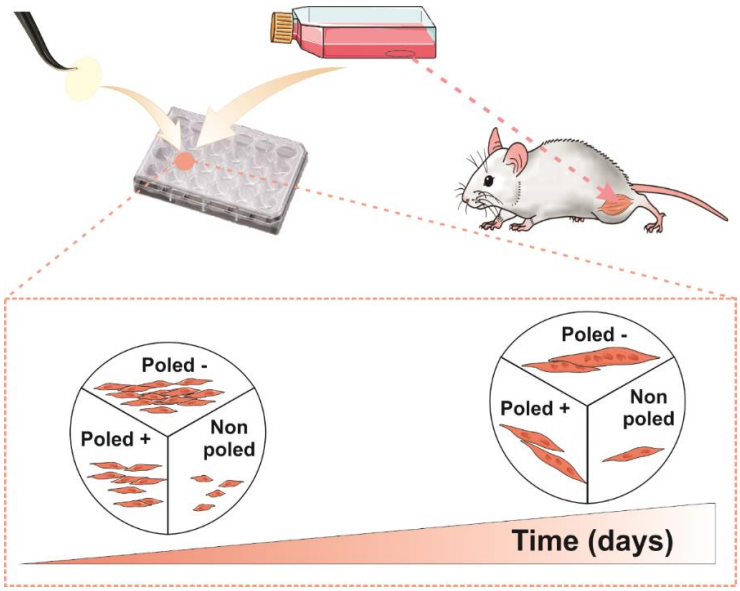

Figure 5.1. Schematic representation of the work on C2C12 myoblast proliferation and differentiation on β-PVDF films with different polarization states.

However, the physical interactions and role of cell adhesion, i.e. cell-substrate forces, mediating these effects are not entirely clear, though there is increasing evidence of their relevance in transmitting signals in the development and maintenance of tissues, regulation of cell cycle, migration, differentiation and survival [18]. Three stages characterize the static *in vitro* cell adhesion process: the initial stage is the attachment of the cell body to the material via ligand binding; subsequently, the cell body flattens and spreads due to reorganization of cytoskeletal actin; and lastly, the formation of FAs between cell and the material due to the further actin organization and recruitment of integrins [19]. The more cells that attach and spread on the material's surface, the greater the number of cell adhesive bonds and, therefore, stronger cell adhesion is expected. Similarly, the adhesion force is related to the number and strength of chemical bonds on the cell surface according to cell adhesion models [19, 20]. These dynamic processes

of cell adhesion are inextricably linked to changes in cytoskeletal tension and activation of signaling cascades that regulate cell proliferation and differentiation (i.e. gene expression). Most studies to date correlate the material surface properties with cell proliferation and differentiation, which are typically ascertained using conventional staining and fluorescent techniques. Furthermore, the extent of the associated cell adhesion is still often extrapolated from morphological observations such as cells spreading or rounding up, without considering the strength of adhesion [21], or determined using general washing assays by counting the number of cells remaining on the substrate. Therefore, the binding specificity (e.g. type of integrin) and adhesion forces at the cell-material interface are not fully quantified, yet the latest models (e.g. clutch model) show they are critical for transmitting the signals from the material through to the cell's interior [22].

Numerous techniques have been developed to analyze cell adhesion events, including those of single cells [23]. One of these techniques, Single Cell Force Spectroscopy (SCFS), is based on Atomic Force Microscopy (AFM) and represents a versatile approach to quantify single cell adhesion on different substrates, between different cell types, and is showing potential application in mechanobiology [24]. The general idea of SCFS is to replace the tip of the AFM cantilever by a living cell [25]. SCFS offers a large range of detectable forces (e.g. from piconewtons to several nanonewtons), where the measurement of cell detachment enables direct quantification of molecular-level interactions and the forces required to detach a single cell from the substrate. SCFS is a technique more suitable for shorter times studies, i.e. seconds to minutes, as longer contact times and adhesion to the surface may eventually exceed the binding of the cell to the AFM cantilever.

In this study, we aimed to further understand the effect of piezoelectric β-PVDF (poled samples) surface charge on the C2C12 myoblast cell adhesion. Morphological observations with immunofluorescence staining was used to investigate the cell interactions with two different PVDF surfaces, including those that are non-poled (overall zero charge) and "poled" (positive or negative surface charge). In addition, the Atomic Force Microscopy-based technique, Single Cell Force Spectroscopy, was used to provide further insight into the effect of surface charge on the de-adhesion forces and energy required to detach single cells from the PVDF surfaces.

5.2 Experimental Section

5.2.1 Materials

PVDF (Solef 5130, M_W 1,000-1,200 kg/mol) and DMF were purchased from Solvay and Merck, respectively.

5.2.2 Preparation of the samples

The procedure detailed for the preparation of the PVDF films was done as described on Chapter 4 (section 4.2.2) obtaining the same films with the same properties (d_{33} coefficient of the poled samples is ≈ |24| pC.N^{-1}. Non-poled samples present an overall zero net charge, whereas, once poled, β-PVDF samples can present an overall negative, "poled –", or positive, "poled +", surface charge [16].

5.2.3 Cell Culture

C2C12 myoblast cells (*ATCC*) were cultivated with the same composition of the medium and the conditions of cell culture as described on Chapter 2 (section 2.2.3.3.2). For the AFM measurements and vinculin staining, a suspension of C2C12 with a density of 8x10^4 cells.mL^{-1} (CO_2-independent media) and 0.8x10^4 cells.mL^{-1}, respectively, was used. For vinculin staining, the suspension of C2C12 was prepared with and without serum for the immunofluorescence assays.

5.2.4 Immunofluorescence staining

C2C12 cells, with and without protein presence, seeded on different samples were subjected to immunofluorescence staining in order to analyse the presence of FAs contact after 3 h of culture in basal medium. The nucleus, actin and vinculin were stained by DAPI, Tetramethylrhodamine B isothiocyanate (TRITC) and anti-vinculin–FITC antibody (*Sigma-Aldrich*), respectively. At this time, the medium of each well was removed and the cells were washed with PBS 1x and fixed in 4% formaldehyde for 10 minutes at 37 °C. After this, the samples were again washed with PBS 1x and then incubated with anti-vinculin–FITC antibody (1:50 in PBS 1x) in the dark at room temperature for 1 h. The cells were subsequently counterstained with TRITC (1:200) and DAPI (1 μg.mL^{-1}) at room temperature in the dark for 30 and 5 min, respectively. In the end, the samples were rinsed in PBS 1x and after with distilled water, and finally mounted on slides. The samples were visualized using a fluorescence microscope (*Olympus Bx51*) with the appropriate filter sets. The *imageJ* software was used to measure the length and width of the cytoskeleton and also the diameter of the nucleus on all the samples with *feret's* diameter measurement. Experiments were performed on three samples for each condition, and by analyzing ten images for each sample. Data are presented as mean ± SD. The graphs were designed in OriginPro 8.5, and Photoshop CS5 was used to assembly the figures for publication. Results were analyzed by Graph Pad Prism Version X for windows (Graph Pad Software, San Diego, CA, U.S.A.). To determine the statistical significances, one-way ANOVA was used. Differences were considered to be significant when $p < 0.05$.

5.2.5 Single Cell Force Spectroscopy

5.2.5.1 Cantilever functionalization

The cantilevers were incubated overnight in 50 µL droplets of biotin-BSA solution in a humidified chamber at 37 °C. After that, the cantilevers were washed by immersing and gently moving them in 20 mL of PBS (without Ca^{2+} and Mg^{2+}) filled into a petri dish, performing a total of three washes. The cantilevers were incubated for 30 min in 50 µL droplets of the diluted streptavidin solution in a humidified chamber at room temperature. Thereafter, the cantilevers were washed again three times in 20 mL PBS (without Ca^{2+}/Mg^{2+}), as previously described. To finish the functionalization, the cantilevers were incubated in 50 µL droplets of diluted concanavalin A-biotin solution in a humidified chamber for 30 min at room temperature. After this time, they were washed three times with PBS and stored in a petri dish containing 10 mL PBS (without Ca^{2+} or Mg^{2+}) at 4 °C for at least one week.

5.2.5.2 Attachment of Single Cell onto AFM Probes

SCFS was performed using a JPK Biowizard II Atomic Force Microscope (JPK, Germany) mounted on a fully automated Nikon inverted optical microscope. The AFM-inverted optical microscope was fully enclosed in a cell incubation system for temperature and humidity control. The PVDF film was placed in the liquid cell and 600 µl of CO_2-independent medium was injected, with heating applied to enable the CO_2-independent media (without proteins) to reach thermal equilibration at 37 °C. The Concanavalin functionalized tipless cantilever was then brought into approximately 50 µm above the PVDF surface. A further 300 µl of CO_2-independent medium containing the C2C12 cells with a concentration of approximately 80 000 cells.ml^{-1} was then injected into the liquid cell and the cells allowed to settle onto the PVDF surface for a period of 5-10 min. Rounded up cells that were yet to adhere were located with the optical microscope and the functionalized AFM probe was positioned over a single cell. The cell was attached manually to the apex of the cantilever by lowering the stepper motor in 1 µm steps and making contact with the cell until an applied force of 0.5 nN had been reached. After attaching the cell, the cantilever was retracted 50 µm and the optical microscope was used to confirm that the cell was positioned correctly at the end of the cantilever. Afterwards, the single cell was allowed to adhere for 5 min to ensure the strength of cell attachment to the cantilever was greater than to the PVDF surface during the SCFS. According to previous studies, this procedure combined with the use of short cell contact times (e.g. seconds) with the substrate ensured that the cell adhesion to the cantilever was greater than adhesion to the opposing surface [26].

5.2.5.3 Force Measurements

Force measurements were performed according to modifications of previous methods [27, 28]. After attachment of the cell, the live single cell probe was repositioned over a cell-free region of the PVDF surface and force-distance (F-D) curves were performed with a loading force of 500 pN, contact-time of 1 s and retraction speed of 20 μm.sec^{-1} for all experiments. In this study, a 100 μm z-extended travel stage (provided by the JPK Company) was employed to accommodate the longer-range interactions (≈ 10-80 μm) between the cell and PVDF sample, which could be significantly greater than the standard z-travel stage (max 15 μm). At least 10 different cells were measured on each PVDF sample (non-poled and "poled –") and up to 20 force-distance, F-D, curves collected for each cell (from 4 different positions on the sample), giving a total of 200 F-D curves per sample for the analysis.

5.2.5.4 Force-distance curve analysis

Analysis of the F-D curves was performed using the JPK Data Processing software (Version spm-5.1.11), which enabled the quantification of adhesion force, adhesion energy and detachment length. Raw curves were converted into F-D curves using the measured detection sensitivity and cantilever spring constant [29]. Box-whisker plots were plotted using Origin Pro (2015) b9.2.272 and presented as the mean ± s.e.m..

5.3 Results

5.3.1 Cell adhesion on different β-PVDF materials

In order to determine if there are significant differences in the cytoskeletal organization of C2C12 cells on the different β-PVDF samples, the cells were stained for vinculin (green), a FA protein, as well as F-actin (red). The fluorescent images obtained are presented in Figure 5.2. Vinculin is a 117 kDa cytoplasmic protein, a component of the membrane that is associated to the adhesion complexes, as these linker proteins connect the integrins (bound to the ECM) to the actomyosin cytoskeleton [30]. Also, vinculin is a key protein in the regulation of the contractile forces transmission whereby if the vinculin is absent or present, the contractile force generation is reduced or enhanced, respectively [31, 32]. As a first approach, a comparison of the density of vinculin-expressing FAs, cell dimensions (length and width), and cell morphology was made between C2C12 myoblast cells on the different β-PVDF film samples, including the non-poled, “poled +” and “poled –”.

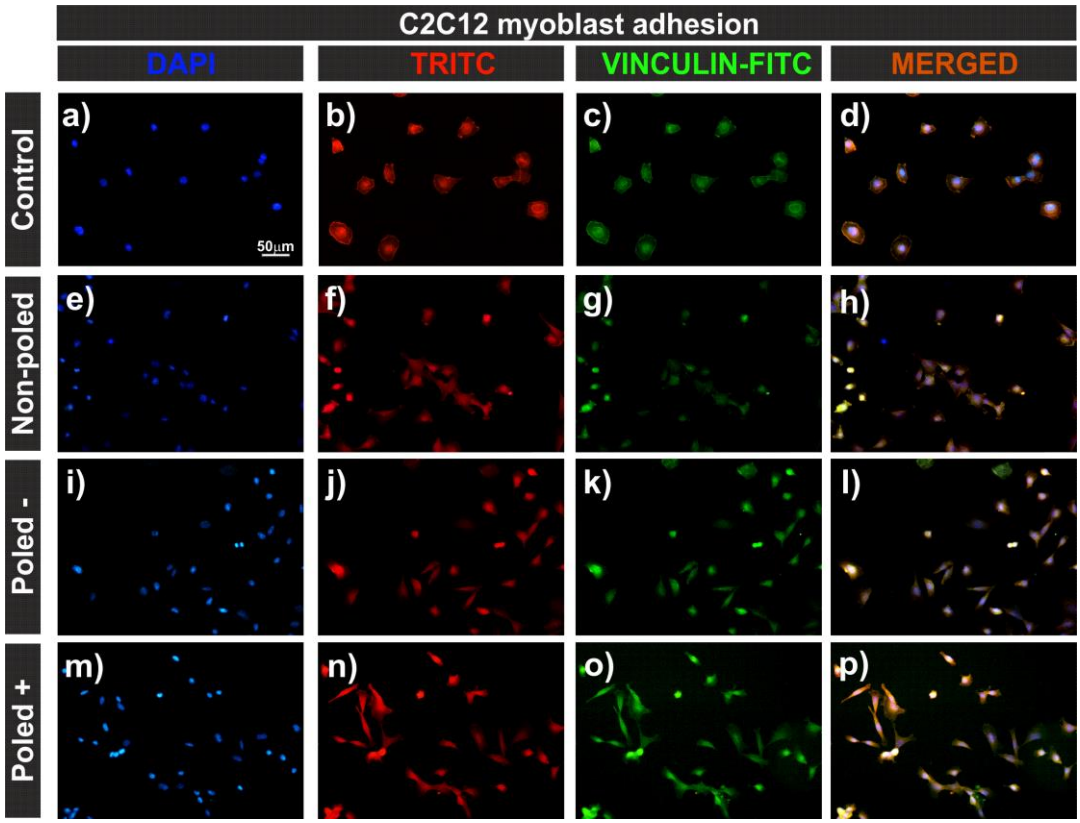

Figure 5.2. C2C12 myoblast cells cultured on the surface of polystyrene plate and β-PVDF films after 3h. Fluorescence images of DAPI stained cell nuclei (blue) in (a), (e), (i) and (m), vinculin expression (green) in (b), (f), (j) and (n), F-actin staining (cytoskeleton, red) in (c), (g), (k) and (o), overlay in (d), (h), (l) and (p). For comparison cells cultured on polystyrene plate are shown in (a, b, c, d) and those on the different β-PVDF samples are non-poled in (e, f, g, h), "poled –" in (i, j, k, l) and "poled +" in (m, n, o, p). The scale bar (50 µm) is valid for all the images.

Immunofluorescence was performed to observe myoblast adhesion and cytoskeletal structure on the different substrates. After 3 h of cell seeding, it was observed that the number of attached cells was similar for all the samples (Figure 5.2). Moreover, it was observed that C2C12 cells cultured on poled β-PVDF surfaces showed a greater spreading morphology compared with those on the non-poled β-PVDF and control. In particular, the cell shape on the different substrates were different, especially compared to the control where the cells were distinctly rounded. In addition, staining with vinculin-FITC (green, Figure 5.2) showed that vinculin was present throughout the cytoplasm of C2C12 cell in all the samples, independently of the sample surface characteristics. In order to quantitatively assess their morphology, the values of length and width of the cytoskeleton, and the nucleus diameter were calculated (Table 5.1). Table 5.1 shows that there was an approximately two-fold higher length-to-width ratio on the poled β-PVDF samples, specifically ≈ 2.80, compared to 1.33 for non-poled β-PVDF samples, indicating that the

cells on the charged surfaces acquired a more elongated morphology. However, there was no significant difference in the cell dimensions, length-to-width ratio, and nucleus size between the differently poled PVDF (Table 5.1). Hence, these results demonstrate that changes in the C2C12 cell morphology and spreading in response to cell attachment to the PVDF surface was dependent on the existence of surface charge but independent of the polarization state (negative or positive surface charge). It is to notice that the wettability of the samples can have an important role on the cell adhesion, once the poled samples present higher hydrophilicity than the non-poled ones. It is to notice, nevertheless, that in the present case, the wettability of the samples is determined by the surface charge, once surface roughness and surface chemistry are the same, as those issues are not affected by the poling procedure [16]. In this way, the discussion is focused on the surface charge of the samples and its influence on the cell adhesion.

Table 5.1 - Length and width of the myoblast cells and nucleus diameter after 3 h of incubation in the β-PVDF samples with different surface charges. The values are presented as average ± SD. $^{\#}p \leq 0.0001$ *vs Control and* $^{*}p \leq 0.0001$ *vs* Non-poled for each parameter.

Samples	Length (µm)	Width (µm)	Length/width	Nucleus diameter (µm)
Control	27.91 ± 4.88	22.84 ± 4.77	1.27 ± 0.21	10.73 ± 1.44
Non-poled	30.81 ± 7.16 $^{\#}$	23.42 ± 5.13	1.33 ± 0.27	10.24 ± 1.34
"Poled +"	41.02 ± 8.50 $^{\# *}$	15.33 ± 3.75 $^{\# *}$	2.81 ± 0.30	8.29 ± 1.39 $^{\# *}$
"Poled -"	40.91 ± 6.47 $^{\# *}$	15.79 ± 2.56 $^{\# *}$	2.80 ± 0.33	8.26 ± 1.73 $^{\# *}$

Figure 5.3 demonstrates the FAs and the morphology of the C2C12 myoblast cells cultured on the β-PVDF samples. The higher resolution images of single cells after 3 h confirm that C2C12 myoblast cells cultured on poled samples are more elongated than those cultured on non-poled samples (figure 5.3), in agreement with the literature [14]. Further, relative to the control sample, it seems that the vinculin expression and intensity are higher on all PVDF samples, forming a ring around the nucleus and smaller regions around the edge of the cell. There are no significative differences between the samples with and without proteins.

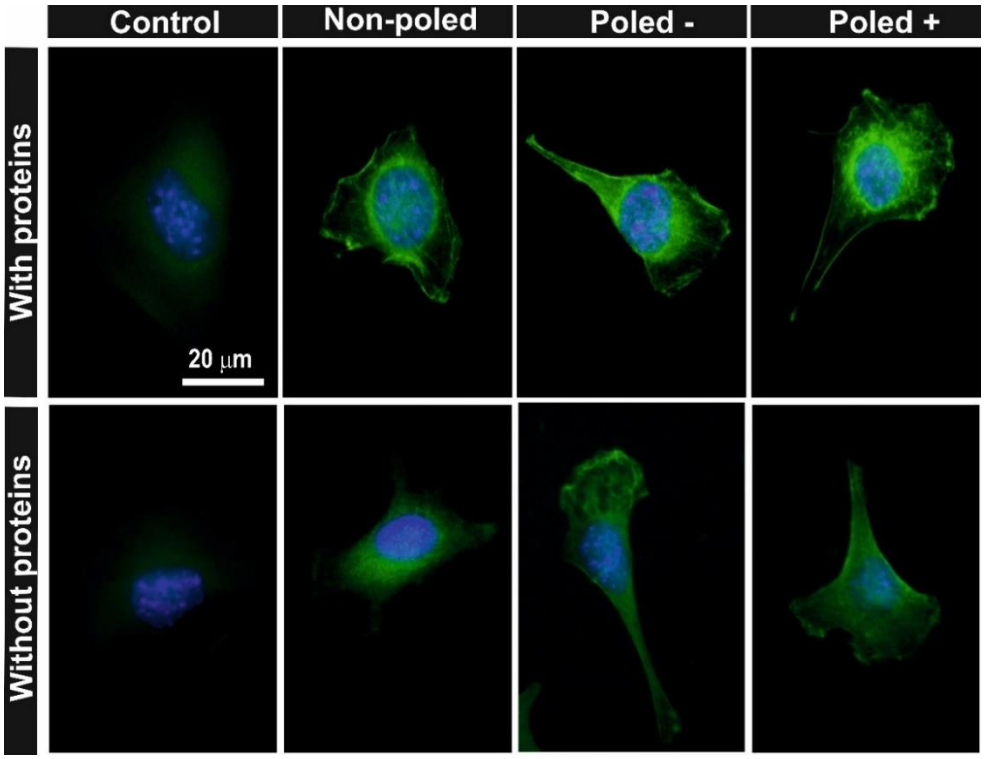

Figure 5.3. Immunofluorescence to analyze de focal adhesion by anti-vinculin FITC antibody staining of the C2C12 myoblast cells cultured 3 h on the control and β-PVDF samples (non-poled, "poled –" and "poled +") with and without proteins. The scale bar of 20 μm is valid for all the images.

5.3.2 Single Cell Force Spectroscopy

As mentioned, poled β-PVDF was previously shown to promote the elongation of C2C12 myoblasts [14], which is in agreement with our observations in Figure 5.2 and 5.3, and the length-to-width ratio values in Table 5.1. In the same study, the "poled –" β-PVDF, (negatively charged surface) enhanced the C2C12 proliferation (after 3 days) compared to the non-poled and "poled +" β-PVDF samples [14]. Given that the cell adhesion is an important process underlying these different cell responses [33], we attempt to evaluate the adhesion forces measured by SCFS. To this end, this SCFS initial investigation was used to directly probe the ability of the PVDF support the initial C2C12 myoblast cell adhesion without proteins. For that, the negatively charged ("poled –") β-PVDF film versus the non-charged - zero average charge - (non-poled) β-PVDF film were selected in order to study the influence of a charged surface relative to a non-charged surface (non-poled sample). More specifically, the negatively charged surface was a focus as these surfaces enhanced the cell proliferation and differentiation [14]. For the SCFS experiments, a single C2C12 cell was attached to a functionalized cantilever (Figure 5.4a). The attached cell was then lowered to the β-PVDF substrate (Figure 5.4b) until a pre-set force was reached. After a contact time of

1-3 sec to allow the formation of adhesive interactions, the cantilever was retracted until the cell and substrate were completely separated (Figure 5.4c). During the approach and retraction of the cantilever, the force versus distance (F-D) curves were obtained and analysed.

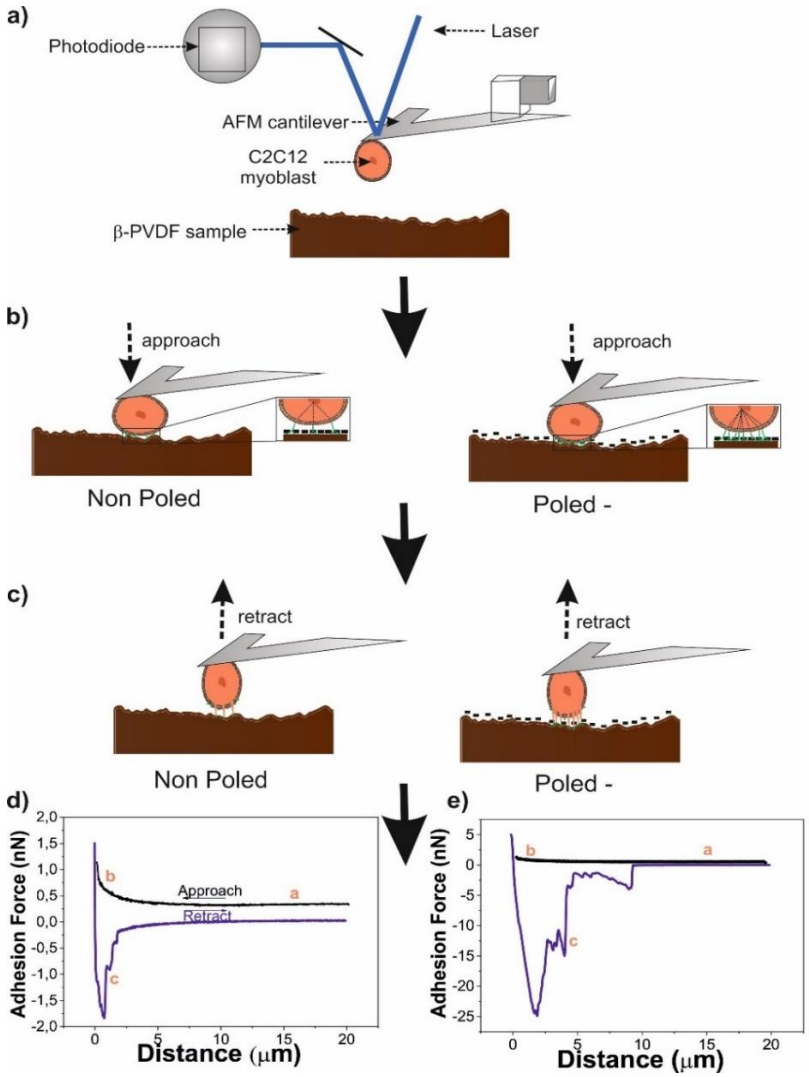

Figure 5.4. Single cell force spectroscopy. (a) All the elements involved in the test and the AFM cantilever is positioned above the cell after the cantilever functionalization. (b) The cantilever-bound cell is lowered towards on the polymer support until a pre-set force is reached. (c) After a given preset contact time, the cantilever is retracted until cell and substrate are completely separated. Representative Force-Distance curves recorded while repeatedly detaching a single C2C12 myoblast cell from β-PVDF samples with different surface charges: (d) Non-poled and (e) "Poled –".

Figure 5.4d and 5.4e show the F-D curves for non-poled and "poled –" β-PVDF obtained by SCFS, respectively. The F-D curves show that C2C12 myoblast cells on the negative poled β-PVDF present

significantly higher peak forces in the retraction curves (figure 5.4e) compared to those on the non-poled β-PVDF (figure 5.4d). Here, the peak maximum represents a measure of the bulk single cell de-adhesion [24] although the presence of subsequent peaks indicates the sequential detachment of fewer, remaining adhesive bonds. Thus, the F-D curves confirmed that higher de-adhesion forces occurred on the negatively charged β-PVDF surfaces, presumably due to stronger electrostatic interactions between the PVDF and charged cell surface molecules (non-specific interaction) and also, given that there are no proteins present in the medium. The larger magnitude of cell de-adhesion on the negatively charged β-PVDF surfaces was also evident by the presence of several larger peaks in Figure 5.4e, in addition to the greater de-adhesion energy that is given by the integrated area under the retraction curve. From analysis of the F-D curves, the maximum de-adhesion force (maximum peak force), de-adhesion energy (integrated area under the F-D curve) and the distance required to completely detach the cell from the surface are shown in Figure 5.5.

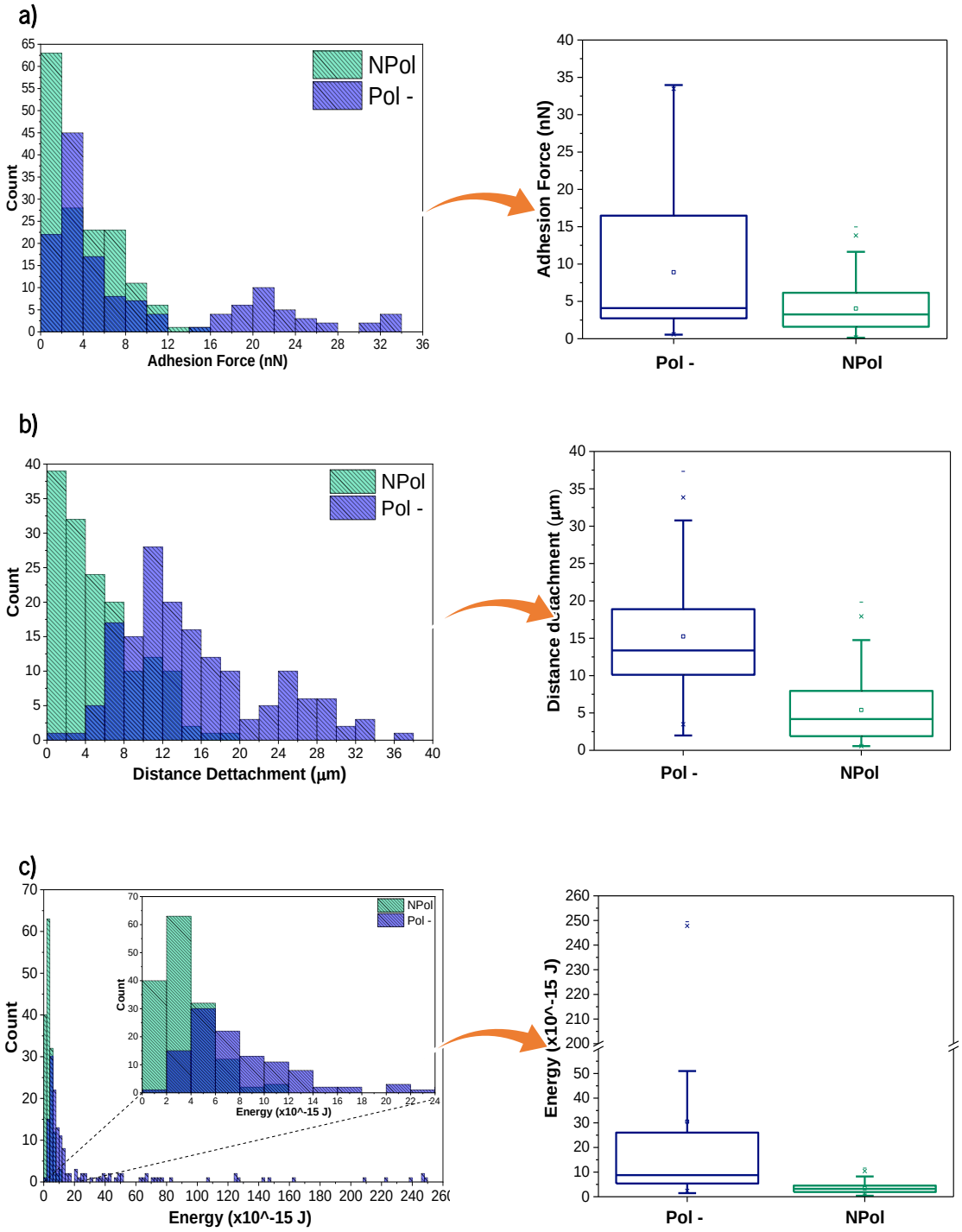

Figure 5.5. Comparison of histograms for the (a) maximum de-adhesion force, (b) distance detachment and (c) adhesion energy.

Whisker plots verified that the de-adhesion force of individual C2C12 cells was higher on "poled –" β-PVDF samples (8.92 ± 0.45 nN) than on non-poled substrates (4.06 ± 0.20 nN) (Figure 5.5a). The higher de-adhesion force value of "poled –" β-PVDF was associated with an increase in de-adhesion energy (30.34 ± 1.52 × 10^{-15} J) and detachment distance (15.28 ± 0.76 µm) of the C2C12 myoblast cell

compared to the non-poled surface ($3.38 \pm 0.17 \times 10^{-15}$ J and 5.27 ± 0.26 μm), respectively (Figure 5.5c and 5.5b). Furthermore, histograms of de-adhesion force (Figure 5.5a) and distance detachment (Figure 5.5b) revealed that the "poled –" β-PVDF samples consisted to two peak distribution, but this was not observed for the de-adhesion energy (Figure 5.5c). The peak values of these distributions were 4 ± 0.2 nN and 22 ± 1.1 nN for the de-adhesion force, and 12 ± 0.6 and 26 ± 1.3 μm for distance detachment. In contrast, the non-poled β-PVDF samples showed only a single distribution, with the appearance of a half-normal distribution for de-adhesion force (Figure 5.5a) and distance detachment (Figure 5.5b). Specifically, the distribution for de-adhesion forces overlapped with the lower peak distribution of the "poled –" β-PVDF samples (Figure 5.5a) though for the detachment distance the non-poled β-PVDF distribution was lower than both distributions of the "poled –" β-PVDF samples (Figure 5.5b).

5.4 Discussion and Conclusion

In this study, two different approaches were performed to distinguish the effect of PVDF material properties on the cell response, firstly via immunofluorescence staining of cells after 3 h in serum-containing media to elucidate the surface charge effects on the cell morphology and FA - vinculin. The results demonstrated that the poled (surface charged) PVDF enhanced cell spreading morphology and greater expression of vinculin compared to the control, suggesting that this cell adhesion promoted by the electrical poling of PVDF is importantly related to previous observations of increased myoblast differentiation and maturation of myotubes on the same surfaces.

Having confirmed the effects from our previous studies, the focus of the study was to then probe the C2C12 cell adhesive interactions on the non-poled versus poled PVDF. This was done using SCFS and on the negatively charged surfaces but in this case under serum-free conditions to investigate purely the initial electrostatic interactions. During the initial adhesion process, electrostatic interactions may also influence the myoblasts, promoting cell adhesion and subsequent responses such as morphology elongation. Thus, as a first step to elucidate the different cell adhesion mechanisms, such as electrostatic interaction, hydrophobic interaction, and biological interaction [34], the SCFS was performed in the aforementioned serum-free media.

It has been commonly assumed that positively charged substrates promote cell adhesion through electrostatic interaction, e.g. through use of positively charged poly-l-lysine on cell culture substrates, with the negative charge of the cell membrane, while negatively charged substrates would be expected to suppress cell adhesion. However, previous studies demonstrate that cells adhere to both positively and

negatively charged surfaces, even within short periods of incubation [34]. Also, the influence of gold nanoparticles positively- and negatively- charged groups on their internalization by HOB cells was investigated and it has been shown that different surface charges can be internalized, irrespective of the presence or absence of serum proteins in the media [35]. The surface charge density can also improve the penetration efficiency [36]. In this study, the SCFS directly verified that single C2C12 cells could adhere strongly to negatively charged surfaces without adsorbed proteins within contact times of seconds. In contrast, de-adhesion forces comprising significantly fewer interactions occurring over much smaller distances, presumably also responsible for the reduced de-adhesion energy, were observed on the non-poled (non-charged). These findings are in agreement with a previous study of *Hoshiba* and co-authors, where it was demonstrated that the cell adhesion force was higher on charged surfaces, it is independent of the proteins presence or absence [34].

The box-whisker plots showed clear differences in the cells de-adhesion, however, the histogram analysis revealed a more complex response of the cell de-adhesion. For instance, two peak distributions (blue peaks) were observed for the negatively poled surface, suggesting that the surface charge distribution of the "poled –" β-PVDF is not homogeneous due to the semicrystalline nature of the polymer [37], leading to some regions where the cell can form stronger adhesion and less adhesion in other regions. In particular, the peak values of ≈ 20-25 nN in the higher distribution, are remarkably high for the single cell de-adhesion in comparison to those measured in other SCFS studies where the single cell forces are typically < 1 nN [38]. We suggest that the high de-adhesion values may be related to either the high charge density of electroactive PVDF [1] and/or possible effects from the approach and contact of the cantilever with the PVDF surface that generates a mechanical stimulus, which in turn induces electrical polarization of the PVDF.

In conclusion, the molecular interactions between C2C12 myoblast cell and piezoelectric polymer films, β-PVDF, with different surface charges, positive, negative or neutral, were analysed with the AFM-based SCFS technique and immunofluorescence tests. It was demonstrated that surface charge promotes cell elongation and negative polarization improves cell-material adhesion. The de-adhesion energy required to detach the cell is higher on negative charged surfaces, which is concomitant with higher de-adhesion force exerted on the cantilever. This study is the first in vitro study to directly quantify the adhesive forces of cells on PVDF, including the effect of negative polarization state and surface charge of piezoelectric β-PVDF films on C2C12 cells. β-PVDF with polarization offers potential for skeletal muscle TE applications, allowing one to tune cell-surface interactions via electrical poling and also dynamically from the piezoelectric effect.

A key issue is that the SCFS reveals a distinct difference in cell interaction (forces, energy) for poled versus non-poled samples which in turn affects the cell behaviour with respect to the cell adhesion. This fact is evidenced by the results obtained from the morphological and fluorescence observations (figure 5.2), where cells cultured on charged surfaces present an more elongated morphology, in agreement with previous studies showing that charged surfaces promote an earlier formation of myocytes, which are necessary for differentiation of myoblasts into myotubes, and consequently skeletal muscle tissue [12]. Through physical attachment to actin filaments within the cellular network, FAs allow cells to pull or push themselves along a matrix during migration. The substrate properties such as stiffness, topography and surface energy/charge are important parameters determining the resistance of the substrate to deformation by cell traction forces, which enable cells to travel with persistent direction [39]. Molecular pathways underlying cell proliferation are also regulated via contractile forces imparted by the actin network and sensed by focal FAs.

Regarding cell morphological observations and forces measured by SCFS, it is proposed that cell spreading and elongation correlates with larger adhesion to the charged surface. The increased tensile forces (i.e. the forces the cell feels when it "pulls" on the surface otherwise known as traction forces) activate actin expression/reorganization, enabling cells to increase its area on the substrate. From the SCFS, the charged groups of "poled –" β-PVDF surface act as "ligands" based on electrostatic forces with charged cell membrane molecules, resulting in stronger adhesion forces. Thus, this will enable the cells to spread and elongate.

5.5 References

1. Martins, P., Lopes, A.C. and Lanceros-Mendez, S., *Electroactive phases of poly(vinylidene fluoride): Determination, processing and applications*. Progress in Polymer Science, 2014. **39**(4): p. 683-706.
2. Mould, R.F., *Marie and Pierre Curie and radium: History, mystery, and discovery*. Medical Physics, 1999. **26**(9): p. 1766-1772.
3. Usher, T.D., et al., *The promise of piezoelectric polymers*. Polymer International, 2018. **67**(7): p. 790-798.
4. Zhang, Y., et al., *A new way to promote molecular drug release during medical treatment: A polyelectrolyte matrix on a piezoelectric–dielectric energy conversion substrate*. Small, 2018. **14**(37): p. 1802136.
5. Hu, F., et al., *Recent Advancements in Nanogenerators for Energy Harvesting*. Small, 2015. **11**(42): p. 5611-5628.
6. Ribeiro, C., et al., *Electroactive poly(vinylidene fluoride)-based structures for advanced applications*. Nature Protocols, 2018. **13**(4): p. 681-704.

7. Dhandayuthapani, B., et al., *Polymeric scaffolds in tissue engineering application: A review*. International Journal of Polymer Science, 2011. **2011:** p. 290602.
8. Guo, B. and Ma, P.X., *Synthetic biodegradable functional polymers for tissue engineering: A brief review*. Science China Chemistry, 2014. **57**(4): p. 490-500.
9. Levin, M., *Molecular bioelectricity in developmental biology: New tools and recent discoveries: Control of cell behavior and pattern formation by transmembrane potential gradients*. BioEssays, 2012. **34**(3): p. 205-217.
10. Ribeiro, C., et al., *Piezoelectric polymers as biomaterials for tissue engineering applications*. Colloids and Surfaces B: Biointerfaces, 2015. **136**: p. 46-55.
11. Xiang, H. and Chen, Y., *Energy-Converting Nanomedicine*. Small, 2019. **15**(13): p. 1805339.
12. Bach, A.D., et al., *Skeletal muscle tissue engineering*. Journal of Cellular and Molecular Medicine, 2004. **8**(4): p. 413-422.
13. Ribeiro, C., et al., *Piezoelectric poly(vinylidene fluoride) microstructure and poling state in active tissue engineering*. Engineering in Life Sciences, 2015. **15**(4): p. 351-356.
14. Martins, P.M., et al., *Effect of poling state and morphology of piezoelectric poly(vinylidene fluoride) membranes for skeletal muscle tissue engineering*. RSC Advances, 2013. **3**(39): p. 17938-17944.
15. Ribeiro, S., et al*., Electroactive biomaterial surface engineering effects on muscle cells differentiation*. Materials Science and Engineering C, 2018. **92**: p. 868-874.
16. Serrado Nunes, J., et al., *Relationship between the microstructure and the microscopic piezoelectric response of the α- and β-phases of poly(vinylidene fluoride).* Applied Physics A: Materials Science and Processing, 2009. **95**(3): p. 875-880.
17. Parssinen, J., et al., *Enhancement of adhesion and promotion of osteogenic differentiation of human adipose stem cells by poled electroactive poly(vinylidene fluoride)*. Journal of Biomedical Materials Research - Part A, 2015. **103**(3): p. 919-928.
18. Huang, S. and Ingber, D.E., *The structural and mechanical complexity of cell-growth control*. Nature Cell Biology, 1999. **1**(5): p. E131-E138.
19. Khalili, A.A. and Ahmad, M.R., *A Review of cell adhesion studies for biomedical and biological applications*. International Journal of Molecular Sciences, 2015. **16**(8): p. 18149-18184.
20. Dembo, M., et al., *The reaction-limited kinetics of membrane-to-surface adhesion and detachment*. Proceedings of the Royal Society B: Biological Sciences, 1988. **234**(1274): p. 55-83.
21. Resende, R.R., et al., *Scale/topography of substrates surface resembling extracellular matrix for tissue engineering.* Journal of Biomedical Nanotechnology, 2014. **10**(7): p. 1157-1193.
22. Sun, Z., Guo, S.S. and Fässler, R., *Integrin-mediated mechanotransduction*. Journal of Cell Biology, 2016. **215**(4): p. 445-456.
23. Friedrichs, J., et al., *A practical guide to quantify cell adhesion using single-cell force spectroscopy*. Methods, 2013. **60**(2): p. 169-178.
24. Yu, M., et al., *Increasing throughput of AFM-based single cell adhesion measurements through multisubstrate surfaces*. Beilstein Journal of Nanotechnology, 2015. **6**(1): p. 157-166.
25. Beaussart, A., et al., *Single-cell force spectroscopy of probiotic bacteria*. Biophysical Journal, 2013. **104**(9): p. 1886-1892.

26. Wojcikiewicz, E.P., et al., *Contributions of molecular binding events and cellular compliance to the modulation of leukocyte adhesion*. J Cell Sci, 2003. **116**(12): p. 2531-2539.
27. Zhang, H., et al., *Quantifying molecular-level cell adhesion on electroactive conducting polymers using electrochemical-single cell force spectroscopy*. Scientific Reports, 2015. **5:** p. 13334.
28. Zhang, H., et al., *Effect of electrochemical oxidation and reduction on cell de-adhesion at the conducting polymer–live cell interface as revealed by single cell force spectroscopy*. Biointerphases, 2018. **13**(4): p. 041004.
29. Puckert, C. and Higgins, M.J., *Force Spectroscopy*, in *Compendium of Surface and Interface Analysis*, Kiguchi, M., Editor. Springer-Singapore, 2018. p. 193-200.
30. Peng, X., et al., *New Insights into Vinculin Function and Regulation*. International Review of Cell and Molecular Biology. 2011. **287**: p. 191-231.
31. Mierke, C.T., et al., *Mechano-coupling and regulation of contractility by the vinculin tail domain*. Biophysical Journal, 2008. **94**(2): p. 661-670.
32. Mierke, C.T., *The role of vinculin in the regulation of the mechanical properties of cells*. Cell Biochemistry and Biophysics, 2009. **53**(3): p. 115-126.
33. Chang, H.Y., et al., *Effect of surface potential on epithelial cell adhesion, proliferation and morphology*. Colloids and Surfaces B: Biointerfaces, 2016. **141**: p. 179-186.
34. Hoshiba, T., Yoshikawa, C. and Sakakibara, K., *Characterization of Initial Cell Adhesion on Charged Polymer Substrates in Serum-Containing and Serum-Free Media*. Langmuir, 2018. **34**(13): p. 4043-4051.
35. Allen, C., et al., *Research highlights: investigating the role of nanoparticle surface charge in nano-bio interactions*. Environmental Science: Nano, 2017. **4**(4): p. 741-746.
36. Quan, X., et al., *Molecular understanding of the penetration of functionalized gold nanoparticles into asymmetric membranes*. Langmuir, 2017. **33**(1): p. 361-371.
37. Ribeiro, C., et al., *Enhanced proliferation of pre-osteoblastic cells by dynamic piezoelectric stimulation*. RSC Advances, 2012. **2**(30): p. 11504-11509.
38. Helenius, J., et al., *Single-cell force spectroscopy*. Journal of Cell Science, 2008. **121**(11): p. 1785-1791.
39. Kennedy, K.M., Bhaw-Luximon, A. and Jhurry, D., *Cell-matrix mechanical interaction in electrospun polymeric scaffolds for tissue engineering: Implications for scaffold design and performance*. Acta Biomaterialia, 2017. **50**: p. 41-55.

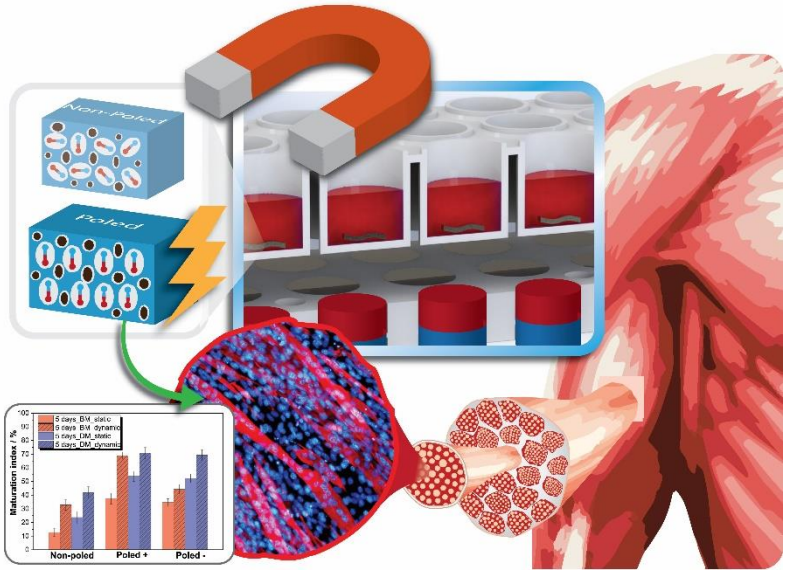

Chapter 6. Magnetically activated electroactive microenvironments for skeletal muscle tissue regeneration

CFO/P(VDF-TrFE) magnetoelectric films were processed and their influence on cell behaviour evaluated. It is shown that these materials have large interest due to their active behaviour (piezoelectric, magnetic and magnetoelectric response). In this chapter, the magnetoelectric composites without and with polarization (positive and negative) were used to investigate their effect on C2C12 myoblast adhesion, proliferation and differentiation. Also, the mechanical and/or electrical stimulation on cell proliferation and differentiation are investigated through the use of an activated electroactive microenvironment produced by two different bioreactors (magnetic and mechanical).

This chapter is based on the following publication: **S. Ribeiro**, E. O. Carvalho, C. Ribeiro, C. R. Tubio, N. Castro, N. Pereira, V. Correia, A. C. Gomes and S. Lanceros-Méndez, *Magnetically activated electroactive microenvironments for skeletal muscle tissue regeneration.* Submitted 2019.

6.1 Introduction

More than 600 individual skeletal muscles can be found in the human body that enabling to perform a variety of functions, such as executing locomotive tasks, breathing, or moving the eyes, among others [1]. This tissue is the most abundant in human body being one of the components of the musculoskeletal system. Further, it is attached to bones by tendons and produce all the movements of body parts in relation to each other [2].

Skeletal muscle is a highly specialized tissue that consists of striated and elongated multinuclear muscle fibres (known as myofibres) encapsulated within connective tissue sheaths [3]. It has the property of plasticity, which mean that when the skeletal muscle is under the influence of physiological changes such as mechanical stress and unloading, the composition of fiber types of skeletal muscle can change [2]. The loss of functional muscle from genetic disease, such as Duchenne muscular dystrophy, traumatic injury or surgical excisions results in a physiologic deficiency that continues to remain without an effective clinical treatment [4].

The replacement and/or regeneration of lost/damaged tissues or organs represent one of the main challenges of the last decades, so in order to address these issues, TE has emerged as a possible solution. In this way, TE represent an alternative and helpful approach for organs/tissues reconstruction/replacing when the conventional pharmaceutical treatments are no more applicable [5]. One of the most important components of the TE multidisciplinary field is the scaffold design that should mimic the naturally exiting extracellular matrix through a complete biomimicking approach, including structural, biochemical and biophysical cues, in order to provide a proper cell growth. In fact, it has been demonstrated that chemical, biological and/or physical signals affect the cell response, enhancing cell target functions such as adhesion, proliferation, migration and differentiation [6]. Among the physical stimuli, it has been shown that mechanical and electrical effects affect biological entities. The cellular responses to mechanical stimuli are mediated by mechanotransduction pathways that can promote tissue development and/or function. Similar to the mechanical stimulation, electrical stimulation influences the survival, proliferation rate, hypertrophy and other properties of muscle cells. *In vitro*, the use of electrical stimulation has been aimed mainly at mimicking the motoneurons action found in their native physiological environment [7].

In the area of muscle TE physical stimuli have been poorly investigated. However, as this tissue reacts to electro-mechanical stimuli during its normal function [7-8], scaffolds that can provide electroactive physical stimuli seems to be a necessary approach. Thus, the application of mechanical and electrical stimulation *in vitro* has shown promise for growing contractile skeletal muscle tissue [9].

In this context, the so-called smart materials and, in particular, smart polymer materials are very interesting for efficient muscle tissue repair strategies. In order to provide those physical stimuli (electrical and mechanical) present in the microenvironment of skeletal muscle tissue, electroactive materials, such as piezoelectric polymers, are being increasingly used in the biomedical context [10-12]. These materials develop voltage when a mechanical stress is applied, or vice-versa, promoting adhesion, proliferation and differentiation of myoblast cells. Although muscle itself is not piezoelectric, it is sensitive to dynamic mechanical and electrical solicitations [11, 13], being this dynamic biomimetic approach particularly relevant as muscle is physiologically subjected to mechano-electrical solicitations related to walking, jumping and running [14-15]. The most representative piezoelectric polymers in this area are PVDF, and its copolymer due to their biocompatibility, bio stability and high piezoelectric coefficients [12, 16].

Most of the research in the area of muscle TE has been conducted in order to develop scaffolds, mainly varying their morphology in the form of films and fibres as well as by the addition of conductive materials [17]. However, so far, the effect of mechano-electrical stimuli on the myotube differentiation thought polymeric biomaterials that can provide both stimuli simultaneously have not been investigated. As a complement to piezoelectric biomaterials, which will now work under static conditions, for example when the patient is immobilized (for example due to serious health problems), ME biomaterials allow to produce magnetically activated mechanical and electrical stimuli. These materials consist on the combination of magnetostrictive particles and piezoelectric materials, the ME effect resulting from the mechanical deformation induced by a magnetic field due to the magnetostriction of one of the components, leading to an electrical polarization variation due to the piezoelectric effect of the other phase. Thus, the use of an external magnetic field allows to remotely control tissue stimulation [18] by inducing both mechanical and/or electrical signals to the surrounding tissues [19]; providing an innovative tool for skeletal muscle that has not been evaluated so far.

In this context, this work reports on the development of magneto-active films based on a piezoelectric polymer - P(VDF-TrFE) – and magnetostrictive nanoparticles - cobalt ferrite nanoparticles ($CoFe_2O_4$). These composites materials have been evaluated as biomaterials for muscle TE by studying the influence of the mechano-electrical stimuli on myotube differentiation both under static and dynamic conditions.

6.2 Materials and methods

6.2.1 Materials

P(VDF-TrFE) was acquired from Solvay, DMF, pure grade from Merck and CFO nanoparticles with 35-55 nm were purchased by Nanoamor.

6.2.2 Preparation of the magnetoelectric nanocomposites

The films were prepared based on the method presented in [20-21] for similar polymer-based composite compositions.

In order to obtain a good dispersion of the magnetostrictive nanoparticles within the polymer matrix, first, the desired content of CFO nanoparticles (20 wt.%) was added to the DMF and placed in an ultrasound bath (ATU ATM3LCD) during 30 min. Then, citric acid (0.02 $g.mL^{-1}$) was added to the mixture, which was in the ultrasound bath for another 3 h. After this time, P(VDF-TrFE) at a concentration of 20/80 polymer/solvent (w/w) was added to the mixture that was kept under mechanical stirring for 2 h. When the polymer reached complete dissolution, the samples were obtained by solvent casting method, by spreading the solution on clean glass substrate and placing them inside an oven for 10 min at 210 °C. The films are obtained with ≈ 40 μm of thickness.

Electrical poling of CFO/P(VDF-TrFE) was achieved as described on chapter 4 (section 4.2.2). The piezoelectric response (d_{33} ≈ |8-10| $pC.N^{-1}$) of the poled films was obtained with range d_{33}-meter (model 8000, APC Int Ltd). After the polarization, average positive charge is obtained in one side of the sample and negative charges on the opposite side. The films used for cell culture are represented in table 6.1.

Table 6.1. Nanocomposites used for cell culture.

Samples	Polarization	$\lvert d_{33} \rvert$ ($pC.N^{-1}$)	Stimuli given to the cells	Denomination
CFO/P(VDF-TrFE)	None	—	Mechanical	non-poled
	Positive	9	Mechano-electrical	"poled +"
	Negative	10	Mechano-electrical	"poled –"

6.2.3 Characterization of nanocomposites

The morphology of the CFO/P(VDF-TrFE) nanocomposites surface was evaluated by SEM as described on Chapter 2 (section 2.2.3.2)

Tapping mode Atomic Force Microscopy (AFM) images were acquired using an AFM equipment (Nano-Observer CSI). The AFM images were processed using Gwyddion software. The average roughness (Ra) was calculated for each image after three measurements performed in different places of each samples.

Magnetic hysteresis loops were measured at room temperature using a vibrating sample magnetometer (VSM) (Microsense 2.2) from -18500 Oe to 18500 Oe.

WCA measurements of the different CFO/P(VDF-TrFE) samples were measured and presented as described on Chapter 2 (section 2.2.3.2).

6.2.3.1 Characterization of the magnetic and electromechanical stimulus

As the ME stimulation of the cells on the prepared films is carried out in a bioreactor that applies a varying magnetic field [19], the magnetic characterization of the surface was performed, at the same height of cell culture, in relation to the permanent magnet table, allowing the comparison with the results obtained through the biological analysis with the magnetic stimuli actually produced.

This characterization was performed using a GM08 gaussmeter, with a PT8029 reference Transverse probe, which allows measuring AC and DC fields with maximum amplitude of 3 000 T, using an RS232 connection to record the acquired data.

In order to ensure the correct measurement of the magnetic field, concentric measurements were performed in the centre of the culture wells by displacing the measuring tip along the two axes, which is coupled to a graduated X-Y table.

To better understand the field format, based on the characteristics of the bioreactor magnets and the values recorded in the measurement, a finite element modelling was performed using the ANSYS Maxwell software, obtaining a three-dimensional analysis of the generated magnetic fields. After the magnetic component was analysed, the magnetically induce deformation of the samples by the magneto-mechanical transduction was also characterized by attaching a strain gauge (L2A-06-062LW-120) to the sample using a LOCTITE Hysol® 3425 two-component araldite glue. The sensor variation measurement is based on a setup developed for this purpose, given the need to obtain a relatively high sampling rate, taking into account the bioreactor operating frequency (200 samples per second), and high resolution, due to the low deformation of the sample.

Resistance variation of the strain gauge was obtained by measuring the voltage at the sensor terminals using a 24 bit sigma delta ADC with reference LTC2440 controlled by Evaluation Board DC590B, connected via USB to the computer. DC590. In order to measure the resistance variation through voltage variation, a precision constant current was applied using Keithley 2400 Source/Meter, where a 1 mA reference current was applied.

Finally, the characterization of the electrical response of the biomaterial –magnetoelectric stimulation- when positioned on the wells of culture plate was performed using an external setup to the bioreactors-biomaterial system. The wide range d_{33}-meter was used to obtain the d_{33} of the samples, and the magnetoeletric effect was characterized by measuring the transverse ME voltage coefficient (α33)

and longitudinal ME coefficient ($\alpha 31$) using the dynamic lock-in amplifier method. The samples were placed in the center of a ME characterization system composed by two sets of concentric Helmholtz coils. A pair of coils was used to generate an AC field with amplitude of 1 Oe, at the resonant frequency of the sample, simulating the AC response applied by the bioreactors. The second set of Helmholtz's coils allows varying the DC magnetic field applied to the sample from 0 to 0.5 T, controlled by a current power source. The voltage generated in the direction of sample thickness was measured using a digital Lock-in amplifier (Stanford Research SR530). ME stress coefficients were calculated from the measured strain using equation 6.1.

$$\alpha_{33} = \frac{\Delta V}{H_{AC} * t} \qquad (6.1)$$

where ΔV is the measured output voltage, H_{AC} is the amplitude of the AC magnetic field, and t is the thickness of the piezoelectric layer.

The characterization of the electrical response in the mechanical bioreactor was performed by measuring the piezoelectric response of the sample under mechanical stimulation. Conductive electrodes were printed on the surface of the sample by screen printing, the sample was connected to a 16 bits high resolution oscilloscope (PicoScope 4262) and the electrical as a function of frequency recorded.

6.2.4 Cell culture assays

6.2.4.1 Samples sterilization

For the *in vitro* assays, circular CFO/P(VDF-TrFE) films (non-poled, "poled +" and "poled –") were cut with 13 mm of diameter. These samples were sterilized as described on Chapter 2 (section 2.2.3.3.1). Then, the samples were placed in a 24-well cell culture plates.

6.2.4.2 Cell culture

C2C12 cells were grown in 75 cm^2 cell-culture flask and cultured in BM. The composition of the medium and the conditions of cell culture are the same as described on Chapter 2 (section 2.2.3.3.2).

6.2.4.3 Adhesion assays

For cell adhesion tests, C2C12 cells were seeded at a cell density of 4 000 cells.cm^{-2} with a drop of 100 µL in 24-well plates and allowed to adhere in CFO/P(VDF-TrFE) nanocomposites for 45 min at 37 °C,

and then 400 µL of DMEM was added to each well (drop method). After 24 h of culture in BM, C2C12 cells were subjected to immunofluorescence staining in order to analyze the presence of FAs as described on Chapter 5 (section 5.2.4).

6.2.4.4 Proliferation and differentiation cell culture assays

C2C12 cells were seeded on the different CFO/P(VDF-TrFE) nanocomposite films at a density of 7 500 and 40 000 cells.cm^{-2} for proliferation and differentiation tests, respectively (figure 6.1). Similarly, to the cell adhesion assays, the drop method was used for the proliferation and differentiation assays.

For cell proliferation studies, two plates at these conditions were incubated with BM at 37 °C in a saturated humidity atmosphere containing 95% air and 5% CO_2 for 24 h to allow cell adhesion. After this time, one plate was maintained at the same conditions (static culture – cell culture without any applied stimuli) and the other was transferred onto a home-made bioreactor [19] system (dynamic culture – cell culture under magnetic stimulation for magneto-mechanical and magneto-electric response) up to 3 days.

For the differentiation experiments, the samples were placed in 24-well plates (three plates) and incubated in BM, as previously described, until reached 90% confluence. Thereafter, in order to induce myotube formation, the BM of half of the samples was changed to differentiation medium (DM). The DM was composed of DMEM supplemented with 2% FBS and 1% P/S. As for the proliferation assay, one plate was maintained at the same conditions (static culture), other was transferred onto the magnetic bioreactor (dynamic culture) and the last one to a mechanical bioreactor (dynamic culture) up to 8 days. In all conditions, the medium was renovated daily.

For the dynamic culture (figure 6.1), the samples placed on the magnetic bioreactor were subjected to the following cycle, as presented in [19]: an active time of 16 h under magnetic stimulus (divided into 5 min of active time and 25 min of repose time) followed by a non-active time of 8 h (no magnetic stimulation). The dynamic culture was performed under magnetic stimulation at a frequency of 0.3 Hz and the 20 mm displacement of permanent magnets below the culture wells.

In parallel, for differentiation tests, another home-made bioreactor system was used with mechanical stimulation (see [22-23]) by placing the culture plate on a vertical vibration module at a frequency of 1 Hz with amplitude of approximately 1 mm. The following cycle has an active time of 16 h under mechanical stimulus followed by a non-active time of 8 h (no mechanical stimulation), in order to mimic the human body mechanical stimulation along a day, such as in the magnetic bioreactor (figure 6.1). In each study, 3 replicates were used for each condition.

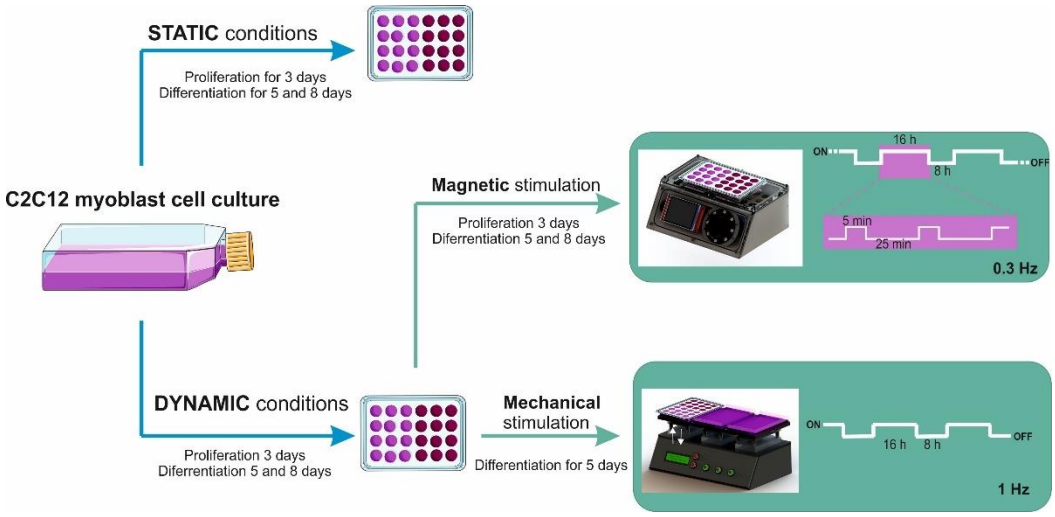

Figure 6.1. Schematic representation of the cell culture assays using static and dynamic (magnetic and mechanical stimulation) conditions and parameters applied by each bioreactor.

6.2.4.4.1 Cell viability

For the proliferation assays, the evaluation of the cell viability of C2C12 myoblast on the different CFO/P(VDF-TrFE) films under static and dynamic conditions was analyzed by MTS assay as described on chapter 2 (section 2.2.3.3.4). The cell proliferation values were determined regarding the cells adhered on the material after 24 h adhesion, just before placing them in contact with the bioreactor (equation 6.2). Experimental data were obtained from four replicates of each sample of three independent experiments and expressed as mean ± SD.

$$Cell\ proliferation\ (\%) = \frac{Abs_{490nm}\ sample}{Abs_{490nm}\ sample\ after\ 24h\ adhesion}\ x\ 100 \qquad (6.2)$$

6.2.4.4.2 Immunofluorescence staining

For proliferation and differentiation studies, immunofluorescence tests were also performed to analyze the cytoskeleton morphology, while also verifying cell viability and the presence of MHC, respectively.

For proliferation tests under static and dynamic (magnetic stimulation) conditions, after 3 days, the same point used for MTS evaluation, some samples were subjected to immunofluorescence staining as described on Chapter 2 (section 2.2.3.3.5).

For differentiation tests under static and dynamic (magnetic and mechanical stimulation) conditions, after 5 and 8 days of differentiation, the samples are submitted to immunofluorescence staining as described on Chapter 4 (section 4.2.5).

6.2.4.4.3 Calculation of fusion and maturation index per area

The fusion and maturation index, length, diameter and myotube number was calculated as presented on chapter 4 (section 4.2.6). Experiments were carried out on three samples for each condition and by analyzing ten images for each sample, for each of the two independent experiments. Data are presented as mean ± s.e.m. from triplicates samples of two independent experiments.

6.2.4.4.4 Quantification of creatine kinase activity

For cell differentiation assessment, creatine kinase activity (CK) was also quantified. For that, the cells present in samples were rinsed with PBS 1x and collected with a cell scraper. After that, the cells were homogenized in an appropriate volume of cold 50 mM potassium phosphate (pH 7.5) buffer and centrifuged at 10 000 × *g* for 15 min at 2-8 °C. After the centrifugation, the supernatant was removed and used for the assay. Creatine kinase activity of the samples was determined using a commercial kit (*Sigma-Aldrich*). The kit is based on enzyme coupled reactions in which creatine phosphate and ADP is converted to creatine and ATP by creatine kinase. The generated ATP is used to phosphorylate glucose by hexokinase to generate glucose-6-phosphate, which is then oxidized by NADP in the presence of glucose-6-phosphate dehydrogenase. The produced NADPH, measured at 340 nm, is proportionate to the CK activity in the sample. Data are presented as mean ± s.e.m. from triplicates of two independent experiments.

6.2.4.5 Statistical Analysis

All quantitative data were analyzed using GraphPad Prism (v6.00, La Jolla, CA, USA). The results were analyzed statistically using the two-way ANOVA followed by Tukey's test. Differences were considered to be statistically significant when p-value < 0.05.

6.3 Results and Discussion

6.3.1 Characterization of CFO/P(VDF-TrFE) nanocomposites

When cells adhere to the surface of a scaffold, a sequence of physico-chemical reactions will occur,

influencing cell fate. The cell attachment is a complex process, affected by numerous aspects, such as material surface properties. Thus, relevant properties of the CFO/P(VDF-TrFE) films surface were investigated.

The CFO/P(VDF-TrFE) composites films with the same amount of CFO nanoparticles (20 wt.%) and different polarization state were analyzed by SEM (figure 6.2a, 6.2b and 6.2c). It is observed random fibril-like microstructure (see inset of figure 6.2a) as a result the characteristic growth of the co-polymer, which crystallization kinetics is hindered by the presence of the CFO nanoparticles, acting as nucleation agents for crystallization [24]. It is also observed that the distribution of the magnetostrictive nanoparticles within the P(VDF-TrFE) polymer matrix is uniform without large agglomerations and that the films are non-porous. Those characteristics are independent of the poling state.

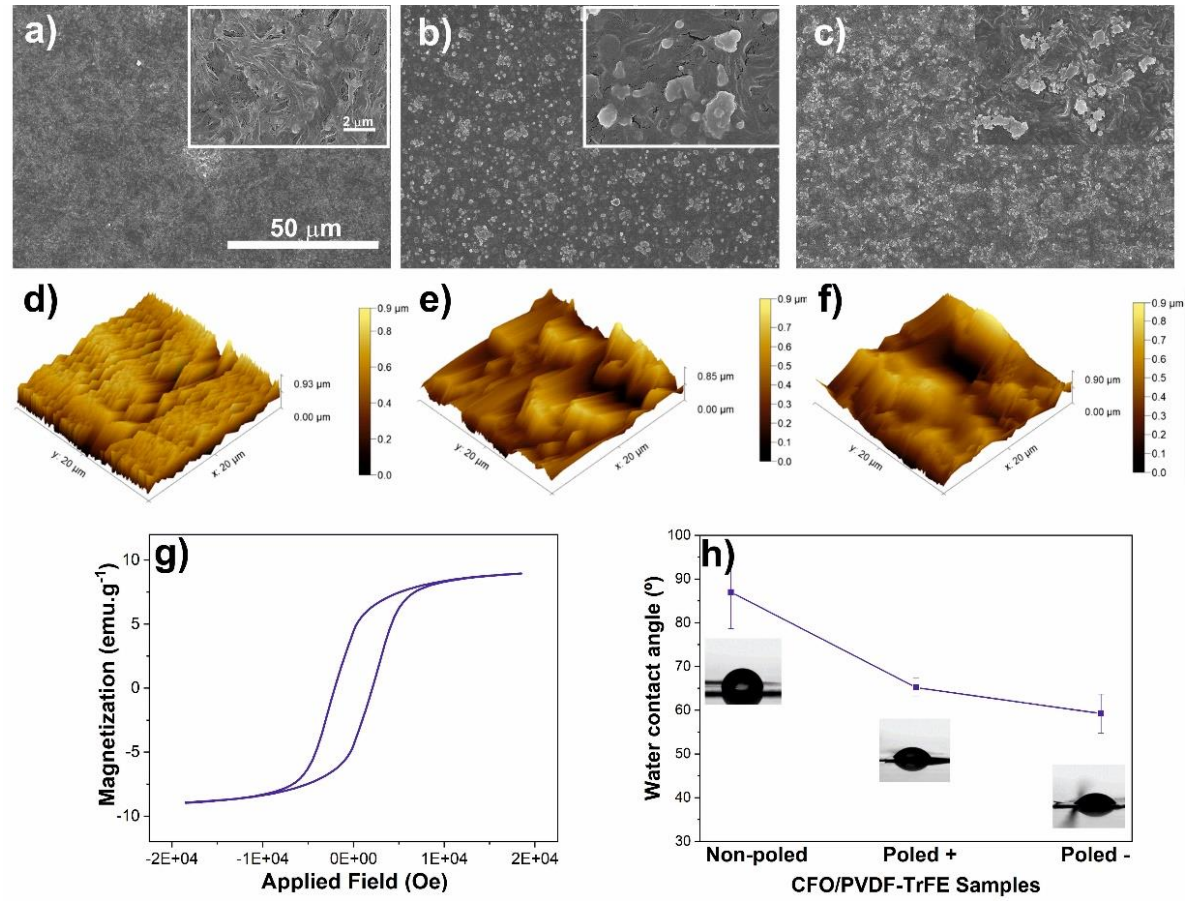

Figure 6.2. Surface morphology obtained by scanning electron microscopy of the CFO/P(VDF-TrFE) nanocomposite films: (a) non-poled, (b) "poled +" and (c) "poled –". The scale bar is 50 µm for all the images and 2 µm for the inset images. The corresponding AFM (20 × 20 µm) results are presented in figures, (d), (e), (f), for CFO/P(VDF-TrFE) non-poled, "poled +" and "poled –" materials, respectively. (g) Room temperature hysteresis loops for CFO/P(VDF-TrFE) films. (h) Water contact angle measurement for CFO/P(VDF-TrFE) films with and without polarization (mean ± SD).

The AFM images of the CFO/P(VDF-TrFE) samples with different polarization are displayed in figure 6.2, maintaining the same scale and scan size for comparison. The inclusion of CFO nanoparticles in the P(VDF-TrFE) matrix lead to an average roughness of ≈ 83 ± 19 nm for the CFO/P(VDF-TrFE) non-poled films. When these samples are subjected to the polarization procedure, a slight decrease in the roughness occurs, with no significant differences between both polarizations states: ≈ 78 ± 21 nm for the negative and ≈ 75 ± 20 nm for the positive one. This decrease can be associated with the fact that the polarization induces more ordered structures [25] and with the homogenization effect of the plasma in the polymer surface [26].

The quantification of the magnetic nanoparticle content within the composites was assessed by VSM technique. The hysteresis curves (figure 6.2g) reveal a typical ferromagnetic behaviour for the nanocomposites with CFO nanoparticles [27], characterized by magnetization curves in which the magnetization increases with increasing magnetic field until saturation, reaching a maximum saturation of 8.9 emu.g^{-1} at approximately 20 000 Oe.

Once the surface wettability (hydrophobocity/hydrophilicity) is an important parameter that affects cell-biomaterial interaction and, therefore, cell behaviour, the wettability of the different samples was assessed through sessile drop technique (figure 6.2h). All samples show contact angles below 90°, presenting a hydrophilic behaviour, which is agreement concordance with the literature [28]. The introduction of CFO nanoparticles (≈ 87 ± 8° for non-poled CFO/P(VDF-TrFE) films slightly increases the contact angle comparatively to the P(VDF-TrFE) film without CFO (≈ 78 ± 5°) [26], further, the polarization process strongly affects the wettability of the samples, leading to a decrease in the contact angle values: with positive polarization, the value decreases to ≈ 65 ± 2°, whereas with negative polarization, the value decreases to ≈ 59 ± 4°. These results are in agreement with previous studies were it was demonstrated that corona treatment produce an increase in the surface wettability [29], based on the alignment of the dipolar moments and, therefore, the net surface charge (positive or negative) in the poled samples [30].

There are numerous approaches in an attempt to promote cell proliferation and cell differentiation, approaches that recently include the incorporation of responsive materials used as scaffolds with electrical, magnetic and/or electromechanical properties, associated with the use of new generations of bioreactors [16], which allow control and stimulation of these new materials. In this way, it is important to characterize the stimuli that actually reach to the material where the cells are in contact. In this work, the materials used are subjected to a variable magnetic field, produced by a home-made magnetic bioreactor [19], where the emergence of a magneto-mechanical oscillation in the magnetostrictive

nanoparticles will produce the electrical response in the piezoelectric polymer, leading to a magnetically activated electroactive microenvironment.

In this way, an experimental setup was developed to measure the quantities effectively applied to the material surface and transmitted to the cells. Given the characteristics of the material used, the first major transduction that occurs corresponds to a magnetic stimulus that translates into an applied mechanical stimulus to the cells. Therefore, in a first phase, the magnetic field dispersion to which the ME film is subjected was measured. It was found that the films are subjected to a magnetic field that varies between 0.22 T and -0.22 T, according to the position of the magnets relative to the material. Thus, a finite element simulation of the field-to-surface dispersion was performed, based on the magnetic bioreactor characteristics, and the fields measured by a gaussmeter (figure 6.3).

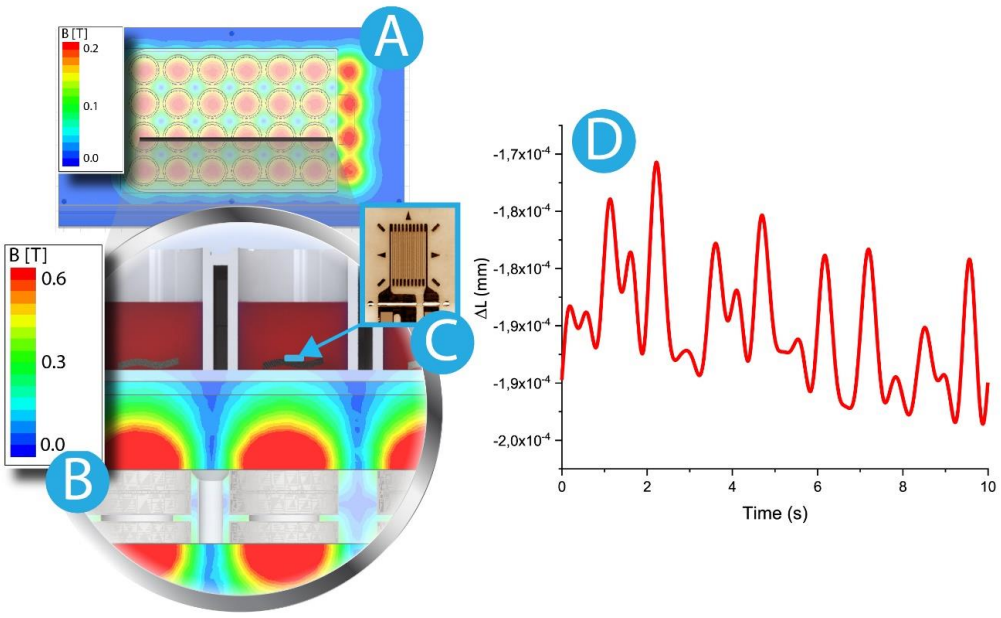

Figure 6.3. (a) Result of the simulation process, along the material surface; (b) cross-section image of the field created along the distance between the permanent magnet and the material surface; (c) detail of the strain gauge sensor for the measurement of the materials deformation; (d) result of the strain measurement, obtained from the measurement of the sensor resistance variation.

Figure 6.3 shows the magnetic field variations, being the magnetic field approximately zero in the central regions between the magnets. Further, there are slightly larger fields in the peripheries of the culture plated when compared to the central region.

After the analysis of the field applied to the ME films, the mechanical strain was measured with a strain gauge sensor (L2A-06-062LW-120, Micro-Measurements) coupled to the film (figure 6.3c). Once the bioreactor is placed into operation, the resistance variation of the strain gauge was obtained, as shown

in figure 6.3b. It is important to note that the sensor was placed at the centre of the well, concentric with the bioreactor excitation magnet, where a displacement cycle was applied allowing the movement of the table until the sensor was concentric with the neighbor magnet, corresponding to a total displacement of 20 mm at a frequency of 0.3 Hz leading to an approximately sinusoidal magnetic excitation with amplitude of approximately 0.22 T in each point. Once the voltage variation at the sensor terminals was collected, the corresponding conversion was carried out to resistance variation, taking into account the reference current through the application of Ohm's law. In order to obtain the mechanical variation of the film, the conversion of the resistance to the deformation variation is performed taking into consideration the gauge factor of the sensor, 2.155, and its length along the measurement axis, 1.52 mm. Thus, the dimensional variation of the sample over the various magnetic excitation cycles is obtained as represented in figure 6.3d, which shows the uniformity of the response over the various magnetic cycles. In this way, it can be concluded that the ME films present a variation of approximately 0.02 μm, which corresponds to a variation of 0.013 $\mu m.mm^{-2}$, since the deformation along the transversal and longitudinal axis is the same, for the already mentioned variation of magnetic field.

Finally, ME characterization (figure 6.4) shows that the samples present a maximum electrical response for an applied DC field of 1500 Oe.

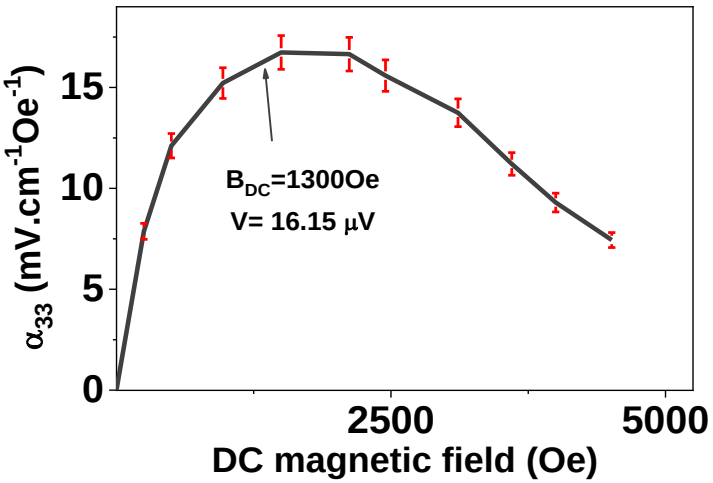

Figure 6.4. Magnetoelectric response of CFO/P(VDF-TrFE) for a DC field from 0 to 5000 Oe at a constant H_{AC} of 1 Oe.

However, the DC component of the magnetic field produced by the home-made magnetic bioreactor is around 2200 Oe (0.22T), being at the biomaterial level around 1300 Oe, which correspond to a magnetoelectric response of the material of 16.15 μV.

Relatively to the electrical response obtained when the sample is placed on the mechanical bioreactor, a response of 64 μV was measured at a mechanical vibration frequency of 1 Hz.

6.3.2 Cell Culture Results

The surface properties of the biomaterials, namely the wettability, roughness and surface charge have demonstrated to be the three most important factors affecting cell adhesion [31]. Regarding the wettability, it is expect that a decrease of WCA lead to an increase of cell adhesion [32]. Relatively to the roughness, it has been demonstrated that the sub-microenvironment variations associated to the microscale roughness lead to different response depending on cell type [33]. Additionally, it has been demonstrated that the surface charge can influence the cell behaviour, where the negative or positive charges can enhance different types of cells, being an essential factor determining the regulation of cell response [34]. Moreover, it has been proven that charged surfaces and piezoelectric materials enhance skeletal muscle tissue regeneration [10-11]. However, the influence of the mechano- and/or mechano-electrical stimuli on muscle proliferation and differentiation has not been studied yet. So, three different samples were used to prove the suitability of the ME materials as a new magnetically activated electroactive microenvironment approach for skeletal muscle tissue regeneration [19]. In the present case, the non-poled samples present higher WCA than the poled ones, with no significant differences between the samples with different surface charge, as verified above. In this way, for the CFO/P(VDF-TrFE) poled samples, the major differences between them is just the surface charge being positive or negative. Taking this into account, the effects of the ME films with different surface charges on myoblast cell adhesion, proliferation and differentiation were first investigated.

6.3.2.1 C2C12 cell adhesion and proliferation on CFO/P(VDF-TrFE) composites

The influence of the surface charge of the CFO/P(VDF-TrFE) films on the adhesion of C2C12 myoblast were first studied after 24 h of cell culture under static conditions. Figure 6.5 shows the fluorescent images in which the cells were stained for nucleus (blue), F-actin (red) and vinculin (green).

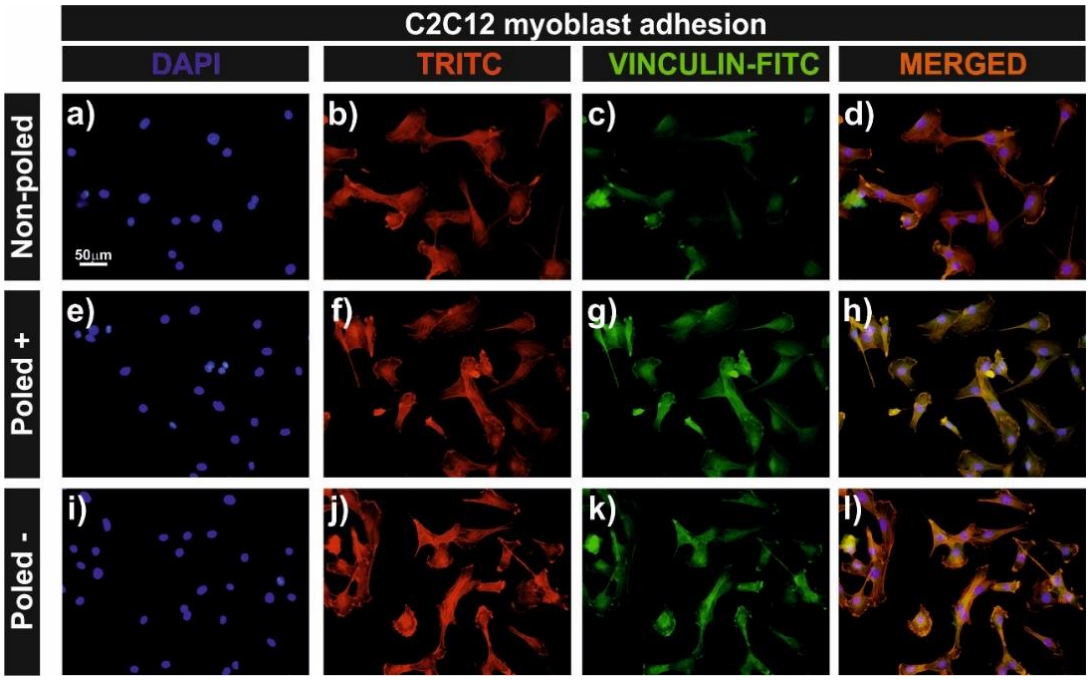

Figure 6.5. C2C12 myoblast cells cultured on the surface of CFO/P(VDF-TrFE) nanocomposite films (non-poled, "poled +" and "poled –") after 24 h of cell adhesion. Fluorescence images of DAPI stained cell nuclei (blue) in (a), (e), and (i); F-actin expression (red) in (b), (f) and (j); vinculin staining (green) in (c), (g) and (k); and overlay in (d), (h) and (l). The scale bar (50 µm) is valid for all the fluorescent images.

The investigation of the cell-matrix contacts in the cells cultured on CFO/P(VDF-TrFE) nanocomposite films with different charges is a relevant issue to understand the influence of substrate polarization on FA characteristics. It has been reported that cell adhesion to a substrate is a key factor determining the function of adhesion receptors in the recruitment of proteins that link the adhesion receptor to the actin cytoskeleton [35]. In this sense, figure 6.5 shows the presence of vinculin, a cytoplasmic actin-binding protein, throughout all the cytoplasm of C2C12 cell in all the samples, independently of the sample surface charge and properties. Relatively to the intensity, it appears to be higher on poled samples than on the non-poled one, and between the different surface charges, it seems to be slightly higher on the positive ones. Analyzing the morphology of C2C12 cells, it is observed that C2C12 cells cultured on poled (negative and positive) CFO/P(VDF-TrFE) surfaces demonstrate a greater spreading morphology with those on the non-poled CFO/P(VDF-TrFE). The same behaviour was observed in the C2C12 myoblast cells cultured on piezoelectric β-PVDF film [36].

As previously indicated, muscle tissue reacts to an electro-mechanical environment and for that, piezoelectric polymers can deliver a mechanical (with non-poled samples) or mechano-electrical signal to the cells (with poled samples) in order to mimic signals and effects present in living tissue. It has been in

fact proven that surface charge of β-PVDF poled samples have impact on C2C12 myoblast adhesion, proliferation [10] and differentiation [11]. However, the effect of mechanical and or electrical stimuli on the cell behaviour through the use of electroactive biomaterials has not been studied yet. In order to address those issues, ME samples, that consist on the combination of magnetostrictive (CFO) and piezoelectric (P(VDF-TrFE)) materials are proposed. These materials allow to investigate the three kind of effects on the proliferation and differentiation of C2C12 myoblast cells: 1) at static conditions, the potential of these films and the influence of the surface charge; 2) at dynamic conditions, with the non-poled samples, the mechanical stimulation and 3) at dynamic conditions, with the poled samples, the mechano-electrical stimulation (figure 6.6).

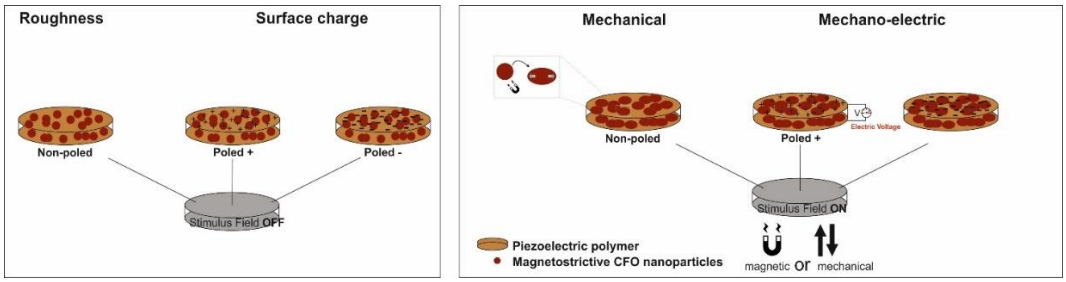

Figure 6.6. Representative images of the stimuli provided to the cells by the different samples under different conditions.

The morphology and proliferation of C2C12 myoblasts on the different samples (non-poled, "poled +" and "poled –") were analyzed up to 3 days of cell culture under static and dynamic conditions with immunocytochemistry and MTS assay, respectively (figure 6.7).

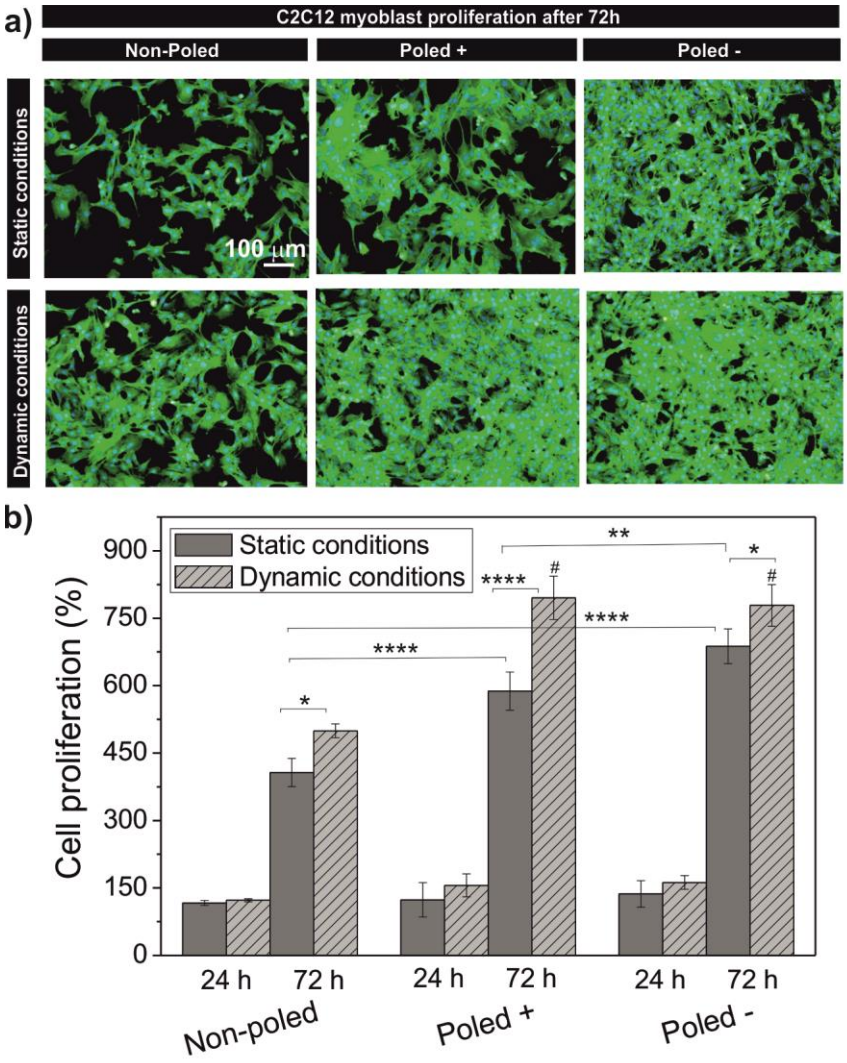

Figure 6.7. (a) Representative immunofluorescence images (nucleus stained with DAPI - blue and cytoskeleton stained with FITC - green). Scale bar (100 μm) is valid for all images. (b) Cell proliferation of C2C12 myoblast culture up to 72 h on CFO/P(VDF-TrFE samples (non-poled, "poled +" and "poled –") under static and dynamic conditions. The cell proliferation values were determined regarding the cells adhered on the material after 24 h adhesion, just before placed in contact with the bioreactor. The results are expressed as the mean ± SD of three independent assays. $^{*}p \leq 0.05$, $^{**}p \leq 0.01$, $^{****}p \leq 0.0001$ *and* $^{\#}p \leq 0.0001$ *vs* non-poled after 72 h at dynamic conditions.

Figure 6.7a shows that cell proliferation increases in all samples under static and dynamic conditions from 24 h to 72 h, which is in agreement with the obtained values for cell proliferation (Figure 6.7b).

Under static conditions, and after 24 h of cell culture, the cell proliferation on all CFO/P(VDF-TrFE) materials are similar, with a little difference between the non-poled samples and poled ones. After 72 h, as expected, all samples demonstrated an increase of cell proliferation, with the lower value for the non-

poled samples (≈ 405%) and the higher for the "poled –" CFO/P(VDF-TrFE) films (≈ 685%). This behaviour is in agreement with a previous study where was stated that negative surface charges promote higher proliferation rates of C2C12 myoblast cells [10].

Under dynamic conditions (figure 6.1), the influence of the mechanical and/or electrical stimulation on cell proliferation was studied, showing that both stimulations improve cell proliferation, being significantly higher (figure 6.7b) with the mechano-electrical stimuli (with poled samples, ≈ 780%), being no significant differences between both polarizations, confirming the myoblast sensitivity to the mechano-electric stimuli.

6.3.2.2 C2C12 cell differentiation on the CFO/P(VDF-TrFE) samples

During differentiation of C2C12 cells, myoblasts undergo remodeling to form mature myotubes with increased expression of muscle specific genes [37]. Final differentiation into contractile units is concomitant with the expression of sarcomeric proteins such as skeletal muscle MHC. The expression of MHC isoforms is often a measure of *in vitro* myotube differentiation and efficiency [38]. In this study, C2C12 myoblasts were grown on the materials in the presence of two different culture media: basal medium, in order to evaluate just the physical stimuli, and differentiation medium, used to assess the effect of the biochemical stimulus. Further, two different conditions of culture were used: static and dynamic. These parameters were selected to access the influence of surface charge and mechano-electric stimuli in the expression of the myogenic differentiation marker MHC. Figure 6.8 shows the fluorescent images of C2C12 myoblasts cultured on the different CFO/P(VDF-TrFE) films surfaces, as well some relevant properties of the formed myotubes formed, including fusion and maturation index, length, aspect ratio between length and width and the number of myotubes per 1 mm^2.

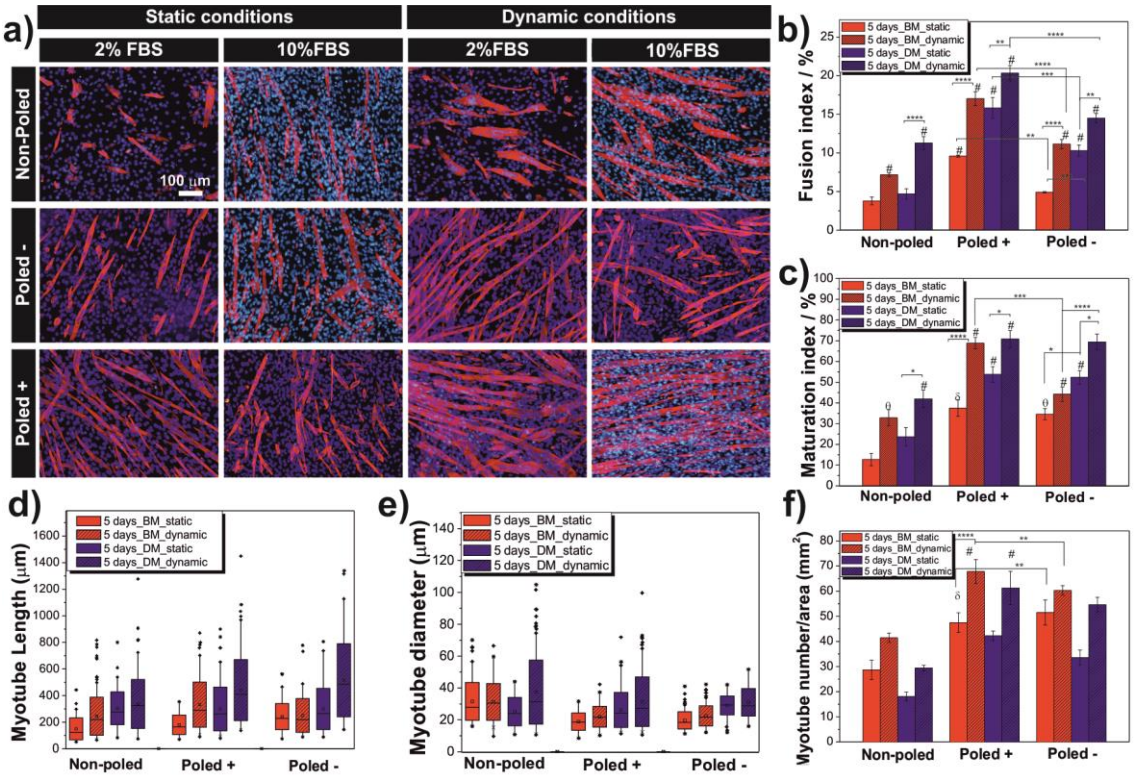

Figure 6.8. (a) Immunofluorescent staining of myosin heavy chain after 5 days of C2C12 cells differentiation on the different samples. Row 1 shows the C2C12 cells present on non-poled, row 2 shows them on "poled +" and row 3 shows the cells on "poled –" CFO/P(VDF-TrFE) samples. The columns 1 and 2 show the cells under static condition with DM and BM, respectively; columns 3 and 4 show them under dynamic conditions (magnetic stimulation) with DM and BM, respectively. Quantitative analysis on (b) fusion index, (c) maturation index, (d) myotube length and (e) diameter of the obtained myotubes and (f) myotube number. Data are expressed as the mean ± s.e.m. $^{*}p \leq 0.05$, $^{**}p \leq 0.01$, $^{***}p \leq 0.001$, $^{****}p \leq 0.0001$; *and* $^{\delta}p \leq 0.01$ *vs* non-poled with BM and static conditions, $^{\theta}p \leq 0.001$ *vs* non-poled with BM and static conditions and $^{\#}p \leq 0.0001$ *vs* non-poled with BM and static conditions.

Figure 6.8a shows that all the ME materials with and without surface charge promote myogenic differentiation of C2C12 myoblast that can be confirmed by the presence of MHC in all the samples after 5 days of cell culture in all the conditions. Regarding the fusion index (figure 6.8b) at static conditions, with BM, the sample "poled +" show higher values comparatively to the other samples that shows similar values. When the medium was changed to DM, significative differences were observed in both poled samples. Also, it is possible to verify significant differences between the polarization surface charges, with higher values for the positively charged samples. Previous studies show related results, proving that electrically poled β-PVDF samples promote higher fusion index values [11], with also higher values for

the positive ones. This fact indicates that positively charged samples improves C2C12 myoblast differentiation.

After analyzing the myogenic fusion index, i.e. the number of fused cells per total cell number, it is also important to evaluate the maturity of the formed myotubes.

Relatively to the maturation index (figure 6.8c) at static conditions, it is verified with BM that poled samples present significant higher values compared to the non-poled ones, but with no significant difference between the polarization types. Changing the medium to DM, the same behaviour as the one observed in the fusion index was observed: all samples present higher values with DM but with no significant difference for the non-poled samples and significant difference for the poled ones. However, comparing the poled samples, contrarily to the fusion index, no significant differences were observed among them.

The differentiation assays on the same scaffolds using the drop method (figure 6.1) under dynamic conditions were performed at the same time. It is observed (figure 6.8b and 6.8c) that for all samples with and without DM under dynamic conditions, the values of fusion and maturation index were higher than under static condition. After 5 days of differentiation it is evident, for cell culture in both media, that the fusion index was more significative in charged samples, in particular in “poled +” with DM (≈ 20%). Although significant differences between the polarizations on fusion index values were observed, similar maturation values were verified for “poled +” and “poled –” with DM (≈ 71 and 69% respectively). The non-poled samples showed ≈ 11 and 42% for fusion and maturation index, respectively, demonstrating that mechanical and mechano-electrical stimuli promote C2C12 myoblast differentiation.

In order to assess the myotube formation, myotube length (figure 6.8d), diameters (figure 6.8e) and numbers/area (figure 6.8f) were evaluated for cell culture with the two media (BM and DM), under static and dynamic conditions. It is verified that non-poled samples lead to higher myotubes diameters and that the poled samples lead to higher myotubes length. Relatively to the myotube number per area, it is verified that the dynamic conditions improve the number of myotubes, with higher values for the poled samples, which is in agreement with the obtained results of fusion and maturation index.

After examination of the myogenic differentiation on CFO/P(VDF-TrFE) samples by the presence of MHC, the major structural protein in myotubes, another muscle-specific structural gene, muscle creatine kinase was evaluated during the differentiation phase. Creatine kinase is a relevant muscle-specific gene in muscle fiber-type maturation of the myotubes. Figure 6.9 shows the creatine kinase values obtained for C2C12 myoblast cells cultured on CFO/P(VDF-TrFE) films with and without polarization for 5 days of cell differentiation under static and dynamic conditions.

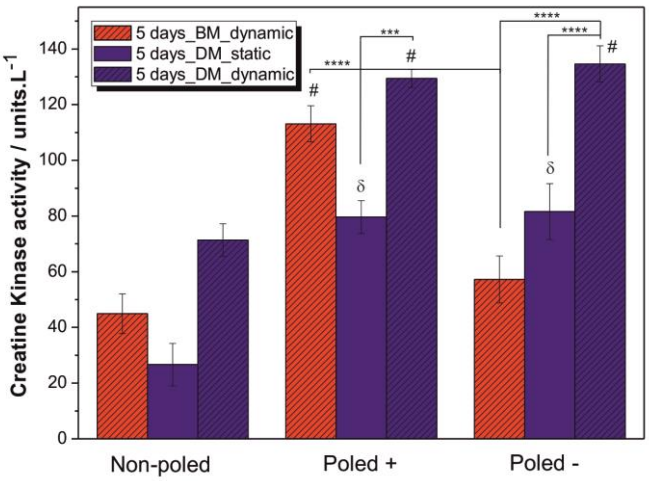

Figure 6.9. Creatine kinase activity values after 5 days of C2C12 cell differentiation cultured on the different CFO/P(VDF-TrFE) samples: non-poled, "poled +" and "poled –". All the values are presented as average ± s.e.m. $^{***}p \leq 0.001$, $^{****}p \leq 0.0001$; $^{\delta}p \leq 0.01$ *vs* non-poled with BM and dynamic conditions and $^{\#}p \leq 0.0001$ *vs* non-poled with BM and dynamic conditions.

Comparing the static and dynamic conditions with DM it is evident that the samples cultured under dynamic conditions yield the highest values of creatine kinase activity. Further, the poled samples present higher values compared with the non-poled ones, being no significative differences among samples with different surface charge. Analyzing the samples under dynamic conditions but with and without DM, it is verified that no significant differences are obtained for non-poled and "poled +" samples, contrary to the "poled –" samples, where significant differences are observed, with higher values with DM. Once, as already stated before, the creatine kinase values are associated to the more mature myotubes. Thus, it is verified that these results are in agreement with the values of the maturation index (figure 6.8c).

The study of cell differentiation was kept up to 8 days and after this time, immunofluorescence staining of myosin heavy chain was investigated (figure 6.10).

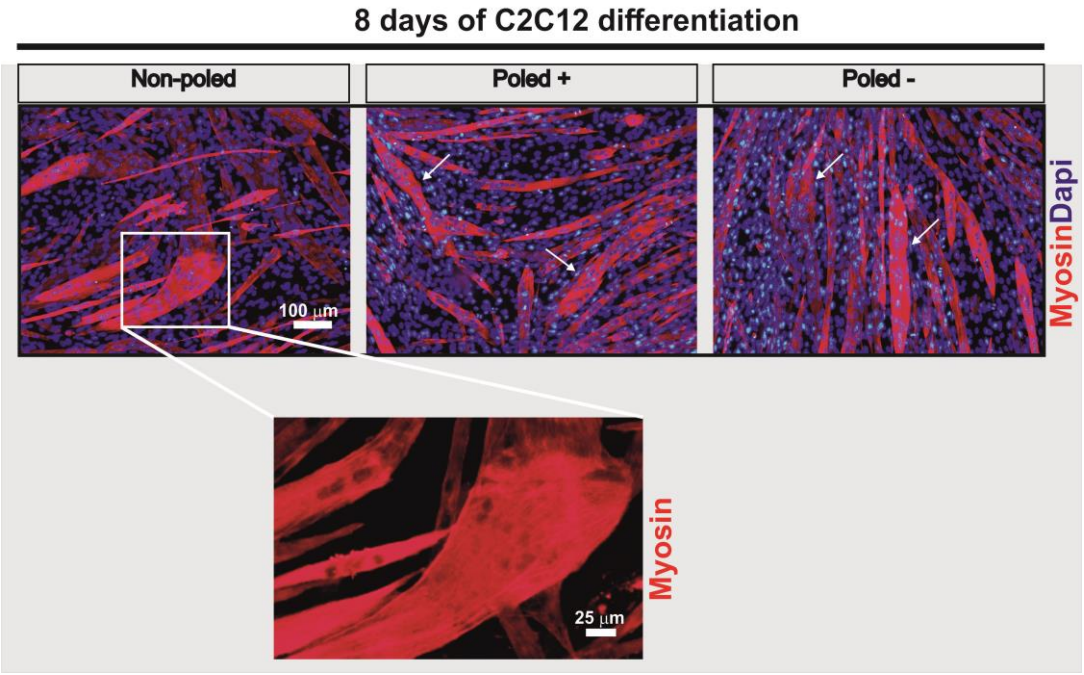

Figure 6.10. Immunofluorescence microscopy images of C2C12 myoblast differentiated on different CFO/P(VDF-TrFE) films for 8 days with BM under dynamic conditions. Myotubes were fixed and stained with a MHC-specific antibody (red) and the nuclei counterstained with DAPI (blue). Scale bars represent 100 µm for all upper images.

Figure 10 shows the immunofluorescent staining of MHC images of C2C12 myoblast cells differentiated under dynamic conditions (magnetic stimulation) with BM. After 8 days of differentiation, it is verified that myotubes continue to grow with the same profile obtained after 5 days of differentiation, i.e just more mature myotubes are observed in all the samples when compared with the same sample and conditions. Namely, it is observed higher myotubes diameter on the non-poled samples and higher length in the poled ones. The same behaviour was observed for the others conditions (data not shown), with similar differences between the samples and conditions observed after 5 days of differentiation.

Observing all the results obtained after evaluation of the influence of the surface charge (polarization) of the biomaterial and the stimuli provided to the cells (mechanical and/or electrical), it can be concluded that the polarization and also these stimuli enhance the myoblast differentiation, leading to more mature myotubes. Also, comparing the poled samples, it is verified that when only the physical stimuli was provided (BM at dynamic conditions), the samples with positive polarization lead to significantly higher fusion and maturation index. This can be related to the fact that the cellular plasma membrane presents a negative charge [39]. Also, it has been demonstrated that the positive and negative charge can enhance/inhibit different phases of cell behaviour. For example, the use of positive charged nanoparticles

has demonstrated to inhibit stem cell proliferation but not differentiation [40]. However, when the physical stimuli is combined with the chemical one (DM), no significant differences are observed between cell culture on samples with different surface polarization.

Another important parameter for skeletal muscle TE is the alignment of the cells. This is important once the natural skeletal muscle presents a highly organized structure, with long parallel bundles of multinucleated myotubes. Besides that, a non-proper myotube alignment leads to an ineffective force transmission and contractility for regeneration of functional muscle fibres [41].

In this way, it is important the biomaterials to prevent random fusion and to lead to a proper elongation and alignment of myotubes. The fused myotubes formed in the different samples at different conditions have been this studied (Figure 6.11).

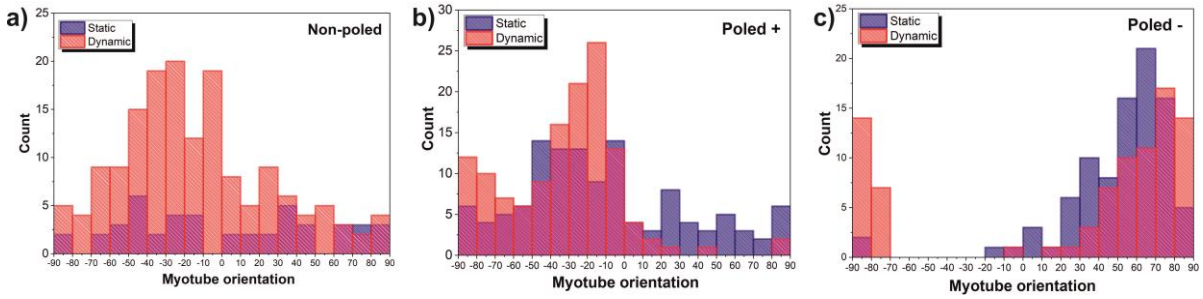

Figure 6.11. Distribution of myotube orientation on the different CFO/P(VDF-TrFE) samples: (a) non-poled, (b) "poled +" and (c) "poled –"; with DM under static and dynamic conditions after 5 days of differentiation.

Regarding the distribution of myotube orientation on the different CFO/P(VDF-TrFE) samples, the polarization of the samples seems to induce some myotube orientation. When the mechanical and/or electrical stimuli are provided, it is verified that these stimuli induce the myotube orientation in all the samples; being more evident on the non-poled samples compared with the static conditions where no myotube orientation was verified. Therefore, these results demonstrate that, together with the enhancement of myoblast differentiation, the developed materials lead to the myotubes alignment. In this way, ME biomaterials show strong potential to be used for skeletal muscle TE. Therefore, this effect can be combined also with scaffolds with fibrillar morphology [42] which as has been shown to strengthen the alignment of myotubes [11].

The previous results thus demonstrated that the mechano-electrical stimuli (provided by the magnetic home-made bioreactor) have large influence on proper C2C12 differentiation. However, it is possible to directly mechanically stimulate these ME samples [22] with a home-made vibration bioreactor

(see figure 6.1), obtaining a mechanically activated electroactive microenvironment. With this bioreactor a direct mechanical stimulation of the materials is provided, evaluating directly the piezoelectric response. Thus, studying this two kind of stimulation by different bioreactors, it is possible prove the positive influence of mechano-electric stimuli on the cells by two different approaches (magnetoelectric stimulation and direct piezoelectric stimulation). The study in this mechanical home-made bioreactor was performed with different CFO/P(VDF-TrFE) samples and no chemical stimuli (BM), for 5 days of cell differentiation, in order to evaluate and compare only the physical stimuli.

The figure 6.12 shows the immunofluorescent images and some myotube quantitative parameters obtained on the CFO/P(VDF-TrFE) samples with BM under dynamic conditions through the use of the mechanical home-made bioreactor.

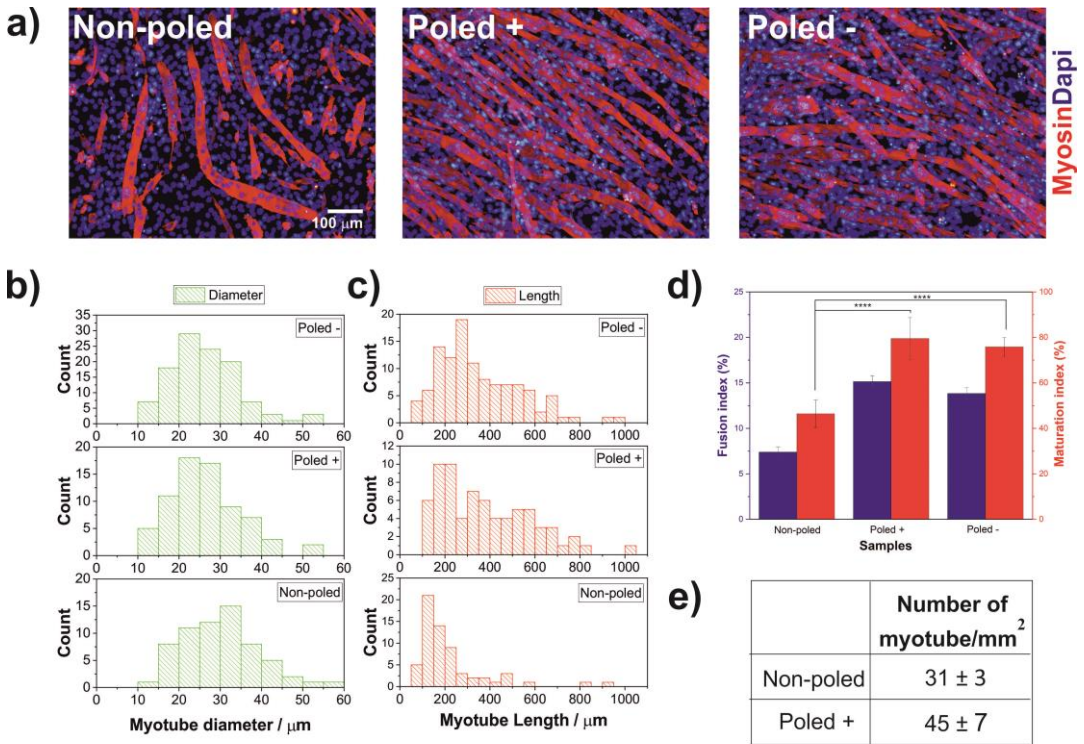

	Number of myotube/mm^2
Non-poled	31 ± 3
Poled +	45 ± 7
Poled -	53 ± 5

Figure 6.12. (a) Immunofluorescent staining of myosin heavy chain (MHC) after 5 days of C2C12 cells differentiation under dynamic condition (mechanical stimulation) with BM on the different CFO/P(VDF TrFE) samples. Scale bars represent 100 μm for all images. Quantification of (b) myotube diameter, (c) myotube length, (d) fusion and maturation index and (e) number of myotubes.mm^{-2}. Data are expressed as the mean ± s.e.m., $^{****}p \leq 0.0001$.

Figure 6.12a shows that all materials under mechanical stimulation promote C2C12 differentiation, where the electrically charged materials lead to higher fusion and maturation index values (Figure 6.12d)

than samples without charge (non-poled), in which just mechanical and not mechano-electric stimulation occurs. It is to notice that these results are fully in agreement with the ones obtained with the magnetic home-made bioreactor.

Also, no significant differences between samples cultured on "poled +" and "poled –" samples were obtained. The size of myotubes, more specifically their length (figure 6.12c) and diameter (figure 6.12b) shows that higher values of maturation index are also associated with longer myotubes. The "poled +" CFO/(PVDF-TrFE) samples support the biggest myotubes with 391.05 ± 34.19 μm, with no significant differences compared to the "poled –", 356.28 ± 24.34 μm. Relatively to the distribution of the myotube diameter (figure 6.12b), it is observed that the diameter average values obtained for all samples ranged between 26.38 ± 1.04 and 30.50 ± 1.18 μm, with the non-poled samples leading to the largest diameter. Myotube number was also quantified (figure 6.12e) and the results demonstrate that the mechano-electrical stimulus promotes higher differentiation, and consequently, higher myotube formation, with no significative differences between both polarization states, 45 ± 7 and 53 ± 5, for "poled +" and "poled –", respectively.

The use of a home-made bioreactor system with mechanical solicitations at 1 Hz confirmed the relevance of the mechano-electric stimuli for muscle differentiation. With this approach (direct mechanical stimuli), higher values of electrical stimuli (64 μV) are provided (as calculated from the piezoelectric coefficient of the materials) to the cells.

An overview of the cell response obtained by the use of the different home-made bioreactors are compared in Table 6.2, showing the data of the fusion and maturation index obtained in the different samples with BM at static and dynamic conditions in the two bioreactors.

Table 6.2. Quantitative comparison of MHC among the different samples after 5 days of differentiation under static and dynamic (magnetic and mechanical stimulation) conditions.

Conditions	Medium	Bioreactor Stimulus	Samples	Fusion index	Maturation index
Static	BM	-------	Non-poled	3.78 ± 0.51	12.73 ± 2.96
			Poled +	9.59 ± 0.13	37.52 ± 4.01
			Poled -	4.9 ± 0.1	34.59 ± 2.72
Dynamic		Magnetic	Non-poled	7.17 ± 0.24	32.85 ± 3.90
			Poled +	17.03 ± 0.89	68.88 ± 2.67
			Poled -	11.15 ± 0.60	44.24 ± 3.49
		Mechanical	Non-poled	7.38 ± 0.58	46.41 ± 5.97
			Poled +	15.14 ± 0.95	79.52 ± 11.23
			Poled -	13.83 ± 0.73	75.88 ± 4.17

Regarding the table 6.2, it is verified that the fusion and maturation index values are slightly higher with direct mechanical stimulation. Once the values of electrical stimuli provided by this bioreactor are superior to those provided by the magnetic one, it is concluded than the mechanical but mostly the electrical cues, play a key role on muscle differentiation. In this way, electromechanical microenvironments, either directly mechanically or magnetically activated show an excellent potential for skeletal muscle TE, by providing the necessary physical stimuli present in the natural tissue in the human body.

6.4 Conclusions

Skeletal muscle TE requires novel and more efficient strategies to mimic the natural tissue microenvironment. This work demonstrates the relevance of electromechanically active microenvironments for muscle TE. The mechanical and electrical activation of the microenvironment has been performed either directly (direct application of mechanical solicitation to produce the piezoelectric response of the material) or indirectly (magnetically activated) by using magnetoelectric biomaterials - that allows triggering cellular response by non-contact external stimulation. Herein, the suitability of the magnetoelectric effect for skeletal muscle TE was demonstrated with CFO/P(VDF-TrFE) films with different

surface charges. It is shown that the introduction of 20 wt.% $CoFe_2O_4$ filler increases the water surface angle with respect to the pristine polymer, but that the water contact is reduced after the poling process, leading to lower water contact angles for the charged samples: ≈ 59 ± 4° for negative and ≈ 67 ± 2° for positive surface charge. Further, surface roughness also increases with the introduction of the magnetic fillers with respect to pristine PVDF-TrFE. These biomaterials allowed mechanical (0.013 μm.mm^{-2}) and electrical (16.15 μV and 64 μV, thought magnetic an mechanical bioreactor, respectively) stimulation of the cells. Relatively to the myogenic cell differentiation, this study showed that at dynamic conditions, the application of mechanical (non-poled samples) and mechano-electrical ("poled +" and "poled -" samples) stimuli promote the C2C12 cells differentiation (higher presence of MHC) comparatively to the static conditions. As verified in the cell proliferation, charged samples show higher maturation index, with no significant differences in positive and negatively charged surfaces. A magnetically or mechanically activated electroactive microenvironment was provided to the cells by the use of a magnetic or mechanical bioreactor, respectively. Comparing both stimulation procedures, it is concluded that the mechanical but mostly the electrical cues play a key role on muscle differentiation. Concluding, this study proves the need of biomimetic electroactive microenvironments for muscle tissue engineering and demonstrated how to apply these stimuli remotely by magnetoelectric biomaterials.

6.5 References

1. Meyer, U., et al., *Fundamentals of tissue engineering and regenerative medicine*. Fundamentals of Tissue Engineering and Regenerative Medicine , 2009. p. 1-1049.
2. Tabebordbar, M., Wang, E.T. and Wagers, A.J., *Skeletal muscle degenerative diseases and strategies for therapeutic muscle repair*. Annual Review of Pathology: Mechanisms of Disease, 2013. **8**: p. 441-475.
3. Frontera, W.R. and Ochala, J., *Skeletal Muscle: A Brief Review of Structure and Function.* Behavior Genetics, 2015. **45**(2): p. 183-195.
4. Guiraud, S. and Davies, K.E., *Regenerative biomarkers for Duchenne muscular dystrophy.* Neural Regeneration Research, 2019. **14**(8): p. 1317-1320.
5. Shafiee, A. and Atala, A., *Tissue Engineering: Toward a New Era of Medicine*. Annual Review of Medicine, 2017. **68**: p. 29-40.
6. Pérez, R.A., et al., *Naturally and synthetic smart composite biomaterials for tissue regeneration.* Advanced Drug Delivery Reviews, 2013. **65**(4): p. 471-496.
7. Rangarajan, S., Madden, L. and Bursac, N., *Use of flow, electrical, and mechanical stimulation to promote engineering of striated muscles.* Annals of Biomedical Engineering, 2014. **42**(7): p. 1391-1405.
8. Dao, T.T. and Tho, M.C.H.B., *A systematic review of continuum modeling of skeletal muscles: Current trends, limitations, and recommendations.* Applied Bionics and Biomechanics, 2018. **2018:** p. 7631818.

9. Liao, I.C., et al., *Effect of Electromechanical Stimulation on the Maturation of Myotubes on Aligned Electrospun Fibers.* Cellular and molecular bioengineering, 2008. **1**(2-3): p. 133-145.
10. Martins, P.M., et al., *Effect of poling state and morphology of piezoelectric poly(vinylidene fluoride) membranes for skeletal muscle tissue engineering.* RSC Advances, 2013. **3**(39): p. 17938-17944.
11. Ribeiro, S., et al., *Electroactive biomaterial surface engineering effects on muscle cells differentiation.* Materials Science and Engineering C, 2018. **92**: p. 868-874.
12. Cardoso, V.F., et al., *Fluorinated polymers as smart materials for advanced biomedical applications.* Polymers, 2018. **10**(2): p. 161.
13. Koppes, R.A., Schiele, N.R. and Corr, D.T., *An electromechanical bioreactor for scaffold-free skeletal muscle tissue engineering*. in ASME 2011 Summer Bioengineering Conference, 2011. P. 135-136.
14. Gazendam, M.G.J. and Hof, A.L., *Averaged EMG profiles in jogging and running at different speeds.* Gait and Posture, 2007. **25**(4): p. 604-614.
15. Sasaki, K. and Neptune, R.R., *Muscle mechanical work and elastic energy utilization during walking and running near the preferred gait transition speed.* Gait and Posture, 2006. **23**(3): p. 383-390.
16. Ribeiro, C., et al., *Piezoelectric polymers as biomaterials for tissue engineering applications.* Colloids and Surfaces B: Biointerfaces, 2015. **136**: p. 46-55.
17. Guo, B. and Ma, P.X., *Conducting Polymers for Tissue Engineering.* Biomacromolecules, 2018. **19**(6): p. 1764-1782.
18. Dobson, J., *Remote control of cellular behaviour with magnetic nanoparticles.* Nature Nanotechnology, 2008. **3**(3): p. 139-143.
19. Ribeiro, C., et al., *Proving the suitability of magnetoelectric stimuli for tissue engineering applications.* Colloids and Surfaces B: Biointerfaces, 2016. **140**: p. 430-436.
20. Martins, P., et al., *Optimizing piezoelectric and magnetoelectric responses on $CoFe_2O_4$/P(VDF-TrFE) nanocomposites.* Journal of Physics D: Applied Physics, 2011. **44**(49): p. 495303.
21. Ribeiro, C., et al., *Electroactive poly(vinylidene fluoride)-based structures for advanced applications.* Nature Protocols, 2018. **13**(4): p. 681-704.
22. Ribeiro, C., et al., *Enhanced proliferation of pre-osteoblastic cells by dynamic piezoelectric stimulation.* RSC Advances, 2012. **2**(30): p. 11504-11509.
23. Ribeiro, C., et al., *Dynamic piezoelectric stimulation enhances osteogenic differentiation of human adipose stem cells.* Journal of Biomedical Materials Research - Part A, 2015. **103**(6): p. 2172-2175.
24. Prabhakaran, T. and Hemalatha, J., *Poly(vinylidene fluoride)-Based Magnetoelectric Polymer Nanocomposite Films*, in *Magnetoelectric Polymer-Based Composites*. Editors: S.Lanceros-Mendez and P.Martins, Editors. Wiley VHC, 2017. p. 87-113.
25. Martins, P., Lopes, A.C. and Lanceros-Mendez, S., *Electroactive phases of poly(vinylidene fluoride): Determination, processing and applications.* Progress in Polymer Science, 2014. **39**(4): p. 683-706.
26. Correia, D.M., et al., *Surface wettability modification of poly(vinylidene fluoride) and copolymer films and membranes by plasma treatment.* Polymer, 2019. **169**: p. 138-147.

27. Gonçalves, R., et al., *Development of magnetoelectric $CoFe_2O_4$/poly(vinylidene fluoride) microspheres.* RSC Advances, 2015. **5**(45): p. 35852-35857.
28. Yuan, Y. and Lee, T.R., *Contact angle and wetting properties*. Springer Series in Surface Sciences, 2013. **51**(1): p. 3-34.
29. Ribeiro, C., et al., *Fibronectin adsorption and cell response on electroactive poly(vinylidene fluoride) films.* Biomedical Materials, 2012. **7**(3): p. 035004.
30. Serrado Nunes, J., et al., *Relationship between the microstructure and the microscopic piezoelectric response of the α- And β-phases of poly(vinylidene fluoride).* Applied Physics A: Materials Science and Processing, 2009. **95**(3): p. 875-880.
31. Ranella, A., et al., *Tuning cell adhesion by controlling the roughness and wettability of 3D micro/nano silicon structures.* Acta Biomaterialia, 2010. **6**(7): p. 2711-2720.
32. Webb, K., Hlady, V. and Tresco, P.A., *Relative importance of surface wettability and charged functional groups on NIH 3T3 fibroblast attachment, spreading, and cytoskeletal organization.* Journal of Biomedical Materials Research, 1998. **41**(3): p. 422-430.
33. Ribeiro, C., et al., *Surface roughness dependent osteoblast and fibroblast response on poly(L-lactide) films and electrospun membranes.* Journal of Biomedical Materials Research - Part A, 2015. **103**(7): p. 2260-2268.
34. Metwally, S. and Stachewicz, U., *Surface potential and charges impact on cell responses on biomaterials interfaces for medical applications.* Materials Science and Engineering C, 2019. **104**: p. 109883.
35. Bays, J.L. and DeMali, K.A., *Vinculin in cell–cell and cell–matrix adhesions.* Cellular and Molecular Life Sciences, 2017. **74**(16): p. 2999-3009.
36. Parssinen, J., et al., *Enhancement of adhesion and promotion of osteogenic differentiation of human adipose stem cells by poled electroactive poly(vinylidene fluoride).* Journal of Biomedical Materials Research - Part A, 2015. **103**(3): p. 919-928.
37. Nakayama, K.H., Shayan, M. and Huang, N.F., *Engineering Biomimetic Materials for Skeletal Muscle Repair and Regeneration.* Advanced Healthcare Materials, 2019. **8**(5): p. 1801168.
38. Chal, J. and Pourquié, O., *Making muscle: Skeletal myogenesis in vivo and in vitro.* Development (Cambridge), 2017. **144**(12): p. 2104-2122.
39. Chen, Y.S., Harn, H.J. and Chiou, T.W., *The Role of Biomaterials in Implantation for Central Nervous System Injury.* Cell Transplantation, 2018. **27**(3): p. 407-422.
40. Li, J.J., Kawazoe, N. and Chen, G., *Gold nanoparticles with different charge and moiety induce differential cell response on mesenchymal stem cell osteogenesis.* Biomaterials, 2015. **54**: p. 226-236.
41. Jana, S., Levengood, S.K.L. and Zhang, M., *Anisotropic Materials for Skeletal-Muscle-Tissue Engineering.* Advanced Materials, 2016. **28**(48): p. 10588-10612.
42. Maciel, M.M., et al., *Relation between fiber orientation and mechanical properties of nano-engineered poly(vinylidene fluoride) electrospun composite fiber mats.* Composites Part B: Engineering, 2018. **139**: p. 146-154.

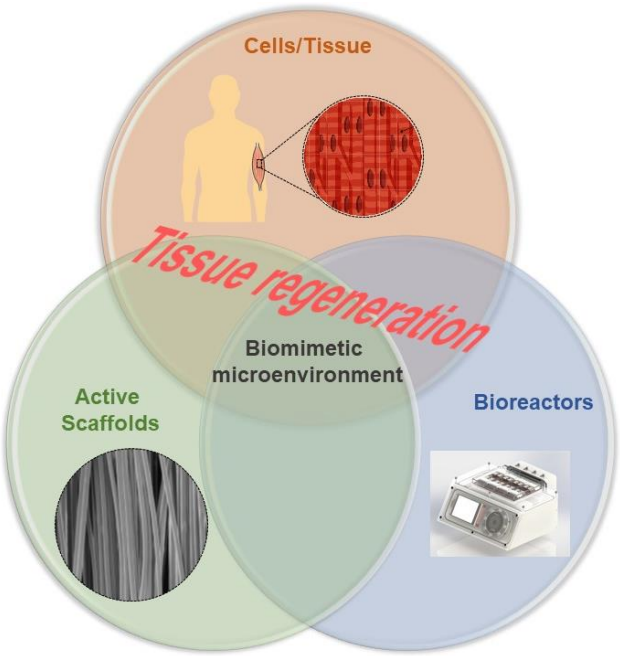

Chapter 7. Conclusions and future works

This chapter presents the main conclusions of this work, devoted to the development of multifunctional platforms for muscle regeneration, and their influence on cell muscle behaviour. The potential of piezoelectric and magnetoelectric polymeric biomaterials for skeletal muscle tissue engineering was shown, and the relevance of mechano-electrical stimuli for myotube differentiation was confirmed. Suggestions for future works are also put forward.

7.1 Conclusions

The biomimicry of the natural microenvironment of tissues with engineered scaffolds remains one of the largest challenges of TE. The microenvironment is a complex 3D microstructure of signaling molecules, interacting cells and structural components. With each of these components playing a critical role in healthy tissue, it is essential to understand their interactions in order to identify methods to properly repair tissue damaged in disease states. Furthermore, by thoroughly understanding the microenvironment contribution to cell fate determination, it will allow more accurate and specifically designed TE strategies. It has been demonstrated that muscle cells differentiate optimally when the physical signals resemble the cues encountered by the cells in their natural environment. Also, it is well known that muscle tissue reacts to electrical and mechanical stimuli. In this way, piezoelectric biomaterials emerge as possible solution to provide these electromechanically active stimuli for a more biomimetic TE approach.

This work was thus devoted to the use of β-PVDF polymer for muscle TE applications, mainly due to its high piezoelectric response, allowing to provide the electromechanical stimuli that the muscle tissue needs. The suitability of the piezoelectric effect for tissue regeneration has already been proven for bone and it was already demonstrated the relevance of surface charge on muscle regeneration. In this way, β-PVDF films (non-poled - no average surface charge, “poled +” - positive surface charge and “poled –” - negative surface charge) were successfully obtained by solvent casting and corona discharge for the poled samples, and PVDF fibres were obtained by electrospinning obtaining directly fibres on electroactive phase (β-phase). These fibres can mimic the extracellular matrix of the human body promoting alignment of cells. The mechanical properties of the scaffold are an essential parameter in order to get controlled mechanotransduction of the cells. The effective Young’s modulus for the oriented fibres depends significantly on the stretching direction. Being 225, 27 and 23 MPa for deformation along the 0°, 45° and 90° angles with respect to fiber orientation, respectively. The electroactive β phase of the pure PVDF fibres is above 75%, independently of the orientation direction.

As electroactive materials are a suitable platform for advanced muscle TE strategies, new functional properties were added to the materials. Thus, SiNPs and magnetic nanoparticles were introduced in the piezoelectric matrix. SiNPs were selected in order to improve the nucleation of β-phase of PVDF and to provide a platform for loading growth/differentiation factors in mesoporous silica nanoparticles. Magnetic nanoparticles, on the other hand, were introduced in order to provide magneto-mechanical and/or magneto-electric stimulation to the cells.

In the case of SiNPs, particles with different diameters and functionalizations were produced and introduced in different contents into PVDF leading to composites with different morphology, porosity and

electroactive phase. It was verified that 8 wt.% of SiNPs with positive functionalization (NMe_3^+) promotes an increase on β-phase content up to ≈ 53%. The obtained samples demonstrated to be not cytotoxic and promoted cell proliferation, being a good approach for TE applications.

The introduction of CFO within PVDF fibres increases the electroactive β phase content up to ≈ 92% and the stretching does not alter significatively these values. The same happen for the mechanical properties that increase to 308.71 MPa with 10 wt.% of $CoFe_2O_4$ nanoparticles.

All the developed materials represent active multifunctional platforms for skeletal muscle tissue engineering depending. Thus, it was important evaluate the effect on cells of some relevant parameters.

In this way, cell response was evaluated in β-PVDF films (non-poled - no charge, "poled +" - positive charge and "poled –" - negative charge) obtained by solvent casting and corona discharge for the poled samples, and PVDF fibres obtained by electrospinning. It was observed that both charged surfaces of PVDF films promote myogenic differentiation of C2C12 cells. After 8 days of differentiation, it is shown that without chemical stimuli (basal medium), the positively charged surface of β-PVDF samples show higher fusion index comparatively to the other samples. On the other hand, the maturation index values of the obtained myotubes are higher when the cells grown on surface charged samples, with no significant differences among positively or negatively charged surfaces when combined with the chemical stimuli (differentiation medium) (≈ 5 fold higher when compared with the control: 5 days of differentiation with BM) and also without chemical stimuli (basal medium) (≈ 3 fold higher when compared with the control: 5 days of differentiation with BM). So, it was demonstrated that the combination of surface charge (physical stimuli) and differentiation medium (chemical stimuli) promote myotubes more mature than samples without polarization.

Together with the surface charge of the materials, their morphology also plays a relevant role in determining cell fate. Thus, with respect to the effect of the scaffold morphology, it was verified that oriented electrospun PVDF fibres promote the alignment of the cells that is important for the differentiation and morphology of skeletal muscle tissue in the human body.

Analyzing the effect of β-PVDF surface charge on cell adhesion, it was shown that surface charge promotes cell elongation (≈ 41 μm) and negative polarization improves cell-material adhesion force (≈ 8.92 ± 0.45 nN). In this way, the de-adhesion energy required to detach cells is higher on negative charged surfaces (≈ $30.34 \pm 1.52 \times 10^{-15}$ J), which is in agreement with higher de-adhesion force exerted on the cantilever. These results demonstrate that polarization allows to tune cell-surface interactions via electrical surface charge and also dynamically from the piezoelectric effect, that leads to surface charge variations upon mechanical solicitations.

With respect to the materials with magnetostrictive CFO nanoparticles, the adhesion, proliferation and differentiation of myoblast C2C12 cells was studied under both static and dynamic conditions. Under static conditions, it was observed that the surface charge allows the elongation of the cells (similar for both polarization states) as verified for the PVDF films. Further, cell proliferation shows an increase in cell viability and differentiation, with higher fusion and maturation index of the myotubes comparatively to the samples without surface charge. In this case, no physical stimuli are being applied to cells. In order to stimulate the environment found in the human body, bioreactors are needed to provide the appropriate stimuli to the biomaterials. This introduces a new technology that combines a new generation of active biomaterials for TE with the use of bioreactors that can provide the appropriate stimuli. By applying dynamic stimulation, to the magnetoelectric films, the cells will sense mechanical stimuli of 0.013 $\mu m.mm^{-2}$ and an electrical stimuli of 16.15 μV. With this approach the influence of the mechano-electrical stimuli on the myoblast cell differentiation was evaluated and it was shown that these stimuli promote skeletal muscle regeneration, obtaining more mature myotubes, with no significant differences in positive and negatively charged surfaces. Also, another bioreactor with mechanical solicitation was used in order to prove the relevance of such stimuli, where similar but slightly higher values of electrical (64 μV) stimuli were applied to the cells. The results obtained shows higher maturation index values than the obtained by the use of the magnetic bioreactor, concluding that the mechanical and mostly the electrical stimuli play a key role on muscle differentiation. Therefore, this study proves the suitability of physical stimuli to improve tissue regeneration. It is also proved that magnetoelectric biomaterials are highly interesting to provide the mechano- and electrically-active dynamic microenvironment.

Thus, this work successfully demonstrates that mechanical and electrical stimuli are essential elements for proper muscle regeneration and that piezoelectric and magnetoelectric materials represent a promising approach for muscle TE.

7.2 Future work

This work demonstrated that piezoelectric and magnetoelectric polymers are promising candidates for skeletal muscle TE applications. However, it is essential to continue this line of research to better understand how the developed materials support skeletal muscle regeneration.

- In this study, only one cell type has been studied: cell line C2C12. As different cell types respond differently to different material surface characteristics, it will be important to evaluate the influence of the electro-mechanical stimuli with other muscle cell types such as cardiac muscle cells. In particular, the

study of these effects on human muscle cells and also on induced pluripotent stem cells (IPSCs) seem to be interesting challenges.

- Some important characteristics of myoblast cells must be quantified, such as the expression of marker genes that play distinct roles during myogenesis. This quantification can be due under static and dynamic conditions in order to understand how the surface charge and the piezoelectric effect affect the intracellular pathways of the cells. With these results it will be possible develop a more targeted and effective approach for muscle regeneration.
- The developed fibre platform with silica nanoparticles can be produced with silica mesoporous nanoparticles in order to combine the piezoelectric polymers with the release of bioactive materials to target specific applications goals.
- Evaluate the physiological function of the differentiated muscle function.
- Validate the electro-mechanical bioreactor as a widespread tool for tissue regeneration.